The Multituberculates as Living Animals: New Insights into the Ecomorphology, Behavior, and Life History of One of the Most Successful Mammalian Lineages

Lucas N. Weaver

A dissertation

submitted in partial fulfillment of the

requirements for the degree of

Doctor of Philosophy

University of Washington

2021

Reading Committee:

Gregory P. Wilson Mantilla, Chair

Christian A. Sidor

Raymond R. Rogers

Program Authorized to Offer Degree:

Biology

University of Washington

Abstract

The Multituberculates as Living Animals: New Insights into the Ecomorphology, Behavior, and Life History of One of the Most Successful Mammalian Lineages

Lucas N. Weaver

Chair of the Supervisory Committee:

Gregory P. Wilson Mantilla

Biology

Mammals from the Mesozoic and early Cenozoic exploited a diversity of ecological niches, approaching the complexity and specialization of extant therian mammals. Among the most evolutionarily diverse and numerically abundant of these early mammals were the Multituberculata, an extinct group of mostly small-bodied (< 1 kg) herbivores and omnivores whose fossil record spans the Middle Jurassic (ca. 170 Ma) through the end of the Eocene (ca. 35 Ma). Despite their predominance in early mammalian fossil assemblages, the paleobiology of multituberculates remains relatively obscure, due in part to their lack of modern descendants, and in part to their highly specialized, non-analogous dental and skeletal morphology. In this dissertation, I use a combination of linear morphometrics, comparative anatomy, functional morphology, sedimentology, taphonomy, and bone histology to shed further light on the

ecomorphology, behavior, and life history of multituberculates. In particular, this dissertation focuses on the fossil record of the multituberculate subgroup Cimolodonta from the Late Cretaceous through early Paleogene of the Western Interior of North America. In Chapter 2, a co-author and I examine how the shape of the blade-like lower premolars (p4s) of cimolodontans changed from the mid-Cretaceous through early Paleogene, and we find that the cimolodontan chewing cycle may have functionally constrained p4 shape and that their specialized blade-like dentitions may have limited their ability to exploit a broader array of herbivorous niches. In Chapter 3, co-authors and I describe exceptionally preserved skeletons of a cimolodontan from the Late Cretaceous Egg Mountain locality of Montana; therein, we describe a new genus, *Filikomys*, and infer that it was capable of burrowing. We then examine how the skeletons were preserved and hypothesize that these animals were preserved in burrows and that they were aggregating in life, thereby exhibiting the earliest evidence of mammalian social behavior. In Chapter 4, co-authors and I investigate the bone tissue microstructure (bone histology) of extant marsupial and placental mammals and discover that the bone histology of those groups are distinct and likely reflect their divergent reproductive strategies. We then apply our histological correlate of reproductive strategies to a sample of multituberculate femora from the Late Cretaceous and Paleocene of Montana and find that their bone histology is nearly identical to that of placentals, indicating that they likely had placental-like life histories. Those findings shed new light on the marsupial-placental dichotomy and challenge the hypothesis that Cenozoic rise of placental mammals was driven by unique reproductive innovations. In sum, this dissertation suggests that at least some multituberculates approached the level of behavioral and reproductive complexity of extant small-bodied placental mammals, and that their highly-specialized dentitions facilitated their Mesozoic success, but also their Cenozoic demise.

TABLE OF CONTENTS

LIST OF FIGURES

CHAPTER 2: SHAPE DISPARITY IN THE BLADE-LIKE PREMOLARS OF MULTITUBERCULATE MAMMALS: FUNCTIONAL CONSTRAINTS AND THE EVOLUTION OF HERBIVORY

CHAPTER 3: EARLY MAMMALIAN SOCIAL BEHAVIOUR REVEALED BY MULTITUBERCULATES FROM A DINOSAUR NESTING SITE

CHAPTER 4: MULTITUBERCULATE MAMMALS SHOW EVIDENCE OF A LIFE HISTORY STRATEGY SIMILAR TO THAT OF PLACENTALS, NOT MARSUPIALS

LIST OF TABLES

CHAPTER 2: SHAPE DISPARITY IN THE BLADE-LIKE PREMOLARS OF MULTITUBERCULATE MAMMALS: FUNCTIONAL CONSTRAINTS AND THE EVOLUTION OF HERBIVORY

CHAPTER 3: EARLY MAMMALIAN SOCIAL BEHAVIOUR REVEALED BY MULTITUBERCULATES FROM A DINOSAUR NESTING SITE

CHAPTER 4: MULTITUBERCULATE MAMMALS SHOW EVIDENCE OF A LIFE HISTORY STRATEGY SIMILAR TO THAT OF PLACENTALS, NOT MARSUPIALS

ACKNOWLEDGMENTS

For each research chapter, I will thank the specific people and funding that supported my work, but here I want to thank the people who made my entire graduate experience possible. First, I am deeply indebted and grateful to my advisor, Greg Wilson Mantilla; thank you for your mentorship, friendship, and for teaching me how to be a rigorous scientist and a competent writer. Many thanks to my dissertation committee, Chris Sidor, Caroline Strömberg, Patricia Kramer, and Ray Rogers, for your guidance and advice as I navigated both my research and my academic career. I would like to give special thanks to the Rogers family, Ray, Kristi, Lucy, Hatcher, and Uncle Jeff for supporting and encouraging me throughout my graduate career; I learned more about research, academia, and life sitting in your living room than just about anywhere else. Many thanks also to my 'unofficial' committee, Dave Grossnickle, Meg Whitney, Tom Tobin, and Eric Sargis, for reading countless manuscript and grant drafts, helping me navigate the twists and turns of academia, and for sharing a beer, laugh, and word of encouragement when I needed it most. Thank you to Dave Krause, Anne Weil, Craig Scott, and Bolor Minjin for your advice and perspective on all things multituberculate, many of the ideas presented here grew out of our conversations. I am also incredibly grateful to have had the chance to work with and learn from Bill Clemens, my academic grandfather, who taught me much about early mammals and the geology and paleontology of the Hell Creek area of northeastern Montana, and whose legacy of rigorous, specimen- and field-based research I hope to carry on in my own career. He is deeply missed.

I was extremely fortunate to be able to do my graduate work in the Department of Biology at the University of Washington. Thank you to my dear friends and cohort-mates, Ana Maria Bedoya Ovale and Will Brightly, who were my biggest sounding boards for venting

frustrations and celebrating successes. Thank you to the Wilson Mantilla lab members, past and present, with whom I learned so much, shared so many fond memories, and forged such strong friendships: Alex Brannick, Brody Hovatter, Henry Fulghum, Steph Smith, Dave DeMar, Jonathan Calede, Jordan Claytor, Paige Wilson, and Meng Chen. Thank you to the UW Paleobiology group for forming such a strong community and welcoming me from day one, in particular: Brandon Peecook, Zoe Kulik, Savannah Olroyd, Camilla Crifo, Alice Novello, Tim Ghallager, Alex Lowe, and Elena Stiles. Thank you to the UW Biology community as a whole; listing everyone who made an impact on me would spill across multiple pages, but the graduate students, postdocs, faculty, and staff have made this department my home for the past six years and I am so grateful.

Fieldwork has been my highlight of this entire process, and I am very thankful to the people of Jordan, Montana, who opened their doors to me, welcomed me into their community, and supported me in many ways. In particular, thank you to the Engdahls, Twitchells, Tharps, McKeevers, Phipps, Sinks, and the Hell Creek Bar staff. Thanks to the U.S. Bureau of Land Management, Montana State Parks, Charles M. Russell Wildlife Refuge, and Hell Creek State Park for your support, permitting, and access to field sites. Thanks also to Mike D'Emic, for letting me crash your Cloverly fieldwork, and to the Sidor lab field crew and Petrified Forest National Park for letting me dip my toes into the Triassic.

None of this would have been possible with the unwavering love, support, and encouragement of my family. Thank you to my parents, Tom and Jillon, for telling me to be true to myself and pursue my passions, words can never describe how deeply and truly grateful I am (and I'm so happy that you now know what a multituberculate is!). Thank you to my in-laws, Julie, Brian, and Mark, and my extended family: my uncles Steve, Bill, Randy, Rick, and Rob,

my aunts Rhonda, Rosie, and Sharon, and my cousins Britt, Mitch, Aaron, Tia, Kyle, and Allison—you all have supported and encouraged me throughout this process. I want to give a special thanks to Barb, Woody, and Lauren (the original Doctor of Philosophy in the family); you three were my academic refugium in family get-togethers and some of my fondest memories are chatting with you and telling you all about my latest academic exploits. And Woody, thank you for the Brunton compass, I still use it today.

Finally, I owe every single one of my successes, big and small, to my wife, Chloe. From day one, you pushed me to excel, to never settle, and to take advantage of every opportunity that came my way. Thank you for never letting me feel sorry for myself, for supporting me through thick and thin, and for being the best partner and dog mom a guy could ask for. I love you more than words can tell.

This dissertation is dedicated to Tom Bown and Kim Nichols, who ignited in me a passion for ancient mammals and prehistoric landscapes, and instilled in me the importance of good friends and good bourbon in solving scientific puzzles.

This paper is a study in paleobiology, an attempt to consider a very ancient and long extinct group of mammals not as bits of broken bone but as flesh and blood beings. The group so considered has many claims to such a study. It includes members of the very oldest known mammalian faunas and it subsisted practically from the beginning of reptilian dominance on into that of mammalian ascendency. What role these small beasts played in that savage medieval world and what peculiar advantage secured their unparalleled longevity are questions which have long excited the imagination. An attempt is here made to answer these questions by interpreting the mute and fragmentary remains of the animals themselves.

—George Gaylord Simpson, 'The Multituberculates as Living Animals,' 1926

CHAPTER 1: INTRODUCTION

When George Gaylord Simpson penned his first treatise on the paleobiology of multituberculate mammals (Simpson 1926), that group already had a long history of sparking confusion and debate among early paleontologists. Variably regarded as marsupials (Falconer 1957; Owen 1971) or monotremes (Broom 1910, 1914), herbivores (Falconer 1962; Gidley 1909) or carnivores (Owen 1971; Cope 1884; Broom 1910, 1914), arborealists (Gidley 1909) or terrestrialists (Broom 1910), the specialized hard-tissue anatomy of multituberculates perplexed comparative anatomists of the late 19th and early 20th centuries. Simpson was the first to clarify both the general ecological habits of multituberculates (Simpson 1926; Simpson and Elftman 1928) and their distinct phylogenetic position relative to modern mammalian lineages (Simpson 1928, 1929; Granger and Simpson 1929; Simpson 1937). Their procumbent incisors, serrated and blade-like premolars, and low-crowned molars hosting longitudinally arranged rows of cusps, all likely reflected adaptations for an herbivorous diet (Simpson 1926). Their postcranial skeleton exhibited an odd array of characters (Granger and Simpson 1929) that bespoke a unique, abducted gait and a scansorial or arboreal locomotor mode (Simpson 1926; Simpson and Elftman 1928). They were closely related to neither monotremes nor marsupials, but rather represented a separate and wholly extinct mammalian lineage that perhaps arose independently from the stock of non-mammalian cynodonts that gave rise to extant mammals (Simpson 1928, 1937, 1959).

In broad strokes, our current conceptualization of multituberculate paleobiology is fairly similar to that envisaged by Simpson, yet in the 95 years since he set out to understand the multituberculates as living animals, countless advances have been made. For example, it is likely that only some multituberculates were specialized herbivores, whereas the rest were probably

omnivorous (e.g., Krause 1982; Wall and Krause 1992; Gambaryan and Kielan-Jaworowska 1995; Wilson et al. 2012). Although some multituberculates were likely arboreal (Jenkins and Krause 1982; Krause and Jenkins 1983), others were terrestrial (Kielan-Jaworowska and Gambaryan 1994) or even fossorial (Kielan-Jaworowska and Qi 1990). We also now know that they likely had a keen sense of smell (e.g., Kielan-Jaworowska and Lancaster 2004), relatively poor hearing (e.g., Hurum 1998), and many were probably nocturnal (e.g., Krause 1986). Although Simpson regarded Multituberculata as a lineage outside of what we would now consider 'Crown Mammalia' (a view maintained by some and, as of yet, not fully refuted; e.g., Butler and Macintyre 1994; Butler 2000; Butler and Hooker 2005), the current consensus is that multituberculates were crown mammals, more closely related to therians than to monotremes (e.g., Rowe 1988; Luo et al. 2002).

Nevertheless, many of the key questions that inspired Simpson to explore multituberculate paleobiology nearly a century ago continue to fascinate and perplex paleontologists today. What selective pressures drove the evolution of their bizarre dentition? What made them so successful for well over 100 million years? Why did they decline so precipitously in the early Cenozoic? What are the phylogenetic relationships among multituberculate species? How did they behave? What ecological roles did they fill in dinosaur-dominated ecosystems? Were multituberculates specialized in biological aspects other than their hard-tissue anatomy? If so, how do those specializations compare to their mammalian contemporaries or modern mammals?

In this dissertation, I attempt to address aspects of all of these questions from the perspective of the Late Cretaceous and early Paleogene record of multituberculates from the Western Interior of North America. In particular, this work focuses on the Cimolodonta, perhaps

the most iconic multituberculates, characterized by their large, blade-like lower fourth premolars (p4) (Kielan-Jaworowska and Hurum 2001). The origins of the Cimolodonta are murky, but they first appear in the fossil record of the late Early Cretaceous (Cifelli 1997) and may have arisen from a group closely related to the Asian Eobaataridae (Kielan-Jaworowska et al. 1987; Kielan-Jaworowska and Hurum 2001). Whereas most North American multituberculates from the Late Jurassic and Early Cretaceous fall within the 'Plagiaulacida,' a paraphyletic grade characterized by a number of multituberculate plesiomorphies (e.g., up to four lower premolars that form a low, composite blade), cimolodontans vastly outnumbered 'plagiaulacidans' in terms of relative abundance and species richness by the mid-Cretaceous (early Cenomanian, ca. 100 Ma) and were the only multituberculate lineage to survive into the Late Cretaceous and early Paleogene (Eaton 1995; Eaton and Cifelli 2001; Weaver et al. 2019) (but see Flynn 1986 for a putative occurrence of two lower premolars of a 'plagiaulacidan' from the late Campanian of the San Juan Basin, New Mexico). Among mammalian communities in the Late Cretaceous of North America, cimolodontans were the most numerically abundant and taxonomically rich (e.g., Clemens 1964; Fox 1971; Montellano 1992; Eaton 2002; Wilson 2014), and beginning in the Campanian they underwent an adaptive radiation that coincided with the ecological rise of angiosperms (Wilson et al. 2012). In the early aftermath of the Cretaceous-Paleogene (K-Pg) mass extinction, cimolodontans continued to proliferate, rivaling contemporaneous eutherians in terms of both diversity and abundance (e.g., Wilson 2014; Smith et al. 2018). Indeed, cimolodontans continued to diversify well into the Paleocene before declining precipitously at the end of that epoch (Krause 1986; Wilson et al. 2012). Although cimolodontans persisted into the Eocene, they eventually went extinct before the onset of the Oligocene (Krishtalka et al. 1982; Swisher and Prothero 1990; Schumaker and Kihm 2006).

Herein, I aim to better illuminate the paleobiology and evolutionary history of North American cimolodontans through a series of chapters investigating their ecomorphology, behavior, and life history. In Chapter 2, a co-author and I focus on the most defining feature of Cimolodonta—their large, blade-like p4—and explore how p4 shape disparity changed from the mid-Cretaceous through the early Paleogene in North America. That study sheds new light on the selective pressures that constrain tooth shape in mammals with blade-like dentitions, and clarifies macroevolutionary trends among the Cimolodonta. In Chapter 3, co-authors and I describe exceptionally preserved skeletons of a cimolodontan from the late Campanian Egg Mountain locality of western Montana. Therein, we use a combination of geological, taphonomic, and functional morphological analyses to explore the preservational setting of the fossils and the locomotor mode of the species, revealing new insights into their ecology and behavior. In Chapter 4, co-authors and I investigate the life history of multituberculates from the latest Cretaceous and earliest Paleocene of northeastern Montana by studying their bone tissue microstructure (bone histology) and comparing it to that of extant, small-bodied marsupial and placental mammals. That study provides a new perspective on the evolution of mammalian reproduction and development and casts doubt on classic hypotheses about the drivers of placental diversification in the early Cenozoic.

Although focused on a single group of mammals, from a single geographic region, from a relatively narrow swath of geologic time, these studies have major implications for our understanding of early mammalian evolution. They reveal aspects of multituberculate paleobiology that heretofore have never been observed in any Mesozoic mammal, and challenge long-held beliefs about when in geologic time, and where taxonomically, key mammalian traits evolved. Yet, in many ways (and as is often the case), these studies raise more questions than

they answer, and they are almost certainly mere approximations of the real truth of the story. Nevertheless, an attempt is made herein to answer some of the fundamental questions about multituberculate evolution, "by interpreting the mute and fragmentary remains of the animals themselves" (Simpson 1926:228).

1.1 REFERENCES

Broom, R. (1910). On *Tritylodon*, and on the relationships of the Multituberculata. *Proceedings of the Zoological Society of London* **80**:760–769.

Broom, R. (1914). On the structure and affinities of the Multituberculata. *Bulletin of the American Museum of Natural History* **33**:115–134.

Butler, P. M. (2000). Review of the early allotherian mammals. *Acta Palaeontologica Polonica* **45**:317–342.

Butler, P. M., and Hooker, J. J. (2005). New teeth of allotherian mammals from the English Bathonian, including the earliest multituberculates. *Acta Palaeontologica Polonica* **50**:185–207.

Butler, P. M., and Macintyre, G. T. (1994). Review of the British Haramiyidae (?Mammalia, Allotheria), their molar occlusion and relationships. *Philosophical Transactions of the Royal Society B* **345**:433–458.

Cifelli, R. L. (1997). First notice on the Mesozoic mammals from Oklahoma. *Oklahoma Geology Notes* **57**:4–17.

Clemens, W. A. (1964). Fossil mammals of the type Lance Formation, Wyoming: part I. Introduction and Multituberculata. *University of California Publications in Geological Sciences* **48**:1–105.

Cope, E. D. (1884). The Tertiary Marsupialia. *The American Naturalist* **18**:686–697.

Eaton, J. G. (1995). Cenomanian and Turonian (early Late Cretaceous) multituberculate mammals from southwestern Utah. *Journal of Vertebrate Paleontology* **15**:761–784.

Eaton, J. G. (2002). Multituberculate mammals from the Wahweap (Campanian, Aquilan) and Kaiparowits (Campanian, Judithian) formations, within and near Grand Staircase-Escalante National Monument, southern Utah. *Miscellaneous Publications of the Utah Geological Survey* **02-4**:1–66.

Eaton, J. G., and Cifelli, R. L. (2001). Multituberculate mammals from near the Early-Late Cretaceous boundary, Cedar Mountain Formation, Utah. *Acta Palaeontologica Polonica* **46**:453–518.

Falconer, H. (1957). Description of two species of the fossil mammal genus *Plagiaulax* from Purbeck. *Quarterly Journal of the Geological Society* **13**:261–282.

Falconer, H. (1962). On the disputed affinity of the mammalian genus *Plagiaulax*. *Quarterly Journal of the Geological Society* **18**:348–369.

Flynn, L. J. (1986). Late Cretaceous mammal horizons from the San Juan Basin, New Mexico. *American Museum Novitates* **2845**:1–30.

Fox, R. C. (1971). Early Campanian multituberculates (Mammalia: Allotheria) from the Upper Milk River Formation, Alberta. *Canadian Journal of Earth Sciences* **8**:916–938.

Gambaryan, P. P., and Kielan-Jaworowska, Z. (1995). Masticatory musculature of Asian taeniolabidoid multituberculate mammals. *Acta Palaeontologica Polonica* **40**:45–108.

Gidley, J. W. (1909). Notes on the fossil mammalian genus *Ptilodus*, with descriptions of new species. *Proceedings of the United States National Museum* **36**:611–626.

Granger, W., and Simpson, G. G. (1929). A revision of the Tertiary Multituberculata. *Bulletin of the American Museum of Natural History* **56**:601–676.

Hurum, J. H. (1998). The inner ear of two Late Cretaceous multituberculate mammals, and its implications for multituberculate hearing. *Journal of Mammalian Evolution* **5**:65–93.

Jenkins, F. A., Jr., and Krause, D. W. (1982). Adaptations for climbing in North American multituberculates (Mammalia). *Science* **220**:712–715.

Kielan-Jaworowska, Z., Dashzeveg, D., and Trofimov, B. A. (1987). Early Cretaceous multituberculates from Mongolia and a comparison with Late Jurassic forms. *Acta Palaeontologica Polonica* **32**:3–47.

Kielan-Jaworowska, Z., and Gambaryan, P. P. (1994). Postcranial anatomy and habits of Asian multituberculate mammals. *Fossils and Strata* **36**:1–92.

Kielan-Jaworowska, Z., and Hurum, J. H. (2001). Phylogeny and systematics of multituberculate mammals. *Palaeontology* **44**:389–429.

Kielan-Jaworowska, Z., and Lancaster, T. E. (2004). A new reconstruction of multituberculate endocranial casts and encephalization quotient of Kryptobaatar. *Acta Palaeontologica Polonica* **49**:117–188.

Kielan-Jaworowska, Z., and Qi, T. (1990). Fossorial adaptations of a taeniolabidoid multituberculate mammal from the Eocene of China. *Vertebrata PalAsiatica* **28**:83–94.

Krause, D. W. (1982). Jaw movement, dental function, and diet in the Paleocene multituberculate Ptilodus. *Paleobiology* **8**:265–281.

Krause, D. W. (1986). Competitive exclusion and taxonomic displacement in the fossil record: the case of rodents and multituberculates in North America. In *Vertebrates, Phylogeny,*

and Philosophy, Flanagan, K. M., and Lillegraven, J. A., eds. (Contributions to Geology, University of Wyoming, Special Paper 3), pp. 95–117.

Krause, D. W., and Jenkins, F. A., Jr. (1983). The postcranial skeleton of North American multituberculates. *Bulletin of the Museum of Comparative Zoology* **150**:199–246.

Krishtalka, L. R., Emry, R. J., Storer, J. E., and Sutton, J. F. (1982). Oligocene multituberculates (Mammalia: Allotheria): youngest known record. *Journal of Paleontology* **56**:791–794.

Luo, Z.-X., Kielan-Jaworowska, Z., and Cifelli, R. L. (2002). In quest for a phylogeny of Mesozoic mammals. *Acta Palaeontologica Polonica* **47**:1–78.

Montellano, M. (1992). Mammalian fauna of the Judith River Formation (Late Cretaceous, Judithian), northcentral Montana. *University of California Publications in Geological Sciences* **136**:1–115.

Owen, R. (1971). Monograph of the fossil Mammalia of the Mesozoic formations. *Palaeontographical Society* **24**.

Rowe, T. (1988). Definition, diagnosis, and origin of Mammalia. *Journal of Vertebrate Paleontology* **8**:241–264.

Schumaker, K. K., and Kihm, A. J. (2006). Multituberculates from the Medicine Pole Hills local fauna (Chadronian) of Bowman County, North Dakota. *Paludicola* **6**:9–21.

Simpson, G. G. (1926). Mesozoic Mammalia, IV: the multituberculates as living animals. *American Journal of Science* **11**:228–250.

Simpson, G. G. (1928). *A Catalogue of the Mesozoic Mammalia in the Geological Department of the British Museum* (British Museum of Natural History, London), pp. 215.

Simpson, G. G. (1929). American Mesozoic Mammalia. *Memoirs of the Peabody Museum of Yale University* **3**:1–235.

Simpson, G. G. (1937). Skull structure of the Multituberculata. *Bulletin of the American Museum of Natural History* **73**:727–763.

Simpson, G. G. (1959). Mesozoic mammals and the polyphyletic origin of mammals. *Evolution* **13**:405–414.

Simpson, G. G., and Elftman, H. O. (1928). Hind limb musculature and habits of a Paleocene multituberculate. *American Museum Novitates* **333**:1–19.

Smith, S. M., Sprain, C. J., Clemens, W. A., Lofgren, D. L., Renne, P. R., and Wilson, G. P. (2018). Early mammalian recovery after the end-Cretaceous mass extinction: a high-resolution view from McGuire Creek area, Montana, USA. *Geological Society of American Bulletin* **130**:2000–2014.

Swisher, C. C., III, and Prothero, D. R. (1990). Single crystal $^{40}Ar/^{39}Ar$ dating of the Eocene-Oligocene transition in North America. *Science* **249**:760–762.

Wall, C. E., and Krause, D. W. (1992). A biomechanical analysis of the masticatory apparatus of *Ptilodus* (Multituberculata). *Journal of Vertebrate Paleontology* **12**:172–187.

Weaver, L. N., Wilson, G. P., Krumenacker, L. J., Moore, J. R., and Varricchio, D. J. (2019). New multituberculate mammals from the mid-Cretaceous (lower Cenomanian) Wayan Formation of southeastern Idaho and implications for the early evolution of Cimolodonta. *Journal of Vertebrate Paleontology* **39**:e1604532.

Wilson, G. P. (2014). Mammalian extinction, survival, and recovery dynamics across the Cretaceous-Paleogene boundary in the northeastern Montana, USA. In *Through the End of the Cretaceous in the Type Locality of the Hell Creek Formation in Montana and Adjacent Areas*, Wilson, G. P., Clemens, W. A., Horner, J. R., and Hartman, J. H., eds. (Geological Society of America, Special Paper 503), pp. 365–392.

Wilson, G. P., Evans, A. R., Corfe, I. J., Smits, P. D., Fortelius, M., and Jernvall, J. (2012). Adaptive radiation of multituberculate mammals before the extinction of dinosaurs. *Nature* **483**:457–460.

CHAPTER 2: SHAPE DISPARITY IN THE BLADE-LIKE PREMOLARS OF MULTITUBERCULATE MAMMALS: FUNCTIONAL CONSTRAINTS AND THE EVOLUTION OF HERBIVORY

Weaver, LN., and Wilson, GP. (2020) Shape disparity in the blade-like premolars of multituberculate mammals: functional constraints and the evolution of herbivory. *Journal of Mammalogy*. doi: 10.1093/jmammal/gyaa029.

2.1 AUTHOR CONTRIBUTIONS

LNW and GPW conceived of the study. LNW collected and analyzed the data. LNW made the figures and wrote the manuscript, with substantial input from GPW.

2.2 ABSTRACT

Cimolodontan multituberculates were a diverse and long-lived group of mammals characterized by large, blade-like lower fourth premolars (p4). Blade-like (plagiaulacoid) dentitions have evolved numerous times in distantly related mammalian lineages. Here we investigate how p4-shape disparity changed through time in the Cimolodonta. We address two hypotheses: (H_1) blade-like dentitions constrain the ability of plagiaulacoid mammals to evolve novel dental morphologies, (H_2) cimolodontan dental evolution proceeded gradually along a morphocline during the Late Cretaceous. We quantify functionally important aspects of p4 shape, including ratios reflecting height (H:L), symmetry (L1:L), and mesial-face height (H1:H), in a large sample of cimolodontans spanning the mid-Cretaceous through early Paleogene of North America (ca. 100–35 Mya). Our results do not support the morphocline hypothesis (H_2) and, instead, show that cimolodontans evolved a wide range of p4 shapes by the mid-Cretaceous and that p4-shape disparity remained stable through the Late Cretaceous. We hypothesize that the two-stage

cimolodontan chewing cycle (slicing-crushing then grinding) imposed functional constraints on p4 morphology. After the Cretaceous-Paleogene boundary, p4-shape disparity increased sharply, driven by the appearance of the Taeniolabidoidea, Microcosmodontidae, and Eucosmodontidae, in the early Paleocene. We contend that the slicing-crushing functions of the p4 became less important in those taxa, relaxing functional constraints on p4 morphology. Cimolodontans that retained both the slicing-crushing and grinding function of the p4 had a more limited range of p4 morphologies, and were probably largely restricted to animal-dominated omnivory. Taxa that shifted the initial slicing-crushing function from the p4 to the incisors had fewer functional constraints on p4 morphology, and were able to increase their molar grinding capacity to exploit plant-dominated omnivory and herbivory. That the p4 was reduced in herbivorous taxa rather than modified into a broader, multi-cusped tooth lends support to the morphological constraint hypothesis (H_1), and this relationship between p4 morphology and function suggests that retaining a large, blade-like p4 might have limited the range of herbivorous diets cimolodontans could exploit. These findings highlight the ecological and evolutionary limitations that specialized dentitions can impose on mammals by restricting their morphological and, in turn, functional diversification.

2.3 INTRODUCTION

Mammals have evolved a stunning array of dental types (Ungar 2010). Among the most distinctive is the plagiaulacoid type, which is characterized by one or more of the lower cheek teeth being modified to form a large, laterally compressed, serrated blade (Abel 1931; Simpson 1933). This type arose independently in a number of distantly related mammalian clades, including multituberculates, carpolestid plesiadapiforms, and diprotodont marsupials (Simpson

1933). Functional analyses of the masticatory patterns in multituberculates and carpolestids show that the plagiaulacoid blade served to slice and to wedge food apart prior to the food being ground by the molars (Krause 1982a; Biknevicius 1986; Wall and Krause 1992). Indeed, the dietary ecology of extant diprotodont marsupials with plagiaulacoid dentition (*Bettongia*, *Aepyprymnus*, *Hypsiprymnodon*, and *Burramys*) suggests that this type of dentition reflects a commitment to herbivory (Simpson 1926, 1933; but see Clemens and Kielan-Jaworowska 1979) or omnivory (Parker 1977; Schlager 1981). Likewise, ecomorphological analyses of the teeth and jaws of extinct multituberculates imply that plagiaulacoidy is associated with omnivorous to herbivorous diets (Wilson et al. 2012; Grossnickle and Polly 2013).

Despite the evolutionary success achieved by plagiaulacoid mammals, such specialized dentition may have constrained their abilities to evolve novel dental morphologies (Wilson et al. 2012; Vander Linden and Wilson 2014). For example, multi-cusped teeth are not known to have evolved from a blade-like precursor, although such a transformation has been suggested for sudamericid gondwanatherians (Gurovich and Beck 2009) and sthenurine kangaroos (Prideaux 2004). Nevertheless, the extent to which plagiaulacoid dentitions are morphologically constrained remains unclear because investigation is lacking into how the plagiaulacoid form has varied within any particular lineage over time. To this end, we quantified morphological variation in the blade-like lower fourth premolar (p4) of North American cimolodontan multituberculates, the longest-lived clade of plagiaulacoid mammals (note that ‘p4’ refers to a permanent lower fourth premolar, from either side of the mouth).

Cimolodontan multituberculates have a fossil record extending from the late Early Cretaceous (ca. 110 Ma; Cifelli 1997) to the late Eocene (ca. 35 Ma; Krishtalka et al. 1982; Swisher and Prothero 1990), and were the most numerically abundant and taxonomically diverse

mammals in the Late Cretaceous and early Paleocene faunas of the northern hemisphere (Kielan-Jaworowska et al. 2004; Weil and Krause 2008). In the Late Cretaceous (by at least 80 Ma) cimolodontans underwent an adaptive radiation that did not slow across the Cretaceous-Paleogene boundary and was broadly coincident with the ecological rise of angiosperms (Wilson et al. 2012; Grossnickle and Polly 2013). This adaptive radiation was characterized by increases in taxonomic richness, body-size disparity, and dietary breadth, to include herbivory (Wilson et al. 2012). Nearing the end of the Paleocene, however, the abundance and diversity of cimolodontans declined rapidly (Van Valen and Sloan 1966; Krause 1986; Wilson 2014), and by the end of the Eocene, multituberculates were extinct. This decline and eventual extinction has been attributed to the competitive inferiority of multituberculates to eutherian herbivores that were beginning to diversify in the early Cenozoic (Van Valen and Sloan 1966; Hopson 1967; Krause 1986; Adams et al. 2019). Here, we investigate the patterns of cimolodontan p4 morphology through the Late Cretaceous and early Paleogene to elucidate the role that this specialized, blade-like dentition might have played in either facilitating or limiting dietary flexibility in plagiaulacoid mammals.

Cimolodontans differ from other multituberculates in their p4 morphology (Kielan-Jaworowska and Hurum 2001) and in their resulting chewing mechanics (Krause 1982a). Cimolodontans likely arose from an unknown group of 'plagiaulacidan' multituberculates in the Early Cretaceous (Kielan-Jaworowska and Hurum 2001). The 'Plagiaulacida' were a paraphyletic assemblage of early multituberculates in which up to four lower premolars were modified to form a composite blade (Figure 2.1A); this group persisted from the Middle Jurassic (ca. 166 Ma; Butler and Hooker 2005) to the early Late Cretaceous (ca. 97 Ma; Eaton and Cifelli 2001). Cimolodontans differ from 'plagiaulacidans' by a loss of all anterior lower premolars

except for a peg-like p3 and by a p4 that is enlarged to form an arcuate, serrated blade (Figure 2.1A).

In the first phase of the multituberculate chewing cycle, the upper and lower dentitions come into initial contact (Krause 1982a; Lazzari et al. 2010), but the pattern of this first phase differs between 'plagiaulacidans' and cimolodontans. 'Plagiaulacidans' had what is interpreted as the plesiomorphic pattern (Krause 1982a; Lazzari et al. 2010): the lower jaw moved both orthally (upwards) and palinally (backwards) to initiate the chewing cycle at an angle oblique to the upper dentition. The functional interpretation of this pattern is that the lower premolars engaged in grinding (Hahn 1971; Lazzari et al. 2010). In contrast, in the cimolodontan *Ptilodus*, the enlarged p4 is thought to have functioned first in slicing and crushing as the lower jaw moved strictly orthally, then in grinding once the teeth were in occlusion and the jaw moved palinally (Krause 1982a; Wall and Krause 1992). We further illuminate macroevolutionary patterns within the Cimolodonta by quantifying changes in p4 shape and disparity through time.

Cimolodontan dental evolution has previously been framed as having proceeded gradually along a morphocline from a primitive '*Paracimexomys*-grade' in the mid-Cretaceous (ca. 113–94 Ma), in which the p4 was mesiodistally long in comparison to the lower molars but did not dorsally protrude above them, to a derived 'Ptilodontoid-grade' in the latest Cretaceous and Paleocene, in which the p4 was greatly enlarged and protruded well above the level of the molars (Clemens and Kielan-Jaworowska 1979; Archibald 1982). Along this morphocline, the molar row increased in relative size and surface complexity, whereas the p4 underwent little morphological change prior to the origin of 'Ptilodontoid-grade' cimolodontans near the end of the Cretaceous (Archibald 1982). In the last 25 years, significant additions have been made to the fossil record of cimolodontans, particularly those from the mid-Cretaceous, revealing a greater

diversity of p4 morphologies than was previously appreciated (e.g., Eaton 1995; Eaton and Cifelli 2001; Weaver et al. 2019). For example, the discovery of a p4 assigned to a clade nested within the Cimolodonta (Cimolodontidae) near the Early–Late Cretaceous boundary suggests that cimolodontans were already diversifying by the early Late Cretaceous (Weaver et al. 2019). These findings call the morphocline hypothesis into question and prompted us to re-evaluate the pattern of p4-shape evolution in the Cimolodonta.

In this paper we address two hypotheses: (H_1) specialized, blade-like dentitions constrain the ability of plagiaulacoid mammals to evolve novel dental morphologies, and (H_2) cimolodontan dental evolution proceeded gradually along a morphocline. We quantified functionally important aspects of p4 shape (Figure 2.1B), including ratios reflecting height (H:L), symmetry (L1:L), and height of the mesial face (H1:H), in a sample of 363 cimolodontan specimens representing eight families, 36 genera, and 94 species, from the mid-Cretaceous to early Paleogene (ca. 100–35 Ma) of North America. Our results shed new light on the macroevolution of cimolodontan multituberculates, demonstrating that their p4-shape disparity was not correlated with increases in taxonomic richness, body size disparity, and dietary breadth during the Late Cretaceous (Wilson et al. 2012). Furthermore, our results suggest that the chewing cycle of cimolodontans imposed functional constraints on their p4 morphologies, limiting their ability to exploit herbivorous niches. These findings provide a compelling example of decoupling between taxonomic diversity and morphological disparity in mammalian evolution, and highlight the limitations that specialized dentitions can impose on mammals by restricting their future dietary diversification.

2.4 MATERIALS AND METHODS

Sampling—We compiled a database of p4 measurements from cimolodontan multituberculates spanning the Late Cretaceous (ca. 100–66 Ma) and early Paleogene (ca. 66–35 Ma) of North America (Figure 2.2–4; Supplemental Data SD1). Sampling intensity varied considerably across our different time bins, owing to both the paucity of p4 specimens known from certain time intervals and the availability of specimens (e.g., whether or not the p4 of a particular species had been published and illustrated). In many cases, only a single p4 of a particular species was available for inclusion in our dataset, whereas in other cases we had access to numerous p4 specimens for a given species (e.g., species of *Mesodma* from our 'Lancian' and 'Puercan' time bins; Supplementary Data SD1). Furthermore, our data may have been affected by a multitude of taphonomic, paleoenvironmental, and paleobiological factors that could have varied both among and within our time bins. Although we recognize that this imperfect sampling may affect the analyses presented herein, this dataset represents the most comprehensive survey to date of the known p4s of cimolodontans from the Late Cretaceous and early Paleogene of North America.

Whenever possible, we measured the relevant specimens or casts directly using a Leica MZ9.5 binocular dissecting microscope and a custom measuring stage that has capability of reading to 0.001 mm. When that approach was not possible, we took the following approaches in order of preference: (1) we used ImageJ to measure specimens from images in published figures or from images that we acquired; (2) we used digital calipers to measure specimen images directly from the printed version of published figures; or (3) we took measurements available from the published literature (see Supplemental Data SD1 for notes on the methods used to acquire specific measurements). In 13 cases where we had access to specimens that also were

included in published figures, we measured both the actual specimen and the illustrated specimen, using either ImageJ (for electronic copies) or digital calipers (for print copies), then compared these measurements using the 'Method comparison' function in XLSTAT (version 2015.5; Supplementary Data SD2). For each measurement, *t*-tests show that the mean values for measurements of specimens versus measurements of illustrations do not differ significantly. The mean differences between measurements (biases) are small (Bias = -0.101 mm for L, -0.059 mm for H, -0.065 mm for L1, and 0.002 mm for H1), and the standard deviation ranged from -0.259 to 0.082 mm. In evaluating the Bland and Altman plots (Bland and Altman 1986), we noted that the majority of measurements were randomly clustered around the mean (0), and that all but one fall within the 95% confidence interval range (Supplementary Data SD2). These different methods for obtaining linear measurements therefore are unlikely to significantly have biased the results of our analyses.

Preservation biases are another potential source of error in our analyses. Dentigerous jaws are rare in the Cretaceous and Paleocene fossil record, and many multituberculate taxa are known only from isolated teeth. As a consequence, some taxa that were present during particular time intervals are omitted from our dataset because no complete p4 specimens have been attributed to them. For example, the Cimolomyidae first appeared in the middle–late Santonian (ca. 85 Ma; Eaton 2013) and persisted until the end of the Cretaceous (Figure 2.5); nonetheless, cimolomyid p4s are known only from the Judithian and Lancian North American Land Mammal 'ages' (e.g., Clemens 1964; Fox 1980; Cifelli et al. 2004). Thus, in our 'Pre-Aquilan' and 'Aquilan' time bins, cimolomyids only are represented by fragmentary p4s, and isolated upper premolars and molars (e.g., Fox 1971; Eaton 2013). The effect on p4-shape disparity only should be minor if the p4 shape of the omitted taxon is not expected to strongly diverge from those of

the other taxa in that time bin (Foote 1993). Although it currently is impossible to know the p4 morphologies of these early cimolomyids, these are represented in both the 'Judithian' and 'Lancian' time bins, and their presence in these time bins does not significantly increase p4-shape disparity relative to the preceding time bins. We thus contend that these missing p4 morphologies would not radically have been different from those seen in later Late Cretaceous time intervals.

p4 measurement conventions—Our multituberculate p4 measurements (Figure 2.1B) and ratios follow Novacek and Clemens (1977) and Hunter et al. (1997), with p4s oriented according to Novacek and Clemens (1977:Figure 2.2). We define a p4 serration as any sharp, dorsal projection from the blade profile, regardless of whether it is accompanied by a buccal or lingual ridge; this definition includes the mesial-most serration sometimes referred to as a 'pseudoserration' (sensu Krause 1982b), and thus could affect the measurement of the height of the crown at the first serration (H1; Figure 2.1B). All measurements were rounded to the nearest 0.01 mm.

Measurement abbreviations—**L**, length; **L1**, length to the apex of the crown; **H**, height; **H1**, height to the first serration (Figure 2.1B).

Analysis of p4-shape evolution—Using our database of p4 measurements, we calculated three ratios—H:L, L1:L, and H1:H—for each specimen, and plotted them through geologic time and according to taxonomic group (Figs. 2 – 4). We chose these ratios for this analysis because they are commonly used to describe cimolodontan p4 shape (e.g., Novacek and Clemens 1977; Archibald 1982; Hunter et al. 1997) and because they reflect important functional aspects of p4-shape evolution. H:L is the ratio of total height to total length of the crown: a high value corresponds to a tall profile. L1:L is the ratio of the length from the mesial face to the tallest

point on the crown relative to the total length of the crown: a value of 0.5 corresponds to a symmetrical profile, and higher and lower values correspond to more skewed profiles (distally or mesially, respectively). H1:H is the ratio of the height of the first serration to the total height of the crown; a high value corresponds to a p4 with a high mesial face. Together, these ratios make up our p4 morphospace.

We assigned each specimen in our dataset to one of 10 time bins; its approximate age was based upon either the geologic age (Gradstein et al. 2012) of the rock unit in which it was discovered or the North American Land Mammal 'age' (NALMA; Woodburne 2004) to which its fauna had been assigned. Thus, every plotted point represents a single measured specimen, except in cases where multiple specimens from the same family had the same ratio value and, therefore, are overlapping (Figs. 2 – 4). To quantify changes in morphological disparity through time, we calculated the variance of all mean species values of each ratio per time bin (Figs. 2 – 4; Supplemental Data SD3). We also ran resampling analyses to account for differences in sample size across our different time bins (Supplementary Data SD4). We drew five random samples from the species ratio values of each time bin (Supplementary Data SD3) and calculated the variance of each of these subsamples. For each ratio, we repeated this resampling at both 100 and 1,000 iterations, to generate 95% confidence intervals for each mean measure of variance (Supplementary Data SD4). The disparity values plotted in Figures 2 – 4 represent the mean ratio variances and 95% confidence intervals derived from our 100 iteration resampling analyses. In every case, the patterns were comparable to those generated using our raw data (Supplementary Data SD3), and 95% confidence intervals were non-overlapping (Figs. 2 – 4; Supplementary Data SD4), suggesting that these disparity patterns are independent of sample size. We opted not to assess statistical significance of these patterns using an *F*–test because the number of species

present in each of our time bins is relatively small (as low as five species in some cases). The sensitivity of an *F*–test depends highly on degrees of freedom and normally distributed data and, given the limited sample sizes of our dataset, such a test would impose an overly high burden of proof and thus be prone to Type II error.

Specimens from the lower Cenomanian-age Mussentuchit Member of the Cedar Mountain Formation of central Utah (Eaton and Nelson 1991; Eaton and Cifelli 2001) and Wayan Formation of southeastern Idaho (Weaver et al. 2019) were assigned to a 'mid-Cretaceous' bin (ca. 100–95 Ma). Specimens from upper Cenomanian–Santonian deposits (e.g., Eaton 1995, 2006) were assigned to a 'pre-Aquilan' bin (ca. 95–84 Ma). All other Late Cretaceous and Paleocene specimens were assigned to time bins according to NALMAs (Woodburne 2004). One taxon in our dataset, *Nidimys occultus*, has been assigned to the Edmontonian NALMA (Hunter et al. 2010), but we include it in our Judithian bin (ca. 79–69 Ma) because the Edmontonian has not been well sampled and is poorly characterized (Cifelli et al. 2004). All Eocene-age specimens were assigned to an 'Eocene' bin (ca. 55–35 Ma); however, most of these specimens belong to the early Eocene Wasatchian NALMA (ca. 55–50 Ma; e.g., McKenna 1960; Krause 1982c), with only one specimen belonging to the late Eocene, Chadronian NALMA (ca. 38–35 Ma; Schumaker and Kihm 2006). Note that these time bins vary considerably in duration. All else being equal, we would expect to see higher p4-shape disparity in the longer time bins (e.g., the pre-Aquilan, Judithian, and Eocene) because there was more time for evolution to produce disparate shapes, but this does not appear to be the case for our results. In addition, by lumping together smaller time intervals into a larger bin, we might have aggregated more granular changes in p4-shape disparity that occurred within each of those intervals. Nevertheless, because of the uneven sampling of cimolodontan fossils from the Late

Cretaceous and early Paleogene and the uncertainty in the absolute ages of certain rock units, we were unable to consistently group our data into small time bins (ca. 3–5 Ma).

Species-richness data—To compare p4-shape disparity to trends in cimolodontan taxonomic diversity, we compiled a database of all known cimolodontan multituberculate species from the Late Cretaceous and early Paleogene of North America (see Supplementary Data SD5 for the list of species per time interval, and the sources of those data). These species-richness data are presented graphically in Figure 5 as raw species counts for each time interval. The same time bins were used for both the p4-shape-disparity data and the species-richness data to maximize comparisons between them; nonetheless, we did include an Edmontonian species list in Supplementary Data SD5 for the sake of completeness (but note that these data are not displayed graphically). Many tentative species were omitted from our species tally (e.g., ?*Cimolomys* spp. A and B; Eaton 2013) but when a tentative occurrence represented the only record of a particular genus or species for a given time bin, it was included in our list. One such tentative occurrence worth noting is that of the Taeniolabidoidea in the Lancian (Figure 2.5; Supplementary Data SD5). We list three ?Taeniolabidoidea species as occurring in the Lancian; however, one of these species, *Bubodens magnus*, is poorly known (known only from a single molar; Wilson 1987), and its assignment to the Taeniolabidoidea is tentative (Kielan-Jaworowska et al. 2004). The other two species, '*Catopsalis*' *johnstoni* and '*Valenopsalis*' sp. cf. '*V.*' *joyneri* (formerly '*Catopsalis*' *joyneri*; Williamson et al. 2015), are from localities that are poorly constrained temporally (Cifelli et al. 2004; Lofgren et al. 2004). To convey the uncertainty associated with these occurrences, Lancian taeniolabidoids are highlighted in gray in Figure 2.5.

2.5 RESULTS

Our results show a pattern in the evolution of p4 shape in North American cimolodontans that consists of three parts and holds across all three ratios (Figs. 2 – 4). First, p4-shape disparity was low from the mid-Cretaceous through the Lancian (ca. 100–66 Ma). Second, p4-shape disparity increased sharply in the Puercan (ca. 66–63 Ma). Third, p4-shape disparity decreased after the Puercan (ca. 63–60 Ma). The range of p4 heights (H:L ≈ 0.4–0.6; Figure 2.2) and symmetries (L1:L ≈ 0.4–0.6; Figure 2.3) that characterized Late Cretaceous cimolodontans largely were established by the mid-Cretaceous and varied little until the Puercan. During this interval, two cimolodontan groups, the Neoplagiaulacidae (circles) and Cimolodontidae (squares) occupied the low and high ends, respectively, of the range of p4-height ratios (Figure 2.2); the '*Paracimexomys* group' (dashes) had intermediate values. As the Cimolomyidae (triangles) diversified in the Lancian (Figure 2.5), some taxa in this group surpassed cimolodontids in p4-height ratio (Figure 2.2). In contrast, the relative p4-symmetry ratios of higher-level taxa varied through the Late Cretaceous (Figure 2.3). The Neoplagiaulacidae (circles) tended to have more mesially skewed p4 profiles (L1:L < 0.5) and the Cimolodontidae (squares) tended to have more distally skewed profiles (L1:L > 0.5), but this pattern does not hold for every time bin. For example, in the Aquilan the cimolodontid *Cimolodon similis* (UMNH VP7592) had a mesially skewed profile equal to that of coeval neoplagiaulacids, and in the Lancian the neoplagiaulacid ?*Neoplagiaulax burgessi* (UCMP 116893, 116894) had a distally skewed profile exceeding that of coeval cimolodontids. The pattern of the p4-mesial-face-height ratio (Figure 2.4) differed from those for p4 height and symmetry. The range of the p4-mesial-face-height ratio (H1:H ≈ 0.5–0.9) that characterized Late Cretaceous cimolodontans was not established until the pre-Aquilan, and the overall disparity of p4-mesial-face-height ratio

was greater relative to p4 height and symmetry during much of the Late Cretaceous (pre-Aquilan, Judithian, Lancian) and Paleocene (Puercan–Tiffanian; Figure 2.4). As with p4 symmetry, there was considerable variation in p4-mesial-face-height ratios within higher-level taxa. The highest ratio values were seen within the Cimolodontidae (squares) in the pre-Aquilan and the Neoplagiaulacidae (circles) in the Judithian. The lowest ratio values were seen within the '*Paracimexomys* group' (dashes; Figure 2.4) in the pre-Aquilan and the Neoplagiaulacidae in the Lancian.

Disparity in p4 shape (all three ratios) increased sharply in the Puercan (Figs. 2 – 4). This increase was driven primarily by the appearance of the Taeniolabidoidea (crosses) and Microcosmodontidae (asterisks) and the presence of the Eucosmodontidae (X's) in the early Paleocene (Figure 2.5). These clades expanded the range of p4 height, symmetry, and mesial-face-height ratios beyond the limits observed in the Late Cretaceous. Taeniolabidoids expanded the high end of all ratios, microcosmodontids expanded the high end of p4 height and symmetry, and eucosmodontids expanded the low end of p4 symmetry and mesial-face height (Figs. 2 – 4). The Ptilodontidae (diamonds) also diversified in the Puercan, but their ratio values were comparable to those seen in the Late Cretaceous.

In the Torrejonian (63–60 Ma), p4 disparity of all three ratios declined. One factor that might have driven this decline is the associated decline in the taxonomic diversity of both taeniolabidoids and eucosmodontids (Figure 2.5). Another factor is that we were not able to sample any Torrejonian microcosmodontids in our dataset. We excluded one Torrejonian microcosmodontid p4 from our dataset because it was poorly preserved (*Microcosmodon* cf. *M. harleyi*; Clemens and Wilson 2009), and other Torrejonian microcosmodontids are not known from p4s. In the Tiffanian, disparity continued to drop (or at least remained relatively stable in

the case of L1:L) likely reflecting the disappearance of taeniolabidoids and eucosmodontids from our dataset (note that one species of taeniolabidoid is known from the Tiffanian, but has no associated p4; Figure 2.5). Nonetheless, p4-shape disparity across all three ratios did not drop down to Late Cretaceous levels until the Eocene. Microcosmodontids increased in taxonomic diversity in the Tiffanian and persisted into the Clarkforkian (Figure 2.5), expanding the range of all three p4 ratios beyond that exhibited by the other cimolodontan groups during those time periods (Figs. 2–4). This had the effect of buoying p4-shape disparity until microcosmodontids disappeared in the Eocene (Figure 2.5).

Our raw species-richness data reveal that cimolodontan taxonomic diversity was decoupled from p4-shape disparity during the Late Cretaceous and early Paleogene of North America. Unlike the pattern we observed for p4-shape disparity (Figs. 2 – 4), species richness among North American cimolodontans generally increased from the mid-Cretaceous to the Tiffanian (ca. 100–56 Ma; Figure 2.5), then dropped precipitously from the Tiffanian to the Clarkforkian (ca. 56–55 Ma; Figure 2.5). During the Late Cretaceous, species richness increased steadily from seven species in the mid-Cretaceous (ca. 100–95 Ma) to 25 species in the Judithian (ca. 79–69 Ma; Figure 2.5). Species richness increased sharply to 37 species in the Puercan (ca. 66–63 Ma), then increased sharply again to 47 species in the Tiffanian (ca. 60–56 Ma; Figure 2.5). In the Clarkforkian, species richness dropped dramatically to eight species, and only seven cimolodontan species persisted into the Eocene (ca. 55 Ma; Figure 2.5).

2.6 DISCUSSION

Stability of Late Cretaceous p4-shape disparity—The morphocline hypothesis implies a pattern of steady dental morphological change in Cimolodonta over the course of the ca. 34 Ma

of the Late Cretaceous (Clemens and Kielan-Jaworowska 1979; Archibald 1982). Our results, which rely on a fossil database of p4s that is more comprehensive than that available to previous workers, do not support that hypothesis. Instead, we show that by the beginning of the Late Cretaceous (early Cenomanian, ca. 100–95 Ma) North American cimolodontans had already evolved p4-shape disparity on par with that from latest Cretaceous time intervals (e.g., the Lancian), which are better sampled. This unexpected pattern implies that the evolution of the range of p4 shapes, and presumably other aspects of the dentition, (1) occurred rapidly in the mid-Cretaceous or (2) occurred gradually but earlier than previously understood (i.e., Early Cretaceous). Another alternative is that p4 morphology and p4 size were decoupled, such that p4 morphological diversity evolved early, but later changes to p4 size relative to the lower molars occurred gradually during the Late Cretaceous (sensu Archibald 1982). Testing these alternative hypotheses would require a greater sample of Early Cretaceous cimolodontans or the discovery of more complete cimolodontan jaws, with p4–m2 preserved, from the Late Cretaceous of North America. That p4-shape disparity of North American cimolodontans remained stable for the remainder of the Late Cretaceous suggests that factors might have constrained p4 morphological evolution. Structural and developmental constraints might have limited the range of viable p4 morphologies, but we hypothesize that the constraints were primarily functional and related to the chewing cycle of cimolodontan multituberculates.

Functional constraints limit Late Cretaceous p4-shape disparity—If the p4 of cimolodontans functioned in both slicing and grinding, then its morphological evolution would be constrained to certain heights, symmetries, and (to a lesser degree) mesial-face heights that would permit these functions (Figure 2.6). Although the p4 ‘slicing-then-grinding’ cycle was recognized in the Paleocene cimolodontan *Ptilodus* (Krause 1982a), the constrained p4-shape

disparity that we observe among Late Cretaceous North American cimolodontans implies that it might have arisen earlier in cimolodontan evolution.

The slicing-then-grinding cycle would have influenced the viable range of p4 heights (H:L values) among cimolodontans (Figure 2.6A – C). If the p4 were too tall, then it would have prevented the opposing molars from occluding (grinding phase inhibited in Figure 2.6A). If the p4 were too short, then it would have been unable to slice incoming food prior to the opposing molars coming into contact with one another (slicing-crushing phase inhibited in Figure 2.6C). Thus, the range of p4 heights observed among Late Cretaceous cimolodontans might represent an evolutionary trade-off that balanced the slicing and grinding phases of the cimolodontan chewing cycle (Figure 2.6B).

Similarly, if the cimolodontan p4 acted in both slicing and grinding, then the range of symmetries (L1:L values) also would have been restricted (Figure 2.6D–F). The p4 of cimolodontans is set at an angle in the dentary: distally the tooth is set high near the level of the molars, and mesially the tooth is set low at the level of the diastema (Figure 2.6). The mechanical advantage of a blade is proportional to its approach angle; i.e., the angle between the long axis of the blade and the line perpendicular to the direction of movement (Abler 1992; Evans and Sanson 1998; Evans and Sanson 2003; Evans and Pineda-Munoz 2018). For point cutting (i.e., slicing) to occur as a blade (e.g., the p4) contacts a horizontal surface (e.g., the upper tooth row), the approach angle of the blade must be greater than 0º (Evans and Sanson 2003). Given this functional requirement, there would be a selective advantage to increasing the distal skew of p4 because the approach angle of p4 increases as its profile skews distally (Figure 2.6D – F). As p4 skews mesially, the mechanical advantage of the blade will decrease, limiting the slicing function of the tooth (slicing-crushing phase inhibited in Figure 2.6F). In contrast, as p4 skews

distally, less of the mesial portion of the tooth comes into contact with the upper dentition, limiting the amount of p4 surface area available for grinding (grinding phase inhibited in Figure 2.6D). Thus, as with p4 height, the range of p4 symmetries observed among Late Cretaceous cimolodontans might represent an evolutionary trade-off that maintained both the slicing and grinding function of the p4 (Figure 2.6E).

Compared to the p4-height and p4-symmetry ratios, the p4-mesial-face-height ratio (H1:H) has a higher overall disparity. This is because H1:H values correspond to the height at which the p4 serration series begins, rather than dictating gross changes in the shape of the p4 profile. Extreme changes in p4 height and symmetry would prohibit either one or both phases of the cimolodontan chewing cycle, but extreme changes in the height of the serration series would not prohibit slicing-crushing or grinding. Thus, H1:H could vary more than H:L or L1:L without incurring similar negative functional consequences. Nevertheless, the range of p4-mesial-face-height ratios was small in the Late Cretaceous compared to in the earliest Paleocene. This suggests that there might have been other functional constraints on the height of the p4 serration series that were related to the chewing cycle of cimolodontans (Figure 2.6G – I). A high H1:H value (> ~0.9) would not affect the grinding function of p4 because only the serrations near or distal to the p4 apogee occlude with the upper dentition during the cimolodontan chewing cycle (Krause 1982a; Figure 2.6G). In contrast, because serrated blades decrease the amount of orthal force needed to slice food materials (Abler 1992), maintaining serrations along the mesial portion of the tooth (H1:H < ~0.9) would provide a functional advantage during the slicing phase of the chewing cycle (Figure 2.6H). If the serration series began too low on the blade, neither slicing nor grinding would be inhibited, but those first few serrations would be ‘non-functional’ because they would fall below the active chewing surface of the p4 (Krause 1982a; Figure 2.6I).

Thus, neither of these scenarios would prohibit slicing or grinding, but they would decrease the efficiency of the p4 to perform these functions (Figure 2.6G, I).

Relaxed functional constraints drive earliest Paleocene increases in p4-shape disparity—The Taeniolabidoidea, Eucosmodontidae, and Microcosmodontidae, drove the increase in p4-shape disparity in the earliest Paleocene (Puercan). When we remove these clades from our analyses, the Puercan increase in p4-shape disparity disappears (see Supplemental Data SD6). Unlike other cimolodontan groups, the Taeniolabidoidea, Eucosmodontidae, and Microcosmodontidae exhibit a relative decrease in p4 size and an increase in molar-row length (Figure 2.7). This relative lengthening of the molar row would have increased the grinding capacity of these taxa. Taeniolabidoids, eucosmodontids, and microcosmodontids, also exhibit large, robust incisors that have a ventrobuccally restricted band of enamel and in turn were self-sharpening (Krause 1986; Kielan-Jaworowska and Hurum 2001). This suite of morphological changes suggests that (1) the role of the p4-slicing at the beginning of the chewing cycle was de-emphasized (Sloan 1979; Krause 1986), (2) incisor-gnawing (similar to that seen in Rodentia) became important to the initial breakdown of food items, and (3) molar-grinding was emphasized in the masticatory cycle of these cimolodontan groups (Figure 2.7).

We hypothesize that this modification of the masticatory cycle relaxed the functional constraints on the p4 morphology of taeniolabidoids, microcosmodontids, and eucosmodontids. Taeniolabidoids modified their p4 from a blade to a mesiodistally and dorsoventrally short and buccolingually expanded tooth (Figure 2.7A, D, G). Both microcosmodontids and eucosmodontids retained a blade-like p4, but in microcosmodontids it was reduced in both height and length (Figure 2.7B, E, H), and in eucosmodontids it was reduced in height (Figure 2.7C, F, I). For taeniolabidoids (Figure 2.7A, D) and microcosmodontids (Figure 2.7B, E), the p4 was so

reduced in both height and length that high H:L and L1:L values likely would not have interfered with the grinding phase of the chewing cycle. Also, if these groups de-emphasized the initial p4-slicing phase of their chewing cycle, there would have been no functional advantage to maintaining serrations along the mesial face of the tooth. This may explain their high H1:H values (Figure 2.7G, H). In eucosmodontids, the p4 is not significantly reduced in length, but it is reduced in height, resulting in low H:L values (Figure 2.7C). Their low L1:L values may reflect their emphasis on the grinding phase of their chewing cycle, because a mesially skewed p4 profile would allow more of the p4 surface to be used in grinding (Figure 2.7F). Eucosmodontids also exhibit the lowest H1:H values. This may be related to the fact that their p4s often are set at a lower angle in the jaw than those of other cimolodontans (e.g., Sloan and Van Valen 1965:fig. 4; Figure 2.7C, F, I); their serration series therefore could have begun lower on the tooth while still falling along the active chewing surface of the p4 (Figure 2.7I). Each of these groups took a different approach to reducing the slicing-crushing function of their p4 and, as a result, their p4 morphologies were able to expand beyond the morphological limits imposed on every other group of North American cimolodontans (Figure 2.7).

Impact of p4 shape on the evolution of herbivory in multituberculates—Our results show that the breadth of p4 shapes that characterized Late Cretaceous cimolodontans from North America evolved by ca. 100 Ma, prior to their adaptive radiation ca. 80 Ma (Wilson et al. 2012). That is, p4-shape disparity did not increase in-step with taxonomic richness, body-size disparity, or dietary breadth during the late Late Cretaceous. Although this adaptive radiation was recognized at the global scale, we also see that p4-shape disparity and cimolodontan species richness were decoupled during the Late Cretaceous and early Paleogene of North America (compare Figure 2.2 – 4 with Figure 2.5). A possible explanation is that the evolution of plant-

dominated omnivory and herbivory in some multituberculate groups had more to do with increases in the relative size and complexity of the molar row than increases in p4-shape disparity (Wilson et al. 2012). This explanation is consistent with our functional constraint hypothesis. The cimolodontan groups that retained the slicing-crushing and grinding function of the p4 (e.g., Neoplagiaulacidae) had a more limited range of p4 morphologies, and had dental complexity values (i.e., orientation patch count rotated values) that suggest they were largely animal-dominated omnivores; whereas the taxa that shifted the initial slicing-crushing function from the p4 to the incisors (e.g., Taeniolabidoidea) had fewer functional constraints on p4 morphology, and were able to increase their molar grinding capacity at the expense of p4 size and shape to exploit plant-dominated omnivory and herbivory (Wilson et al. 2012). One exception to this rule are the Cimolomyidae, which had relatively limited p4 morphologies (Figure 2.2 – 4), but also have been inferred as plant-dominated omnivores and herbivores (Wilson et al. 2012). Nevertheless, compared to the other cimolodontan groups that had limited p4 morphologies, cimolomyids exhibited a decrease in both the height and length of the p4 relative to the lower molars (or at least no increase in p4 size proportional to the increase in molar size; Clemens and Kielan-Jaworowska 1979; Archibald 1982). That their p4 morphologies did not greatly expand the p4 morphospace may be related to the fact that cimolomyid incisors were not rodent–like, as they were in the Taeniolabidoidea, Eucosmodontidae, and Microcosmodontidae (Archibald 1982; Kielan-Jaworowska and Hurum 2001). Thus, the initial slicing-crushing function of the p4 probably was not shifted to the incisors in the Cimolomyidae, and their p4 morphologies likely were still limited by functional constraints associated with the cimolodontan chewing cycle.

This relationship between p4 morphology and function suggests that retaining a large,

blade-like p4 might have limited the range of herbivorous diets cimolodontans could exploit. Functional analyses of the chewing mechanics of cimolodontans and carpolestids have shown that their plagiaulacoid blades functioned by fracturing and dividing plant-based foods with brittle or ductile exteriors and soft, fleshy interiors (e.g., fruits and nuts), rather than grinding foliage (Krause 1982a; Biknevicius 1986; Wall and Krause 1992). Mammals with folivorous diets typically expand the occlusal surface area of their cheek tooth rows because breaking down fibrous stems and leaves requires prolonged grinding by the cheek teeth (Rensberger 1986; Hunter and Jernvall 1995). Retaining a long, narrow, blade-like p4 would significantly limit the occlusal surface area of the cimolodontan cheek tooth row and would therefore be ill suited for a folivorous diet. Although it has been proposed that a multi-cusped tooth can evolve from a blade-like precursor in some cases (Prideaux 2004; Gurovich and Beck 2009), the fact that cimolodontans compensated for this problem by increasing the relative size of their molars at the expense of the p4 implies that there might have been some developmental, functional, or structural constraints that prohibited modifying p4 into a broader, multi-cusped tooth (Wilson et al. 2012). This lends support to the hypothesis that specialized, blade-like dentitions constrain the ability of plagiaulacoid mammals to evolve novel dental morphologies. Therefore, the evolution of an enlarged, slicing-crushing p4 might have been an important adaptation for early cimolodontans, but it had the potential consequence of limiting their dietary flexibility.

Implications for the extinction of multituberculates—Competitive exclusion by archaic ungulates (i.e., 'condylarths'), plesiadapiforms, and rodents, in particular, long has been cited as the cause for the early Paleogene decline of multituberculates (Van Valen and Sloan 1966; Krause 1986; Adams et al. 2019). This hypothesis is supported by the marked decline in the number of multituberculates that were inferred to have been plant-dominated omnivores or

herbivores in the Paleocene (Wilson et al. 2012), just as herbivorous eutherian mammals were beginning to increase in both taxonomic diversity and numerical abundance (Van Valen and Sloan 1966; Krause 1986). Functional constraints on cimolodontan dental morphology might have contributed to this decline by putting Paleocene multituberculates at a selective disadvantage relative to contemporaneous eutherian herbivores.

Our findings suggest that although the plagiaulacoid type of mammalian dentition has arisen independently in a number of distantly related and evolutionarily successful lineages, it might have also limited the range of diets that these lineages could exploit. More broadly, these findings highlight the evolutionary trade-offs associated with dental specialization. Specialized dentitions have allowed mammalian lineages to exploit novel food resources, but they have also reduced future dietary options.

2.7 ACKNOWLEDGMENTS

We thank W. H. Brightly for his help with our resampling analyses, D. W. Krause and C. S. Scott for feedback on our species-richness data, D. M. Grossnickle, M. R. Whitney, A. L. Brannick, B. T. Hovatter, and J. R. Claytor for helpful comments and discussions concerning this manuscript and research, S. M. Smith and P. K. Wilson for thoughtful critiques and suggestions that improved the figures, C. Levitt-Bussian (Natural History Museum of Utah) for access to specimens, R. L. Cifelli, B. M. Davis, and K. Davies (Sam Noble Oklahoma Museum of Natural History), P. A. Holroyd and W. A. Clemens (University of California Museum of Paleontology), and B. Crowley (Burke Museum) for access to casts, R. A. Powell, L. A. Ruedas and four anonymous reviewers for their suggestions that improved the manuscript, and M. I. Pardi for organizing, and R. A. Powell for editing, this special issue. We also gratefully acknowledge

financial support provided by a NSF Graduate Research Fellowship and a Doris O. and Samuel P. Welles Research Fund travel grant (LNW) and by the University of Washington Department of Biology, the Burke Museum, and the Myhrvold & Havranek Charitable Family Fund (LNW and GPW).

2.8 LITERATURE CITED

ABEL, O. 1931. Die stellung des menschen im rahmen der wirbeltiere. Gustav Fischer. Jena, Germany.

ABLER, W. L. 1992. The serrated teeth of tyrannosaurid dinosaurs, and biting structures in other animals. Paleobiology 18:161–183.

ADAMS, N. F., E. J. RAYFIELD, P. G. COX, S. N. COBB, AND I. J. CORFE. 2019. Functional tests of the competitive exclusion hypothesis for multituberculate extinction. Royal Society Open Science 6:181536.

ARCHIBALD, J. D. 1982. A study of Mammalia and geology across the Cretaceous-Tertiary boundary in Garfield County, Montana. University of California Publications in Geological Sciences 122:1–286.

BIKNEVICIUS, A. R. 1986. Dental function and diet in the Carpolestidae (Primates, Plesiadapiformes). American Journal of Physical Anthropology 71:157–171.

BLAND, J. M., AND D. G. ALTMAN. 1986. Statistical methods for assessing agreement between two methods of clinical measurement. The Lancet 327:307–310.

BUTLER, P. M., AND J. J. HOOKER. 2005. New teeth of allotherian mammals from the English Bathonian, including the earliest multituberculates. Acta Palaeontologica Polonica 50:185–207.

CIFELLI, R. L. 1997. First notice on Mesozoic mammals from Oklahoma. Oklahoma Geology Notes 57:4–17.

CIFELLI, R. L., J. J. EBERLE, D. L. LOFGREN, J. A. LILLEGRAVEN, AND W. A. CLEMENS. 2004. Mammalian biochronology of the latest Cretaceous. Pp. 21–42 in Late Cretaceous and Cenozoic mammals of North America: biostratigraphy and geochronology (M. O. Woodburne, ed.). Columbia University Press. New York, New York.

CLEMENS, W. A. 1964. Fossil mammals of the type Lance Formation, Wyoming: part I. Introduction and Multituberculata. University of California Publications in Geological Sciences 48:1–105.

CLEMENS, W. A., AND Z. KIELAN-JAWOROWSKA. 1979. Multituberculata. Pp. 99–149 in Mesozoic mammals: the first two-thirds of mammalian history (J. A. Lillegraven, Z. Kielan-Jaworowska, and W. A. Clemens, eds.). University of California Press. Berkeley, California.

CLEMENS, W. A., AND G. P. WILSON. 2009. Early Torrejonian mammalian local faunas from northeastern Montana, U.S.A. Pp. 111–158 in Papers on geology, vertebrate paleontology, and biostratigraphy in honor of Michael O. Woodburne (L. B. Albright, III, ed.). Museum of Northern Arizona Bulletin 65. Flagstaff, Arizona.

EATON, J. G. 1995. Cenomanian and Turonian (early Late Cretaceous) multituberculate mammals from southwestern Utah. Journal of Vertebrate Paleontology 15:761–784.

EATON, J. G. 2006. Santonian (Late Cretaceous) mammals from the John Henry Member of the Straight Cliffs Formation, Grand Staircase-Escalante National Monument, Utah. Journal of Vertebrate Paleontology 26:446–460.

EATON, J. G. 2013. Late Cretaceous mammals from Bryce Canyon National Park and vicinity,

Paunsaugunt Plateau, southwestern Utah. Pp. 329–369 in At the top of the Grand Staircase: the Late Cretaceous of southern Utah (A. L. Titus and M. A. Loewen, eds.). Indiana University Press. Bloomington, Indiana.

EATON, J. G., AND R. L. CIFELLI. 2001. Multituberculate mammals from near the Early-Late Cretaceous boundary, Cedar Mountain Formation, Utah. Acta Palaeontologica Polonica 46:453–518.

EATON, J. G., AND M. E. NELSON. 1991. Multituberculate mammals from the Lower Cretaceous Cedar Mountain Formation, San Rafael Swell, Utah. Contributions to Geology, University of Wyoming 29:1–12.

EVANS, A. R., AND S. PINEDA-MUNOZ. 2018. Inferring mammal dietary ecology from dental morphology. Pp. 37–51 in Methods in paleoecology: reconstructing Cenozoic environments and ecological communities (D. A. Croft, D. F. Su, and S. W. Simpson, eds.). Springer Nature. Cham, Switzerland.

EVANS, A. R., AND G. D. SANSON. 1998. The effect of tooth shape on the breakdown of insects. Journal of Zoology 246:391–400.

EVANS, A. R., AND G. D. SANSON. 2003. The tooth of perfection: functional and spatial constraints on mammalian tooth shape. Biological Journal of the Linnean Society 78:173–191.

FOOTE, M. 1993. Contributions of individual taxa to overall morphological disparity. Paleobiology 19:403–419.

FOX, R. C. 1971. Early Campanian multituberculates (Mammalia: Allotheria) from the Upper Milk River Formation, Alberta. Canadian Journal of Earth Sciences 8:916–938.

FOX, R. C. 1980. Mammals from the Upper Cretaceous Oldman Formation, Alberta. IV.

Meniscoessus Cope (Multituberculata). Canadian Journal of Earth Sciences 17:1480–1488.

GRADSTEIN, F. M., J. G. OGG, M. D. SCHMITZ, AND G. M. OGG (EDS.). 2012. The geologic time scale 2012. Elsevier Scientific Publishing. Amsterdam, Netherlands.

GROSSNICKLE, D. M., AND P. D. POLLY. 2013. Mammal disparity decreases during the Cretaceous angiosperm radiation. Proceedings of the Royal Society B 280:1–8.

GUROVICH, Y., AND R. BECK. 2009. The phylogenetic affinities of the enigmatic mammalian clade Gondwanatheria. Journal of Mammalian Evolution 16:25–49.

HAHN, G. 1971. The dentition of the Paulchoffatiidae (Multituberculata, upper Jurassic). Memória dos Serviços Geológicos de Portugal 17:7–39.

HOPSON, J. A. 1967. Comments on the competitive inferiority of the multituberculates. Systematic Zoology 16:352–355.

HUNTER, J. P., J. H. HARTMAN, AND D. W. KRAUSE. 1997. Mammals and mollusks across the Cretaceous-Tertiary boundary from Makoshika State Park and vicinity (Williston Basin), Montana. Contributions to Geology, University of Wyoming 32:61–114.

HUNTER, J. P., R. E. HEINRICH, AND D. B. WEISHAMPEL. 2010. Mammals from the St. Mary River Formation (Upper Cretaceous), Montana. Journal of Vertebrate Paleontology 30:885–898.

HUNTER, J. P., AND J. JERNVALL. 1995. The hypocone as a key innovation in mammalian evolution. Proceedings of the National Academy of Sciences of the United States of America 92:10718–10722.

KIELAN-JAWOROWSKA, Z., R. L. CIFELLI, AND Z.-X. LUO. 2004. Mammals from the age of dinosaurs: origins, evolution, and structure. Columbia University Press. New York, New

York.

KIELAN-JAWOROWSKA, Z., AND J. H. HURUM. 2001. Phylogeny and systematics of multituberculate mammals. Palaeontology 44:389–429.

KRAUSE, D. W. 1982a. Jaw movement, dental function, and diet in the Paleocene multituberculate *Ptilodus*. Paleobiology 8:265–281.

KRAUSE, D. W. 1982b. Evolutionary history and paleobiology of early Cenozoic Multituberculata (Mammalia), with emphasis on the family Ptilodontidae. Ph.D. dissertation, University of Michigan. Ann Arbor, Michigan.

KRAUSE, D. W. 1982c. Multituberculates from the Wasatchian Land-Mammal Age, early Eocene, of western North America. Journal of Paleontology 56:271–294.

KRAUSE, D. W. 1986. Competitive exclusion and taxonomic displacement in the fossil record: the case of rodents and multituberculates in North America. Pp. 95–117 in Vertebrates, phylogeny, and philosophy (K. M. Flanagan and J. A. Lillegraven, eds.). Contributions to Geology, University of Wyoming, Special Paper 3. Laramie, Wyoming.

KRISHTALKA, L., R. J. EMRY, J. E. STORER, AND J. F. SUTTON. 1982. Oligocene multituberculates (Mammalia: Allotheria): youngest known record. Journal of Paleontology 56:791–794.

LAZZARI, V., J. A. SCHULTZ, P. TAFFOREAU, AND T. MARTIN. 2010. Occlusal pattern in paulchoffatiid multituberculates and the evolution of cusp morphology in mammaliamorphs with rodent-like dentitions. Journal of Mammalian Evolution 17:177–192.

LOFGREN, D.L., J. A. LILLEGRAVEN, W. A. CLEMENS, P. D. GINGERICH, AND T. E. WILLIAMSON. 2004. Paleocene biochronology: the Puercan through Clarkforkian land mammal ages. Pp. 43–105 in Late Cretaceous and Cenozoic mammals of North America:

biostratigraphy and geochronology (M. O. Woodburne, ed.). Columbia University Press. New York, New York.

MCKENNA, M. C. 1960. Fossil Mammalia from the early Wasatchian Four Mile fauna, Eocene of northwest Colorado. University of California Publications in Geological Sciences 37:1–130.

NOVACEK, M., AND W. A. CLEMENS. 1977. Aspects of intrageneric variation and evolution of *Mesodma* (Multituberculata, Mammalia). Journal of Paleontology 51:701–717.

PARKER, P. J. 1977. Aspects of the biology of *Bettongia penicilata*. Ph.D. dissertation, Yale University. New Haven, Connecticut.

PRIDEAUX, G. J. 2004. Systematics and evolution of the sthenurine kangaroos. University of California Publications in Geological Sciences 146:1–623.

RENSBERGER, J. M. 1986. Early chewing mechanisms in mammalian herbivores. Paleobiology 12:474–494.

SCHLAGER, F. E. 1981. Evaluation of factors influencing status and distribution of the rufous bettong, *Aepyprymnus rufescens*, in New South Wales. Bulletin of the Australian Mammalogy Society 7:1–58.

SCHUMAKER, K. K., AND A. J. KIHM. 2006. Multituberculates from the Medicine Pole Hills local fauna (Chadronian) of Bowman County, North Dakota. Paludicola 6:9–21.

SIMPSON, G. G. 1926. Mesozoic Mammalia, IV: the multituberculates as living animals. American Journal of Science 11:228–250.

SIMPSON, G. G. 1933. The 'plagiaulacoid' type of mammalian dentition: a study of convergence. Journal of Mammalogy 14:97–101.

SLOAN, R. E. 1979. Multituberculata. Pp. 492–498 in The encyclopedia of paleontology (R. W.

Fairbridge and D. Jablonski, eds.). Dowden, Hutchinson, and Ross, Inc. Stroudsburg, Pennsylvania.

SLOAN, R. E., AND L. VAN VALEN. 1965. Cretaceous mammals from Montana. Science 148:220–227.

SWISHER, C. C., III, AND D. R. PROTHERO. 1990. Single-crystal $^{40}Ar/^{39}Ar$ dating of the Eocene-Oligocene transition in North America. Science 249:760–762.

UNGAR, P. S. 2010. Mammal teeth: origin, evolution, and diversity. Johns Hopkins University Press. Baltimore, Maryland.

VAN VALEN, L., AND R. E. SLOAN. 1966. The extinction of the multituberculates. Systematic Zoology 15:261–278.

VANDER LINDEN, A. R., AND G. P. WILSON. 2014. Functional constraint and convergent evolution of plagiaulacoid dentition in extant marsupials. Integrative and Comparative Biology 54:E361.

WALL, C. E., AND D. W. KRAUSE. 1992. A biomechanical analysis of the masticatory apparatus of *Ptilodus* (Multituberculata). Journal of Vertebrate Paleontology 12:172–187.

WEAVER, L. N., G. P. WILSON, L. J. KRUMENACKER, J. R. MOORE, AND D. J. VARRICCHIO. 2019. New multituberculate mammals from the mid-Cretaceous (lower Cenomanian) Wayan Formation of southeastern Idaho and implications for the early evolution of Cimolodonta. Journal of Vertebrate Paleontology, 39(2):e1604532.

WEIL, A., AND D. W. KRAUSE. 2008. Multituberculata. Pp. 19–38 in Evolution of Tertiary mammals of North America, Volume 2 (C. M. Janis, G. F. Gunnell, and M. D. Uhen, eds.). Cambridge University Press. Cambridge, United Kingdom.

WILLIAMSON, T. E., S. L. BRUSATTE, R. SECORD, AND S. SHELLEY. 2015. A new taeniolabidoid

multituberculate (Mammalia) from the middle Puercan of the Nacimiento Formation, New Mexico, and a revision of taeniolabidoid systematics and phylogeny. Zoological Journal of the Linnean Society 177:183–208.

WILSON, G. P. 2014. Mammalian extinction, survival, and recovery dynamics across the Cretaceous-Paleogene boundary in northeastern Montana, USA. Pp. 365–392 in Through the end of the Cretaceous in the type locality of the Hell Creek Formation in Montana and adjacent areas (G. P. Wilson, W. A. Clemens, J. R. Horner, and J. H. Hartman, eds.). Geological Society of America, Special Paper 503. Boulder, Colorado.

WILSON, G. P., A. R. EVANS, I. J. CORFE, P. D. SMITS, M. FORTELIUS, AND J. JERNVALL. 2012. Adaptive radiation of multituberculate mammals before the extinction of dinosaurs. Nature 483:457–460.

WILSON, R. W. 1987. Late Cretaceous (Fox Hills) multituberculates from the Red Owl local fauna of western South Dakota. Dakoterra 3:118–132.

WOODBURNE, M. O. (ED.). 2004. Late Cretaceous and Cenozoic mammals of North America: biostratigraphy and geochronology. Columbia University Press. New York, New York.

2.9 FIGURES

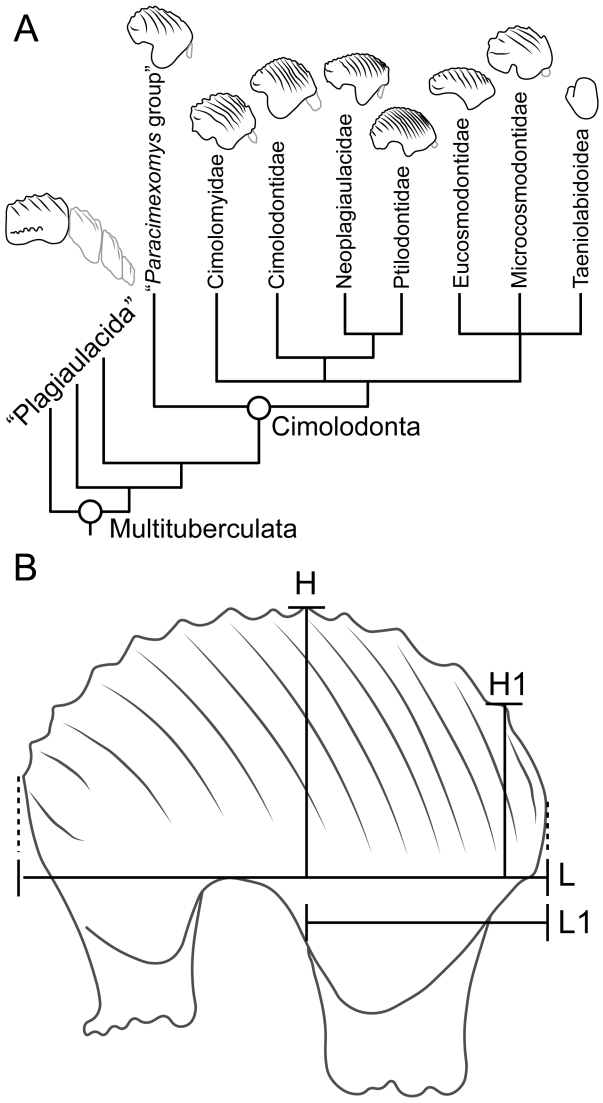

Figure 2.1.—A, Hypothetical cladogram showing the possible interrelationships of North American cimolodontan multituberculates (based on Kielan-Jaworowska and Hurum 2001). Outline drawings of the lower premolars from representatives of each group are shown above; p4 is outlined in black and anterior premolars are outlined in gray. **B**, The measurement scheme of this study illustrated on a right p4 in buccal view. **Abbreviations: L**, length; **L1**, length to the highest point of the p4 profile; **H**, maximum height of the p4 profile; **H1**, height to the first serration.

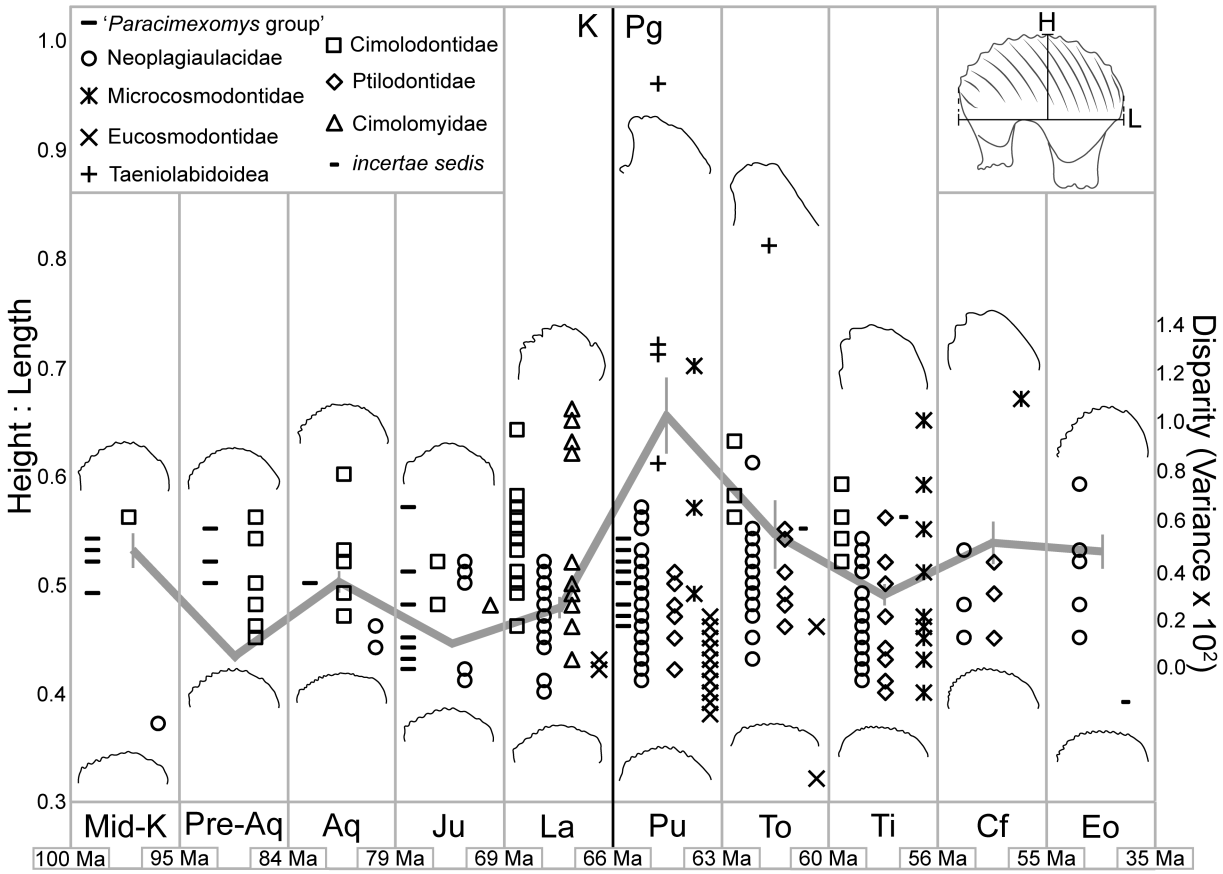

Figure 2.2.— H:L values and disparity of cimolodontan p4s through time. Ratio values are given on the left vertical axis and different markers correspond to the H:L values of different cimolodontan groups (see legend). Outline drawings of the right p4s in buccal profile depict the specimens with the maximum and minimum values for each time bin. The bold gray line represents disparity through time with disparity values on the right vertical axis. The ages that bracket the temporal bins are approximate values and based on Gradstein et al. (2012) and Woodburne (2004). Note that widths of temporal bins are not to scale. Inset shows measurement scheme for H:L values. **Abbreviations: Mid-K**, mid-Cretaceous (including specimens from the Mussentuchit and Wayan formations); **Pre-Aq**, pre-Aquilan (including specimens from the upper Cenomanian–Santonian); **Aq**, Aquilan; **Ju**, Judithian; **La**, Lancian; **Pu**, Puercan; **To**, Torrejonian; **Ti**, Tiffanian; **Cf**, Clarkforkian; **Eo**, Eocene (including specimens from the

Wasatchian and Chadronian NALMAs).

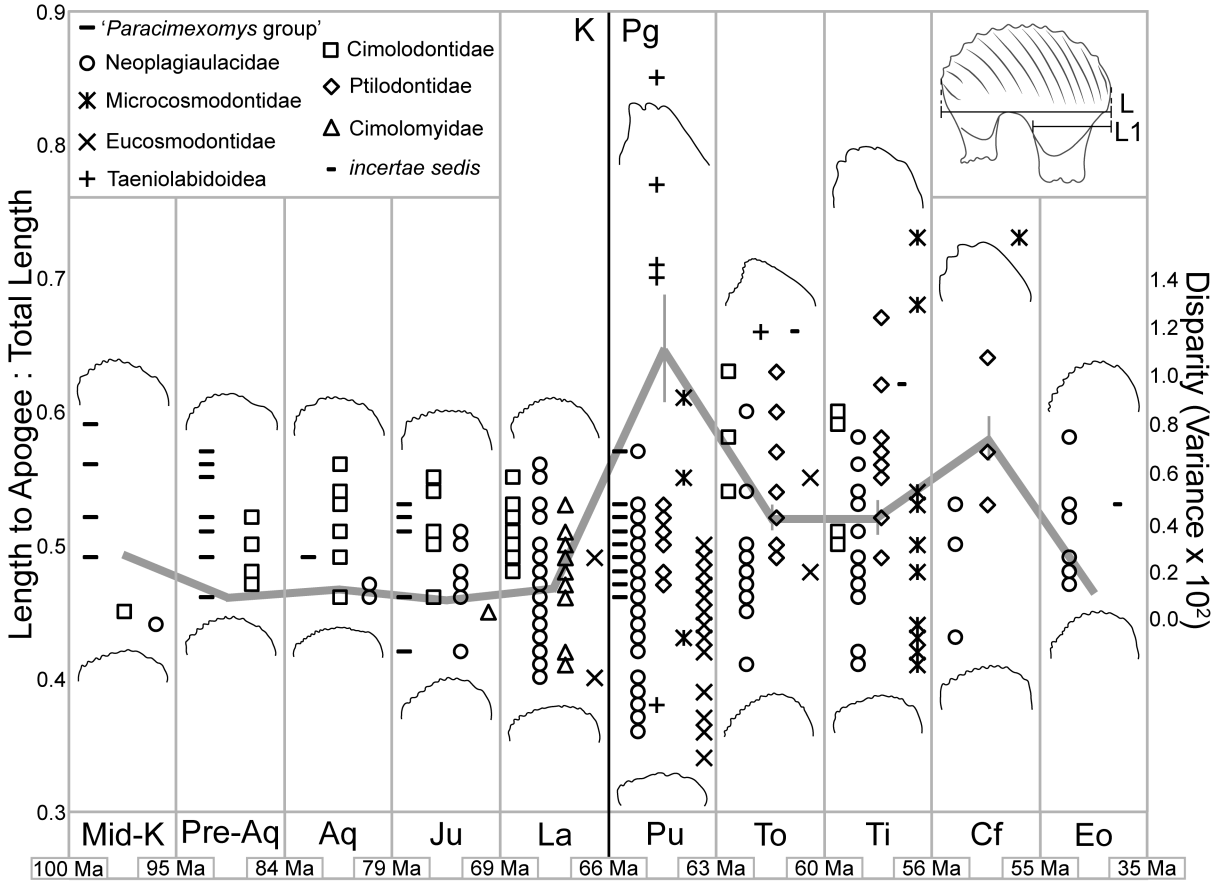

Figure 2.3.—L1:L values and disparity of cimolodontan p4s through time. See Figure 2.2 caption for other details.

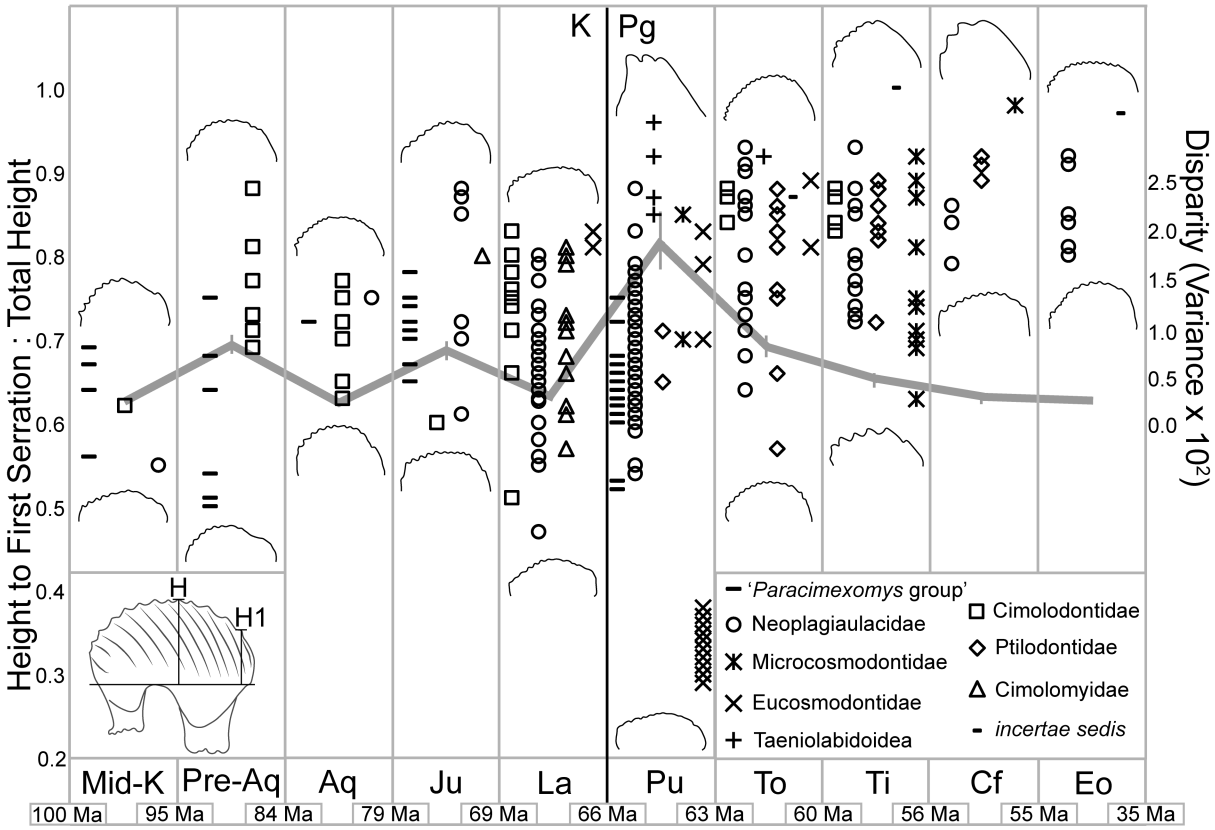

Figure 2.4.—H1:H values and disparity of cimolodontan p4s though time. See Figure 2.2 caption for other details.

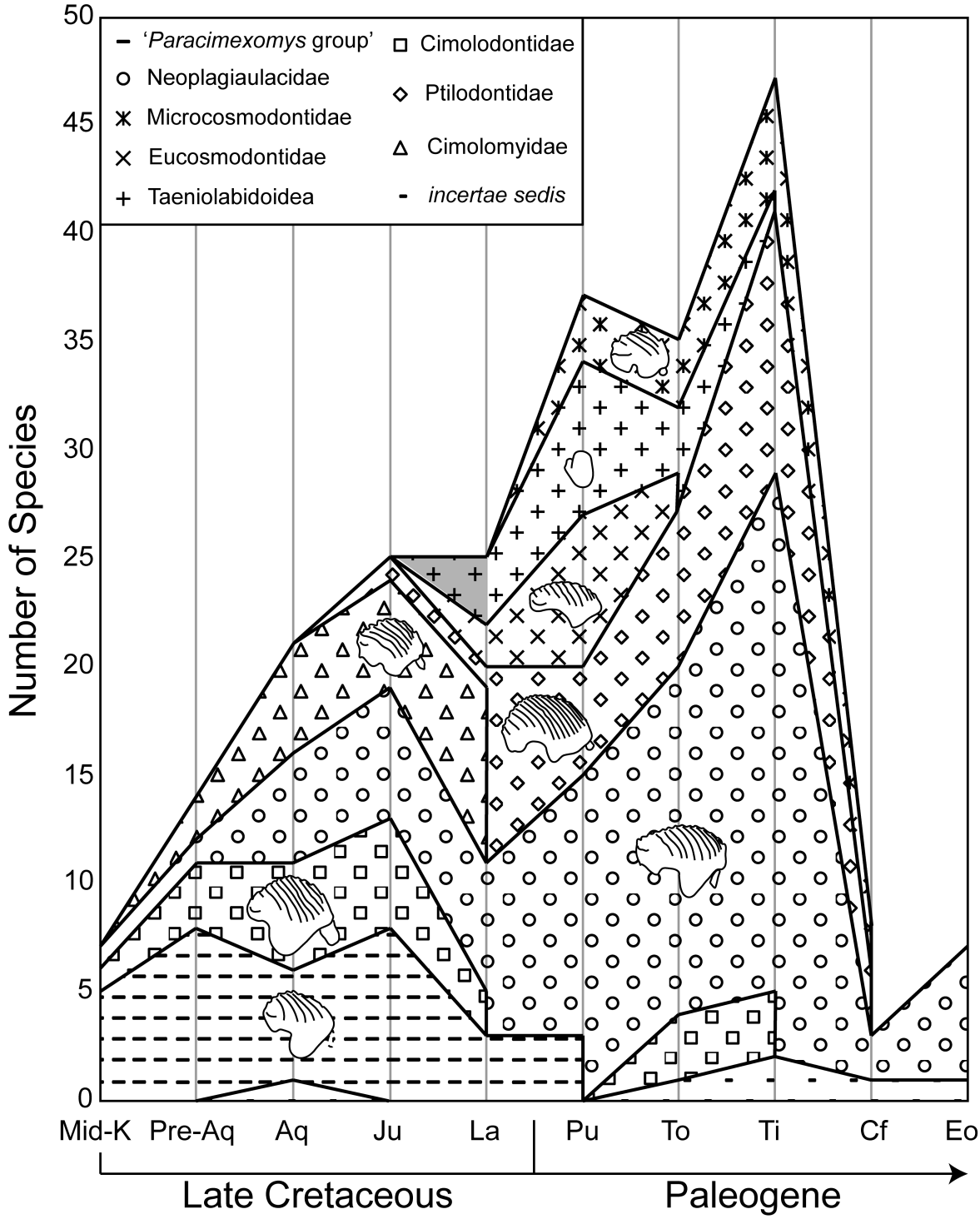

Figure 2.5.—Raw species richness of cimolodontan multituberculates from the Late Cretaceous and early Paleogene of North America. Each time bin is represented by a gray vertical line. The vertical thickness of each marker-filled area corresponds to the number of species for that taxon

in that given time bin. Data for each time bin is plotted at the gray vertical line and interpolated between these lines. See Figs. 2–4 for approximate durations of time bins and Figure 2.2 caption for abbreviation definitions. Outline drawings of the lower premolars from representatives of each group are provided within plot. The Lancian value for taeniolabidoids is shaded gray because of the uncertainty associated with the presence of these taxa in this time bin (see 'Materials and Methods' for details).

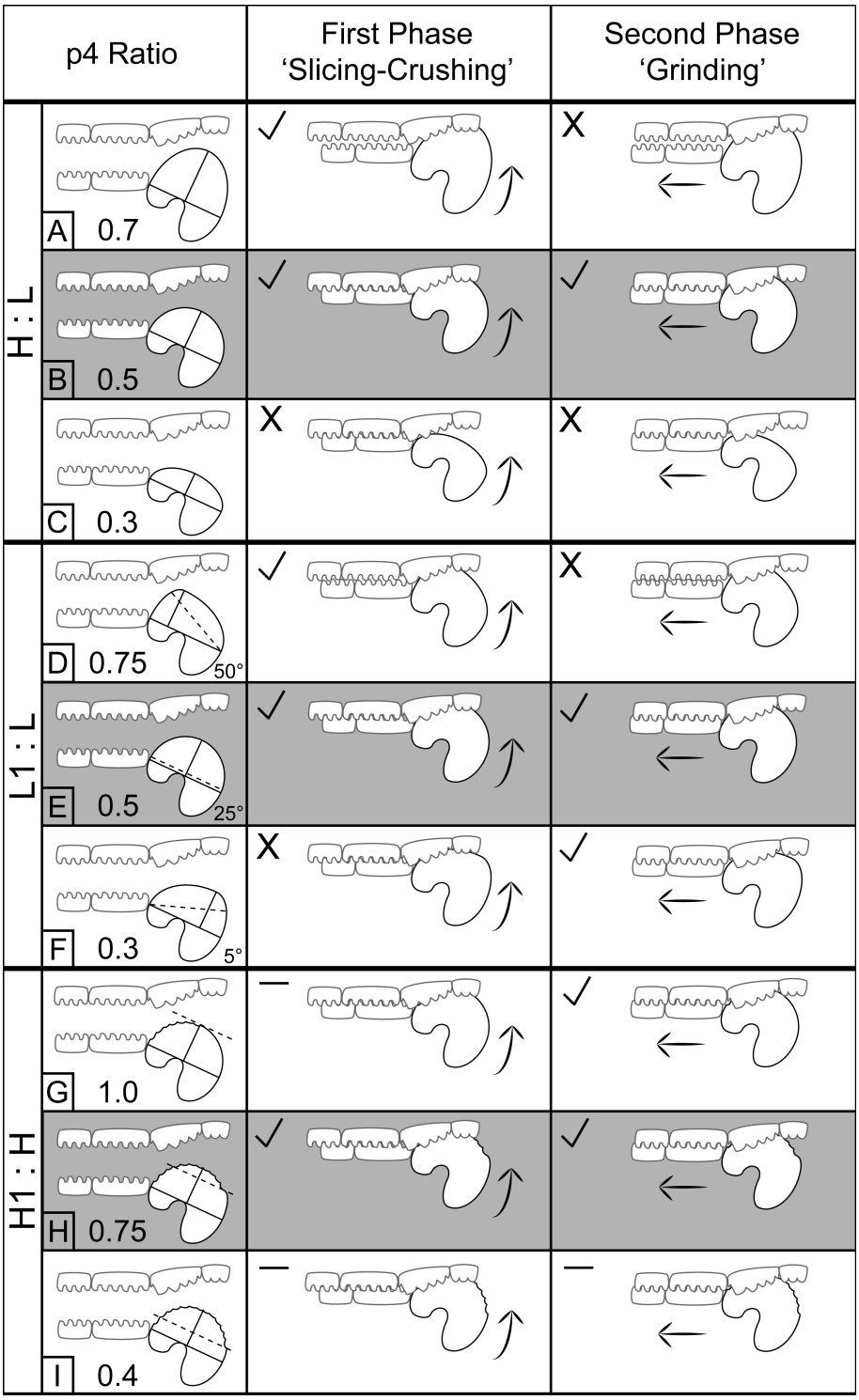

Figure 2.6.—Schematic of cimolodontan cheek tooth rows showing the potential effects of different p4 height (**A**–**C**), symmetry (**D**–**F**), and mesial-face height (**G**–**I**) ratio values on the slicing-crushing and grinding phases of the chewing cycle. The p4 is outlined in black, molars

and upper premolars are outlined in gray. Black arrows indicate direction of movement of the lower tooth row during the first (upwards) and second (backwards) phases of the cimolodontan chewing cycle. Solid lines within the p4s represent the hypothetical measurements that would produce the ratio values for each row. The dotted lines in the L1:L schematics (**D**–**F**) demonstrate how the long axis of the p4 changes with distal vs. mesial skew, thus affecting the approach angle of the blade (given in the lower right-hand corner). The dotted lines in the H1:H schematics (**G**–**I**) represent the height at the first serration (H1). White shaded boxes represent ratio values that inhibit one or two phases of the chewing cycle; gray shaded boxes represent values that do not inhibit either phase of the chewing cycle. Xs denote a morphology that inhibits that particular phase of the chewing cycle; check marks denote a morphology that does not inhibit that particular phase of the chewing cycle.

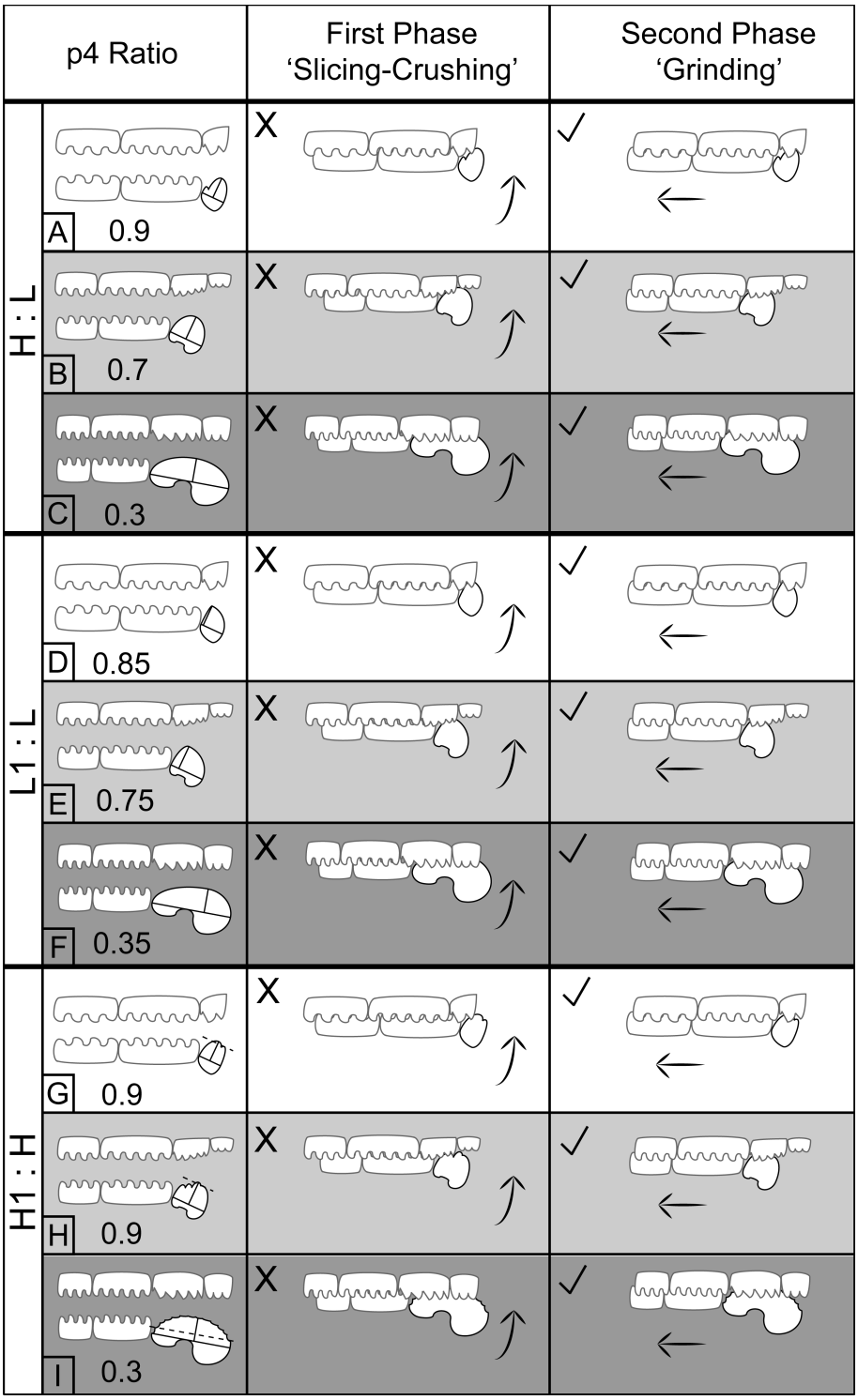

Figure 2.7.—Schematic of the dentition of the Taeniolabidoidea (white shaded boxes; **A**, **D**, **G**), Microcosmodontidae (light-gray shaded boxes; **B**, **E**, **H**), and Eucosmodontidae (dark-gray shaded boxes; **C**, **F**, **I**) showing how their p4 morphologies were able to expand the range of p4

ratios by mostly abandoning the slicing-crushing phase of their chewing cycle.

2.10 APPENDIX I: LIST OF SPECIES AND SPECIMENS INVESTIGATED

The North American cimolodontan p4 specimens used in the study are listed below by species in alphabetical order. The format is as follows: **Genus species**: Specimen number—age, locality, formation, county, state/province, country. For pre-Aquilan specimens, their approximate geologic age is provided, otherwise the North American Land Mammal 'age' is provided. **Museum abbreviations**: **AMNH**, American Museum of Natural History, New York, New York, U.S.A.; **CCM**, Carter County Museum, Ekalaka, Montana, U.S.A.; **DMNS** or **DMNH**, Denver Museum of Nature and Science, Denver, Colorado, U.S.A.; **KU**, Kansas University Biodiversity Institute and Natural History Museum, Lawrence, Kansas, U.S.A.; **MCZ**, Museum of Comparative Zoology, Harvard University, Cambridge, Massachusetts, U.S.A.; **MNA**, Museum of Northern Arizona, Flagstaff, Arizona, U.S.A.; **MOR**, Museum of the Rockies, Bozeman, Montana, U.S.A.; **NMMNH**, New Mexico Museum of Natural History and Science, Albuquerque, New Mexico, U.S.A.; **OMNH**, Sam Noble Oklahoma Museum of Natural History, Norman, Oklahoma, U.S.A.; **PTRM**, Pioneer Trails Regional Museum, Bowman, North Dakota, U.S.A.; **PU** or **YPM-PU**, Princeton University collections, Yale Peabody Museum, New Haven, Connecticut, U.S.A.; **TMP**, Royal Tyrrell Museum of Paleontology, Drumheller, Alberta, Canada; **UA** or **UALVP**, Laboratory of Vertebrate Paleontology, University of Alberta, Edmonton, Alberta, Canada; **UCM**, University of Colorado Museum, Boulder, Colorado, U.S.A.; **UCMP**, University of California Museum of Paleontology, Berkeley, California, U.S.A.; **UM**, Museum of Paleontology, University of Michigan, Ann Arbor, Michigan, U.S.A.; **UMNH**, Utah Museum of Natural History, Salt Lake City, Utah, U.S.A.; **UMVP**, University of

Minnesota, Vertebrate Paleontology Collections, Minneapolis, Minnesota, U.S.A.; **USNM**, United States National Museum of Natural History, Washington, D.C., U.S.A.; **UW**, University of Wyoming, Collection of Fossil Vertebrates, Laramie, Wyoming, U.S.A.

Acheronodon garbanii: UCMP 116953—Puercan, UCMP Locality V74111, Tullock Member, Fort Union Formation, Garfield County, Montana, U.S.A.

Acheronodon vossae: UALVP 24550—Tiffanian, Cochrane 2 Locality, Paskapoo Formation, Rocky View County, Alberta, Canada.

Allocosmodon woodi: UALVP 40475, 40494—Tiffanian, DW-2 Locality, Paskapoo Formation, Rocky View County, Alberta, Canada; UM 84199—Tiffanian, Douglass Quarry, Fort Union Formation, Sweetgrass County, Montana, U.S.A.; MCZ 19963—Tiffanian, New Anthill Locality, Shotgun Member, Fort Union Formation, Fremont County, Wyoming, U.S.A.; UMVP 5001—Tiffanian, Circle Locality, Tongue River Member, Fort Union Formation, McCone County, Montana, U.S.A.

Anconodon cochranensis: USNM V9765—Torrejonian, Douglass Quarry, Fort Union Formation, Sweetgrass County, Montana, U.S.A.; UALVP 44135—Torrejonian, Who Nose? Locality, Paskapoo Formation, Rocky View County, Alberta, Canada.; UM 84131, 84117, PU 14619B—Tiffanian, Douglass Quarry, Fort Union Formation, Sweetgrass County, Montana, U.S.A.

Anconodon gidleyi: TMP 2011.090.0371—Torrejonian, TMP Locality L2395, Paskapoo Formation, Rocky View County, Alberta, Canada.; UM 84146—Tiffanian, Douglass Quarry, Fort Union Formation, Sweetgrass County, Montana, U.S.A.

Baiotomeus douglassi: UM 77928—Torrejonian, Rock Bench Quarry, Fort Union Formation,

Sweetgrass County, Montana, U.S.A.

Baiotomeus lamberti: YPM-PU 18221A—Torrejonian, Medicine Rocks I, Fort Union Formation, Carter County, Montana, U.S.A.

Baiotomeus rhothonion: UALVP 44132—Torrejonian, Who Nose? Locality, Paskapoo Formation, Rocky View County, Alberta, Canada.

Bryceomys fumosus: MNA V5639, V7476—Turonian, Bryce Valley, Smoky Hollow Member, Straight Cliffs Formation, Garfield County, Utah, U.S.A.

Bryceomys intermedius: OMNH 34405—lower Cenomanian, San Rafael Swell, Mussentuchit Member, Cedar Mountain Formation, Emery County, Utah, U.S.A.

Catopsalis alexanderi: UCMP 34979—Puercan, UCMP Locality V74110, Tullock Member, Fort Union Formation, Garfield County, Montana, U.S.A.

Catopsalis fissidens: NMMNH P-8608—Torrejonian, 'Torrejon beds', Nacimiento Formation, San Juan County, New Mexico, U.S.A.

***Catopsalis* sp.**: UCMP 10998—Puercan, UCMP Locality V70201, Tullock Member, Fort Union Formation, Garfield County, Montana, U.S.A.

Cedaromys bestia: OMNH 26636—lower Cenomanian, San Rafael Swell, Mussentuchit Member, Cedar Mountain Formation, Emery County, Utah, U.S.A.

Cedaromys minimus: UMNH VP12836—upper Cenomanian, UMNH VP Locality 162, middle member of the Naturita Formation, Cedar Canyon, Iron County, Utah, U.S.A.

Cedaromys parvus: OMNH 32987, 27497—lower Cenomanian, San Rafael Swell, Mussentuchit Member, Cedar Mountain Formation, Emery County, Utah, U.S.A.

Cimexomys arapahoensis: UCM 34938—Puercan, UCM Locality 77267, Denver Formation, Arapahoe County, Colorado, U.S.A.

Cimexomys gratus: UCMP 133835—Puercan, UCMP Locality V87114, Tullock Member, Fort Union Formation, McCone County, Montana, U.S.A.; UCMP 117000, 150082—Puercan, UCMP V74111, Tullock Member, Fort Union Formation, Garfield County, Montana, U.S.A.

Cimexomys judithae: AMNH 77100—Judithian, Clambank Hollow, Judith River Formation, Chouteau County, Montana, U.S.A.; UCMP 131505—Judithian, UCMP Locality V-77803, Judith River Formation, Hill County, Montana, U.S.A.; MOR 302—Judithian, MOR Locality TM-006, Two Medicine Formation, Teton County, Montana, U.S.A.; two uncatalogued specimens—Judithian, MOR Locality TM-006, Two Medicine Formation, Teton County, Montana, U.S.A.

Cimexomys minor: UCMP 69232—Puercan, UCMP Locality V65127, Tullock Member, Fort Union Formation, McCone County, Montana, U.S.A.; UCMP 92666, 111614, 111615, 111617, 111618, 111619, 111629, 111631, 111632, 111633, 111637, 111638—Puercan, UCMP Locality V70201, Tullock Member, Fort Union Formation, McCone County, Montana, U.S.A.

***Cimexomys* sp.**: YPM-PU 14499—Puercan, Mantua Lentil, Polecat Bench Formation, Park County, Wyoming, U.S.A.

Cimexomys* sp. cf. *C. judithae: OMNH 22315—Judithian, OMNH Locality V5, Kaiparowits Formation, Kane County, Utah, U.S.A.; MNA V5312—Judithian, MNA Locality 704-1, Kaiparowits Formation, Kane County, Utah, U.S.A.

Cimolodon akersteni: IMNH 50879—lower Cenomanian, Idaho Museum of Natural History Locality 2167, Wayan Formation, Caribou County, Idaho, U.S.A.

Cimolodon electus: UA 5310—Aquilan, Locality UA-MR-4, upper Milk River Formation, Verdigris Coulee, County of Warner No. 5, Alberta, Canada.

Cimolodon foxi: OMNH 20483—Judithian, OMNH Locality V9, Kaiparowits Formation, Kane

County, Utah, U.S.A.

Cimolodon nitidus: UA 2333—Lancian, KUA-1 Locality, Scollard Formation, County of Stettler No. 6, Alberta, Canada; UCMP 116899, 116898, 185873—Lancian, UCMP Locality V73087, Hell Creek Formation, Garfield County, Montana, U.S.A.; UCMP 168716, 168716—Lancian, UCMP Locality V77130, Hell Creek Formation, Garfield County, Montana, U.S.A.; UCMP 50068, 51446—Lancian, UCMP Locality V5620, Lance Formation, Niobrara County, Wyoming, U.S.A.; UCMP 52109—Lancian, UCMP Locality V5815, Lance Formation, Niobrara County, Wyoming, U.S.A.; UCMP 52062—Lancian, UCMP Locality V5817, Lance Formation, Niobrara County, Wyoming, U.S.A.; UCMP 153586—Lancian, UCMP Locality V73078, Hell Creek Formation, Garfield County, Montana, U.S.A.; UCMP 116901—Lancian, UCMP Locality V73039, Hell Creek Formation, Garfield County, Montana, U.S.A.; UCMP 153509—Lancian, UCMP Locality V77132, Hell Creek Formation, Garfield County, Montana, U.S.A.; UCMP 187798—Lancian, UCMP Locality V99369, Garfield County, Montana, U.S.A.; UW 26213—Lancian, UW Locality V-92027, Hanna Basin, Ferris Formation, Carbon County, Wyoming, U.S.A.

Cimolodon similis: UMNH VP7592—Aquilan, UMNH Locality 77, Wahweap Formation, Kane County, Utah, U.S.A.; UA 5360—Aquilan, Locality UA-MR-6, upper Milk River Formation, Verdigris Coulee, County of Warner No. 5, Alberta, Canada.

Cimolodon **sp. cf.** ***C. foxi***: UMNH VP1782—Santonian, UMNH Locality 781, John Henry Member, Straight Cliffs Formation, Bryce Canyon National Park, Garfield County, Utah, U.S.A.

Cimolodon **sp. cf.** ***C. nitidus***: UMNH VP6915, VP5106—?lower Campanian, UMNH Locality 10, ?Wahweap Formation, Iron County, Utah, U.S.A.; UMNH VP7978—Aquilan, UMNH Locality 130, Wahweap Formation, Kane County, Utah, U.S.A.

Cimolodon* sp. cf. *C. similis: MNA V5863, V5881, V6030—upper Cenomanian, Paunsaugunt Plateau, middle member of the Naturita Formation, Kane County, Utah, U.S.A.; OMNH 20347, 22313—Judithian, OMNH Locality V5, Kaiparowits Formation, Kane County, Utah, U.S.A.; OMNH 20484—Judithian, OMNH Locality V9, Kaiparowits Formation, Kane County, Utah, U.S.A.; MNA V7532—Judithian, MNA Locality 704-1, Kaiparowits Formation, Kane County, Utah, U.S.A.

***Cimolodon* sp. (small)**: MNA V4525—Aquilan, MNA Locality 455-1, Wahweap Formation, Kane County, Utah, U.S.A.

Cimolodon wardi: UMNH VP14027—Aquilan, UMNH Locality 10, Wahweap Formation, Iron County, Utah, U.S.A.

Cimolomys gracilis: UCMP 45708, 51570—Lancian, UCMP Locality V5620, Lance Formation, Niobrara County, Wyoming, U.S.A.; UCMP 52107—Lancian, UCMP Locality V5815, Lance Formation, Niobrara County, Wyoming, U.S.A.; UCMP 187778—Lancian, UCMP Locality V99369, Hell Creek Formation, Garfield County, Montana, U.S.A.

Clemensodon megaloba: AMNH 57623, UCMP 47149—Lancian, UCMP Locality V5620, Lance Formation, Niobrara County, Wyoming, U.S.A.

Dakotamys malcomi: MNA V6056, V5874, UMNH VP12855, VP12854—upper Cenomanian, Paunsaugunt Plateau, middle member of the Naturita Formation, Kane County, Utah, U.S.A.

Ectypodus elaphus: UALVP 45994—Tiffanian, DW-2 Locality, Paskapoo Formation, Rocky View County, Alberta, Canada.

Ectypodus powelli: mean—Tiffanian, Princeton Quarry, Fort Union Formation, Park County, Wyoming, U.S.A.; UM 71783—Clarkforkian, UM Locality SC-188, Willwood Formation, Park County, Wyoming, U.S.A.; UM 69868—Clarkforkian, UM Locality SC-195, Willwood

Formation, Park County, Wyoming, U.S.A.

***Ectypodus* sp.**: UW 26211, 26212—Puercan, UW Locality V-92031, Ferris Formation, Hanna Basin, Ferris Formation, Carbon County, Wyoming, U.S.A.; UA 16099, 16100—Puercan, MHBT Quarry, Ravenscrag Formation, near Ravenscrag, Saskatchewan, Canada.; UM 84198, 84197—Tiffanian, Douglass Quarry, Fort Union Formation, Sweetgrass County, Montana, U.S.A.

Ectypodus* sp. cf. *E. childei: UCMP 44023—Wasatchian, UCMP Locality V5352, Hiawatha Member, Wasatch Formation, Moffat County, Colorado, U.S.A.

Ectypodus lovei: PTRM 10427—Chadronian, PTRM Locality V89002, ?Chadron Formation, Bowman County, North Dakota.

Ectypodus* sp. cf. *E. szalayi: UALVP 44073—Torrejonian, Who Nose? Locality, Paskapoo Formation, Rocky View County, Alberta, Canada.

Ectypodus sylviae: AMNH 100939—Torrejonian, Swain Quarry, Fort Union Formation, Carbon County, Wyoming, U.S.A.

Ectypodus szalayi: AMNH 35536—Torrejonian, Gidley Quarry, Fort Union Formation, Sweetgrass County, Montana, U.S.A.

Ectypodus tardus: UCMP 44041—Wasatchian, UCMP Locality V5348, Hiawatha Member, Wasatch Formation, Moffat County, Colorado, U.S.A.; UCMP 44004, 44010—Wasatchian, UCMP Locality V5357, Hiawatha Member, Wasatch Formation, Moffat County, Colorado, U.S.A.; UCMP 44007—Wasatchian, UCMP Locality V5352, Hiawatha Member, Wasatch Formation, Moffat County, Colorado, U.S.A.

Eucosmodon americanus: AMNH 3028—Puercan, 'upper Puerco beds', Nacimiento Formation, San Juan County, New Mexico, U.S.A.

Eucosmodon molestus: AMNH 3029—Torrejonian, 'Torrejon beds', Nacimiento Formation, San Juan County, New Mexico, U.S.A.

Eucosmodon primus: AMNH 16327—Puercan, 'lower Puerco beds', Nacimiento Formation, San Juan County, New Mexico, U.S.A.

Fractinus palmorum: UW 27063—Tiffanian, UW Locality V-90043, Hanna Formation, Carbon County, Wyoming, U.S.A.

Kimbetohia campi: AMNH 58392—Puercan, Betonnie Tsosie Wash, Nacimiento Formation, San Juan County, New Mexico, U.S.A.

?*Kimbetohia mziae*: UCM 34329, 34615, 34947, 35031, 35097, 35098, 38858, 38868, 39546—Puercan, UCM Locality 77267, Denver Formation, Arapahoe County, Colorado, U.S.A.

Krauseia clemensi: AMNH 87855, 87856, UMVP 6034, 6035—Torrejonian, Swain Quarry, Fort Union Formation, Carbon County, Wyoming, U.S.A.; KU 14032—Torrejonian, KU Locality 9, Nacimiento Formation, San Juan County, New Mexico, U.S.A.

Meniscoessus major: UA 15182—Judithian, Red Deer River Valley, Oldman Formation, County of Newell, Special Area No. 2, Alberta, Canada.

Meniscoessus robustus: UCMP 46875, 47132, 51507, 51508—Lancian, UCMP Locality V5620, Lance Formation, Niobrara County, Wyoming, U.S.A.; UCMP 107405— Lancian, UCMP Locality V73051, Hell Creek Formation, Garfield County, Montana, U.S.A.; YPM 10613—Lancian, Hatcher Collection, Lance Formation, Niobrara County, Wyoming, U.S.A.

Meniscoessus* sp. cf. *M. robustus: DMNH 52225—Lancian, DMNH Locality 3322, Laramie Formation, Weld County, Colorado, U.S.A.

Mesodma archibaldi: MNA V7533—Judithian, MNA Locality 704-1, Kaiparowits Formation, Kane County, Utah, U.S.A.).

Mesodma formosa: UCMP 46407, 47025, 45724, 45722, 45726, 45795, 46407, 47011, 47025, 47208—Lancian, UCMP Locality V5620, Lance Formation, Niobrara County, Wyoming, U.S.A.; UCMP 115931—Lancian, UCMP Locality V73087, Hell Creek Formation, Garfield County, Montana, U.S.A.; UCMP 187898—Lancian, UCMP Locality V99220, Hell Creek Formation, Garfield County, Montana, U.S.A.

Mesodma hensleighi: UCMP 115924, 115930, 115932, 185868—Lancian, UCMP Locality V73087, Hell Creek Formation, Garfield County, Montana, U.S.A.; UCMP 170839, 174209—Lancian, UCMP Locality V75162, Hell Creek Formation, Garfield County, Montana, U.S.A.; UCMP 153522—Lancian, UCMP Locality V84130, Hell Creek Formation, Garfield County, Montana, U.S.A.; UCMP 187723—Lancian, UCMP Locality V99230, Hell Creek Formation, Garfield County, Montana, U.S.A.; UCMP 45727, 47191, 47202, 51461, 51746, 51856—Lancian, UCMP Locality V5620, Lance Formation, Niobrara County, Wyoming, U.S.A.

Mesodma primaeva: AMNH 77121—Judithian, Clambank Hollow, Judith River Formation, Chouteau County, Montana, U.S.A.

Mesodma pygmaea: UALVP 44049—Torrejonian, Who Nose? Locality, Paskapoo Formation, Rocky View County, Alberta, Canada.; UM 84194, 84195—Tiffanian, Douglass Quarry, Fort Union Formation, Sweetgrass County, Montana, U.S.A.

Mesodma senecta: UA 5378—Aquilan, Locality UA-MR-4, upper Milk River Formation, Verdigris Coulee, County of Warner No. 5, Alberta, Canada.

?*Mesodma* sp.: OMNH 27563—lower Cenomanian, San Rafael Swell, Mussentuchit Member, Cedar Mountain Formation, Emery County, Utah, U.S.A.

Mesodma* sp. cf. *M. formosa: UCMP 150116, 150117, 150118, 150119, 150120, 150121, 150122, 150123, 150124—Puercan, UCMP Locality V65127, Tullock Member, Fort Union

Formation, McCone County, Montana, U.S.A.; UCMP 150108, 150109, 150110, 150111, 150112, 150113, 150114, 150115—Puercan, UCMP Locality V71203, Tullock Member, Fort Union Formation, McCone County, Montana, U.S.A.; UCMP 150102, 150103—Puercan, UCMP Locality V72210, Tullock Member, Fort Union Formation, Garfield County, Montana, U.S.A.; UCMP 116875, 116626, 116636, 150107—Puercan, UCMP Locality V74111, Tullock Member, Fort Union Formation, Garfield County, Montana, U.S.A.; UCMP 187532—Puercan, UCMP Locality V96268, Tullock Member, Fort Union Formation, Garfield County, Montana, U.S.A.

***Mesodma* sp. (large)**: UMNH VP7642—Judithian, UMNH Locality 24, Kaiparowits Formation, Kane County, Utah, U.S.A.

Mesodma* sp. cf. *M. thompsoni: UCMP 150079, 150085, 150086—Puercan, UCMP Locality V65127, Tullock Member, Fort Union Formation, McCone County, Montana, U.S.A.; UCMP 150087, 150088—Puercan, UCMP Locality V70199, Tullock Member, Fort Union Formation, McCone County, Montana, U.S.A.; UCMP 150089, 150090, 150091, 150092—Puercan, UCMP Locality V70201, Tullock Member, Fort Union Formation, McCone County, Montana, U.S.A.; UCMP 150093, 150094, 150095, 150096, 150097, 150098—Puercan, UCMP Locality V71203, Tullock Member, Fort Union Formation, McCone County, Montana, U.S.A.; UCMP 116622, 116635, 150099, 150100—Puercan, UCMP Locality V74111, Tullock Member, Fort Union Formation, Garfield County, Montana, U.S.A.; UCMP 150101—Puercan, UCMP Locality V77087, Tullock Member, Fort Union Formation, Garfield County, Montana, U.S.A.; UCMP 186794, 186796, 187512, 187529—Puercan, UCMP Locality V96268, Tullock Member, Fort Union Formation, Garfield County, Montana, U.S.A.

Mesodma thompsoni: UCMP 47217—Lancian, UCMP Locality V5620, Lance Formation,

Niobrara County, Wyoming, U.S.A.; UCMP 187559—Lancian, UCMP Locality V75178, Hell Creek Formation, Garfield County, Montana, U.S.A.; UCMP 108053—Lancian, UCMP Locality V72212, Hell Creek Formation, Garfield County, Montana, U.S.A.; UCMP 116604—Lancian, UCMP Locality V73087, Hell Creek Formation, Garfield County, Montana, U.S.A.; UCMP 116605—Lancian, UCMP Locality V74116, Hell Creek Formation, Garfield County, Montana, U.S.A.; UCMP 137546, 174275, 187559—Lancian, UCMP Locality V75178, Hell Creek Formation, Garfield County, Montana, U.S.A.; UCMP 153516, 168710, 168712—Lancian, UCMP Locality V77130, Hell Creek Formation, Garfield County, Montana, U.S.A.; UCMP 156129—Lancian, UCMP Locality V80092, Hell Creek Formation, Garfield County, Montana, U.S.A.

Microcosmodon arcuatus: mean—Puercan, MHBT Quarry, Ravenscrag Formation, near Ravenscrag, Saskatchewan, Canada.

Microcosmodon conus: UALVP 42831, 40690—Tiffanian, Gao Mine Locality, Paskapoo Formation, Rocky View County, Alberta, Canada; UM 71657—Tiffanian, UM Locality SC-187, Fort Union Formation, Park County, Wyoming, U.S.A.; UM 81702—Tiffanian, UM Locality SC-165, Fort Union Formation, Park County, Wyoming, U.S.A.

Microcosmodon harleyi: UCMP 144449—Puercan, UCMP Locality V75193, Tullock Member, Fort Union Formation, Garfield County, Montana, U.S.A.

Microcosmodon rosei: UM 72662—Clarkforkian, UM Locality SC-188, Willwood Formation, Park County, Wyoming, U.S.A.

Mimetodon silberlingi: UALVP 44066—Torrejonian, Who Nose? Locality, Paskapoo Formation, Rocky View County, Alberta, Canada.

Neoliotomus ultimus: AMNH 16103—Wasatchian, Pat O'Hara Creek, Willwood Formation,

Park County, Wyoming, U.S.A.

?*Neoplagiaulax burgessi*: UCMP 116893, 116894, 116895, 116896, 116897, 185870—Lancian, UCMP Locality V73087, Hell Creek Formation, Garfield County, Montana, U.S.A.

Neoplagiaulax cimolodontoides: UALVP 46201, 46196, 46197—Tiffanian, DW-2 Locality, Paskapoo Formation, Rocky View County, Alberta, Canada.

Neoplagiaulax donaldorum: UM 84178, 84184—Tiffanian, Douglass Quarry, Fort Union Formation, Sweetgrass County, Montana, U.S.A.

Neoplagiaulax hazeni: UM 73397, 73619, 77323, 85365, 86243, YPM-PU 14422—Tiffanian, Princeton Quarry, Fort Union Formation, Park County, Wyoming, U.S.A.

Neoplagiaulax hunteri: UM 84157, 84184—Tiffanian, Douglass Quarry, Fort Union Formation, Sweetgrass County, Montana, U.S.A.

Neoplagiaulax jepi: mean—Tiffanian, Cedar Point Quarry, Fort Union Formation, Park County, Wyoming, U.S.A.

Neoplagiaulax kremnus: mean—Puercan, MHBT Quarry, Ravenscrag Formation, near Ravenscrag, Saskatchewan, Canada.

Neoplagiaulax macintyrei: AMNH 58667—Puercan, Betonnie Tsosie Wash, Nacimiento Formation, San Juan County, New Mexico, U.S.A.

Neoplagiaulax paskapooensis: UALVP 46138, 46157—Tiffanian, DW-2 Locality, Paskapoo Formation, Rocky View County, Alberta, Canada.

Neoplagiaulax serrator: UALVP 46025, 46080, 46087—Tiffanian, DW-2 Locality, Paskapoo Formation, Rocky View County, Alberta, Canada.

Neoplagiaulax* sp. cf. *N. hunteri: AMNH 100963—Torrejonian, Swain Quarry, Fort Union Formation, Carbon County, Wyoming, U.S.A.

Nidimys occultus: MOR 2501, 2514—Edmontonian, MOR Locality 703, St. Mary River Formation, Glacier County, Montana, U.S.A.

Paracimexomys magister: UA 5390—Aquilan, Locality UA-MR-4, upper Milk River Formation, Verdigris Coulee, County of Warner No. 5, Alberta, Canada.

Parectypodus armstrongi: mean— Puercan, MHBT Quarry, Ravenscrag Formation, near Ravenscrag, Saskatchewan, Canada.

Parectypodus corystes: UALVP 40679, 44081—Torrejonian, Who Nose? Locality, Paskapoo Formation, Rocky View County, Alberta, Canada.

Parectypodus laytoni: YPM-PU 14464—Tiffanian, Princeton Quarry, Fort Union Formation, Park County, Wyoming, U.S.A.; UM 68290—Clarkforkian, UM Locality SC-143, Willwood Formation, Park County, Wyoming, U.S.A.

Parectypodus lunatus: AMNH 59648—Wasatchian, UCMP Locality V5357, Hiawatha Member, Wasatch Formation, Moffat County, Colorado, U.S.A.

Parectypodus sinclairi: TMP.2011.090.0130—Torrejonian, TMP Locality L2395, Paskapoo Formation, Rocky View County, Alberta, Canada.

***Parectypodus* sp.**: UA 15119—Puercan, MHBT Quarry, Ravenscrag Formation, near Ravenscrag, Saskatchewan, Canada.

Parectypodus vanvaleni: AMNH 58641—Puercan, Betonnie Tsosie Wash, Nacimiento Formation, San Juan County, New Mexico, U.S.A.

Paressonodon nelsoni: UWBM 90886—Lancian, DMNH Locality 3322, Laramie Formation, Weld County, Colorado, U.S.A.

Parikimys carpenter: DMNH 52224—Lancian, DMNH Locality 3322, Laramie Formation, Weld County, Colorado, U.S.A.

Pentacosmodon bowensis: UALVP 42806, 42805—Tiffanian, Cochrane 2 Locality, Paskapoo Formation, Rocky View County, Alberta, Canada.

Pentacosmodon pronus: MCZ 20066—Tiffanian, Jepsen Valley Quarry, Fort Union Formation, Park County, Wyoming, U.S.A.; YPM-PU 19027—Tiffanian, unknown locality, Fort Union Formation, Park County, Wyoming, U.S.A.; UALVP 42803—Tiffanian, Gao Mine Locality, Paskapoo Formation, Rocky View County, Alberta, Canada.

Prochetodon cavus: YPM-PU 19099—Tiffanian, unnamed locality, Fort Union Formation, Park County, Wyoming, U.S.A.

Prochetodon foxi: YPM-PU 21223—Tiffanian, Long Draw Quarry, Fort Union Formation, Carbon County, Bighorn Basin, Montana, U.S.A.

Prochetodon* sp. cf. *P. cavus: PU 14542—Clarkforkian, UM Locality SC-143, Willwood Formation, Park County, Wyoming, U.S.A.

Prochetodon* sp. cf. *P. foxi: UALVP 42977—Tiffanian, Gao Mine Locality, Paskapoo Formation, Rocky View County, Alberta, Canada.

Prochetodon speirsae: UALVP 45682, 45689, 45703, 45690—Tiffanian, Cochrane 2 Locality, Paskapoo Formation, Rocky View County, Alberta, Canada.

Prochetodon taxus: UM 71311—Clarkforkian, UM Locality SC-226, Willwood Formation, Park County, Wyoming, U.S.A.

Ptilodus gnomus: UALVP 45148, 18670—Tiffanian, Cochrane 2 Locality, Paskapoo Formation, Rocky View County, Alberta, Canada.

Ptilodus mediaevus: AMNH 3022a—Torrejonian, unknown locality, Nacimiento Formation, San Juan County, New Mexico, U.S.A.; AMNH 100497—Torrejonian, Swain Quarry, Fort Union Formation, Carbon County, Wyoming, U.S.A.

Ptilodus montanus: UALVP 44117, 44113—Torrejonian, Who Nose? Locality, Paskapoo Formation, Rocky View County, Alberta, Canada.

***Ptilodus* sp.**: UCM 41271—Clarkforkian, UCM Locality 78009, 'Plateau Valley beds', Mesa County, Colorado, U.S.A.

***Ptilodus* sp. 'T'**: UALVP 18620—Tiffanian, Cochrane 2 Locality, Paskapoo Formation, Rocky View County, Alberta, Canada.

***Ptilodus* '*titanus*'**: PU 14584—Tiffanian, Douglass Quarry, Fort Union Formation, Sweetgrass County, Montana, U.S.A.

Ptilodus tsosiensis: AMNH 59800— Torrejonian, Betonnie Tsosie Wash, Nacimiento Formation, San Juan County, New Mexico, U.S.A.

Ptilodus wyomingensis: TMP 2011.090.0001—Torrejonian, TMP Locality L2395, Paskapoo Formation, Rocky View County, Alberta, Canada.

Stygimys jepseni: USNM 9769—Torrejonian, Gidley Quarry, Fort Union Formation, Sweetgrass County, Montana, U.S.A.

Stygimys kuszmauli: UCMP 105416, 150080, 150081—Puercan, UCMP Locality V65127, Tullock Member, Fort Union Formation, McCone County, Montana, U.S.A.; UCMP 92525, 92526, 92527, 99078, 102147, 102226, 102574, 102885, 103098, 111686, 111687, 111689, 111690; 111691; 111692; 111693; 111694; 111695; 111696; 111697, 150077, 150078—Puercan, UCMP Locality V70201, Tullock Member, Fort Union Formation, McCone County, Montana, U.S.A.; UCMP 116920, 116921—Puercan, UCMP Locality V74111, Tullock Member, Fort Union Formation, Garfield County, Montana, U.S.A.; UCMP 134601—Puercan, UCMP Locality V87071, Tullock Member, Fort Union Formation, McCone County, Montana, U.S.A.; UCMP 145448, 145547—Puercan, UCMP Locality V96268, Tullock Member, Fort

Union Formation, Garfield County, Montana, U.S.A.

Taeniolabis lamberti: CCM 70-110—Puercan, UCMP Locality V76175, Ludlow Formation, Fallen County, Montana, U.S.A.

Valenopsalis joyneri: UCMP 73828—Puercan, UCMP Locality V65127, Tullock Member, Fort Union Formation, McCone County, Montana, U.S.A.

Xanclomys mcgrewi: AMNH 87587—Torrejonian, Swain Quarry, Fort Union Formation, Carbon County, Wyoming, U.S.A.

Xyronomys robinsoni: UCM 34975—Puercan, UCM Locality 77267, Denver Formation, Arapahoe County, Colorado, U.S.A.

***Xyronomys* sp.**: mean—Puercan, MHBT Quarry, Ravenscrag Formation, near Ravenscrag, Saskatchewan, Canada.

Xyronomys swainae: AMNH 87897—Torrejonian, Swain Quarry, Fort Union Formation, Carbon County, Wyoming, U.S.A.

2.11 APPENDIX II: SUPPLEMENTARY DATA

2.11.1 SUPPLEMENTARY DATA SD1

Table 2.11.1—Table of all p4 measurements and ratios used in this study. **L** = length, **H** = height, **L1** = length to the apogee of the p4 profile, **H1** = height of the first serration. Measurements were taken on either casts or actual specimens when possible using a Leica MZ9.5 binocular dissecting microscope and a custom measuring stage that has the capability of reading to 0.001 mm. When specimens were unavailable, measurements were either obtained from the published literature or captured in ImageJ. $^{=}$ = measurements taken from casts, * =

specimen measured in ImageJ using published scale for calibration, # = specimen measured in ImageJ using published tooth length for calibration, + = specimen measured from print version of publication using digital calipers, ^ = specimen measured in ImageJ from photograph taken with a scale bar.

Family	***Genus***	***species***	**Specimen**	**L**	**H**	**L1**	**H1**	**H:L**	**L1:L**	**H1:H**	**Age**	**Source**
"*Paracimexomys* group"	*Cedaromys*	*bestia*	OMNH 26636	4.08	2.22	2.27	1.49	0.54	0.56	0.67	mid-K	Weaver et al. 2019
"*Paracimexomys* group"	*Cedaromys*	*parvus*	OMNH 32987	3.5	1.86	2.06	1.19	0.53	0.59	0.64	mid-K	Weaver et al. 2019
"*Paracimexomys* group"	*Cedaromys*	*parvus*	OMNH 27497	3.95	2.07	2.06	1.43	0.52	0.52	0.69	mid-K	Eaton and Cifelli 2001*
"*Paracimexomys* group"	*Bryceomys*	*intermedius*	OMNH 34405	2.72	1.32	1.33	0.74	0.49	0.49	0.56	mid-K	Weaver et al. 2019
Cimolodontidae	*Cimolodon*	*akersteni*	IMNH 50879	3.32	1.86	1.51	1.16	0.56	0.45	0.62	mid-K	Weaver et al. 2019
?Neoplagiaulacidae	?*Mesodma*	sp.	OMNH 27563	2.48	0.92	1.08	0.51	0.37	0.44	0.55	mid-K	Eaton and Cifelli 2001*
"*Paracimexomys* group"	*Cedaromys*	*minimus*	UMNH VP12839	2.33	1.17	1.28	-	0.5	0.55	-	pre-Aquilan	Eaton 2009*
"*Paracimexomys* group"	*Dakotamys*	*malcomi*	MNA V6056	2.48	1.36	1.26	0.87	0.55	0.51	0.64	pre-Aquilan	Eaton 1995*

Family	*Genus*	*species*	Specimen	L	H	L1	H1	H:L	L1:L	H1:H	Age	Source
"*Paracimexomys* group"	*Dakotamys*	*malcomi*	MNA V5874	2.52	1.31	1.42	0.98	0.52	0.56	0.75	pre-Aquilan	Eaton 1995*
"*Paracimexomys* group"	cf. *Dakotamys*	*malcomi*	UMNH VP12855	2.13	1.1	1.22	0.56	0.52	0.57	0.5	pre-Aquilan	Weaver et al. 2019
"*Paracimexomys* group"	cf. *Dakotamys*	*malcomi*	UMNH VP12854	2.1	1.04	1.03	0.71	0.5	0.49	0.68	pre-Aquilan	Weaver et al. 2019
"*Paracimexomys* group"	*Bryceomys*	*fumosus*	MNA V5639	2.54	1.27	1.17	0.69	0.5	0.46	0.54	pre-Aquilan	Weaver et al. 2019
"*Paracimexomys* group"	*Bryceomys*	*fumosus*	MNA V7476	2.82	1.4	1.46	0.71	0.5	0.52	0.51	pre-Aquilan	Weaver et al. 2019
Cimolodontidae	*Cimolodon*	sp. cf. *C. similis*	MNA V5863	3.89	2.11	2.03	1.54	0.54	0.52	0.73	pre-Aquilan	Eaton 1995*
Cimolodontidae	*Cimolodon*	sp. cf. *C. similis*	MNA V5881	4.43	2.4	2.13	2.11	0.54	0.48	0.88	pre-Aquilan	Eaton 1995*
Cimolodontidae	*Cimolodon*	sp. cf. *C. similis*	MNA V6030	5.13	2.38	2.39	1.93	0.46	0.47	0.81	pre-Aquilan	Eaton 1995*
Cimolodontidae	*Cimolodon*	*similis*?	MNA V6030	5	2.42	2.36	1.71	0.48	0.47	0.71	pre-Aquilan	Weaver et al. 2019
Cimolodontidae	*Cimolodon*	sp. cf. *C. nitidus*	UMNH VP6915	5.12	2.87	2.66	1.99	0.56	0.52	0.69	pre-Aquilan	Eaton 2006*
Cimolodontidae	*Cimolodon*	sp. cf. *C. nitidus*	UMNH VP5106	5.97	3	2.99	2.12	0.5	0.5	0.71	pre-Aquilan	Eaton 2006*

Family	*Genus*	*species*	Specimen	L	H	L1	H1	H:L	L1:L	H1:H	Age	Source
Cimolodontidae	*Cimolodon*	sp. cf. *C. foxi*	UMNH VP17582	2.44	1.11	1.15	0.85	0.45	0.47	0.77	pre-Aquilan	Eaton 2013*
"*Paracimexomys* group"	*Paracimexomys*	*magister*	UA 5390	3.9	1.95	1.92	1.4	0.5	0.49	0.72	Aquilan	Fox 1971[#]
Cimolodontidae	*Cimolodon*	*wardi*	UMNH VP14027	3.52	1.82	1.9	1.14	0.52	0.54	0.63	Aquilan	Weaver et al. 2019
Cimolodontidae	*Cimolodon*	sp. cf. *C. nitidus*	UMNH VP7978	5.14	3.25	2.87	2.42	0.63	0.56	0.74	Aquilan	Weaver et al. 2019
Cimolodontidae	*Cimolodon*	*electus*	UA 5310	6.2	3.69	3.27	2.84	0.6	0.53	0.77	Aquilan	Fox 1971[#]
Cimolodontidae	*Cimolodon*	*similis*	UMNH VP7592	3.42	1.62	1.59	1.17	0.47	0.46	0.72	Aquilan	Eaton 2002*
Cimolodontidae	*Cimolodon*	*similis*	UA 5360	4.6	2.74	2.26	1.78	0.6	0.49	0.65	Aquilan	Fox 1971[#]
Cimolodontidae	*Cimolodon*	sp. (small)	MNA V4525	3.01	1.59	1.55	1.19	0.53	0.51	0.75	Aquilan	Eaton 2002*
Neoplagiaulacidae	*Mesodma*	*senecta*	UA 5378	4.6	2.11	2.12	1.58	0.46	0.46	0.75	Aquilan	Fox 1971[#]
Neoplagiaulacidae	*Mesodma*	*senecta*	mean	4.36	1.9	2.04	-	0.44	0.47	-	Aquilan	Novacek and Clemens 1977
"*Paracimexomys* group"	*Cimexomys*	cf. *judithae*	OMNH 22315	3.16	1.42	1.34	0.99	0.45	0.42	0.7	Judithian	Eaton 2002*
"*Paracimexomys* group"	*Cimexomys*	cf. *judithae*	MNA V5312	3.2	1.38	1.63	0.99	0.43	0.51	0.72	Judithian	Eaton 2002*
"*Paracimexomys* group"	*Cimexomys*	*judithae*	AMNH 77100	3	1.71	1.38	1.12	0.57	0.46	0.65	Judithian	Sahni 1972[#]
"*Paracimexomys* group"	*Cimexomys*	*judithae*	UCMP 131505	3.18	1.62	1.46	1.2	0.51	0.46	0.74	Judithian	Montellano 1992*

Family	*Genus*	*species*	Specimen	L	H	L1	H1	H:L	L1:L	H1:H	Age	Source
"*Paracimexomys* group"	*Cimexomys*	*judithae*	UCMP 131505	3.08	1.49	1.58	1.12	0.48	0.51	0.75	Judithian	This paper[=]
"*Paracimexomys* group"	*Cimexomys*	*judithae*	MOR 302	3.18	1.41	1.67	1.1	0.44	0.53	0.78	Judithian	This paper[=]
"*Paracimexomys* group"	*Cimexomys*	*judithae*	Uncataloged	3.58	1.55	1.86	1.1	0.43	0.52	0.71	Judithian	This paper
"*Paracimexomys* group"	*Cimexomys*	*judithae*	Uncataloged	2.89	1.22	1.53	0.82	0.42	0.53	0.67	Judithian	This paper
Cimolodontidae	*Cimolodon*	*foxi*	OMNH 20483	3.77	1.82	2.02	1.1	0.48	0.54	0.6	Judithian	Eaton 2002*
Cimolodontidae	*Cimolodon*	sp. cf. *C. similis*	OMNH 20347	4.3	-	2.19	-	-	0.51	-	Judithian	Eaton 2002
Cimolodontidae	*Cimolodon*	sp. cf. *C. similis*	OMNH 20484	4.04	2.11	2	-	0.52	0.5	-	Judithian	Eaton 2002*
Cimolodontidae	*Cimolodon*	sp. cf. *C. similis*	OMNH 22313	4.3	-	1.98	-	-	0.46	-	Judithian	Eaton 2002
Cimolodontidae	*Cimolodon*	sp. cf. *C. similis*	MNA V7532	4.26	-	2.34	-	-	0.55	-	Judithian	Eaton 2002
Neoplagiaulacidae	*Mesodma*	sp. (large)	UMNH VP7642	3.55	1.83	1.64	1.28	0.52	0.46	0.7	Judithian	This paper
Neoplagiaulacidae	*Mesodma*	*archibaldi*	MNA V7533	2.92	1.19	1.36	0.86	0.41	0.47	0.72	Judithian	Eaton 2002*
Neoplagiaulacidae	*Mesodma*	*primaeva*	AMNH 77121	4.77	2.48	2.29	1.51	0.52	0.48	0.61	Judithian	Sahni 1972[#]
Neoplagiaulacidae	*Mesodma*	*primaeva*	mean	4.74	1.99	2.37	-	0.42	0.5	-	Judithian	Novacek and Clemens 1977
Cimolomyidae	*Meniscoessus*	*major*	UA 15182	5.6	2.7	2.52	2.15	0.48	0.45	0.8	Judithian	Fox 1980[#]
Neoplagiaulacidae	*Nidimys*	*occultus*	MOR 2501 (L)	4.5	2.34	1.9	2.03	0.52	0.42	0.87	Edmontonian	Hunter et al. 2010

Family	*Genus*	*species*	Specimen	L	H	L1	H1	H:L	L1:L	H1:H	Age	Source
Neoplagiaulacidae	*Nidimys*	*occultus*	MOR 2501 (R)	4.5	2.31	2.08	2.03	0.51	0.46	0.88	Edmonton	Hunter et al. 2010
Neoplagiaulacidae	*Nidimys*	*occultus*	MOR 2514	4.55	2.27	2.32	1.92	0.5	0.51	0.85	Edmonton	Hunter et al. 2010
Cimolodontidae	*Cimolodon*	*nitidus*	UA 2333	6.82	3.48	3.52	2.77	0.51	0.52	0.8	Lancian	This paper[=]
Cimolodontidae	*Cimolodon*	*nitidus*	UCMP 116899	5.88	3.79	3.05	2.79	0.64	0.52	0.74	Lancian	Archibald 1982[+]
Cimolodontidae	*Cimolodon*	*nitidus*	UCMP 116898	5.22	2.88	2.66	-	0.55	0.51	-	Lancian	Archibald 1982
Cimolodontidae	*Cimolodon*	*nitidus*	UCMP 168716	5.2	2.95	2.57	2.09	0.56	0.49	0.71	Lancian	Weaver et al. 2019
Cimolodontidae	*Cimolodon*	*nitidus*	UCMP 50068	7.92	3.95	4.17	2.99	0.5	0.53	0.76	Lancian	Weaver et al. 2019
Cimolodontidae	*Cimolodon*	*nitidus*	UCMP 51446	5.97	2.74	3.12	1.4	0.46	0.52	0.51	Lancian	Weaver et al. 2019
Cimolodontidae	*Cimolodon*	*nitidus*	UCMP 52109	6.6	3.57	3.18	2.69	0.54	0.48	0.75	Lancian	Weaver et al. 2019
Cimolodontidae	*Cimolodon*	*nitidus*	UCMP 52062	6.13	3.31	2.95	2.64	0.54	0.48	0.8	Lancian	Weaver et al. 2019
Cimolodontidae	*Cimolodon*	*nitidus*	UCMP 153586	6.03	2.95	2.97	1.96	0.49	0.49	0.66	Lancian	Weaver et al. 2019
Cimolodontidae	*Cimolodon*	*nitidus*	UCMP 185873	5.08	2.69	2.54	1.92	0.53	0.5	0.71	Lancian	Weaver et al. 2019

Family	*Genus*	*species*	Specimen	L	H	L1	H1	H:L	L1:L	H1:H	Age	Source
Cimolodontidae	*Cimolodon*	*nitidus*	UCMP 116901	6.41	3.47	3.11	2.57	0.54	0.49	0.74	Lancian	Weaver et al. 2019
Cimolodontidae	*Cimolodon*	*nitidus*	UCMP 168716	6.76	3.62	3.38	2.81	0.54	0.5	0.78	Lancian	Weaver et al. 2019
Cimolodontidae	*Cimolodon*	*nitidus*	UCMP 153509	6.07	3.5	3.12	2.91	0.58	0.51	0.83	Lancian	Weaver et al. 2019
Cimolodontidae	*Cimolodon*	*nitidus*	UCMP 187798	8.06	4.12	4.07	3.11	0.51	0.5	0.75	Lancian	Weaver et al. 2019
Cimolodontidae	*Cimolodon*	*nitidus*	UW 26213	5.55	3.16	3.06	-	0.57	0.55	-	Lancian	Eberle and Lillegraven 1998
Neoplagiaulacidae	*Mesodma*	*hensleighi*	UCMP 115924	2.82	1.32	1.39	-	0.47	0.49	-	Lancian	J. D. Archibald notes
Neoplagiaulacidae	*Mesodma*	*hensleighi*	UCMP 115932	2.89	1.39	1.3	-	0.48	0.45	-	Lancian	J. D. Archibald notes
Neoplagiaulacidae	*Mesodma*	*hensleighi*	UCMP 45727	3.74	1.83	1.81	1.18	0.49	0.48	0.64	Lancian	This paper^
Neoplagiaulacidae	*Mesodma*	*hensleighi*	UCMP 47191	3.5	1.44	1.74	1.06	0.41	0.5	0.74	Lancian	This paper^
Neoplagiaulacidae	*Mesodma*	*hensleighi*	UCMP 47202	3.31	1.6	1.59	0.96	0.48	0.48	0.6	Lancian	This paper^
Neoplagiaulacidae	*Mesodma*	*hensleighi*	UCMP 51461	3.51	1.56	1.52	0.98	0.44	0.43	0.63	Lancian	This paper^
Neoplagiaulacidae	*Mesodma*	*hensleighi*	UCMP 51746	3.66	1.77	1.47	1.13	0.48	0.4	0.64	Lancian	This paper^

Family	*Genus*	*species*	Specimen	L	H	L1	H1	H:L	L1:L	H1:H	Age	Source
Neoplagiaulacidae	*Mesodma*	*hensleighi*	UCMP 51856	3.77	1.86	1.74	1.25	0.49	0.46	0.67	Lancian	This paper^
Neoplagiaulacidae	*Mesodma*	*hensleighi*	UCMP 115930	3.3	1.6	1.57	1.04	0.48	0.48	0.65	Lancian	This paper^
Neoplagiaulacidae	*Mesodma*	*hensleighi*	UCMP 185868	3.5	1.53	1.68	1.01	0.44	0.48	0.66	Lancian	This paper^
Neoplagiaulacidae	*Mesodma*	*hensleighi*	UCMP 170839	3.21	1.59	1.48	1	0.49	0.46	0.63	Lancian	This paper^
Neoplagiaulacidae	*Mesodma*	*hensleighi*	UCMP 174209	3.47	1.75	1.65	1.14	0.5	0.48	0.65	Lancian	This paper^
Neoplagiaulacidae	*Mesodma*	*hensleighi*	UCMP 153522	3.65	1.64	1.64	1.21	0.45	0.45	0.74	Lancian	This paper^
Neoplagiaulacidae	*Mesodma*	*hensleighi*	UCMP 187723	3.16	1.4	1.31	0.96	0.44	0.41	0.69	Lancian	This paper^
Neoplagiaulacidae	*Mesodma*	sp. cf. *M. hensleighi*	UCMP 150084	3.62	1.85	1.48	1.07	0.51	0.41	0.58	Lancian	This paper^
Neoplagiaulacidae	*Mesodma*	*formosa*	UCMP 46407	3.31	1.49	1.6	0.82	0.45	0.48	0.55	Lancian	This paper=
Neoplagiaulacidae	*Mesodma*	*formosa*	UCMP 47025	3.4	1.35	1.68	0.64	0.4	0.49	0.47	Lancian	This paper=
Neoplagiaulacidae	*Mesodma*	*formosa*	UCMP 45724	3.37	1.38	1.64	0.89	0.41	0.49	0.64	Lancian	This paper=
Neoplagiaulacidae	*Mesodma*	*formosa*	UCMP 45722	4.24	2.08	2.01	1.35	0.49	0.47	0.65	Lancian	This paper^
Neoplagiaulacidae	*Mesodma*	*formosa*	UCMP 45726	4.4	1.97	2.11	1.52	0.45	0.48	0.77	Lancian	This paper^
Neoplagiaulacidae	*Mesodma*	*formosa*	UCMP 45795	4.08	2.03	2.01	1.51	0.5	0.49	0.74	Lancian	This paper^
Neoplagiaulacidae	*Mesodma*	*formosa*	UCMP 46407	4.25	2.18	1.8	1.62	0.51	0.42	0.74	Lancian	This paper^
Neoplagiaulacidae	*Mesodma*	*formosa*	UCMP 47011	4.19	2.13	1.93	1.57	0.51	0.46	0.74	Lancian	This paper^

Family	*Genus*	*species*	Specimen	L	H	L1	H1	H:L	L1:L	H1:H	Age	Source
Neoplagiaulacidae	*Mesodma*	*formosa*	UCMP 47025	4.21	1.94	1.89	1.42	0.46	0.45	0.73	Lancian	This paper^
Neoplagiaulacidae	*Mesodma*	*formosa*	UCMP 47208	4.16	2.09	2.05	1.31	0.5	0.49	0.63	Lancian	This paper^
Neoplagiaulacidae	*Mesodma*	*formosa*	UCMP 115931	3.74	1.69	1.78	1.09	0.45	0.48	0.64	Lancian	This paper^
Neoplagiaulacidae	*Mesodma*	*formosa*	UCMP 187898	4.19	2.19	1.87	1.4	0.52	0.45	0.64	Lancian	This paper^
Neoplagiaulacidae	*Mesodma*	sp. cf. *M. formosa*	UCMP 115931	3.09	1.44	1.29	-	0.47	0.42	-	Lancian	Archibald 1982
Neoplagiaulacidae	*Mesodma*	*thompsoni*	UCMP 47217	4	1.6	1.88	1	0.4	0.47	0.625	Lancian	This paper=
Neoplagiaulacidae	*Mesodma*	*thompsoni*	UCMP 187559	4.5	1.98	2.12	1.1	0.44	0.47	0.56	Lancian	This paper=
Neoplagiaulacidae	*Mesodma*	*thompsoni*	UCMP 108053	5.49	2.58	2.31	1.9	0.47	0.42	0.74	Lancian	This paper^
Neoplagiaulacidae	*Mesodma*	*thompsoni*	UCMP 116604	5.69	2.53	2.69	2.02	0.44	0.47	0.8	Lancian	This paper^
Neoplagiaulacidae	*Mesodma*	*thompsoni*	UCMP 116605	5.71	2.53	2.37	2.11	0.44	0.42	0.8	Lancian	This paper^
Neoplagiaulacidae	*Mesodma*	*thompsoni*	UCMP 137546	5.05	2.27	2.53	1.68	0.45	0.5	0.74	Lancian	This paper^
Neoplagiaulacidae	*Mesodma*	*thompsoni*	UCMP 174275	5.25	2.47	2.31	1.68	0.47	0.44	0.68	Lancian	This paper^
Neoplagiaulacidae	*Mesodma*	*thompsoni*	UCMP 187559	5.55	2.65	2.39	1.76	0.48	0.43	0.66	Lancian	This paper^
Neoplagiaulacidae	*Mesodma*	*thompsoni*	UCMP 153516	5.51	2.52	2.36	1.61	0.46	0.43	0.64	Lancian	This paper^
Neoplagiaulacidae	*Mesodma*	*thompsoni*	UCMP 168710	5.5	2.48	2.51	1.76	0.45	0.46	0.71	Lancian	This paper^
Neoplagiaulacidae	*Mesodma*	*thompsoni*	UCMP 168712	5.57	2.53	2.54	1.74	0.45	0.46	0.69	Lancian	This paper^

Family	*Genus*	*species*	Specimen	L	H	L1	H1	H:L	L1:L	H1:H	Age	Source
Neoplagiaulacidae	*Mesodma*	*thompsoni*	UCMP 156129	5.11	2.31	2.11	1.72	0.45	0.41	0.74	Lancian	This paper^
Neoplagiaulacidae	?*Neoplagiaulax*	*burgessi*	UCMP 116893	4.87	2.3	2.74	1.81	0.47	0.56	0.79	Lancian	This paper^
Neoplagiaulacidae	?*Neoplagiaulax*	*burgessi*	UCMP 116894	4.43	2.18	2.49	1.75	0.49	0.56	0.8	Lancian	This paper^
Neoplagiaulacidae	?*Neoplagiaulax*	*burgessi*	UCMP 116895	4.52	2.22	2.5	1.64	0.49	0.55	0.74	Lancian	This paper^
Neoplagiaulacidae	?*Neoplagiaulax*	*burgessi*	UCMP 116896	4.55	2.2	2.39	1.76	0.48	0.53	0.8	Lancian	This paper^
Neoplagiaulacidae	?*Neoplagiaulax*	*burgessi*	UCMP 116897	4.57	2.18	2.36	1.52	0.48	0.52	0.7	Lancian	This paper^
Neoplagiaulacidae	?*Neoplagiaulax*	*burgessi*	UCMP 185870	4.62	2.18	2.39	1.61	0.47	0.52	0.74	Lancian	This paper^
Neoplagiaulacidae	*Parikimys*	*carpenteri*	DMNH 52224	3.96	1.83	1.88	1.26	0.46	0.47	0.69	Lancian	Wilson et al. 2010
Cimolomyidae	*Cimolomys*	*gracilis*	UCMP 45708	5.67	2.6	3	1.9	0.46	0.53	0.73	Lancian	This paper^
Cimolomyidae	*Cimolomys*	*gracilis*	UCMP 51570	5.63	2.71	2.63	1.79	0.48	0.47	0.66	Lancian	This paper^
Cimolomyidae	*Cimolomys*	*gracilis*	UCMP 187778	5.75	2.82	2.75	2.25	0.49	0.48	0.8	Lancian	This paper^
Cimolomyidae	*Cimolomys*	*gracilis*	UCMP 52107	5.35	2.66	2.66	2.15	0.5	0.5	0.81	Lancian	This paper^
Cimolomyidae	*Meniscoessus*	*robustus*	YPM 10613	6.47	3.99	3.05	-	0.62	0.47	-	Lancian	Archibald 1982
Cimolomyidae	*Meniscoessus*	*robustus*	AMNH 14414	7.02	4.63	2.9	-	0.66	0.41	-	Lancian	J. D. Archibald notes
Cimolomyidae	*Meniscoessus*	*robustus*	UCMP 46875	6.31	3.97	2.89	3.14	0.63	0.46	0.79	Lancian	This paper^
Cimolomyidae	*Meniscoessus*	*robustus*	UCMP 47132	8.24	4.02	3.96	2.31	0.49	0.48	0.57	Lancian	This paper^

Family	*Genus*	*species*	Specimen	L	H	L1	H1	H:L	L1:L	H1:H	Age	Source
Cimolomyidae	*Meniscoessus*	*robustus*	UCMP 51507	7.66	5	3.87	3.57	0.65	0.51	0.71	Lancian	This paper^
Cimolomyidae	*Meniscoessus*	*robustus*	UCMP 51508	7.66	5.03	3.73	3.42	0.66	0.49	0.68	Lancian	This paper^
Cimolomyidae	*Meniscoessus*	*robustus*	UCMP 107405	7.56	4.89	3.63	3.54	0.65	0.48	0.72	Lancian	This paper^
Cimolomyidae	*Meniscoessus*	sp. cf. *M robustus*	DMNH 52225	5.67	2.46	2.71	1.5	0.43	0.48	0.61	Lancian	Wilson et al. 2010
Cimolomyidae	*Paressonodon*	*nelsoni*	UWBM 90886	5.07	2.63	2.13	1.64	0.52	0.42	0.62	Lancian	This paper^
Eucosmodontidae	*Clemensodon*	*megaloba*	AMNH 57623	6.03	2.61	2.39	2.16	0.43	0.4	0.83	Lancian	Krause 1992*
Eucosmodontidae	*Clemensodon*	*megaloba*	UCMP 47149	5.5	2.33	2.69	1.89	0.42	0.49	0.81	Lancian	Krause 1992*
"*Paracimexomys* group"	*Cimexomys*	*minor*	UCMP 69232	2.74	1.26	1.39	0.79	0.46	0.51	0.63	Puercan	This paper^
"*Paracimexomys* group"	*Cimexomys*	*minor*	UCMP 92666	2.95	1.57	1.41	1.05	0.53	0.48	0.67	Puercan	This paper^
"*Paracimexomys* group"	*Cimexomys*	*minor*	UCMP 111614	3.26	1.58	1.56	0.83	0.48	0.48	0.53	Puercan	This paper^
"*Paracimexomys* group"	*Cimexomys*	*minor*	UCMP 111615	3.4	1.83	1.78	1.13	0.54	0.52	0.62	Puercan	This paper^
"*Paracimexomys* group"	*Cimexomys*	*minor*	UCMP 111617	3.3	1.77	1.72	1.17	0.54	0.52	0.66	Puercan	This paper^
"*Paracimexomys* group"	*Cimexomys*	*minor*	UCMP 111618	3.41	1.79	1.69	1.14	0.52	0.5	0.64	Puercan	This paper^
"*Paracimexomys* group"	*Cimexomys*	*minor*	UCMP 111619	3.38	1.73	1.67	1.17	0.51	0.49	0.68	Puercan	This paper^
"*Paracimexomys* group"	*Cimexomys*	*minor*	UCMP 111629	3.23	1.73	1.59	1.05	0.54	0.49	0.61	Puercan	This paper^
"*Paracimexomys* group"	*Cimexomys*	*minor*	UCMP 111631	3.78	1.72	2.16	1.29	0.46	0.57	0.75	Puercan	This paper^

Family	*Genus*	*species*	Specimen	L	H	L1	H1	H:L	L1:L	H1:H	Age	Source
"*Paracimexomys* group"	*Cimexomys*	*minor*	UCMP 111632	3.45	1.86	1.8	1.23	0.54	0.52	0.66	Puercan	This paper^
"*Paracimexomys* group"	*Cimexomys*	*minor*	UCMP 111633	3.27	1.58	1.57	1.01	0.48	0.48	0.64	Puercan	This paper^
"*Paracimexomys* group"	*Cimexomys*	*minor*	UCMP 111637	3.53	1.87	1.86	1.13	0.53	0.53	0.6	Puercan	This paper^
"*Paracimexomys* group"	*Cimexomys*	*minor*	UCMP 111638	3.12	1.58	1.57	1.03	0.51	0.5	0.65	Puercan	This paper^
"*Paracimexomys* group"	*Cimexomys*	*minor*	UCMP 116984	3.34	1.68	1.72	1.21	0.5	0.51	0.72	Puercan	This paper^
"*Paracimexomys* group"	*Cimexomys*	*gratus*	UCMP 133835	3.49	1.74	1.6	1.31	0.5	0.46	0.75	Puercan	This paper^
"*Paracimexomys* group"	*Cimexomys*	*gratus*	UCMP 150082	4.98	2.47	2.57	1.28	0.5	0.52	0.52	Puercan	This paper^
"*Paracimexomys* group"	*Cimexomys*	*gratus*	UCMP 117000	4.24	2.01	2.19	-	0.47	0.52	-	Puercan	Archibald 1982
"*Paracimexomys* group"	*Cimexomys*	*gratus*	UCMP 133835	3.62	1.74	1.69	1.31	0.48	0.47	0.75	Puercan	This paper=
"*Paracimexomys* group"	*Cimexomys*	sp.	YPM-PU 14499	4.15	2.19	2.07	-	0.53	0.5	-	Puercan	Middleton and Dewar 2004
"*Paracimexomys* group"	*Cimexomys*	*arapahoensis*	UCM 34938	4.4	2.11	2.28	-	0.48	0.52	-	Puercan	Middleton and Dewar 2004
Neoplagiaulacidae	*Mesodma*	*formosa*	mean	3.18	1.63	1.43	-	0.51	0.45	-	Puercan	Johnston and Fox 1984
Neoplagiaulacidae	*Mesodma*	sp. cf. *M. formosa*	UCMP 150116	4.42	2.18	2.11	1.4	0.49	0.48	0.64	Puercan	This paper^
Neoplagiaulacidae	*Mesodma*	sp. cf. *M. formosa*	UCMP 150117	4.47	2.11	2.2	1.65	0.47	0.49	0.78	Puercan	This paper^

Family	*Genus*	*species*	Specimen	L	H	L1	H1	H:L	L1:L	H1:H	Age	Source
Neoplagiaulacid	*Mesodma*	sp. cf. *M.*	UCMP	4.72	2.15	2.18	1.63	0.46	0.46	0.76	Puerca	This
ae		*formosa*	150118								n	paper^
Neoplagiaulacid	*Mesodma*	sp. cf. *M.*	UCMP	4.46	2.18	2.15	1.43	0.49	0.48	0.66	Puerca	This
ae		*formosa*	150119								n	paper^
Neoplagiaulacid	*Mesodma*	sp. cf. *M.*	UCMP	4.37	2.25	2.01	1.64	0.51	0.46	0.73	Puerca	This
ae		*formosa*	150120								n	paper^
Neoplagiaulacid	*Mesodma*	sp. cf. *M.*	UCMP	4.53	2.11	2.34	1.45	0.47	0.52	0.69	Puerca	This
ae		*formosa*	150121								n	paper^
Neoplagiaulacid	*Mesodma*	sp. cf. *M.*	UCMP	4.5	2.01	2.14	1.43	0.45	0.48	0.71	Puerca	This
ae		*formosa*	150122								n	paper^
Neoplagiaulacid	*Mesodma*	sp. cf. *M.*	UCMP	4.5	2.12	2.15	1.61	0.47	0.48	0.76	Puerca	This
ae		*formosa*	150123								n	paper^
Neoplagiaulacid	*Mesodma*	sp. cf. *M.*	UCMP	4.45	2.23	2.02	1.46	0.5	0.45	0.65	Puerca	This
ae		*formosa*	150124								n	paper^
Neoplagiaulacid	*Mesodma*	sp. cf. *M.*	UCMP	4.43	2.18	1.91	1.69	0.49	0.43	0.78	Puerca	This
ae		*formosa*	150108								n	paper^
Neoplagiaulacid	*Mesodma*	sp. cf. *M.*	UCMP	4.29	2.08	2.04	1.34	0.48	0.48	0.64	Puerca	This
ae		*formosa*	150109								n	paper^
Neoplagiaulacid	*Mesodma*	sp. cf. *M.*	UCMP	4.28	2.09	2.04	1.46	0.49	0.48	0.7	Puerca	This
ae		*formosa*	150110								n	paper^
Neoplagiaulacid	*Mesodma*	sp. cf. *M.*	UCMP	4.32	2.27	1.71	1.64	0.53	0.4	0.72	Puerca	This
ae		*formosa*	150111								n	paper^
Neoplagiaulacid	*Mesodma*	sp. cf. *M.*	UCMP	4.53	2.27	1.96	1.45	0.5	0.43	0.64	Puerca	This
ae		*formosa*	150112								n	paper^
Neoplagiaulacid	*Mesodma*	sp. cf. *M.*	UCMP	4.38	2.19	1.62	1.44	0.5	0.37	0.66	Puerca	This
ae		*formosa*	150113								n	paper^
Neoplagiaulacid	*Mesodma*	sp. cf. *M.*	UCMP	4.24	2.2	1.97	1.37	0.52	0.46	0.62	Puerca	This
ae		*formosa*	150114								n	paper^
Neoplagiaulacid	*Mesodma*	sp. cf. *M.*	UCMP	4.6	2.27	2.18	1.45	0.49	0.47	0.64	Puerca	This
ae		*formosa*	150115								n	paper^
Neoplagiaulacid	*Mesodma*	sp. cf. *M.*	UCMP	4.56	2.23	2.38	1.59	0.49	0.52	0.71	Puerca	This
ae		*formosa*	150102								n	paper^

Family	*Genus*	*species*	Specimen	L	H	L1	H1	H:L	L1:L	H1:H	Age	Source
Neoplagiaulacidae	*Mesodma*	sp. cf. *M. formosa*	UCMP 150103	4.57	2.24	2.22	1.41	0.49	0.49	0.63	Puercan	This paper^
Neoplagiaulacidae	*Mesodma*	sp. cf. *M. formosa*	UCMP 116875	4.52	2.29	1.77	1.5	0.51	0.39	0.66	Puercan	This paper^
Neoplagiaulacidae	*Mesodma*	sp. cf. *M. formosa*	UCMP 116626	4.6	2.16	1.66	1.61	0.47	0.36	0.75	Puercan	This paper^
Neoplagiaulacidae	*Mesodma*	sp. cf. *M. formosa*	UCMP 116636	4.9	2.31	2.77	1.83	0.47	0.57	0.79	Puercan	This paper^
Neoplagiaulacidae	*Mesodma*	sp. cf. *M. formosa*	UCMP 150106	4.71	2.31	2.26	1.47	0.49	0.48	0.64	Puercan	This paper^
Neoplagiaulacidae	*Mesodma*	sp. cf. *M. formosa*	UCMP 150107	4.49	2.27	1.94	1.52	0.51	0.43	0.67	Puercan	This paper^
Neoplagiaulacidae	*Mesodma*	sp. cf. *M. formosa*	UCMP 187532	4.25	2.07	1.9	1.23	0.49	0.45	0.59	Puercan	This paper^
Neoplagiaulacidae	*Mesodma*	*thompsoni*	mean	3.93	2.03	1.88	-	0.52	0.48	-	Puercan	Johnston and Fox 1984
Neoplagiaulacidae	*Mesodma*	sp. cf. *M. thompsoni*	UCMP 150079	5.18	2.3	2.22	1.38	0.44	0.43	0.6	Puercan	This paper^
Neoplagiaulacidae	*Mesodma*	sp. cf. *M. thompsoni*	UCMP 150085	5.44	2.59	2.61	1.64	0.48	0.48	0.63	Puercan	This paper^
Neoplagiaulacidae	*Mesodma*	sp. cf. *M. thompsoni*	UCMP 150086	5.37	2.53	2.44	1.81	0.47	0.45	0.72	Puercan	This paper^
Neoplagiaulacidae	*Mesodma*	sp. cf. *M. thompsoni*	UCMP 150087	4.72	2.23	2.11	1.37	0.47	0.45	0.61	Puercan	This paper^
Neoplagiaulacidae	*Mesodma*	sp. cf. *M. thompsoni*	UCMP 150088	4.92	2.22	1.82	1.43	0.45	0.37	0.64	Puercan	This paper^

Family	*Genus*	*species*	Specimen	L	H	L1	H1	H:L	L1:L	H1:H	Age	Source
Neoplagiaulacidae	*Mesodma*	sp. cf. *M. thompsoni*	UCMP 150089	5.44	2.43	2.41	1.72	0.45	0.44	0.71	Puercan	This paper^
Neoplagiaulacidae	*Mesodma*	sp. cf. *M. thompsoni*	UCMP 150090	5.19	2.56	2.16	1.68	0.49	0.42	0.66	Puercan	This paper^
Neoplagiaulacidae	*Mesodma*	sp. cf. *M. thompsoni*	UCMP 150091	4.71	2.28	2.06	1.69	0.48	0.44	0.74	Puercan	This paper^
Neoplagiaulacidae	*Mesodma*	sp. cf. *M. thompsoni*	UCMP 150092	5.21	2.52	2.33	1.63	0.48	0.45	0.65	Puercan	This paper^
Neoplagiaulacidae	*Mesodma*	sp. cf. *M. thompsoni*	UCMP 150093	5.62	2.47	2.82	1.64	0.44	0.5	0.66	Puercan	This paper^
Neoplagiaulacidae	*Mesodma*	sp. cf. *M. thompsoni*	UCMP 150094	4.71	2.36	2.14	1.47	0.5	0.45	0.62	Puercan	This paper^
Neoplagiaulacidae	*Mesodma*	sp. cf. *M. thompsoni*	UCMP 150095	4.75	2.36	2	1.56	0.5	0.42	0.66	Puercan	This paper^
Neoplagiaulacidae	*Mesodma*	sp. cf. *M. thompsoni*	UCMP 150096	5	2.19	1.97	1.47	0.44	0.39	0.67	Puercan	This paper^
Neoplagiaulacidae	*Mesodma*	sp. cf. *M. thompsoni*	UCMP 150097	5.08	2.4	2.51	1.51	0.47	0.49	0.63	Puercan	This paper^
Neoplagiaulacidae	*Mesodma*	sp. cf. *M. thompsoni*	UCMP 150098	4.83	2.27	2.29	1.53	0.47	0.47	0.67	Puercan	This paper^
Neoplagiaulacidae	*Mesodma*	sp. cf. *M. thompsoni*	UCMP 116622	5.76	2.44	2.94	1.66	0.42	0.51	0.68	Puercan	This paper^

Family	*Genus*	*species*	Specimen	L	H	L1	H1	H:L	L1:L	H1:H	Age	Source
Neoplagiaulacidae	*Mesodma*	sp. cf. *M. thompsoni*	UCMP 116635	5.21	2.23	2.44	1.85	0.43	0.47	0.83	Puercan	This paper^
Neoplagiaulacidae	*Mesodma*	sp. cf. *M. thompsoni*	UCMP 150099	5.03	2.43	2.1	1.62	0.48	0.42	0.67	Puercan	This paper^
Neoplagiaulacidae	*Mesodma*	sp. cf. *M. thompsoni*	UCMP 150100	4.83	2.25	2.08	1.33	0.47	0.43	0.59	Puercan	This paper^
Neoplagiaulacidae	*Mesodma*	sp. cf. *M. thompsoni*	UCMP 150101	5.41	2.52	2.57	1.93	0.47	0.48	0.77	Puercan	This paper^
Neoplagiaulacidae	*Mesodma*	sp. cf. *M. thompsoni*	UCMP 186794	5.25	2.32	2.51	1.48	0.44	0.48	0.64	Puercan	This paper^
Neoplagiaulacidae	*Mesodma*	sp. cf. *M. thompsoni*	UCMP 186796	5.08	2.18	2.33	1.52	0.43	0.46	0.7	Puercan	This paper^
Neoplagiaulacidae	*Mesodma*	sp. cf. *M. thompsoni*	UCMP 187512	5.2	2.57	2.52	1.66	0.49	0.48	0.65	Puercan	This paper^
Neoplagiaulacidae	*Mesodma*	sp. cf. *M. thompsoni*	UCMP 187529	5.47	2.6	2.5	1.72	0.48	0.46	0.66	Puercan	This paper^
Neoplagiaulacidae	*Neoplagiaulax*	*kremnus*	mean	4.65	2.46	2.29	-	0.53	0.49	-	Puercan	Johnston and Fox 1984
Neoplagiaulacidae	*Neoplagiaulax*	*macintyrei*	AMNH 58667	3.78	1.63	2.02	1.22	0.43	0.53	0.75	Puercan	Sloan 1981[+]
Neoplagiaulacidae	*Ectypodus*	sp.	UW 26211	4.71	2.34	2.14	1.26	0.5	0.45	0.54	Puercan	Eberle and Lillegraven 1998

Family	*Genus*	*species*	Specimen	L	H	L1	H1	H:L	L1:L	H1:H	Age	Source
Neoplagiaulacidae	*Ectypodus*	sp.	UW 26212	4.6	2.6	2.22	1.79	0.57	0.48	0.69	Puercan	Eberle and Lillegraven 1998
Neoplagiaulacidae	*Ectypodus*	sp.	UA 16099	3	1.7	1.4	1.35	0.57	0.47	0.79	Puercan	Johnston and Fox 1984
Neoplagiaulacidae	*Ectypodus*	sp.	UA 16100	3.25	1.8	1.5	-	0.55	0.46	-	Puercan	Johnston and Fox 1984
Neoplagiaulacidae	*Xyronomys*	*robinsoni*	UCM 34975	3.2	1.32	1.67	0.73	0.41	0.52	0.55	Puercan	This paper
Neoplagiaulacidae	*Xyronomys*	sp.	mean	2.98	1.3	1.15	-	0.44	0.39	-	Puercan	Johnston and Fox 1984
Neoplagiaulacidae	*Parectypodus*	*armstrongi*	mean	4.71	2.6	2.17	-	0.55	0.46	-	Puercan	Johnston and Fox 1984
Neoplagiaulacidae	*Parectypodus*	sp.	UA 15119	3.9	2.2	1.5	-	0.56	0.38	-	Puercan	Johnston and Fox 1984
Neoplagiaulacidae	*Parectypodus*	*vanvaleni*	AMNH 58641	3.95	1.94	2.02	1.71	0.49	0.51	0.88	Puercan	Sloan 1981[+]
Ptilodontidae	?*Kimbetohia*	*mziae*	UCM 34329	4.84	2.4	2.5	-	0.5	0.52	-	Puercan	Middleton and Dewar 2004
Ptilodontidae	?*Kimbetohia*	*mziae*	UCM 34615	5.19	2.5	2.61	-	0.48	0.5	-	Puercan	Middleton and Dewar 2004
Ptilodontidae	?*Kimbetohia*	*mziae*	UCM 34947	4.84	2.31	2.51	-	0.48	0.52	-	Puercan	Middleton and

Family	*Genus*	*species*	Specimen	L	H	L1	H1	H:L	L1:L	H1:H	Age	Source
												Dewar 2004
Ptilodontidae	?*Kimbetohia*	*mziae*	UCM 35031	4.96	2.51	2.4	-	0.51	0.48	-	Puercan	Middleton and Dewar 2004
Ptilodontidae	?*Kimbetohia*	*mziae*	UCM 35097	4.84	2.26	2.44	-	0.47	0.5	-	Puercan	Middleton and Dewar 2004
Ptilodontidae	?*Kimbetohia*	*mziae*	UCM 35098	4.78	2.4	2.43	-	0.5	0.51	-	Puercan	Middleton and Dewar 2004
Ptilodontidae	*Kimbetohia*	*mziae*	UCM 38858	5.22	2.33	2.75	1.65	0.45	0.53	0.71	Puercan	This paper[=]
Ptilodontidae	?*Kimbetohia*	*mziae*	UCM 38868	4.96	2.48	2.53	-	0.5	0.51	-	Puercan	Middleton and Dewar 2004
Ptilodontidae	?*Kimbetohia*	*mziae*	UCM 39546	4.79	2.25	2.4	-	0.47	0.5	-	Puercan	Middleton and Dewar 2004
Ptilodontidae	*Kimbetohia*	*campi*	AMNH 58392	5.73	2.4	2.67	1.57	0.42	0.47	0.65	Puercan	Sloan 1981[+]
Eucosmodontidae	*Stygimys*	*kuszmauli*	UCMP 105416	4.98	2.09	2.2	-	0.42	0.44	-	Puercan	J. D. Archibald notes
Eucosmodontidae	*Stygimys*	*kuszmauli*	UCMP 99078	4.79	2.06	2.23	-	0.43	0.47	-	Puercan	J. D. Archibald notes

Family	*Genus*	*species*	Specimen	L	H	L1	H1	H:L	L1:L	H1:H	Age	Source
Eucosmodontidae	*Stygimys*	*kuszmauli*	UCMP 92526	4.77	2.01	2.08	-	0.42	0.44	-	Puercan	J. D. Archibald notes
Eucosmodontidae	*Stygimys*	*kuszmauli*	UCMP 150080	5.74	2.5	2.67	2.14	0.44	0.47	0.37	Puercan	This paper^
Eucosmodontidae	*Stygimys*	*kuszmauli*	UCMP 150081	5.56	2.32	2.17	1.88	0.42	0.39	0.34	Puercan	This paper^
Eucosmodontidae	*Stygimys*	*kuszmauli*	UCMP 92525	5.6	2.35	2.53	1.82	0.42	0.45	0.33	Puercan	This paper^
Eucosmodontidae	*Stygimys*	*kuszmauli*	UCMP 92527	5.94	2.49	2.75	1.85	0.42	0.46	0.31	Puercan	This paper^
Eucosmodontidae	*Stygimys*	*kuszmauli*	UCMP 102147	5.8	2.55	2.28	2.2	0.44	0.39	0.38	Puercan	This paper^
Eucosmodontidae	*Stygimys*	*kuszmauli*	UCMP 102226	6.82	2.72	2.67	2.21	0.4	0.39	0.32	Puercan	This paper^
Eucosmodontidae	*Stygimys*	*kuszmauli*	UCMP 102574	5.2	2.17	2.36	1.64	0.42	0.45	0.32	Puercan	This paper^
Eucosmodontidae	*Stygimys*	*kuszmauli*	UCMP 102885	5.72	2.28	2.11	1.88	0.4	0.37	0.33	Puercan	This paper^
Eucosmodontidae	*Stygimys*	*kuszmauli*	UCMP 103098	5.28	2.44	2.42	1.84	0.46	0.46	0.35	Puercan	This paper^
Eucosmodontidae	*Stygimys*	*kuszmauli*	UCMP 111686	6.17	2.39	2.43	2.08	0.39	0.39	0.34	Puercan	This paper^
Eucosmodontidae	*Stygimys*	*kuszmauli*	UCMP 111687	6.14	2.56	2.93	2.18	0.42	0.48	0.36	Puercan	This paper^
Eucosmodontidae	*Stygimys*	*kuszmauli*	UCMP 111689	4.62	1.89	1.93	1.55	0.41	0.42	0.34	Puercan	This paper^
Eucosmodontidae	*Stygimys*	*kuszmauli*	UCMP 111690	5.49	2.12	2.43	1.66	0.39	0.44	0.3	Puercan	This paper^
Eucosmodontidae	*Stygimys*	*kuszmauli*	UCMP 111691	5.78	2.57	2.58	1.98	0.44	0.45	0.34	Puercan	This paper^
Eucosmodontidae	*Stygimys*	*kuszmauli*	UCMP 111692	5.67	2.41	2.43	1.9	0.43	0.43	0.34	Puercan	This paper^

Family	*Genus*	*species*	Specimen	L	H	L1	H1	H:L	L1:L	H1:H	Age	Source
Eucosmodontidae	*Stygimys*	*kuszmauli*	UCMP 111693	6.05	2.58	2.78	1.96	0.43	0.46	0.32	Puercan	This paper^
Eucosmodontidae	*Stygimys*	*kuszmauli*	UCMP 111694	5.19	2.17	1.87	1.7	0.42	0.36	0.33	Puercan	This paper^
Eucosmodontidae	*Stygimys*	*kuszmauli*	UCMP 111695	5.18	2.08	2.37	1.6	0.4	0.46	0.31	Puercan	This paper^
Eucosmodontidae	*Stygimys*	*kuszmauli*	UCMP 111696	5.3	2.35	2.53	1.89	0.44	0.48	0.36	Puercan	This paper^
Eucosmodontidae	*Stygimys*	*kuszmauli*	UCMP 111697	5.71	2.68	2.52	1.98	0.47	0.44	0.35	Puercan	This paper^
Eucosmodontidae	*Stygimys*	*kuszmauli*	UCMP 150077	4.94	2.15	2.33	1.45	0.44	0.47	0.29	Puercan	This paper^
Eucosmodontidae	*Stygimys*	*kuszmauli*	UCMP 150078	6.15	2.44	2.11	2	0.4	0.34	0.33	Puercan	This paper^
Eucosmodontidae	*Stygimys*	*kuszmauli*	UCMP 116921	6.74	2.86	2.42	2.24	0.42	0.36	0.33	Puercan	This paper^
Eucosmodontidae	*Stygimys*	*kuszmauli*	UCMP 134601	6.18	2.74	2.41	2.16	0.44	0.39	0.35	Puercan	This paper^
Eucosmodontidae	*Stygimys*	*kuszmauli*	UCMP 145448	5.92	2.51	2.54	1.9	0.42	0.43	0.32	Puercan	This paper^
Eucosmodontidae	*Stygimys*	*kuszmauli*	UCMP 145547	6.52	2.94	2.81	2.22	0.45	0.43	0.34	Puercan	This paper^
Eucosmodontidae	*Stygimys*	*kuszmauli*	UCMP 116920	4.7	1.92	2.23	1.59	0.41	0.47	0.83	Puercan	Archibald 1982[+]
Eucosmodontidae	*Stygimys*	*camptorhiza*	mean	4.25	1.98	1.65	-	0.47	0.39	-	Puercan	Johnston and Fox 1984
Eucosmodontidae	*Eucosmodon*	*americanus*	AMNH 3028	10.6	4.08	5.35	3.23	0.38	0.5	0.79	Puercan	Granger and Simpson 1929[#]
Eucosmodontidae	*Eucosmodon*	*primus*	AMNH 16327	9.7	3.72	4.8	2.62	0.38	0.49	0.7	Puercan	Granger and

Family	*Genus*	*species*	Specimen	L	H	L1	H1	H:L	L1:L	H1:H	Age	Source
												Simpson 1929[#]
Microcosmodontidae	*Acheronodon*	*garbanii*	UCMP 116953	1.97	1.13	1.08	0.79	0.57	0.55	0.7	Puercan	This paper^
Microcosmodontidae	*Microcosmodon*	*harleyi*	UCMP 144449	1.8	0.88	1.09	0.75	0.49	0.61	0.85	Puercan	Weil 1998*
Microcosmodontidae	*Microcosmodon*	*arcuatus*	mean	2.15	1.5	0.93	-	0.7	0.43	-	Puercan	Johnston and Fox 1984
Taeniolabidoidea	*Taeniolabis*	*lamberti*	CCM 70-110	5.71	4.11	2.18	3.49	0.72	0.38	0.85	Puercan	Simmons 1987*
Taeniolabidoidea	*Catopsalis*	*alexandeari*	UCM 34979	4.2	2.58	2.98	2.37	0.61	0.71	0.92	Puercan	Middleton 1982[#]
Taeniolabidoidea	*Catopsalis*	*alexandeari*	UCMP 34979	2.97	2.85	2.3	2.47	0.96	0.77	0.87	Puercan	This paper^
Taeniolabidoidea	*Catopsalis*	sp.	UCMP 10998	4.42	3.2	3.11	2.94	0.72	0.7	0.92	Puercan	This paper^
Taeniolabidoidea	*Valenopsalis*	*joyneri*	UCMP 73828	3.39	2.42	2.87	2.33	0.71	0.85	0.96	Puercan	This paper^
Cimolodontidae	*Anconodon*	*cochranensis*	USNM V9765	4.77	2.79	2.56	2.45	0.58	0.54	0.88	Torrejonian	This paper[=]
Cimolodontidae	*Anconodon*	*cochranensis*	UALVP 44135	4.44	2.81	2.59	2.36	0.63	0.58	0.84	Torrejonian	Scott 2003*
Cimolodontidae	*Anconodon*	*gidleyi*	TMP 2011.090.0371	5.9	3.33	3.72	2.89	0.56	0.63	0.87	Torrejonian	Scott et al. 2013*
Neoplagiaulacidae	*Mesodma*	*pygmaea*	UALVP 44049	2.27	1.07	1.03	0.69	0.47	0.45	0.64	Torrejonian	Scott 2003*
Neoplagiaulacidae	*Ectypodus*	sp. cf. *E. szalayi*	UALVP 44073	2.46	1.35	1.11	1.02	0.55	0.45	0.76	Torrejonian	Scott 2003*
Neoplagiaulacidae	*Ectypodus*	*szalayi*	AMNH 35536	2.8	1.37	1.36	1	0.49	0.49	0.73	Torrejonian	Sloan 1981[+]

Family	*Genus*	*species*	Specimen	L	H	L1	H1	H:L	L1:L	H1:H	Age	Source
Neoplagiaulacidae	*Ectypodus*	*sylviae*	AMNH 100939	3.03	1.86	1.5	1.48	0.61	0.5	0.8	Torrejonian	Rigby 1980[+]
Neoplagiaulacidae	*Parectypodus*	*sinclairi*	TMP 2011.090.0130	3.37	1.71	2.01	1.54	0.51	0.6	0.9	Torrejonian	Scott et al. 2013*
Neoplagiaulacidae	*Parectypodus*	*corystes*	UALVP 40679	3.34	1.82	1.6	1.29	0.54	0.48	0.71	Torrejonian	Scott 2003*
Neoplagiaulacidae	*Parectypodus*	*corystes*	UALVP 44081	3.69	2.04	1.53	1.38	0.55	0.41	0.68	Torrejonian	Scott 2003*
Neoplagiaulacidae	*Mimetodon*	*silberlingi*	UALVP 44066	2.76	1.32	1.31	0.99	0.48	0.47	0.75	Torrejonian	Scott 2003*
Neoplagiaulacidae	*Xyronomys*	*swainae*	AMNH 87897	2.9	1.25	1.56	0.85	0.43	0.54	0.68	Torrejonian	Rigby 1980[+]
Neoplagiaulacidae	*Neoplagiaulax*	sp. cf. *N. hunteri*	AMNH 100963	4.35	2.12	2.15	1.69	0.49	0.49	0.8	Torrejonian	Rigby 1980[+]
Neoplagiaulacidae	*Krauseia*	*clemensi*	AMNH 87855	3.12	1.63	1.54	1.42	0.52	0.49	0.87	Torrejonian	Rigby 1980[+]
Neoplagiaulacidae	*Krauseia*	*clemensi*	AMNH 87856	3.08	1.64	1.41	1.52	0.53	0.46	0.93	Torrejonian	Rigby 1980[+]
Neoplagiaulacidae	*Krauseia*	*clemensi*	KU 14032	3.27	1.47	1.51	1.34	0.45	0.46	0.91	Torrejonian	Sloan 1981[+]
Neoplagiaulacidae	*Krauseia*	*clemensi*	UMVP 6034	3.87	1.95	1.83	1.68	0.5	0.47	0.86	Torrejonian	Sloan 1981[+]
Neoplagiaulacidae	*Krauseia*	*clemensi*	UMVP 6035	3.77	1.89	1.85	1.6	0.5	0.49	0.85	Torrejonian	Sloan 1981[+]
Ptilodontidae	*Baiotomeus*	*douglassi*	UM 77928	6.6	3.35	3.32	2.22	0.51	0.5	0.66	Torrejonian	Krause 1987a[#]
Ptilodontidae	*Baiotomeus*	*lamberti*	YPM-PU 18221A	5.8	2.84	2.87	1.61	0.49	0.49	0.57	Torrejonian	Krause 1987a[#]
Ptilodontidae	*Baiotomeus*	*rhothonion*	UALVP 44132	2.9	1.6	1.64	1.3	0.55	0.57	0.81	Torrejonian	Scott 2003
Ptilodontidae	*Ptilodus*	*tsosiensis*	AMNH 59800	6.1	2.79	3.3	2.09	0.46	0.54	0.75	Torrejonian	Krause 1982a[#]

Family	*Genus*	*species*	Specimen	L	H	L1	H1	H:L	L1:L	H1:H	Age	Source
Ptilodontidae	*Ptilodus*	*mediaevus*	AMNH 3022a	7.8	3.76	4.18	3.19	0.48	0.54	0.85	Torrejonian	Krause 1982a[#]
Ptilodontidae	*Ptilodus*	*mediaevus*	AMNH 100497	7.1	3.81	4.45	3.34	0.54	0.63	0.88	Torrejonian	Rigby 1980[+]
Ptilodontidae	*Ptilodus*	*wyomingensis*	TMP 2011.090.0001	7.66	4.24	4.56	3.24	0.55	0.6	0.76	Torrejonian	Scott et al. 2013*
Ptilodontidae	*Ptilodus*	*montanus*	UALVP 44117	7.94	3.79	4.15	3.15	0.48	0.52	0.83	Torrejonian	Scott 2003*
Ptilodontidae	*Ptilodus*	*montanus*	UALVP 44113	8.05	4.39	3.98	3.76	0.55	0.49	0.86	Torrejonian	Scott 2003*
Eucosmodontidae	*Stygimys*	*jepseni*	USNM 9769	4.34	1.4	2.1	1.24	0.32	0.48	0.89	Torrejonian	Lofgren et al. 2005*
Eucosmodontidae	*Eucosmodon*	*molestus*	AMNH 3029	15	6.89	8.22	5.61	0.46	0.55	0.81	Torrejonian	Granger and Simpson 1929[#]
Taeniolabidoidea	*Catopsalis*	*fissidens*	NMMNH P-8608	5	4.05	3.3	3.72	0.81	0.66	0.92	Torrejonian	Lucas et al. 1997[#]
incertae sedis	*Xanclomys*	*mcgrewi*	AMNH 87587	4.75	2.63	3.15	2.28	0.55	0.66	0.87	Torrejonian	Rigby 1980[+]
Cimolodontidae	*Anconodon*	*cochranensis*	UM 84131	5.65	3.32	3.37	2.89	0.59	0.6	0.87	Tiffanian	Scott and Krause 2006*
Cimolodontidae	*Anconodon*	*cochranensis*	UM 84117	5.91	3.17	2.92	2.79	0.54	0.5	0.88	Tiffanian	Scott and Krause 2006*
Cimolodontidae	*Anconodon*	*cochranensis*	PU 14619B	5.38	3.01	2.74	2.54	0.56	0.51	0.84	Tiffanian	Krause and Gingerich 1983*

Family	*Genus*	*species*	Specimen	L	H	L1	H1	H:L	L1:L	H1:H	Age	Source
Cimolodontidae	*Anconodon*	*gidleyi*	UM 84146	6.78	3.5	4.03	2.92	0.52	0.59	0.83	Tiffanian	Scott and Krause 2006*
Neoplagiaulacidae	*Mesodma*	*pygmaea*	UM 84194	2.82	1.26	1.15	0.97	0.45	0.41	0.77	Tiffanian	Scott and Krause 2006*
Neoplagiaulacidae	*Mesodma*	*pygmaea*	UM 84195	2.76	1.19	1.27	0.95	0.43	0.46	0.8	Tiffanian	Scott and Krause 2006*
Neoplagiaulacidae	*Neoplagiaulax*	*donaldorum*	UM 84178	4.33	2.27	2.11	2.1	0.52	0.49	0.93	Tiffanian	Scott and Krause 2006*
Neoplagiaulacidae	*Neoplagiaulax*	*donaldorum*	UM 84184	4.17	1.97	1.98	1.42	0.47	0.47	0.72	Tiffanian	Scott and Krause 2006*
Neoplagiaulacidae	*Neoplagiaulax*	*hunteri*	UM 84157	4.75	2.25	2.75	1.66	0.47	0.58	0.74	Tiffanian	Scott and Krause 2006*
Neoplagiaulacidae	*Neoplagiaulax*	*hunteri*	UM 84166	4.92	2.38	2.34	1.74	0.48	0.48	0.73	Tiffanian	Scott and Krause 2006*
Neoplagiaulacidae	*Neoplagiaulax*	*serrator*	UALVP 46025	4	2.05	2.03	1.51	0.51	0.51	0.74	Tiffanian	Scott 2005*
Neoplagiaulacidae	*Neoplagiaulax*	*serrator*	UALVP 46080	4.64	2.12	2.27	1.68	0.46	0.49	0.79	Tiffanian	Scott 2005*
Neoplagiaulacidae	*Neoplagiaulax*	*serrator*	UALVP 46087	4.87	2.24	2.71	1.71	0.46	0.56	0.76	Tiffanian	Scott 2005*
Neoplagiaulacidae	*Neoplagiaulax*	*paskapooensis*	UALVP 46138	4.92	2.42	2.74	2.05	0.49	0.56	0.85	Tiffanian	Scott 2005*
Neoplagiaulacidae	*Neoplagiaulax*	*paskapooensis*	UALVP 46157	4.55	2.14	2.53	1.63	0.47	0.56	0.76	Tiffanian	Scott 2005*
Neoplagiaulacidae	*Neoplagiaulax*	*cimolodontoides*	UALVP 46201	4	2.04	2.17	1.73	0.51	0.54	0.85	Tiffanian	Scott 2005*

Family	*Genus*	*species*	Specimen	L	H	L1	H1	H:L	L1:L	H1:H	Age	Source
Neoplagiaulacidae	*Neoplagiaulax*	*cimolodontoides*	UALVP 46196	3.84	1.89	2.24	1.66	0.49	0.58	0.88	Tiffanian	Scott 2005*
Neoplagiaulacidae	*Neoplagiaulax*	*cimolodontoides*	UALVP 46197	3.86	2.08	2.1	1.79	0.54	0.54	0.86	Tiffanian	Scott 2005*
Neoplagiaulacidae	*Neoplagiaulax*	*jepi*	mean	4.64	1.89	-	-	0.41	-	-	Tiffanian	Secord 2008
Neoplagiaulacidae	*Neoplagiaulax*	*hazeni*	UM 73397	5.25	2.2	-	-	0.42	-	-	Tiffanian	Secord 2008
Neoplagiaulacidae	*Neoplagiaulax*	*hazeni*	UM 73619	5.05	2.1	-	-	0.42	-	-	Tiffanian	Secord 2008
Neoplagiaulacidae	*Neoplagiaulax*	*hazeni*	UM 77323	4.82	2.13	-	-	0.44	-	-	Tiffanian	Secord 2008
Neoplagiaulacidae	*Neoplagiaulax*	*hazeni*	UM 85365	4.65	2.3	-	-	0.49	-	-	Tiffanian	Secord 2008
Neoplagiaulacidae	*Neoplagiaulax*	*hazeni*	UM 86243	5.28	2.3	-	-	0.44	-	-	Tiffanian	Secord 2008
Neoplagiaulacidae	*Neoplagiaulax*	*hazeni*	YPM-PU 14422	5.03	2.2	-	-	0.44	-	-	Tiffanian	Secord 2008
Neoplagiaulacidae	*Ectypodus*	sp.	UM 84198	3.88	1.59	1.86	1.35	0.41	0.48	0.85	Tiffanian	Scott and Krause 2006*
Neoplagiaulacidae	*Ectypodus*	sp.	UM 84197	3.77	1.63	1.59	1.26	0.43	0.42	0.77	Tiffanian	Scott and Krause 2006*
Neoplagiaulacidae	*Ectypodus*	*elaphus*	UALVP 45994	2.36	1.26	1.24	1	0.53	0.53	0.79	Tiffanian	Scott 2005*
Neoplagiaulacidae	*Ectypodus*	*powelli*	mean	3.2	1.31	-	-	0.41	-	-	Tiffanian	Secord 2008
Neoplagiaulacidae	*Parectypodus*	*laytoni*	YPM-PU 14464	2.9	1.3	-	-	0.45	-	-	Tiffanian	Secord 2008
Ptilodontidae	*Prochetodon*	*foxi*	YPM-PU 21223	8.7	3.72	5.04	3.04	0.43	0.58	0.82	Tiffanian	Krause 1987b[#]

Family	*Genus*	*species*	Specimen	L	H	L1	H1	H:L	L1:L	H1:H	Age	Source
Ptilodontidae	*Prochetodon*	*cavus*	YPM-PU 19099	7.3	3.8	4.54	3.36	0.52	0.62	0.88	Tiffanian	Krause 1987b[#]
Ptilodontidae	*Prochetodon*	*speirsae*	UALVP 45682	8.58	3.48	4.69	3.06	0.41	0.55	0.88	Tiffanian	Scott 2004*
Ptilodontidae	*Prochetodon*	*speirsae*	UALVP 45689	8.78	3.57	4.84	3.16	0.41	0.55	0.89	Tiffanian	Scott 2004*
Ptilodontidae	*Prochetodon*	*speirsae*	UALVP 45703	9.19	3.7	5.28	3.09	0.4	0.57	0.84	Tiffanian	Scott 2004*
Ptilodontidae	*Prochetodon*	*speirsae*	UALVP 45690	8.98	3.93	5.06	3.27	0.44	0.56	0.83	Tiffanian	Scott 2004*
Ptilodontidae	*Prochetodon*	sp. cf. *P. foxi*	UALVP 42977	6.28	3.16	4.21	2.65	0.5	0.67	0.84	Tiffanian	Scott 2004*
Ptilodontidae	*Ptilodus*	sp. "T"	UALVP 18620	8.81	3.9	4.31	2.8	0.44	0.49	0.72	Tiffanian	Scott 2004*
Ptilodontidae	*Ptilodus*	*gnomus*	UALVP 45148	4.61	2.58	2.58	2.17	0.56	0.56	0.84	Tiffanian	Scott et al. 2002*
Ptilodontidae	*Ptilodus*	*gnomus*	UALVP 18670	4.77	2.49	2.63	2.13	0.52	0.55	0.86	Tiffanian	Scott et al. 2002*
Ptilodontidae	*Ptilodus*	*"titanus"*	PU 14584	9.65	4.58	5.01	3.95	0.47	0.52	0.86	Tiffanian	Krause and Gingerich 1983*
Microcosmodontidae	*Acheronodon*	*vossae*	UALVP 24550	1.9	0.89	0.82	0.62	0.47	0.43	0.7	Tiffanian	Fox 2005[#]
Microcosmodontidae	*Allocosmodon*	*woodi*	UALVP 40475	3.3	1.31	1.39	0.97	0.4	0.42	0.74	Tiffanian	Fox 2005[#]
Microcosmodontidae	*Allocosmodon*	*woodi*	UALVP 40494	3.1	1.46	1.37	1.1	0.47	0.44	0.75	Tiffanian	Fox 2005[#]
Microcosmodontidae	*Allocosmodon*	*woodi*	UM 84199	3.14	1.34	1.71	0.85	0.43	0.54	0.63	Tiffanian	Scott and Krause 2006*
Microcosmodontidae	*Allocosmodon*	*woodi*	MCZ 19963	3.2	1.47	1.53	1.04	0.46	0.48	0.71	Tiffanian	Holtzman and

Family	*Genus*	*species*	Specimen	L	H	L1	H1	H:L	L1:L	H1:H	Age	Source
												Wolberg 1977[#]
Microcosmodontidae	*Allocosmodon*	*woodi*	UMVP 5001	3.1	1.39	1.26	0.96	0.45	0.41	0.69	Tiffanian	Holtzman and Wolberg 1977[#]
Microcosmodontidae	*Pentacosmodon*	*pronus*	MCZ 20066	1.8	1.17	-	-	0.65	-	-	Tiffanian	Secord 2008
Microcosmodontidae	*Pentacosmodon*	*pronus*	YPM-PU 19027	2.03	1.03	-	-	0.51	-	-	Tiffanian	Secord 2008
Microcosmodontidae	*Pentacosmodon*	*pronus*	UALVP 42803	1.8	1.06	0.96	0.98	0.59	0.53	0.92	Tiffanian	Fox 2005[#]
Microcosmodontidae	*Pentacosmodon*	*bowensis*	UALVP 42806	1.7	1.11	1.16	0.9	0.65	0.68	0.81	Tiffanian	Fox 2005[#]
Microcosmodontidae	*Pentacosmodon*	*bowensis*	UALVP 42805	1.8	1.06	1.31	0.94	0.59	0.73	0.89	Tiffanian	Fox 2005[#]
Microcosmodontidae	*Microcosmodon*	*conus*	UALVP 42831	1.8	0.99	0.95	0.8	0.55	0.53	0.81	Tiffanian	Fox 2005[#]
Microcosmodontidae	*Microcosmodon*	*conus*	UALVP 40690	1.9	1.12	0.95	0.97	0.59	0.5	0.87	Tiffanian	Fox 2005[#]
Microcosmodontidae	*Microcosmodon*	*conus*	UM 71657	1.72	0.78	-	-	0.45	-	-	Tiffanian	Secord 2008
Microcosmodontidae	*Microcosmodon*	*conus*	UM 81702	1.8	0.85	-	-	0.47	-	-	Tiffanian	Secord 2008
incertae sedis	*Fractinus*	*palmorum*	UW 27063	4.92	2.74	3.04	2.74	0.56	0.62	1	Tiffanian	Higgins 2003
Neoplagiaulacidae	*Ectypodus*	*powelli*	UM 71783	3.37	1.52	1.69	1.27	0.45	0.5	0.84	Clarkforkian	Rose 1981*
Neoplagiaulacidae	*Parectypodus*	*laytoni*	UM 68290	3.32	1.75	1.75	1.51	0.53	0.53	0.86	Clarkforkian	Rose 1981*
Ptilodontidae	*Ptilodus*	sp.	UCM 41271	7.19	3.71	3.78	3.29	0.52	0.53	0.89	Clarkforkian	Krause 1980*

Family	*Genus*	*species*	Specimen	L	H	L1	H1	H:L	L1:L	H1:H	Age	Source
Ptilodontidae	*Prochetodon*	sp. cf. *P. cavus*	PU 14542	7.68	3.46	4.89	3.14	0.45	0.64	0.91	Clarkforkian	Krause 1980*
Ptilodontidae	*Prochetodon*	*taxus*	UM 71311 (R)	8	3.92	4.58	3.61	0.49	0.57	0.92	Clarkforkian	Krause 1987b[#]
Neoplagiaulacidae	*Ectypodus*	*powelli*	UM 69868	3.02	1.45	1.3	1.14	0.48	0.43	0.79	Clarkforkian	Krause 1980*
Microcosmodontidae	*Microcosmodon*	*rosei*	UM 72662	1.44	0.97	1.05	0.95	0.67	0.73	0.98	Clarkforkian	Krause 1980*
Neoplagiaulacidae	*Ectypodus*	*tardus*	UCMP 44041	2.81	1.5	1.48	1.26	0.53	0.53	0.84	Eocene	McKenna 1960[#]
Neoplagiaulacidae	*Ectypodus*	*tardus*	UCMP 44004	2.6	1.16	1.23	0.93	0.45	0.47	0.8	Eocene	McKenna 1960[#]
Neoplagiaulacidae	*Ectypodus*	*tardus*	UCMP 44007	3	1.45	1.57	1.17	0.48	0.52	0.81	Eocene	McKenna 1960[#]
Neoplagiaulacidae	*Ectypodus*	*tardus*	UCMP 44010	3.4	1.76	1.63	1.6	0.52	0.48	0.91	Eocene	McKenna 1960[#]
Neoplagiaulacidae	*Ectypodus*	sp. cf. *E. childei*	UCMP 44023	3.21	1.7	1.58	1.42	0.53	0.49	0.84	Eocene	Krause 1982b*
Neoplagiaulacidae	*Ectypodus*	*lovei*	PTRM 10427	3.51	1.84	1.84	1.56	0.52	0.52	0.85	Eocene	Schumaker and Kihm 2006*
Neoplagiaulacidae	*Parectypodus*	*lunatus*	AMNH 59648	3.47	2.06	2.01	1.9	0.59	0.58	0.92	Eocene	Krause 1982b*
incertae sedis	*Neoliotomus*	*ultimus*	AMNH 16103	11.89	4.66	6.35	4.5	0.39	0.53	0.97	Eocene	Krause 1982b*

LITERATURE CITED

ARCHIBALD, J. D. 1982. A study of Mammalia and geology across the Cretaceous-Tertiary boundary in Garfield County, Montana. University of California Publications in Geological Sciences 122:1–286.

EATON, J. G. 1995. Cenomanian and Turonian (early Late Cretaceous) multituberculate mammals from southwestern Utah. Journal of Vertebrate Paleontology 15:761–784.

EATON, J. G. 2002. Multituberculate mammals from the Wahweap (Campanian, Aquilan) and Kaiparowits (Campanian, Judithian) Formations, within and near Grand Staircase-Escalante National Monument, southern Utah. Miscellaneous Publications of the Utah Geological Survey 02-4:1–66.

EATON, J. G. 2006. Santonian (Late Cretaceous) mammals from the John Henry Member of the Straight Cliffs Formation, Grand Staircase-Escalante National Monument, Utah. Journal of Vertebrate Paleontology 26:446–460.

EATON, J. G. 2009. Cenomanian (Late Cretaceous) mammals from Cedar Canyon, southwestern Utah, and a revision of Cenomanian *Alphadon*-like marsupials. Pp. 97–110 in Papers on geology, vertebrate paleontology, and biostratigraphy in honor of Michael O. Woodburne (L. B. Albright III, ed.). Museum of Northern Arizona Bulletin 65. Flagstaff, Arizona.

EATON, J. G. 2013. Late Cretaceous mammals from Bryce Canyon National Park and vicinity, Paunsaugunt Plateau, southwestern Utah. Pp. 329–369 in At the top of the Grand Staircase: the Late Cretaceous of southern Utah (A. L. Titus and M. A. Loewen, eds.). Indiana University Press. Bloomington, Indiana.

EATON, J. G., AND R. L. CIFELLI. 2001. Multituberculate mammals from near the Early-Late Cretaceous boundary, Cedar Mountain Formation, Utah. Acta Palaeontologica Polonica 46:453–518.

EBERLE, J. J., AND J. A. LILLEGRAVEN. 1998. A new important record of earliest Cenozoic mammalian history: geologic setting, Multituberculata, and Peradectia. Rocky Mountain Geology 33:3–47.

FOX, R. C. 1971. Early Campanian multituberculates (Mammalia: Allotheria) from the Upper Milk River Formation, Alberta. Canadian Journal of Earth Sciences 8:916–938.

FOX, R. C. 1980. Mammals from the Upper Cretaceous Oldman Formation, Alberta. IV. *Meniscoessus* Cope (Multituberculata). Canadian Journal of Earth Sciences 17:1480–1488.

FOX, R. C. 2005. Microcosmodontid multituberculates (Allotheria, Mammalia) from the Paleocene and Late Cretaceous of western Canada. Palaeontographica Canadiana 23:1–109.

GRANGER, W., AND G. G. SIMPSON. 1929. A revision of the Tertiary Multituberculata. Bulletin of the American Museum of Natural History 56:601–676.

HIGGINS, P. 2003. A new species of Paleocene multituberculate (Mammalia: Allotheria) from the Hanna Basin, south-central Wyoming. Journal of Vertebrate Paleontology 23:468–470.

HOLTZMAN, R. C., AND D. L. WOLBERG. 1977. The Microcosmodontidae and *Microcosmodon woodi,* new Multituberculata taxa (Mammalia) from the late Paleocene of North America. Scientific Publications of the Science Museum of Minnesota 4:1–13.

HUNTER, J. P., R. E. HEINRICH, AND D. B. WEISHAMPEL. 2010. Mammals from the St. Mary River Formation (Upper Cretaceous), Montana. Journal of Vertebrate Paleontology 30:885–898.

JOHNSTON, P. A., AND R. C. FOX. 1984. Paleocene and Late Cretaceous mammals from Saskatchewan, Canada. Palaeontographica Abteilung A, 186:163–222.

KRAUSE, D. W. 1980. Multituberculates from the Clarkforkian Land-Mammal Age, late Paleocene–early Eocene, of western North America. Journal of Paleontology 54:1163–1183.

KRAUSE, D. W. 1982a. Evolutionary history and paleobiology of early Cenozoic Multituberculata (Mammalia), with emphasis on the family Ptilodontidae. Ph.D. dissertation, University of Michigan. Ann Arbor, Michigan.

KRAUSE, D. W. 1982b. Multituberculates from the Wasatchian Land-Mammal Age, early Ecoene, of western North America. Journal of Paleontology 56:271–294.

KRAUSE, D. W. 1987a. *Baiotomeus*, a new ptilodontid multituberculate (Mammalia) from the middle Paleocene of western North America. Journal of Paleontology 61:595–603.

KRAUSE, D. W. 1987b. Systematic revision of the genus *Prochetodon* (Ptilodontidae, Multituberculata) from the late Paleocene and early Eocene of western North America. Contributions from the Museum of Paleontology, University of Michigan 27:221–236.

KRAUSE, D. W., AND P. D. GINGERICH. 1983. Mammalian fauna from Douglass Quarry, earliest Tiffanian (Late Paleocene) of the eastern Crazy Mountain Basin, Montana. Contributions from the Museum of Paleontology, University of Michigan 26:157–196.

LOFGREN, D. L., B. E. SCHERER, C. K. CLARK, AND B. STANDHARDT. 2005. First record of *Stygimys* (Mammalia, Multituberculata, Eucosmodontidae) from the Paleocene (Puercan) part of the North Horn Formation, Utah, and a review of the genus. Journal of Mammalian Evolution 12:77–97.

LUCAS, S. G., T. E. WILLIAMSON, AND M. D. MIDDLETON. 1997. *Catopsalis* (Mammalia: Multituberculata) from the Paleocene of New Mexico and Utah: taxonomy and biochronological significance. Journal of Paleontology 71:484–493.

MCKENNA, M. C. 1960. Fossil Mammalia from the early Wasatchian Four Mile Fauna, Eocene of northwest Colorado. University of California Publications in Geological Sciences 37:1–130.

MIDDLETON, M. D. 1982. A new species and additional material of *Catopsalis* (Mammalia, Multituberculata) from the Western Interior of North America. Journal of Paleontology 56:1197–1206.

MIDDLETON, M. D., AND E. W. DEWAR. 2004. New mammals from the early Paleocene Littleton fauna (Denver Formation, Colorado). Pp. 59–80 in Paleogene mammals (S. G. Lucas, K. E. Zeigler, and P. E. Kondrashov, eds.). New Mexico Museum of Natural History and Science Bulletin 26. Albuquerque, New Mexico.

MONTELLANO, M. 1992. Mammalian fauna of the Judith River Formation (Late Cretaceous, Judithian), northcentral Montana. University of California Publications in Geological Sciences 136:1–115.

NOVACEK, M., AND W. A. CLEMENS. 1977. Aspects of intrageneric variation and evolution of *Mesodma* (Multituberculata, Mammalia). Journal of Paleontology 51:701–717.

RIGBY, J. K. 1980. Swain Quarry of the Fort Union Formation, Middle Paleocene (Torrejonian), Carbon County, Wyoming: geologic setting and mammalian fauna. Evolutionary Monographs 3:1-178.

ROSE, K. D. 1981. The Clarkforkian Land-Mammal Age and mammalian faunal composition across the Paleocene-Eocene boundary. University of Michigan Papers on Paleontology 26:1–197.

SAHNI, A. 1972. The vertebrate fauna of the Judith River Formation, Montana. Bulletin of the American Museum of Natural History 147:321–412.

SCHUMAKER, K. K., AND A. J. KIHM. 2006. Multituberculates from the Medicine Pole Hills local fauna (Chadronian) of Bowman County, North Dakota. Paludicola 6:9–21.

SCOTT, C. S. 2003. Late Torrejonian (middle Paleocene) mammals from south central Alberta, Canada. Journal of Paleontology 77:745–768.

SCOTT, C. S. 2004. A new species of ptilodontid multituberculate *Prochetodon* (Mammalia, Allotheria) from the Paleocene Paskapoo Formation of Alberta, Canada. Canadian Journal of Earth Sciences 41:237–246.

SCOTT, C. S. 2005. New neoplagiaulacid multituberculates (Mammalia: Allotheria) from the Paleocene of Alberta, Canada. Journal of Paleontology 79:1189–1213.

SCOTT, C. S., AND D. W. KRAUSE. 2006. Multituberculates (Mammalia, Allotheria) from the earliest Tiffanian (late Paleocene) Douglass Quarry, eastern Crazy Mountain Basin, Montana. Contributions from the Museum of Paleontology, University of Michigan 31:211–243.

SCOTT, C. S., R. C. FOX, AND G. P. YOUZWYSHYN. 2002. New earliest Tiffanian (late Paleocene) mammals from Cochrane 2, southwestern Alberta, Canada. Acta Palaeontologica Polonica 47:691–704.

SCOTT, C. S., D. N. SPIVAK, AND A. R. SWEET. 2013. First mammals from the Paleocene Porcupine Hills Formation of southwestern Alberta, Canada. Canadian Journal of Earth Sciences 50:355–378.

SECORD, R. 2008. The Tiffanian Land-Mammal Age (middle and late Paleocene) in the northern Bighorn Basin, Wyoming. University of Michigan Papers on Paleontology 35:1–192.

SIMMONS, N. B. 1987. A revision of *Taeniolabis* (Mammalia: Multituberculata), with a new species from the Puercan of eastern Montana. Journal of Paleontology 61:794–808.

SLOAN, R. E. 1981. Systematics of Paleocene multituberculates from the San Juan Basin, New Mexico. Pp. 127–160 in Advances in San Juan Basin paleontology (S. G. Lucas, K. J. Rigby, and B. S. Kues, eds.). University of New Mexico Press. Albuquerque, New Mexico.

WEAVER, L. N., G. P. WILSON, L. J. KRUMENACKER, J. R. MOORE, AND D. J. VARRICCHIO. 2019. New multituberculate mammals from the mid-Cretaceous (lower Cenomanian) Wayan Formation of southeastern Idaho and implications for the early evolution of Cimolodonta. Journal of Vertebrate Paleontology, 39(2):e1604532.

WEIL, A. 1998. A new species of *Microcosmodon* (Mammalia: Multituberculata) from the Paleocene Tullock Formation of Montana, and an argument for the Microcosmodontidae. PaleoBios 18:1–15.

WILSON, G. P., M. DECHESNE, AND I. R. ANDERSON. 2010. New latest Cretaceous mammals from northeastern Colorado with biochronologic and biogeographic implications. Journal of Vertebrate Paleontology 30:499–520.

2.11.2 SUPPLEMENTARY DATA SD2

Table 2.11.2A—A, Table comparing p4 measurements taken on actual specimens (gray) vs. figured specimens (white). Measurements taken on figures from Archibald 1982 were taken using digital calipers, all other figure measurements were taken using ImageJ.

Genus	species	Specimen no.	H	L	L1	H1	H:L	L1:L	H1:H	Age	Source
Mesodma	*formosa*	UCMP 46407	3.31	1.49	1.6	0.82	0.45	0.48	0.55	Lancian	This paper

Genus	species	Specimen no.	H	L	L1	H1	H:L	L1:L	H1:H	Age	Source
Mesodma	*formosa*	UCMP 46407	3.39	1.49	1.55	0.91	0.45	0.47	0.61	Lancian	Clemens 1964
Mesodma	*formosa*	UCMP 47025	3.4	1.35	1.68	0.64	0.4	0.49	0.47	Lancian	This paper
Mesodma	*formosa*	UCMP 47025	3.4	1.33	1.66	0.79	0.39	0.49	0.59	Lancian	Clemens 1964
Mesodma	*thompsoni*	UCMP 47217	4	1.6	1.88	1	0.4	0.47	0.625	Lancian	This paper
Mesodma	*thompsoni*	UCMP 47217	4	1.56	1.84	1.1	0.39	0.46	0.71	Lancian	Clemens 1964
Mesodma	sp. cf. *M. thompsoni*	UCMP 116622	5.76	2.44	2.94	1.66	0.42	0.51	0.68	Puercan	This paper
Mesodma	sp. cf. *M. thompsoni*	UCMP 116622	5.07	2.32	2.77	1.42	0.46	0.55	0.61	Puercan	Archibald 1982
Mesodma	sp. (large)	UMNH VP7642	3.55	1.83	1.64	1.28	0.52	0.46	0.7	Judithian	This paper
Mesodma	sp. (large)	UMNH VP7642	3.61	1.76	1.71	1.24	0.49	0.47	0.7	Judithian	Eaton 2002
Cimolodon	*nitidus*	UCMP 116901	6.41	3.47	3.11	2.57	0.54	0.49	0.74	Lancian	This paper
Cimolodon	*nitidus*	UCMP 116901	5.84	3.02	2.63	2.33	0.52	0.45	0.77	Lancian	Archibald 1982
Cimolodon	sp. cf. *C. nitidus*	UMNH VP7978	5.14	2.5	2.88	1.75	0.49	0.56	0.7	Aquilan	This paper
Cimolodon	sp. cf. *C. nitidus*	UMNH V7978	5.26	2.57	2.93	1.83	0.49	0.56	0.71	Aquilan	Eaton 2002
Cimolodon	*wardi*	UMNH VP14027	3.52	1.82	1.9	1.14	0.52	0.54	0.63	Aquilan	This paper
Cimolodon	*wardi*	UMNH VP14027	3.54	1.85	1.92	1.22	0.52	0.54	0.66	Aquilan	Eaton 2006
Cimexomys	*judithae*	UCMP 131505	3.08	1.49	1.58	1.12	0.48	0.51	0.75	Judithian	This paper

Genus	species	Specimen no.	H	L	L1	H1	H:L	L1:L	H1:H	Age	Source
Cimexomys	*judithae*	UCMP 131505	3.18	1.62	1.46	1.2	0.51	0.46	0.74	Judithian	Montellano 1992
Bryceomys	*intermedius*	OMNH 34405	2.72	1.32	1.33	0.74	0.49	0.49	0.56	mid-K	This paper
Bryceomys	*intermedius*	OMNH 34405	2.7	1.24	1.37	0.65	0.46	0.51	0.52	mid-K	Eaton and Cifelli 2001
Bryceomys	*fumosus*	MNA V5639	2.54	1.27	1.17	0.69	0.5	0.46	0.54	pre-Aquilan	This paper
Bryceomys	*fumosus*	MNA V5639	2.58	1.25	1.22	0.83	0.48	0.47	0.66	pre-Aquilan	Eaton 1995
Bryceomys	*fumosus*	MNA V7476	2.82	1.4	1.46	0.71	0.5	0.52	0.51	pre-Aquilan	This paper
Bryceomys	*fumosus*	MNA V7476	2.81	1.3	1.4	0.69	0.46	0.5	0.53	pre-Aquilan	Eaton 1995
?Neoplagiaulax	*burgessi*	UCMP 116896	4.55	2.2	2.39	1.76	0.48	0.53	0.8	Lancian	This paper
?Neoplagiaulax	*burgessi*	UCMP 116896	4.2	2.1	2.25	1.7	0.5	0.54	0.81	Lancian	Archibald 1982

We used the XLSTAT (version 2015.5) function “Method comparison” in order to test whether measurements taken from actual specimens were comparable to measurements taken from published figures. We ran this analysis for each linear measurement. Below we provide the outputs from the bias tests, scatterplots, and Bland and Altman plots. The bias metric is estimated as the mean of the difference between the two measurement methods (including associated standard error and 95% confidence intervals). The scatterplots are simply plots of the figure (vertical axis) vs. the specimen (horizontal axis) measurements. Bland and Altman graphs plot the difference between the figure vs. specimen measurements (vertical axis) against the average

of the results obtained by the two methods (horizontal axis). If the methods are comparable, then the points should be randomly distributed about the mean (0), and the majority of points should fall within the 95% confidence interval brackets.

Table 2.11.2B.—**B**, summary statistics, t-test for two paired samples and Bias test comparing **length** measurements taken on specimens vs. figures.

Summary statistics:

Variable	Observations	Obs. with missing data	Obs. without missing data	Minimum	Maximum	Mean	Std. deviation
Specimen	13	0	13	2.540	6.410	3.908	1.214
Figure	13	0	13	2.580	5.840	3.807	1.028

t-test for two paired samples / Two-tailed test:

95% confidence interval on the difference between the means:

] -0.259 , 0.057 [

Difference	-0.101
t (Observed value)	-1.388
t (Critical value)	2.179
DF	12
P-value (Two-tailed)	0.190
alpha	0.05

Bias test:

–Bias: -0.101

–Standard Error: 0.262

–95% Confidence Intervals for Bias: -0.259, 0.057

Figure 2.11.2B.— scatterplot, and Bland and Altman plot comparing **length** measurements taken on specimens vs. figures.

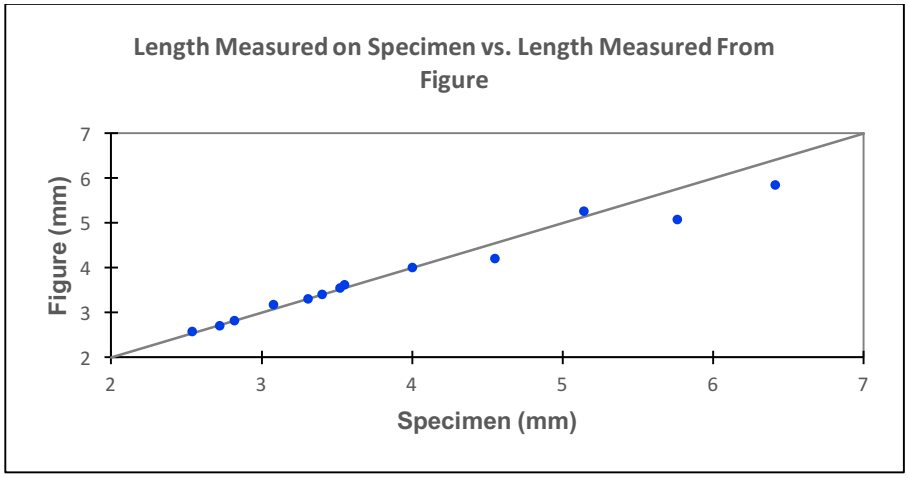

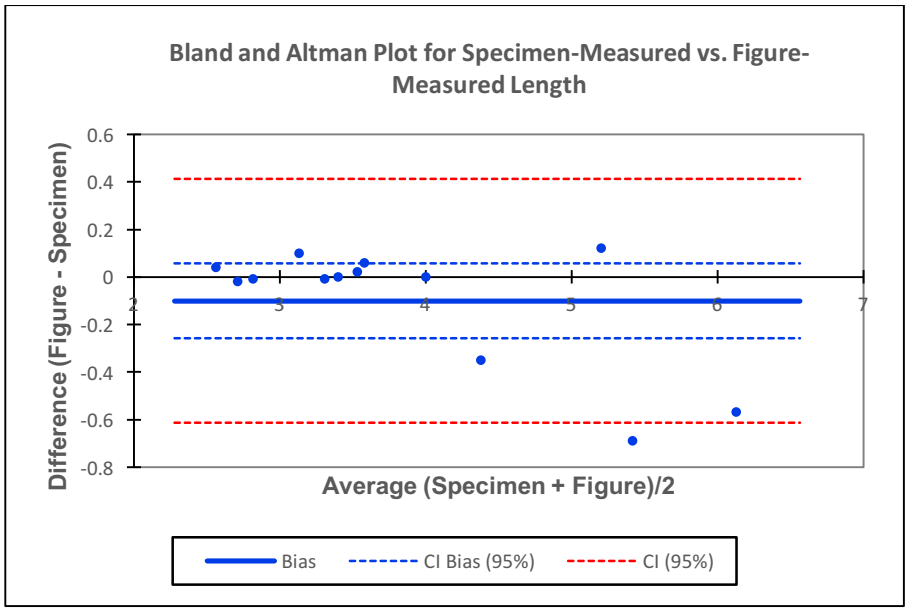

Table 2.11.2C.—C, summary statistics, t-test for two paired samples, and Bias test comparing **height** measurements taken on specimens vs. figures.

Summary statistics:

Variable	Observations	Obs. with missing data	Obs. without missing data	Minimum	Maximum	Mean	Std. deviation
Specimen	13	0	13	1.270	3.470	1.860	0.640
Figure	13	0	13	1.240	3.020	1.801	0.557

t-test for two paired samples / Two-tailed test:

95% confidence interval on the difference between the means:

] -0.142 , 0.024 [

Difference	-0.059
t (Observed value)	-1.550
t (Critical value)	2.179
DF	12
p-value (Two-tailed)	0.147
alpha	0.05

Bias test:

–Bias: -0.059

–Standard Error: 0.138

–95% Confidence Intervals for Bias: -0.142, 0.024

Figure 2.11.2C.—Scatterplot, and Bland and Altman plot comparing **height** measurements taken on specimens vs. figures.

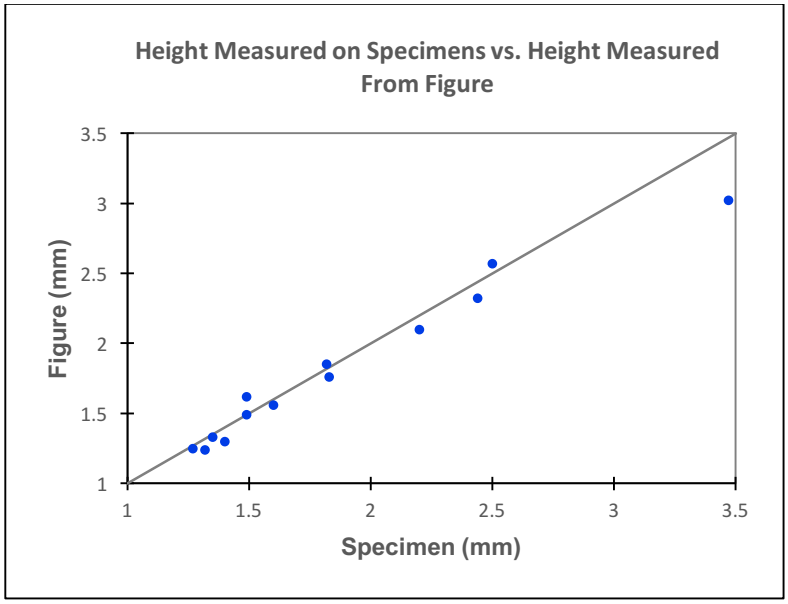

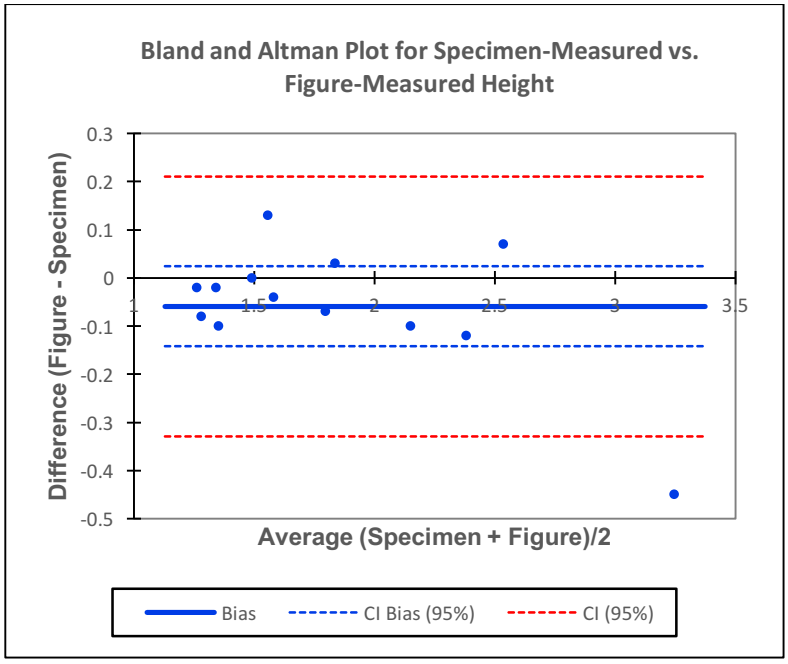

Table 2.11.2D.—**D**, summary statistics, t-test for two paired samples, and Bias test comparing **length to the p4 apogee (L1)** measurements taken on specimens vs. figures.

Summary statistics:

Variable	Observations	Obs. with missing data	Obs. without missing data	Minimum	Maximum	Mean	Std. deviation
Specimen	13	0	13	1.170	3.110	1.966	0.649
Figure	13	0	13	1.220	2.930	1.901	0.569

t-test for two paired samples / Two-tailed test:

95% confidence interval on the difference between the means:

] -0.154 , 0.023 [

Difference	-0.065
t (Observed value)	-1.609
t (Critical value)	2.179
DF	12
P-value (Two-tailed)	0.134
alpha	0.05

Bias test:

–Bias: -0.065

–Standard Error: 0.147

–95% Confidence Intervals for Bias: -0.154, 0.023

Figure 2.11.2D.—Scatterplot, and Bland and Altman plot comparing **length to the p4 apogee (L1)** measurements taken on specimens vs. figures.

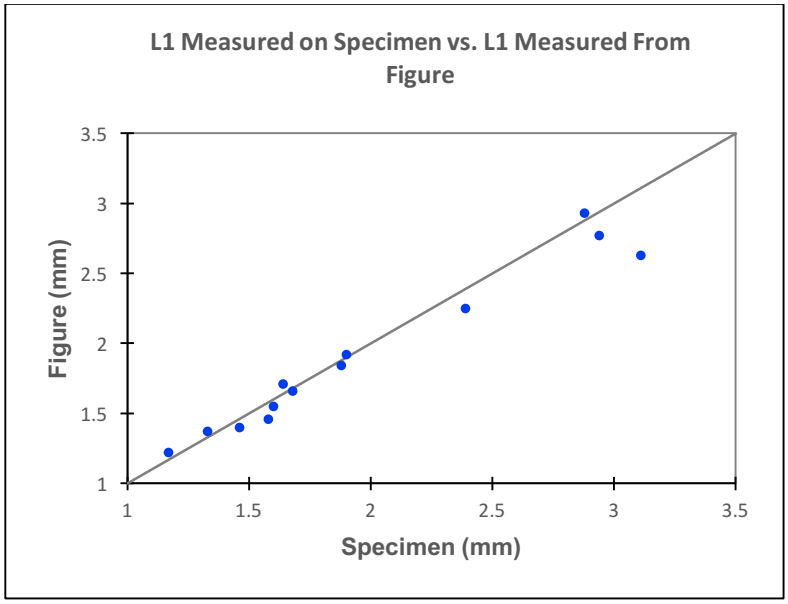

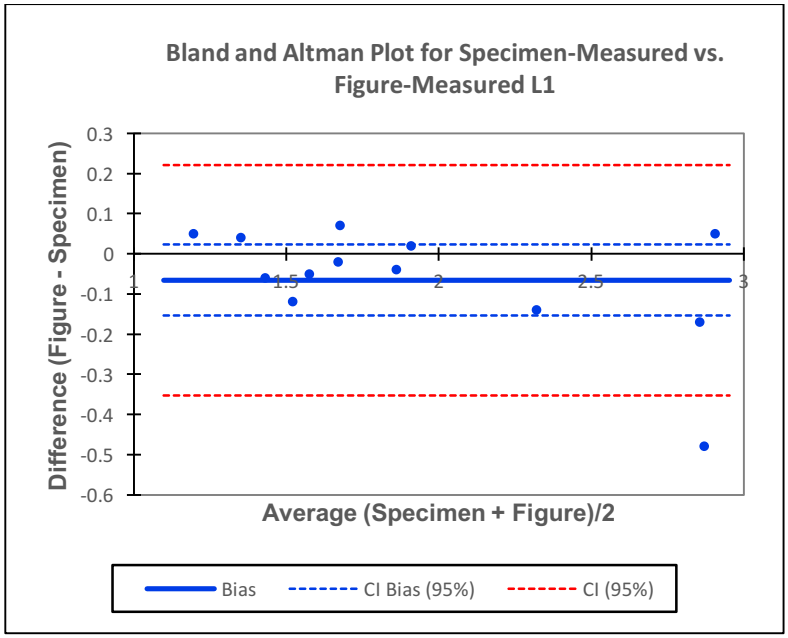

Table 2.11.2E.—**E**, summary statistics, t-test for two paired samples, and Bias test comparing **height to the first serration (H1)** measurements taken on specimens vs. figures.

Summary statistics:

Variable	Observations	Obs. with missing data	Obs. without missing data	Minimum	Maximum	Mean	Std. deviation
Specimen	13	0	13	0.640	2.570	1.222	0.572
Figure	13	0	13	0.650	2.330	1.224	0.494

t-test for two paired samples / Two-tailed test:

95% confidence interval on the difference between the means:

] -0.077 , 0.082 [

Difference	0.002
t (Observed value)	0.063
t (Critical value)	2.179
DF	12
P-value (Two-tailed)	0.951
alpha	0.05

Bias test:

–Bias: 0.002

–Standard Error: 0.132

–95% Confidence Intervals for Bias: -0.077, 0.082

Figure 2.11.2E.—Scatterplot, and Bland and Altman plot comparing **height to the first serration (H1)** measurements taken on specimens vs. figures.

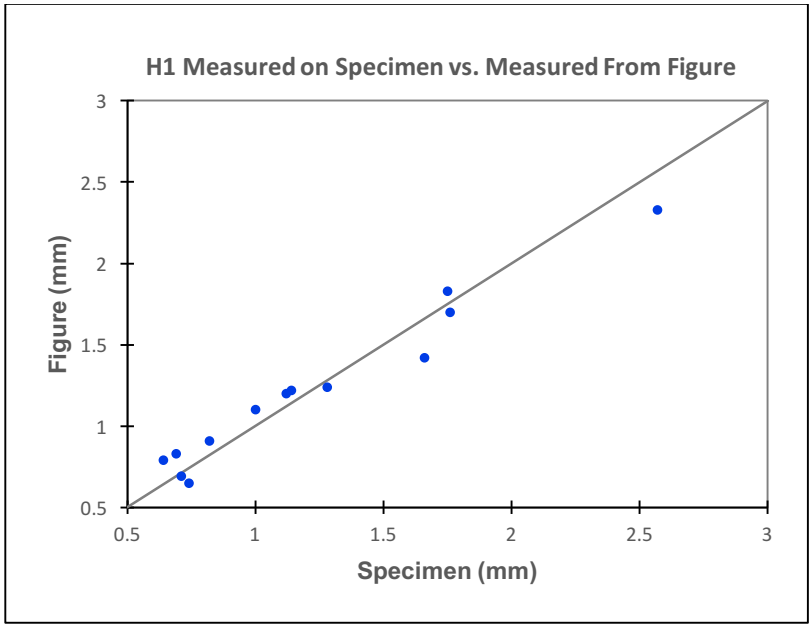

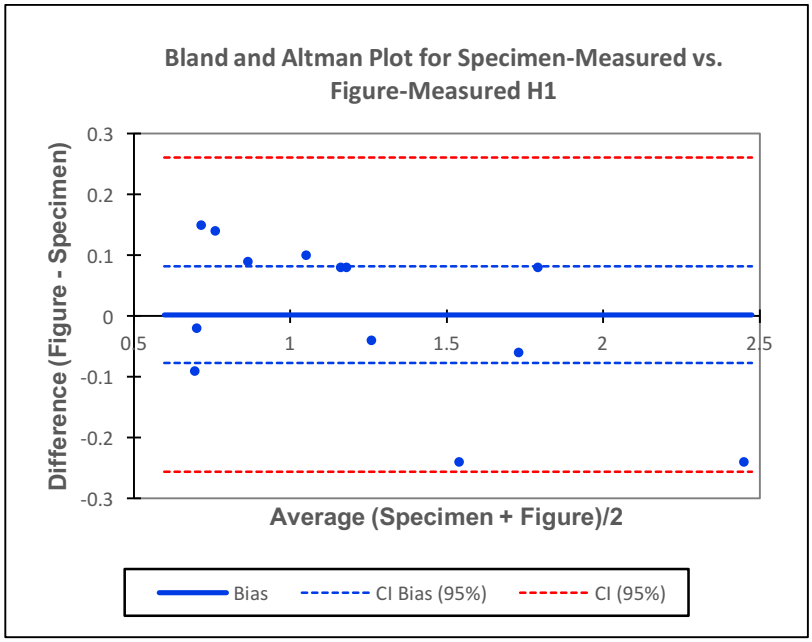

LITERATURE CITED

ARCHIBALD, J. D. 1982. A study of Mammalia and geology across the Cretaceous-Tertiary boundary in Garfield County, Montana. University of California Publications in Geological Sciences 122:1–286.

CLEMENS, W. A. 1964. Fossil mammals of the type Lance Formation, Wyoming: part I. introduction and Multituberculata. University of California Publications in Geological Sciences 48:1–105.

EATON, J. G. 1995. Cenomanian and Turonian (early Late Cretaceous) multituberculate mammals from southwestern Utah. Journal of Vertebrate Paleontology 15:761–784.

EATON, J. G. 2002. Multituberculate mammals from the Wahweap (Campanian, Aquilan) and Kaiparowits (Campanian, Judithian) Formations, within and near Grand Staircase-Escalante National Monument, southern Utah. Miscellaneous Publications of the Utah Geological Survey 02-4:1–66.

EATON, J. G. 2006. Late Cretaceous mammals from Cedar Canyon, southwestern Utah. Pp. 373–402 in Late Cretaceous Vertebrates from the Western Interior (S. G. Lucas and R. M. Sullivan, eds.). New Mexico Museum of Natural History and Science Bulletin 35, Albuquerque, New Mexico.

EATON, J. G., AND R. L. CIFELLI. 2001. Multituberculate mammals from near the Early-Late Cretaceous boundary, Cedar Mountain Formation, Utah. Acta Palaeontologica Polonica 46:453–518.

MONTELLANO, M. 1992. Mammalian fauna of the Judith River Formation (Late Cretaceous, Judithian), northcentral Montana. University of California Publications in Geological Sciences 136:1–115.

2.11.3 SUPPLEMENTARY DATA SD3

Table 2.11.3A.—Mean ratio values for each species per time bin. Because species averages were taken per time bin, the same species may have a different ratio average in different time bins.

Species	H:L average	L1:L average	H1:H average	Age
Cimolodon akersteni	0.56	0.45	0.62	mid-K
Cedaromys bestia	0.54	0.56	0.67	mid-K
Cedaromys parvus	0.525	0.555	0.665	mid-K
Bryceomys intermedius	0.49	0.49	0.56	mid-K
?*Mesodma* sp.	0.37	0.44	0.55	mid-K
Cedaromys minimus	0.5	0.55	–	pre-Aquilan
Dakotamys malcomi	0.523	0.533	0.643	pre-Aquilan
Bryceomys fumosus	0.5	0.49	0.525	pre-Aquilan
Cimolodon* sp. cf. *C. similis	0.505	0.485	0.783	pre-Aquilan
Cimolodon* sp. cf. *C. nitidus	0.53	0.51	0.7	pre-Aquilan
Cimolodon* sp. cf. *C. foxi	0.45	0.47	0.77	pre-Aquilan
Paracimexomys magister	0.5	0.49	0.72	Aquilan
Cimolodon wardi	0.52	0.54	0.63	Aquilan
Cimolodon* sp. cf. *C. nitidus	0.63	0.56	0.74	Aquilan
Cimolodon electus	0.6	0.53	0.77	Aquilan
Cimolodon similis	0.535	0.475	0.685	Aquilan
***Cimolodon* sp. (small)**	0.53	0.51	0.75	Aquilan

Species	H:L average	L1:L average	H1:H average	Age
Mesodma senecta	0.45	0.465	0.75	Aquilan
Cimexomys judithae	0.466	0.493	0.715	Judithian
Cimolodon foxi	0.48	0.54	0.6	Judithian
Cimolodon* sp. cf. *similis	0.52	0.505	–	Judithian
***Mesodma* sp. (large)**	0.52	0.46	0.7	Judithian
Mesodma archibaldi	0.41	0.47	0.72	Judithian
Mesodma primaeva	0.47	0.49	0.61	Judithian
Meniscoessus major	0.48	0.45	0.8	Judithian
Nidimys occultus	0.51	0.463	0.867	Judithian
Cimolodon nitidus	0.537	0.506	0.728	Lancian
Mesodma hensleighi	0.47	0.457	0.655	Lancian
Mesodma formosa	0.471	0.467	0.662	Lancian
Mesodma thompsoni	0.45	0.448	0.699	Lancian
?Neoplagiaulax burgessi	0.48	0.54	0.762	Lancian
Parikimys carpenteri	0.46	0.47	0.69	Lancian
Cimolomys gracilis	0.483	0.495	0.75	Lancian
Meniscoessus robustus	0.599	0.473	0.68	Lancian
Paressonodon nelsoni	0.52	0.42	0.62	Lancian
Clemensodon megaloba	0.425	0.445	0.82	Lancian
Cimexomys minor	0.51	0.507	0.647	Puercan
Cimexomys gratus	0.488	0.493	0.673	Puercan

Species	H:L average	L1:L average	H1:H average	Age
***Cimexomys* sp.**	0.53	0.5	–	Puercan
Cimexomys arapahoensis	0.48	0.52	–	Puercan
Mesodma formosa	0.49	0.46	0.689	Puercan
Mesodma thompsoni	0.466	0.453	0.669	Puercan
Neoplagiaulax kremnus	0.53	0.49	–	Puercan
Neoplagiaulax macintyrei	0.43	0.53	0.75	Puercan
***Ectypodus* sp.**	0.548	0.465	0.673	Puercan
Xyronomys robinsoni	0.41	0.52	0.55	Puercan
***Xyronomys* sp.**	0.44	0.39	–	Puercan
Parectypodus armstrongi	0.55	0.46	–	Puercan
***Parectypodus* sp.**	0.56	0.38	–	Puercan
Parectypodus vanvaleni	0.49	0.51	0.88	Puercan
Kimbethoia mziae	0.484	0.508	0.71	Puercan
Kimbethoia campi	0.42	0.47	0.65	Puercan
Stygimys kuszmauli	0.424	0.429	0.353	Puercan
Stygimys camptorhiza	0.47	0.39	–	Puercan
Eucosmodon americanus	0.38	0.5	0.79	Puercan
Eucosmodon primus	0.38	0.49	0.7	Puercan
Acheronodon garbanii	0.57	0.55	0.7	Puercan
Microcosmodon harleyi	0.49	0.61	0.85	Puercan
Microcosmodon arcuatus	0.7	0.43	–	Puercan

Species	H:L average	L1:L average	H1:H average	Age
Taeniolabis lamberti	0.72	0.38	0.85	Puercan
Catopsalis alexanderi	0.785	0.74	0.895	Puercan
***Catopsalis* sp.**	0.72	0.7	0.92	Puercan
Valenopsalis joyneri	0.71	0.85	0.96	Puercan
Anconodon cochranensis	0.605	0.56	0.86	Torrejonian
Anconodon gidleyi	0.56	0.63	0.87	Torrejonian
Mesodma pygmaea	0.47	0.45	0.64	Torrejonian
Ectypodus szalayi	0.52	0.47	0.745	Torrejonian
Ectypodus sylviae	0.61	0.5	0.8	Torrejonian
Parectypodus sinclairi	0.51	0.6	0.9	Torrejonian
Parectypodus corystes	0.545	0.445	0.695	Torrejonian
Mimetodon silberlingi	0.48	0.47	0.75	Torrejonian
Xyronomys swainae	0.43	0.54	0.68	Torrejonian
Neoplagiaulax* sp. cf. *N. hunteri	0.49	0.49	0.8	Torrejonian
Krauseia clemensi	0.5	0.474	0.884	Torrejonian
Baiotomeus douglassi	0.51	0.5	0.66	Torrejonian
Baiotomeus lamberti	0.49	0.49	0.57	Torrejonian
Baiotomeus rhothonion	0.55	0.57	0.81	Torrejonian
Ptilodus tsosiensis	0.46	0.54	0.75	Torrejonian
Ptilodus mediaevus	0.51	0.585	0.865	Torrejonian

Species	H:L average	L1:L average	H1:H average	Age
Ptilodus wyomingensis	0.55	0.6	0.76	Torrejonian
Ptilodus montanus	0.515	0.505	0.845	Torrejonian
Stygimys jepseni	0.32	0.48	0.89	Torrejonian
Eucosmodon molestus	0.46	0.55	0.81	Torrejonian
Catopsalis fissidens	0.81	0.66	0.92	Torrejonian
Xanclomys mcgrewi	0.55	0.66	0.87	Torrejonian
Anconodon cochranensis	0.563	0.537	0.863	Tiffanian
Anconodon gidleyi	0.52	0.59	0.83	Tiffanian
Mesodma pygmaea	0.44	0.435	0.785	Tiffanian
Neoplagiaulax donaldorum	0.495	0.48	0.825	Tiffanian
Neoplagiaulax hunteri	0.475	0.48	0.735	Tiffanian
Neoplagiaulax serrator	0.477	0.52	0.763	Tiffanian
Neoplagiaulax paskapooensis	0.48	0.56	0.805	Tiffanian
Neoplagiaulax cimolodontoides	0.513	0.553	0.863	Tiffanian
Neoplagiaulax jepi	0.41	–	–	Tiffanian
Neoplagiaulax hazeni	0.442	–	–	Tiffanian
***Ectypodus* sp.**	0.42	0.45	0.81	Tiffanian
Ectypodus elaphus	0.53	0.53	0.79	Tiffanian
Ectypodus powelli	0.41	–	–	Tiffanian
Parectypodus laytoni	0.45	–	–	Tiffanian

Species	H:L average	L1:L average	H1:H average	Age
Prochetodon foxi	0.465	0.625	0.83	Tiffanian
Prochetodon cavus	0.52	0.62	0.88	Tiffanian
Prochetodon speirsae	0.415	0.558	0.86	Tiffanian
***Ptilodus* sp. "T"**	0.44	0.49	0.72	Tiffanian
Ptilodus gnomus	0.54	0.555	0.85	Tiffanian
Ptilodus "titanus"	0.47	0.52	0.86	Tiffanian
Acheronodon vossae	0.47	0.43	0.7	Tiffanian
Allocosmodon woodi	0.442	0.458	0.704	Tiffanian
Pentacosmodon pronus	0.583	0.53	0.92	Tiffanian
Pentacosmodon bowensis	0.62	0.705	0.85	Tiffanian
Microcosmodon conus	0.515	0.515	0.84	Tiffanian
Fractinus palmorum	0.56	0.62	1	Tiffanian
Ectypodus powelli	0.465	0.465	0.815	Clarkforkian
Parectypodus laytoni	0.53	0.53	0.86	Clarkforkian
***Ptilodus* sp.**	0.52	0.53	0.89	Clarkforkian
Prochetodon* sp. cf. *P. cavus	0.45	0.64	0.91	Clarkforkian
Prochetodon taxus	0.49	0.57	0.92	Clarkforkian
Microcosmodon rosei	0.67	0.73	0.98	Clarkforkian
Ectypodus tardus	0.495	0.5	0.84	Eocene
Ectypodus lovei	0.52	0.52	0.85	Eocene
Ectypodus* sp. cf. *E. childei	0.53	0.49	0.84	Eocene

Species	H:L average	L1:L average	H1:H average	Age
Parectypodus lunatus	0.59	0.58	0.92	Eocene
Neoliotomus ultimatus	0.39	0.53	0.97	Eocene

Table 2.11.3B.—Variance values for each ratio per time bin. These values were derived from the mean ratio values (see A above) of each species per time bin. Variance was used as our measure of p4 shape disparity.

	H:L variance	L1:L variance	H1:H variance
mid-Cretaceous	0.005695	0.003205	0.003195
pre-Aquilan	0.000788667	0.000934667	0.0111037
Aquilan	0.004364167	0.001241667	0.002336905
Judithian	0.001323429	0.000866125	0.009137
Lancian	0.002513611	0.001174767	0.003495822
Puercan	0.012353308	0.011748538	0.020742386
Torrejonian	0.007917803	0.004346236	0.009058779
Tiffanian	0.003163706	0.004738444	0.005048522
Clarkforkian	0.006284167	0.0088775	0.003144167
Eocene	0.00535	0.00123	0.00343

2.11.4 SUPPLEMENTARY DATA SD4

Results from resampling analyses. For each ratio, five random mean species values were randomly drawn from each time bin and variance (our measure of disparity) was calculated from this random sample. This was repeated (with replacement) both 100 and 1,000 times for each ratio, and 95% confidence intervals were calculated for the mean ratio variance of each time bin. **H:L** resampling results for **A**, 100 iterations and **B**, 1,000 iterations. **L1:L** resampling results for **C**, 100 iterations and **D**, 1,000 iterations. **H1:H** resampling results for **E**, 100 iterations and **F**, 1,000 iterations. All analyses were performed using the statistical software package R (version 3.4.3 for Mac OS El Capitan).

Table 2.11.4A

	mean	CI
mid.K	0.0049221	0.00063129
pre.Aq	0.000595754	8.77E-05
Aquilan	0.003598375	0.000362207
Judithian	0.001083636	0.000142809
Lancian	0.00248754	0.000327558
Puercan	0.01030285	0.001459072
Torrejonian	0.005426925	0.00133814
Tiffanian	0.00309529	0.000327486
Clarkforkian	0.00512995	0.000752583
Eocene	0.00477655	0.000580043

Figure 2.11.4A

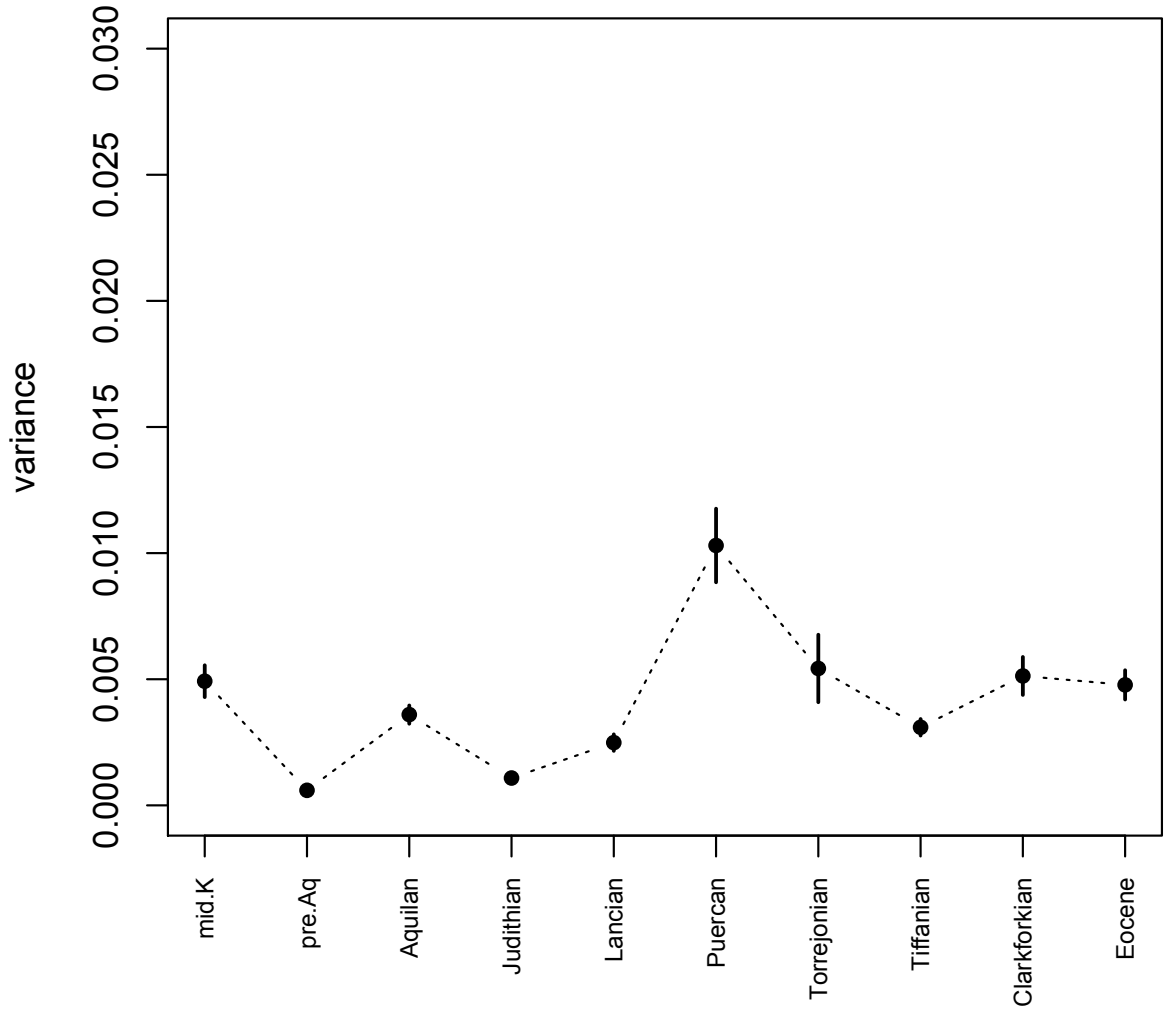

Table 2.11.4B

	mean	CI
mid.K	0.00459966	0.000191437
pre.Aq	0.000665546	2.90E-05
Aquilan	0.003590933	0.000115765
Judithian	0.00119122	5.07E-05
Lancian	0.00230369	0.000107052
Puercan	0.011831536	0.000518045
Torrejonian	0.007434753	0.000534465
Tiffanian	0.003091272	0.000122326
Clarkforkian	0.00518678	0.000243597
Eocene	0.004169225	0.000162029

Figure 2.11.4B

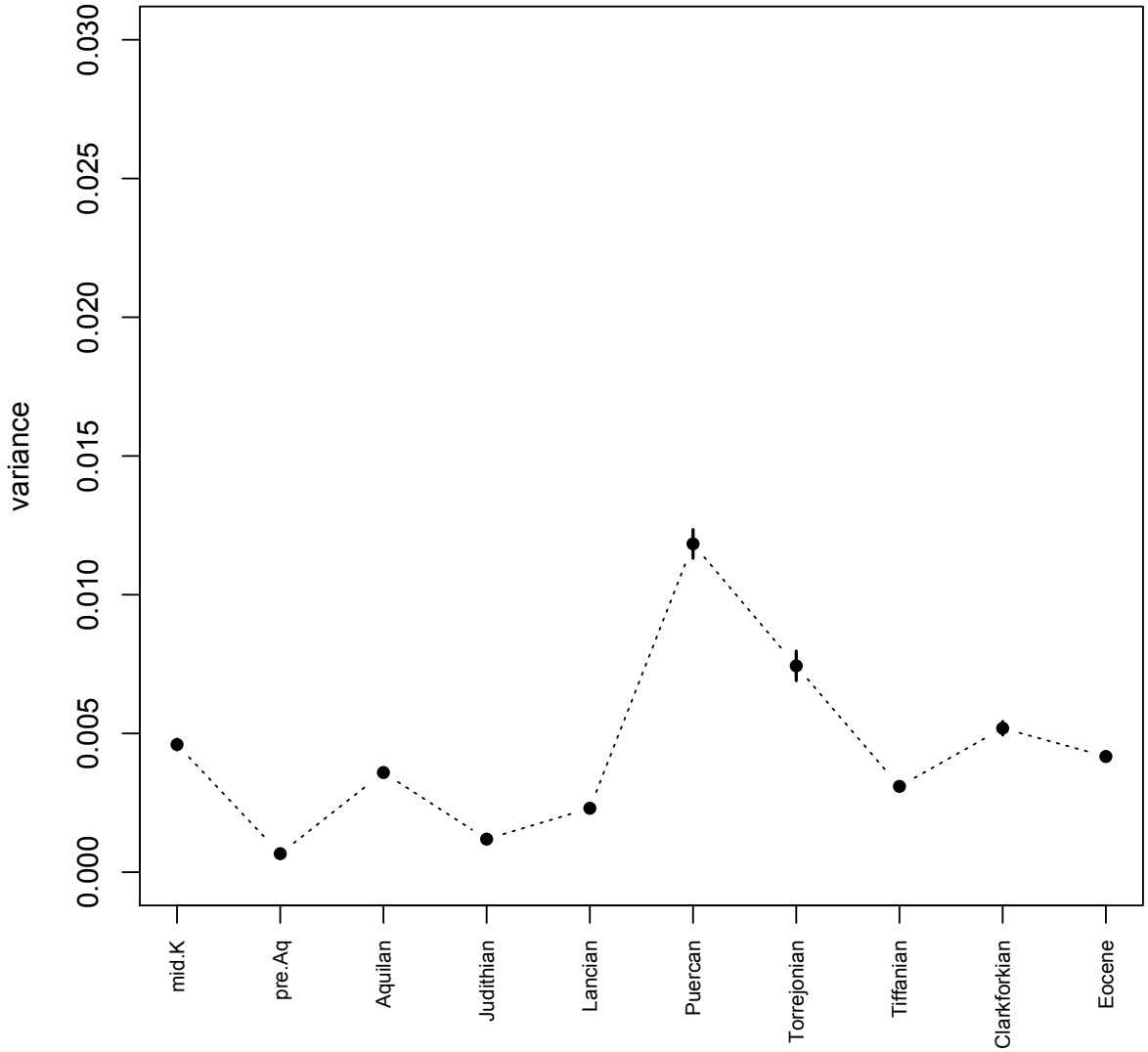

Table 2.11.4C

	mean	CI
mid.K	0.002647575	0.000189512
pre.Aq	0.000729002	7.46E-05
Aquilan	0.001066175	9.95E-05
Judithian	0.000763325	9.48E-05
Lancian	0.001144798	0.000159528
Puercan	0.011208065	0.002140343
Torrejonian	0.004179307	0.000452866
Tiffanian	0.004178589	0.000621459
Clarkforkian	0.00747155	0.000828853
Eocene	0.0010679	0.000113347

Figure 2.11.4C

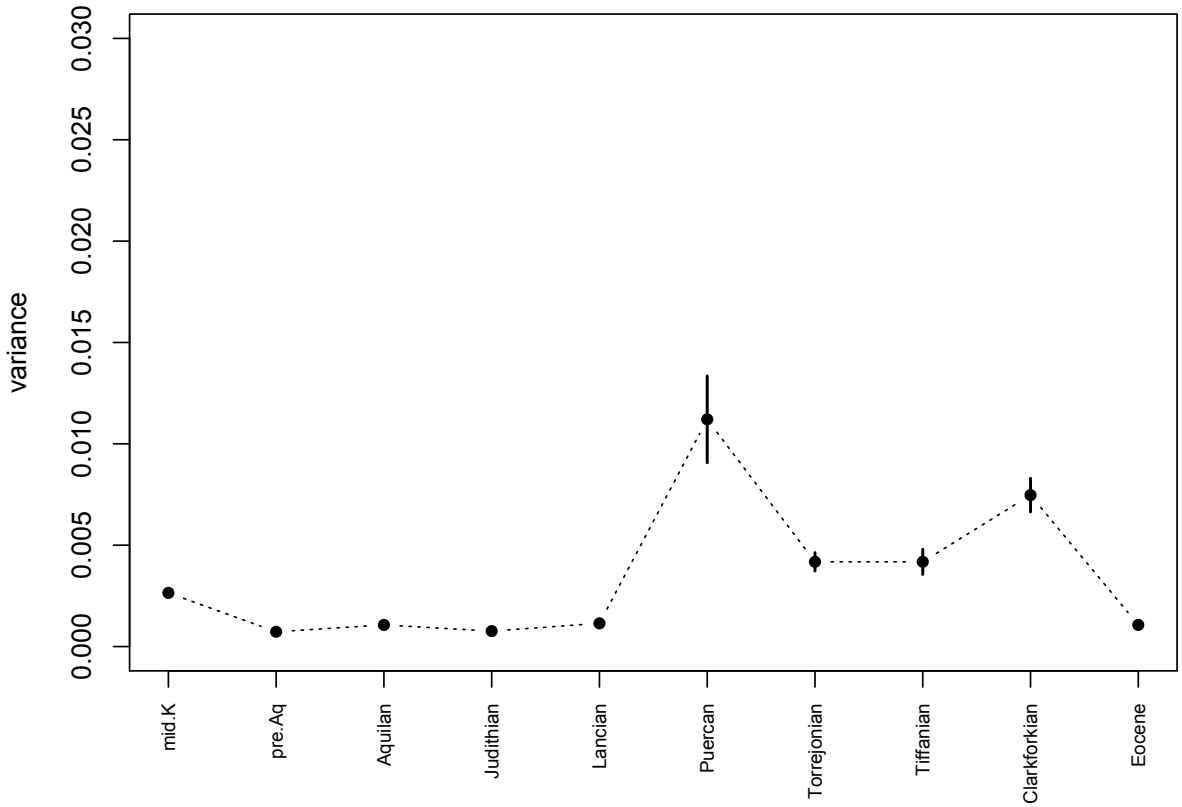

Table 2.11.4D

	mean	CI
mid.K	0.00252843	6.36E-05
pre.Aq	0.000766986	2.32E-05
Aquilan	0.00105348	3.20E-05
Judithian	0.000759155	3.15E-05
Lancian	0.00106265	4.51E-05
Puercan	0.010760653	0.0006847
Torrejonian	0.004058832	0.000147727
Tiffanian	0.004660773	0.000200516
Clarkforkian	0.007466688	0.000271377
Eocene	0.00100814	3.84E-05

Figure 2.11.4D

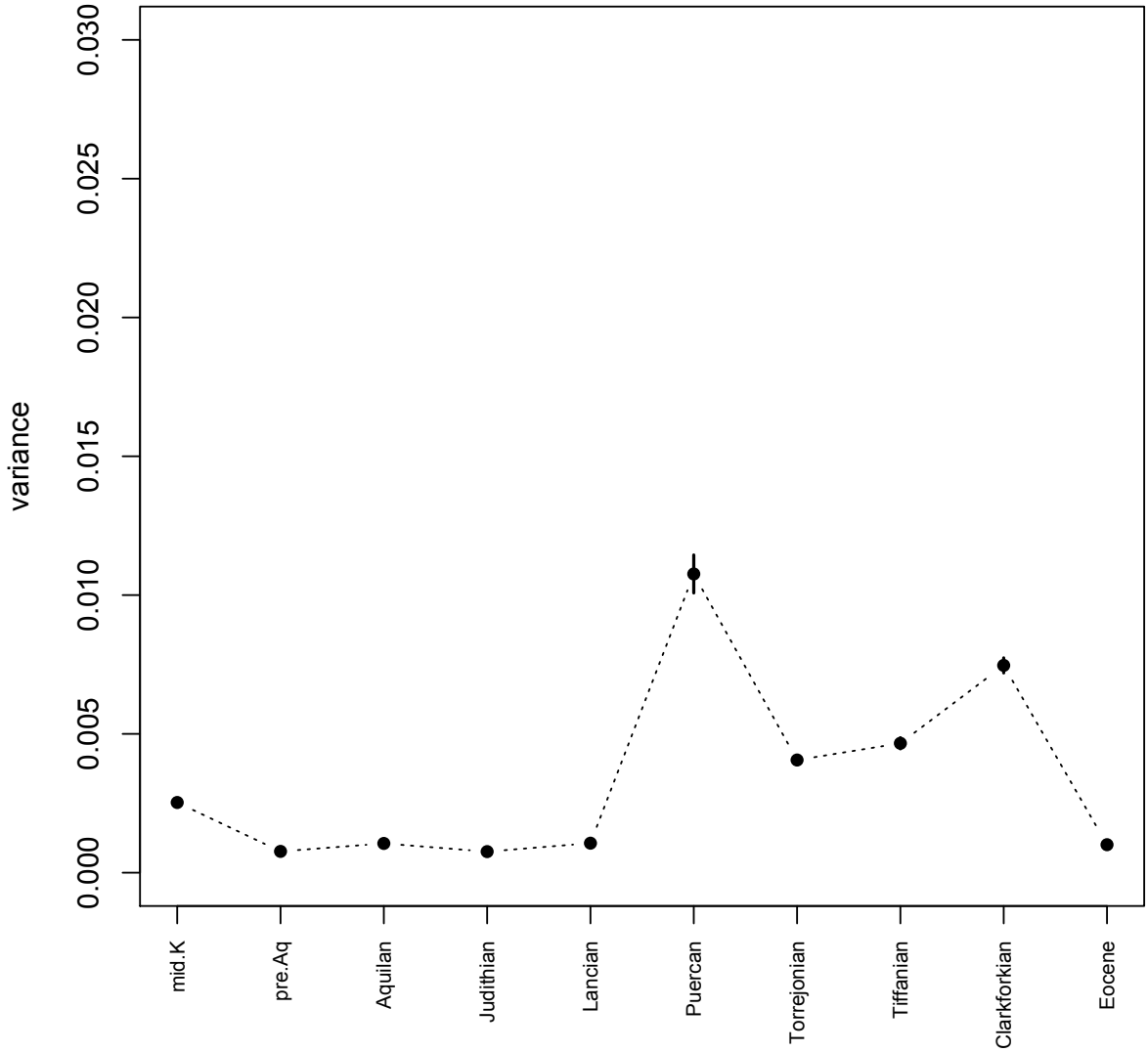

Table 2.11.4E

	mean	CI
mid.K	0.002604325	0.000203193
pre.Aq	0.008535511	0.000917804
Aquilan	0.0019916	0.000260496
Judithian	0.007898262	0.000890197
Lancian	0.002985188	0.000370518
Puercan	0.019309485	0.002884792
Torrejonian	0.008309946	0.001024783
Tiffanian	0.004757991	0.000628878
Clarkforkian	0.002780975	0.000345887
Eocene	0.00271	0.000279188

Figure 2.11.4E

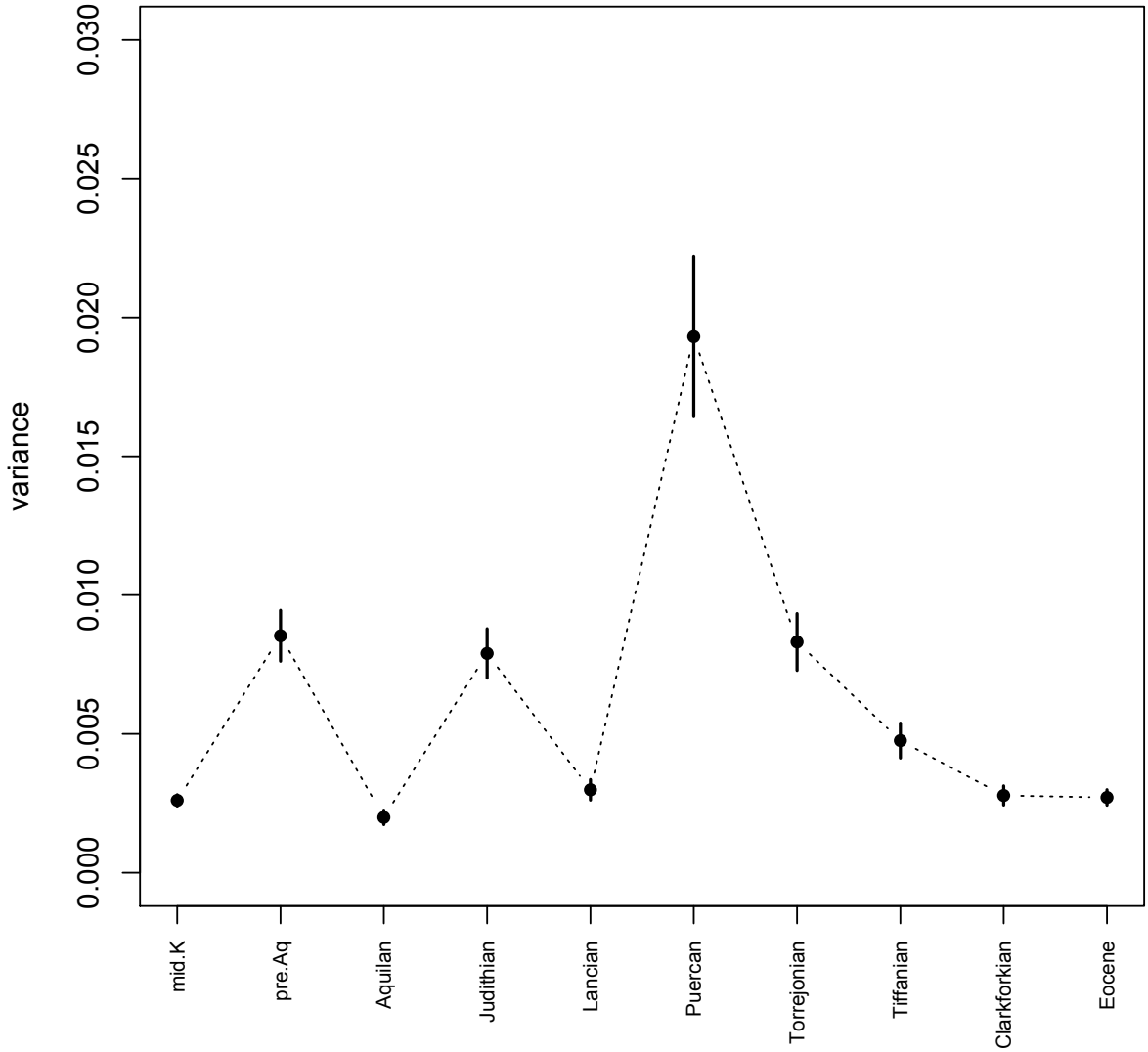

Table 2.11.4F

	mean	CI
mid.K	0.002545455	6.22E-05
pre.Aq	0.008797921	0.000298152
Aquilan	0.001933393	8.14E-05
Judithian	0.007852592	0.000265937
Lancian	0.00326149	0.000125966
Puercan	0.020099697	0.001011532
Torrejonian	0.008825985	0.000342214
Tiffanian	0.004758648	0.000220859
Clarkforkian	0.002739228	0.00010028
Eocene	0.00270128	8.46E-05

Figure 2.11.4F

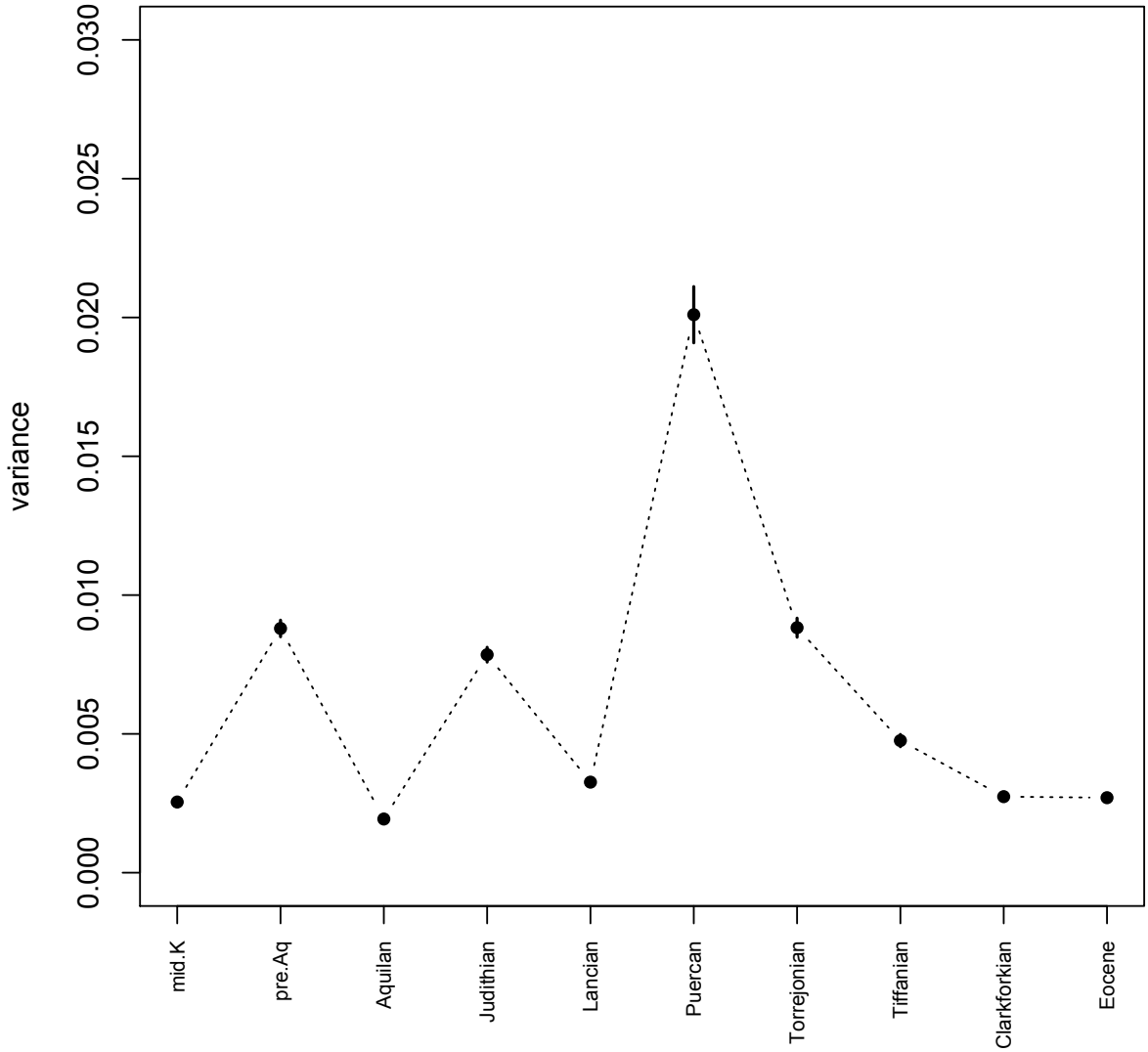

2.11.5 SUPPLEMENTARY DATA SD5

Table 2.11.5.—Cimolodontan species from the Late Cretaceous and early Paleogene of North America used to construct Figure 2.5. Lists are separated by the time bins specified in the main text. Sources for the occurrence of each species is also provided. Note that these are raw species counts, and include some tentative species occurrences (see main text for details).

Mid-Cretaceous		
Family	*Genus species*	Source
"*Paracimexomys* group"	*Bryceomys intermedius*	Kielan-Jaworowska et al. 2004
"*Paracimexomys* group"	*Cedaromys bestia*	Kielan-Jaworowska et al. 2004
"*Paracimexomys* group"	*Cedaromys parvus*	Kielan-Jaworowska et al. 2004
"*Paracimexomys* group"	cf. *Paracimexomys perplexus*	Kielan-Jaworowska et al. 2004
"*Paracimexomys* group"	cf. *Paracimexomys robisoni*	Kielan-Jaworowska et al. 2004
Cimolodontidae	*Cimolodon akersteni*	Weaver et al. 2019
?Neoplagiaulacidae	?*Mesodma* sp.	Kielan-Jaworowska et al. 2004
Pre-Aquilan		

Family	*Genus species*	Source
"*Paracimexomys* group"	*Bryceomys fumosus*	Kielan-Jaworowska et al. 2004
"*Paracimexomys* group"	*Bryceomys hadrosus*	Kielan-Jaworowska et al. 2004
"*Paracimexomys* group"	*Cedaromys minimus*	Eaton 2009
"*Paracimexomys* group"	*Cedaromys* sp. cf. *C. hutchisoni*	Kielan-Jaworowska et al. 2004
"*Paracimexomys* group"	*Paracimexomys* sp. cf. *P. priscus*	Kielan-Jaworowska et al. 2004
"*Paracimexomys* group"	cf. *Paracimexomys robisoni*	Kielan-Jaworowska et al. 2004
"*Paracimexomys* group"	*Dakotamys malcomi*	Kielan-Jaworowska et al. 2004
"*Paracimexomys* group"	*Dakotamys shakespeari*	Eaton 2013
Cimolodontidae	*Cimolodon similis*	Kielan-Jaworowska et al. 2004
Cimolodontidae	*Cimolodon nitidus*	Kielan-Jaworowska et al. 2004
Cimolodontidae	*Cimolodon foxi*	Eaton 2006a

Cimolomyidae	*Meniscoessus intermedius*	Kielan-Jaworowska et al. 2004
Cimolomyidae	*Cimolomys* sp.	Eaton 2013
Neoplagiaulacidae	*Mesodma* sp. cf. *M. minor*	Eaton 2006a

Aquilan

Family	*Genus species*	Source
"*Paracimexomys* group"	*Paracimexomys magister*	Kielan-Jaworowska et al. 2004
"*Paracimexomys* group"	*Bryceomys* sp. cf. *B. fumosus*	Eaton 2002
"*Paracimexomys* group"	*Cedaromys* sp. cf. *C. hutchisoni*	Eaton 2006b
"*Paracimexomys* group"	*Cimexomys antiquus*	Kielan-Jaworowska et al. 2004
"*Paracimexomys* group"	?*Cimexomys gregoryi*	Eaton and Cifelli 2013
Cimolodontidae	*Cimolodon electus*	Kielan-Jaworowska et al. 2004
Cimolodontidae	*Cimolodon similis*	Kielan-Jaworowska et al. 2004
Cimolodontidae	*Cimolodon wardi*	Eaton 2006b
Cimolodontidae	*Cimolodon* sp. cf. *C. nitidus*	Eaton 2002

Cimolodontidae	*Cimolodon* sp. cf. *C. foxi*	Eaton 2002
Cimolomyidae	*Cimolomys milliensis*	Eaton and Cifelli 2013
Cimolomyidae	*Cimolomys*sp. cf. *C. clarki*	Kielan-Jaworowska et al. 2004
Cimolomyidae	*Cimolomys*sp. cf. *C. trochuus*	Eaton 2002
Cimolomyidae	*Meniscoessus ferox*	Kielan-Jaworowska et al. 2004
Cimolomyidae	*Meniscoessus* sp. cf. *M. intermedius*	Eaton 2002
Neoplagiaulacidae	*Mesodma* sp. cf. *M. minor*	Eaton 2006b
Neoplagiaulacidae	*Mesodma* sp. cf. *M. formosa*	Kielan-Jaworowska et al. 2004
Neoplagiaulacidae	*Mesodma* sp. cf. *M. hensleighi*	Eaton and Cifelli 2013
Neoplagiaulacidae	*Mesodma* sp. cf. *M. archibaldi*	Eaton 2013
Neoplagiaulacidae	*Mesodma senecta*	Kielan-Jaworowska et al. 2004
incertae sedis	*Viridomys orbatus*	Kielan-Jaworowska et al. 2004

Judithian

Family	*Genus species*	Source
"*Paracimexomys* group"	*Cedaromys hutchisoni*	Eaton 2002

"*Paracimexomys* group"	*Paracimexomys magnus*	Kielan-Jaworowska et al. 2004
"*Paracimexomys* group"	*Paracimexomys priscus*	Kielan-Jaworowska et al. 2004
"*Paracimexomys* group"	*Cimexomys judithae*	Kielan-Jaworowska et al. 2004
"*Paracimexomys* group"	*Cimexomys* cf. *antiquus*	Kielan-Jaworowska et al. 2004
"*Paracimexomys* group"	?*Cimexomys gregoryi*	Kielan-Jaworowska et al. 2004
"*Paracimexomys* group"	?*Bryceomys* sp.	Kielan-Jaworowska et al. 2004
"*Paracimexomys* group"	*Dakotamys magnus*	Eaton 2002
Cimolodontidae	*Cimolodon nitidus*	Kielan-Jaworowska et al. 2004
Cimolodontidae	*Cimolodon electus*	Kielan-Jaworowska et al. 2004
Cimolodontidae	*Cimolodon similis*	Kielan-Jaworowska et al. 2004
Cimolodontidae	*Cimolodon foxi*	Eaton 2002
?Cimolodontidae	*Kaiparomys cifellii*	Eaton 2002

Cimolomyidae	*Meniscoessus intermedius*	Kielan-Jaworowska et al. 2004
Cimolomyidae	*Meniscoessus major*	Kielan-Jaworowska et al. 2004
Cimolomyidae	*Cimolomys clarki*	Kielan-Jaworowska et al. 2004
Cimolomyidae	*?Cimolomys butleria*	Eaton 2002
Cimolomyidae	?*Essonodon* sp.	Kielan-Jaworowska et al. 2004
Neoplagiaulacidae	*Mesodma archibaldi*	Eaton 2002
Neoplagiaulacidae	*Mesodma minor*	Eaton 2002
Neoplagiaulacidae	*Mesodma primaeva*	Kielan-Jaworowska et al. 2004
Neoplagiaulacidae	*Mesodma* cf. *formosa*	Kielan-Jaworowska et al. 2004
Neoplagiaulacidae	*Mesodma* cf. *hensleighi*	Kielan-Jaworowska et al. 2004
Neoplagiaulacidae	*Mesodma* cf. *senecta*	Kielan-Jaworowska et al. 2004
Ptilodontidae	*Kimbetohia campi*	Kielan-Jaworowska et al. 2004

‘Edmontonian’

Family	*Genus species*	Source
"*Paracimexomys* group"	*Paracimexomys propriscus*	Hunter et al. 2010
Cimolodontidae	*Cimolodon nitidus*	Kielan-Jaworowska et al. 2004
Cimolomyidae	*Cimolomys gracilis*	Kielan-Jaworowska et al. 2004
Cimolomyidae	*Meniscoessus collomensis*	Kielan-Jaworowska et al. 2004
Cimolomyidae	*Meniscoessus* aff. *intermedius*	Kielan-Jaworowska et al. 2004
Cimolomyidae	*Meniscoessus major*	Kielan-Jaworowska et al. 2004
Cimolomyidae	*Meniscoessus robustus*	Kielan-Jaworowska et al. 2004
Neoplagiaulacidae	*Nidimys occultus*	Hunter et al. 2010
Neoplagiaulacidae	*Mesodma thompsoni*	Kielan-Jaworowska et al. 2004

Lancian

Family	*Genus species*	Source
"*Paracimexomys* group"	*Paracimexomys priscus*	Kielan-Jaworowska et al. 2004

"*Paracimexomys* group"	*Cimexomys minor*	Kielan-Jaworowska et al. 2004
"*Paracimexomys* group"	*Cimexomys* cf. *gratus*	Kielan-Jaworowska et al. 2004
Cimolodontidae	*Cimolodon nitidus*	Kielan-Jaworowska et al. 2004
Cimolodontidae	*Cimolodon peregrinus*	Donohue et al. 2013
Cimolomyidae	*Cimolomys gracilis*	Kielan-Jaworowska et al. 2004
Cimolomyidae	*Cimolomys trochuus*	Kielan-Jaworowska et al. 2004
Cimolomyidae	*Essonodon browni*	Kielan-Jaworowska et al. 2004
Cimolomyidae	*Paressonodon nelsoni*	Wilson et al. 2010
Cimolomyidae	*Meniscoessus collomensis*	Kielan-Jaworowska et al. 2004
Cimolomyidae	*Meniscoessus conquistus*	Kielan-Jaworowska et al. 2004
Cimolomyidae	*Meniscoessus robustus*	Kielan-Jaworowska et al. 2004
Cimolomyidae	*Meniscoessus seminoensis*	Kielan-Jaworowska et al. 2004

Neoplagiaulacidae	*Mesodma formosa*	Kielan-Jaworowska et al. 2004
Neoplagiaulacidae	*Mesodma hensleighi*	Kielan-Jaworowska et al. 2004
Neoplagiaulacidae	*Mesodma thompsoni*	Kielan-Jaworowska et al. 2004
Neoplagiaulacidae	?*Neoplagiaulax burgessi*	Kielan-Jaworowska et al. 2004
Neoplagiaulacidae	*Parectypodus foxi*	Kielan-Jaworowska et al. 2004
Neoplagiaulacidae	*Parikimys carpenteri*	Wilson et al. 2010
Ptilodontidae	*Kimbetohia campi*	Kielan-Jaworowska et al. 2004
Eucosmodontidae	*Clemensodon megaloba*	Kielan-Jaworowska et al. 2004
Eucosmodontidae	*Stygimys cupressus*	Kielan-Jaworowska et al. 2004
Taeniolabidoidea?	*Bubodens magnus*	Kielan-Jaworowska et al. 2004
Taeniolabidoidea?	*"Catopsalis" johnstoni*	Kielan-Jaworowska et al. 2004
Taeniolabidoidea?	*"Catopsalis"* cf. *joyneri*	Kielan-Jaworowska et al. 2004

Puercan

Family	*Genus species*	Source
"*Paracimexomys* group"	*Cimexomys minor*	Weil and Krause 2008
"*Paracimexomys* group"	*Cimexomys arapahoensis*	Weil and Krause 2008
"*Paracimexomys* group"	*Cimexomys gratus*	Weil and Krause 2008
Neoplagiaulacidae	*Cernaysia davidi*	Weil and Krause 2008
Neoplagiaulacidae	*Ectypodus* sp.	Weil and Krause 2008
Neoplagiaulacidae	*Mesodma ambigua*	Weil and Krause 2008
Neoplagiaulacidae	*Mesodma formosa*	Weil and Krause 2008
Neoplagiaulacidae	*Mesodma hensleighi*	Weil and Krause 2008
Neoplagiaulacidae	*Mesodma thompsoni*	Weil and Krause 2008
Neoplagiaulacidae	*Neoplagiaulax kremnus*	Weil and Krause 2008
Neoplagiaulacidae	*Neoplagiaulax macintyrei*	Weil and Krause 2008
Neoplagiaulacidae	*Neoplagiaulax nelsoni*	Weil and Krause 2008
Neoplagiaulacidae	*Parectypodus armstrongi*	Weil and Krause 2008
Neoplagiaulacidae	*Parectypodus vanvaleni*	Weil and Krause 2008
Neoplagiaulacidae	*Xyronomys robinsoni*	Weil and Krause 2008
Ptilodontidae	*Baiotomeus* sp.	Weil and Krause 2008
Ptilodontidae	*Kimbetohia campi*	Weil and Krause 2008

Ptilodontidae	*Kimbetohia*? *mziae*	Weil and Krause 2008
Ptilodontidae	*Ptilodus montanus*	Weil and Krause 2008
Ptilodontidae	*Ptilodus tsosiensis*	Weil and Krause 2008
Eucosmodontidae	*Eucosmodon americanus*	Weil and Krause 2008
Eucosmodontidae	*Eucosmodon molestus*	Weil and Krause 2008
Eucosmodontidae	*Eucosmodon primus*	Weil and Krause 2008
Eucosmodontidae	*Stygimys kuszmauli*	Weil and Krause 2008
Eucosmodontidae	*Stygimys camptorhiza*	Weil and Krause 2008
Eucosmodontidae	*Stygimys teilhardi*	Weil and Krause 2008
Eucosmodontidae	*Stygimys vastus*	Weil and Krause 2008
Microcosmodontidae	*Acheronodon garbanii*	Weil and Krause 2008
Microcosmodontidae	*"Microcosmodon" arcuatus*	Weil and Krause 2008
Microcosmodontidae	*"Microcosmodon" harleyi*	Weil and Krause 2008
Taeniolabidoidea	*Catopsalis foliatus*	Weil and Krause 2008
Taeniolabidoidea	*Catopsalis alexanderi*	Weil and Krause 2008
Taeniolabidoidea	*Catopsalis waddleae*	Weil and Krause 2008
Taeniolabidoidea	*Taeniolabis taoensis*	Weil and Krause 2008
Taeniolabidoidea	*Taeniolabis lamberti*	Weil and Krause 2008
Taeniolabidoidea	*Valenopsalis joyneri*	Williamson et al. 2015
Taeniolabidoidea	*Kimbetopsalis simmonsae*	Williamson et al. 2015

Torrejonian

Family	*Genus species*	Source

Cimolodontidae	*Anconodon gidleyi*	Weil and Krause 2008
Cimolodontidae	*Anconodon cochranensis*	Weil and Krause 2008
Cimolodontidae	*Anconodon lewisi*	Weil and Krause 2008
Neoplagiaulacidae	*Ectypodus aphronorus*	Weil and Krause 2008
Neoplagiaulacidae	*Ectypodus szalayi*	Weil and Krause 2008
Neoplagiaulacidae	*Krauseia clemensi*	Weil and Krause 2008
Neoplagiaulacidae	*Mesodma pygmaea*	Weil and Krause 2008
Neoplagiaulacidae	*Mimetodon krausei*	Weil and Krause 2008
Neoplagiaulacidae	*Mimetodon silberlingi*	Weil and Krause 2008
Neoplagiaulacidae	*Neoplagiaulax grangeri*	Weil and Krause 2008
Neoplagiaulacidae	*Neoplagiaulax hunteri*	Weil and Krause 2008
Neoplagiaulacidae	*Neoplagiaulax macintyrei*	Weil and Krause 2008
Neoplagiaulacidae	*Neoplagiaulax macrotomeus*	Weil and Krause 2008
Neoplagiaulacidae	*Neoplagiaulax nelsoni*	Weil and Krause 2008
Neoplagiaulacidae	*Parectypodus corystes*	Weil and Krause 2008
Neoplagiaulacidae	*Parectypodus sinclairi*	Weil and Krause 2008
Neoplagiaulacidae	*Parectypodus sylviae*	Weil and Krause 2008
Neoplagiaulacidae	*Parectypodus trovessartianus*	Weil and Krause 2008
Neoplagiaulacidae	*Xyronomys swainae*	Weil and Krause 2008
Ptilodontidae	*Baiotomeus douglassi*	Weil and Krause 2008
Ptilodontidae	*Baiotomeus lamberti*	Weil and Krause 2008
Ptilodontidae	*Baiotomeus rhothonion*	Weil and Krause 2008
Ptilodontidae	*Ptilodus mediaevus*	Weil and Krause 2008

Ptilodontidae	*Ptilodus gnomus*	Weil and Krause 2008
Ptilodontidae	*Ptilodus montanus*	Weil and Krause 2008
Ptilodontidae	*Ptilodus wyomingensis*	Weil and Krause 2008
Eucosmodontidae	*Eucosmodon molestus*	Weil and Krause 2008
Eucosmodontidae	*Stygimys jepseni*	Weil and Krause 2008
Microcosmodontidae	*Acheronodon* sp.	Weil and Krause 2008
Microcosmodontidae	*Microcosmodon* cf. *M. harleyi*	Clemens and Wilson 2009
Microcosmodontidae?	*Alopocosmodon hadrus*	Scott et al. 2013
Taeniolabidoidea	*Catopsalis calgariensis*	Weil and Krause 2008
Taeniolabidoidea	*Catopsalis fissidens*	Weil and Krause 2008
Taeniolabidoidea	*Catopsalis kakwa*	Scott et al. 2018
incertae sedis	*Xanclomys mcgrewi*	Weil and Krause 2008

Tiffanian

Family	*Genus species*	Source
Cimolodontidae	*Anconodon gidleyi*	Weil and Krause 2008
Cimolodontidae	*Anconodon cochranensis*	Weil and Krause 2008
Cimolodontidae	*Anconodon lewisi*	Weil and Krause 2008
Neoplagiaulacidae	*Ectypodus musculus*	Weil and Krause 2008
Neoplagiaulacidae	*Ectypodus aphronorus*	Weil and Krause 2008
Neoplagiaulacidae	*Ectypodus elaphus*	Weil and Krause 2008
Neoplagiaulacidae	*Ectypodus powelli*	Weil and Krause 2008
Neoplagiaulacidae	*Ectypodus szalayi*	Weil and Krause 2008

Neoplagiaulacidae	*Ectypodus tardus*	Weil and Krause 2008
Neoplagiaulacidae	*Krauseia clemensi*	Weil and Krause 2008
Neoplagiaulacidae	*Mesodma pygmaea*	Weil and Krause 2008
Neoplagiaulacidae	*Mimetodon churchilli*	Weil and Krause 2008
Neoplagiaulacidae	*Mimetodon silberlingi*	Weil and Krause 2008
Neoplagiaulacidae	*Neoplagiaulax cimolodontoides*	Weil and Krause 2008
Neoplagiaulacidae	*Neoplagiaulax hazeni*	Weil and Krause 2008
Neoplagiaulacidae	*Neoplagiaulax hunteri*	Weil and Krause 2008
Neoplagiaulacidae	*Neoplagiaulax jepi*	Weil and Krause 2008
Neoplagiaulacidae	*Neoplagiaulax mckennai*	Weil and Krause 2008
Neoplagiaulacidae	*Neoplagiaulax nanophus*	Weil and Krause 2008
Neoplagiaulacidae	*Neoplagiaulax nelsoni*	Weil and Krause 2008
Neoplagiaulacidae	*Neoplagiaulax paskapooensis*	Weil and Krause 2008
Neoplagiaulacidae	*Neoplagiaulax serrator*	Weil and Krause 2008
Neoplagiaulacidae	*Parectypodus corystes*	Weil and Krause 2008
Neoplagiaulacidae	*Parectypodus laytoni*	Weil and Krause 2008
Neoplagiaulacidae	*Parectypodus sinclairi*	Weil and Krause 2008
Neoplagiaulacidae	*Parectypodus sloani*	Weil and Krause 2008
Neoplagiaulacidae	*Parectypodus sylviae*	Weil and Krause 2008
Ptilodontidae	*Baiotomeus douglassi*	Weil and Krause 2008
Ptilodontidae	*Baiotomeus lamberti*	Weil and Krause 2008
Ptilodontidae	*Baiotomeus russelli*	Weil and Krause 2008
Ptilodontidae	*Prochetodon cavus*	Weil and Krause 2008

Ptilodontidae	*Prochetodon foxi*	Weil and Krause 2008
Ptilodontidae	*Prochetodon speirsae*	Weil and Krause 2008
Ptilodontidae	*Ptilodus mediaevus*	Weil and Krause 2008
Ptilodontidae	*Ptilodus fractus*	Weil and Krause 2008
Ptilodontidae	*Ptilodus gnomus*	Weil and Krause 2008
Ptilodontidae	*Ptilodus kummae*	Weil and Krause 2008
Ptilodontidae	*Ptilodus montanus*	Weil and Krause 2008
Ptilodontidae	*Ptilodus wyomingensis*	Weil and Krause 2008
Microcosmodontidae	*Allocosmodon woodi*	Weil and Krause 2008
Microcosmodontidae	*Acheronodon vossae*	Weil and Krause 2008
Microcosmodontidae	*Microcosmodon conus*	Weil and Krause 2008
Microcosmodontidae	*Pentacosmodon pronus*	Weil and Krause 2008
Microcosmodontidae	*Pentacosmodon bowensis*	Weil and Krause 2008
Taeniolabidoidea	*Catopsalis calgariensis*	Weil and Krause 2008
incertae sedis	*Fractinus palmorum*	Weil and Krause 2008
incertae sedis	*Neoliotomus conventus*	Weil and Krause 2008

Clarkforkian

Family	*Genus species*	Source
Neoplagiaulacidae	*Ectypodus powelli*	Weil and Krause 2008
Neoplagiaulacidae	*Parectypodus laytoni*	Weil and Krause 2008
Ptilodontidae	*Prochetodon taxus*	Weil and Krause 2008
Ptilodontidae	*Prochetodon* sp. cf. *P. cavus*	Krause 1980

Ptilodontidae	*Ptilodus* sp.	Krause 1980
Microcosmodontidae	*Microcosmodon conus*	Weil and Krause 2008
Microcosmodontidae	*Microcosmodon rosei*	Weil and Krause 2008
incertae sedis	*Neoliotomus conventus*	Weil and Krause 2008

Eocene

Family	*Genus species*	Source
Neoplagiaulacidae	*Ectypodus childei*	Weil and Krause 2008
Neoplagiaulacidae	*Ectypodus lovei*	Weil and Krause 2008
Neoplagiaulacidae	*Ectypodus szalayi*	Weil and Krause 2008
Neoplagiaulacidae	*Ectypodus tardus*	Weil and Krause 2008
Neoplagiaulacidae	*Parectypodus simpsoni*	Weil and Krause 2008
Neoplagiaulacidae	*Parectypodus lunatus*	Weil and Krause 2008
incertae sedis	*Neoliotomus ultimus*	Weil and Krause 2008

LITERATURE CITED

CLEMENS, W. A., AND G. P. WILSON. 2009. Early Torrejonian mammalian local faunas from northeastern Montana, U.S.A. Pp. 111–158 in Papers on geology, vertebrate paleontology, and biostratigraphy in honor of Michael O. Woodburne (L. B. Albright, III, ed.). Museum of Northern Arizona Bulletin 65. Flagstaff, Arizona.

DONOHUE, S. L., G. P. WILSON, AND B. H. BREITHAUPT. 2013. Latest Cretaceous multituberculates of the Black Butte Station local fauna (Lance Formation, southwestern

Wyoming), with implications for compositional differences among mammalian local faunas of the Western Interior. Journal of Vertebrate Paleontology 33:677–695.

EATON, J. G. 2002. Multituberculate mammals from the Wahweap (Campanian, Aquilan) and Kaiparowits (Campanian, Judithian) Formations, within and near Grand Staircase-Escalante National Monument, southern Utah. Miscellaneous Publications of the Utah Geological Survey 02-4:1–66.

EATON, J. G. 2006a. Santonian (Late Cretaceous) mammals from the John Henry Member of the Straight Cliffs Formation, Grand Staircase-Escalante National Monument, Utah. Journal of Vertebrate Paleontology 26:446–460.

EATON, J. G. 2006b. Late Cretaceous mammals from Cedar Canyon, southwestern Utah; pp. 373–402 in Late Cretaceous Vertebrates from the Western Interior (S. G. Lucas and R. M. Sullivan, eds.). New Mexico Museum of Natural History and Science Bulletin 35. Albuquerque, New Mexico.

EATON, J. G. 2009. Cenomanian (Late Cretaceous) mammals from Cedar Canyon, southwestern Utah, and a revision of Cenomanian *Alphadon*-like marsupials. Pp. 97–110 in Papers on geology, vertebrate paleontology, and biostratigraphy in honor of Michael O. Woodburne (L. B. Albright III, ed.). Museum of Northern Arizona Bulletin 65. Flagstaff, Arizona.

EATON, J. G. 2013. Late Cretaceous mammals from Bryce Canyon National Park and vicinity, Paunsaugunt Plateau, southwestern Utah. Pp. 329–369 in At the top of the Grand Staircase: the Late Cretaceous of southern Utah (A. L. Titus and M. A. Loewen, eds.). Indiana University Press. Bloomington, Indiana.

EATON, J. G., AND R. L. CIFELLI. 2013. Review of Late Cretaceous mammalian faunas of the Kaiparowits and Paunsaugunt Plateaus, southwestern Utah. Pp. 319–328 in At the top of

the Grand Staircase: the Late Cretaceous of southern Utah (A. L. Titus and M. A. Loewen, eds.). Indiana University Press. Bloomington, Indiana.

HUNTER, J. P., R. E. HEINRICH, AND D. B. WEISHAMPEL. 2010. Mammals from the St. Mary River Formation (Upper Cretaceous), Montana. Journal of Vertebrate Paleontology 30:885–898.

KIELAN-JAWOROWSKA, Z., R. L. CIFELLI, AND Z.-X. LUO. 2004. Mammals from the age of dinosaurs: origins, evolution, and structure. Columbia University Press. New York, New York.

KRAUSE, D. W. 1980. Multituberculates from the Clarkforkian Land-Mammal Age, late Paleocene–early Eocene, of western North America. Journal of Paleontology 54:1163–1183.

SCOTT, C. S., D. N. SPIVAK, AND A. R. SWEET. 2013. First mammals from the Paleocene Porcupine Hills Formation of southwestern Alberta, Canada. Canadian Journal of Earth Sciences 50:355–378.

SCOTT, C. S., A. WEIL, AND J. M. THEODOR. 2018. A new, diminutive species of *Catopsalis* (Mammalia, Multituberculata, Taeniolabidoidea) from the early Paleocene of southwestern Alberta, Canada. Journal of Paleontology 92:896–910.

WEAVER, L. N., G. P. WILSON, L. J. KRUMENACKER, J. R. MOORE, AND D. J. VARRICCHIO. 2019. New multituberculate mammals from the mid-Cretaceous (lower Cenomanian) Wayan Formation of southeastern Idaho and implications for the early evolution of Cimolodonta. Journal of Vertebrate Paleontology, 39(2):e1604532.

WEIL, A., AND D. W. KRAUSE. 2008. Multituberculata. Pp. 19–38 in Evolution of Tertiary mammals of North America, Volume 2 (C. M. Janis, G. F. Gunnell, and M. D. Uhen, eds.). Cambridge University Press. Cambridge, United Kingdom.

WILLIAMSON, T. E., S. L. BRUSATTE, R. SECORD, AND S. SHELLEY. 2015. A new taeniolabidoid multituberculate (Mammalia) from the middle Puercan of the Nacimiento Formation, New Mexico, and a revision of taeniolabidoid systematics and phylogeny. Zoological Journal of the Linnean Society 177:183–208.

WILSON, G. P., M. DECHESNE, AND I. R. ANDERSON. 2010. New latest Cretaceous mammals from northeastern Colorado with biochronologic and biogeographic implications. Journal of Vertebrate Paleontology 30:499–520.

2.11.6 SUPPLEMENTARY DATA SD6

Figure 2.11.6.—The p4 ratio disparity patterns of all cimolodontans in our dataset (gray line) vs. the p4 ratio disparity patterns of all cimolodontans in our dataset except the Taeniolabidoidea, Microcosmodontidae, and Eucosmodontidae (black line). **A**, H:L disparity per time bin; **B**, L1:L disparity per time bin; **C**, H1:H disparity per time bin. Note that for each ratio, there is no peak in disparity in the Puercan when the Taeniolabidoidea, Microcosmodontidae, and Eucosmodontidae are removed from our analyses.

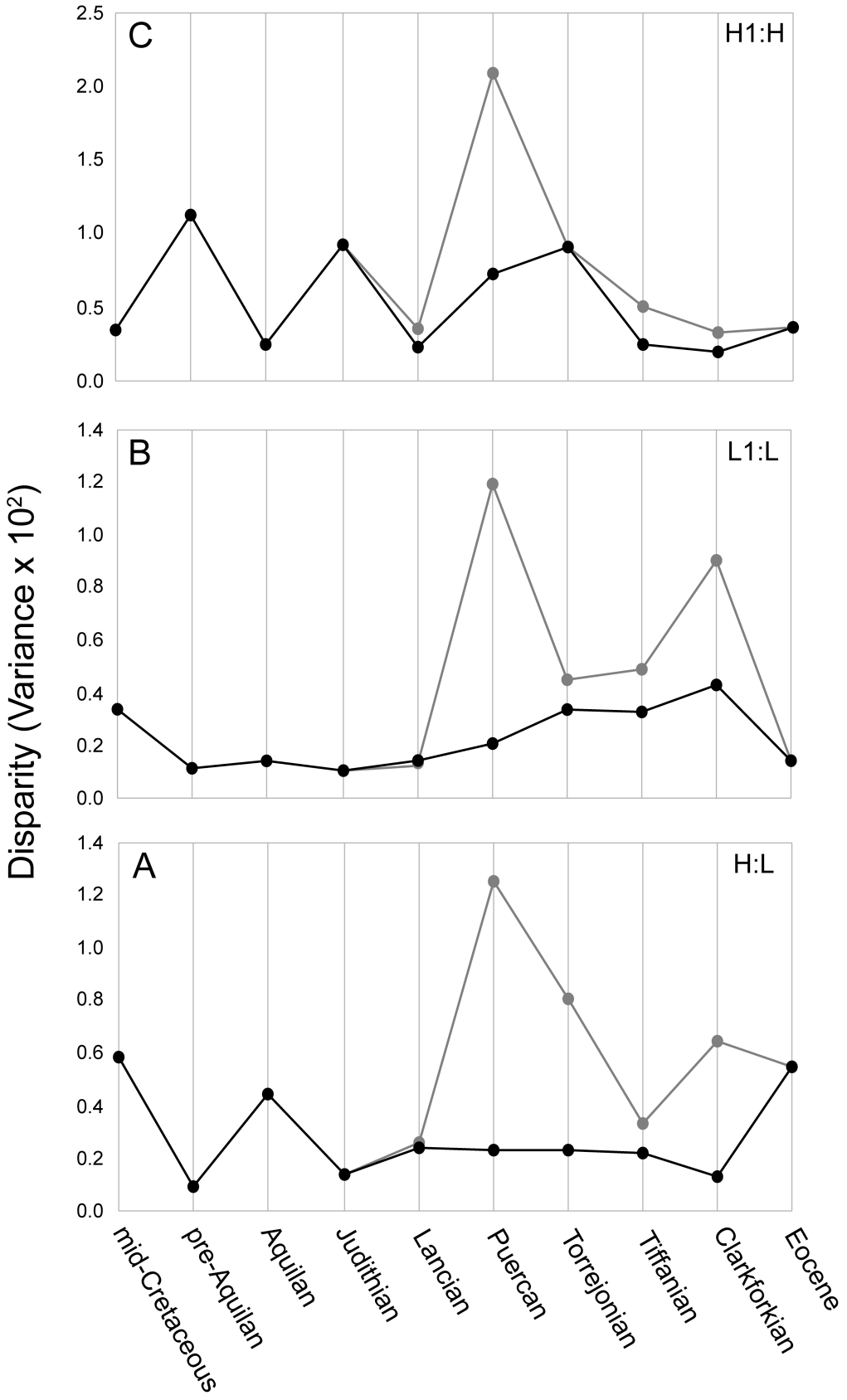
C
H1:H
B
L1:L
A
H:L
Disparity (Variance x 10²)
2.5
2.0
1.5
1.0
0.5
0.0
1.4
1.2
1.0
0.8
0.6
0.4
0.2
0.0
mid-Cretaceous
pre-Aquilan
Aquilan
Judithian
Lancian
Puercan
Torrejonian
Tiffanian
Clarkforkian
Eocene

CHAPTER 3: EARLY MAMMALIAN SOCIAL BEHAVIOUR REVEALED BY MULTITUBERCULATES FROM A DINOSAUR NESTING SITE

Weaver, LN., Varricchio, DJ., Sargis, EJ., Chen, M., Freimuth, WJ., & Wilson Mantilla, GP. (2021) Early mammalian social behavior revealed by multituberculates from a dinosaur nesting site. *Nature Ecology & Evolution* 5:32–37.

3.1 AUTHOR CONTRIBUTIONS

LNW, GPWM, DJV, and EJS conceived of the study. DJV led data collection in the field. LNW, DJV, and WJF led taphonomic analyses. DJV and WJF led geologic and ichnologic analyses. LNW and EJS led functional morphological analyses. MC led quantitative analyses. LNW collected all specimen data. LNW and GPWM led taxonomic analyses. LNW made the figures and wrote the manuscript with substantial input from all coauthors.

3.2 ABSTRACT

When sociality evolved, and in which groups, remain open questions in mammalian evolution, largely due to the fragmentary Mesozoic mammal fossil record. Nevertheless, exceptionally preserved fossils collected within well-constrained geologic and spatial frameworks can provide glimpses into these more fleeting aspects of early mammalian behaviour. Here we report on exceptional specimens of a multituberculate, *Filikomys primaevus* gen. nov., from the Late Cretaceous of Montana, primarily occurring as multi-individual, monospecific aggregates of semi-articulated skulls and skeletons within a narrow stratigraphic (~ 9 cm thick) and geographic (< 32 m^2) interval. Taphonomic and geologic evidence indicates that *F. primaevus* engaged in multi-generational, group-nesting and burrowing behaviour, representing the first example of social behaviour in a Mesozoic mammal. That *F. primaevus* was a digger is further supported by

functional morphological and morphometric analyses of its postcranium. The social behaviour of *F. primaevus* suggests that the capacity for mammals to form social groups extends back to the Mesozoic and is not restricted to therians. Sociality is likely an evolutionary labile trait that has arisen numerous times during the course of mammalian evolution.

3.3 INTRODUCTION

Mammals have evolved a diversity of social behaviours, from small, pair-bonded units to complex eusocial systems[1,2,3,4,5]. Sociality, broadly defined as group-living among conspecifics[1,2], confers advantages in predator avoidance, resource acquisition, and thermoregulation[2,4,5,6]. Solitary living is considered ancestral in mammals because individuals in most extant species (~70%) do not interact with each other outside of reproductive behaviours[1,2,3]. Whereas sociality is absent in Monotremata and is largely restricted to Diprotodontia (e.g., kangaroos) within Marsupialia, it occurs in ~50% of extant orders of Placentalia[2]. Accordingly, this trait was thought to have evolved after the mass extinction event at the Cretaceous-Paleogene (K-Pg) boundary (66 million years ago [Ma]) and with the ensuing evolutionary radiation of Placentalia[1,3]. In contrast, here we establish that social behaviour evolved earlier in mammalian history and beyond Theria (the node based clade of Marsupialia and Placentalia). We report exceptional specimens of a multituberculate mammal, *Filikomys primaevus* gen. nov., from the late Campanian (ca. 75.5 Ma) Egg Mountain locality of western Montana. They occur as tightly packed, multi-individual, monospecific aggregates of semi-articulated skulls and skeletons. Evidence from functional morphology, taphonomy, ichnology, and sedimentology indicates multi-generational, group-nesting and burrowing behaviour in *F.*

primaevus—the first example of social behaviour in a Mesozoic mammal, and the phylogenetically most basal example of sociality within Mammalia.

Multituberculates were mostly small-bodied (< 1 kg), omnivorous or herbivorous mammals that ranged from the Middle Jurassic to the late Eocene (ca. 166–35 Ma)[7,8,9,10]. Associated postcranial and craniodental remains of Mesozoic multituberculates are rare and known mostly from Asia[11,12]. Those specimens strongly influence our understanding of the paleobiology and phylogeny of multituberculates[12,13], but our understanding of multituberculate macroevolution[8,14] stems from North America's larger and more continuous fossil record of mostly isolated teeth and jaws[7]. The material described herein includes the first associated multituberculate skeletons from the Mesozoic of North America and represents the oldest-known case of burrowing capabilities in a Mesozoic multituberculate (Fig. 3.1).

3.4 RESULTS AND DISCUSSION

Mammalia Linnaeus, 1758[15]

Multituberculata Cope, 1884[16]

Cimolodonta McKenna, 1975[17]

Ptilodontoidea Sloan and Van Valen, 1965[18]

Filikomys gen. nov.

Filikomys primaevus (Lambe, 1902)[19]

Etymology. *Filikós* (Greek), friendly or neighborly, in reference to the inferred social behaviour of this animal; -*mys* (Greek), mouse, a common suffix used for multituberculate genera; *Primaevus* (Latin), youthful[19].

Holotype. NMC 1890, right dentary fragment with p4 and m1 preserved.

Diagnosis. Differing from all other cimolodontan multituberculates in: low number of cusps and serrations on its molars and ultimate premolars, but p4 also projects above the level of the molars and is much longer than m1. Full diagnosis in Supplementary Discussion.

A crushed skull, dentaries, and associated vertebrae (MOR 302) were previously described from Egg Mountain[20] and assigned to *Cimexomys judithae*; however, those authors noted differences from the holotype of *C. judithae* (AMNH 77100, isolated p4[21]) and from all other species of *Cimexomys*[20]. We propose that those differences and others (Supplementary Discussion) justify the erection of a new genus, *Filikomys*. *Filikomys* retains character states that are plesiomorphic for Cimolodonta (e.g., low number of cusps on molars and P4) but also exhibits a large p4 that protrudes dorsally above the level of the molars. This derived trait (and others) unites *Filikomys* with the Ptilodontoidea, an endemic group of North American cimolodontans[7] (Supplementary Discussion). We also argue that several Campanian species that were previously assigned to the genus *Mesodma*[22,23] should be reassigned to *Filikomys* (Supplementary Discussion). *Mesodma* is a ptilodontoid genus that survived the K-Pg mass extinction and was the most abundant mammal in the post-K-Pg 'disaster faunas' of North America[24,25]. Our phylogenetic analysis supports an interpretation of *Filikomys* as morphologically intermediate between basal cimolodontans (e.g., *Cimexomys*) and other ptilodontoids (e.g., *Mesodma*; Extended Data Figure 3.9.1); *Filikomys* is most often recovered as the basal-most ptilodontoid (Extended Data Figure 3.9.2; Supplementary Discussion), implying that its behavioural traits (i.e., sociality, burrowing) may be ancestral for *Mesodma* and all other ptilodontoids.

The Egg Mountain locality of the Two Medicine Formation (Campanian, ca. 75.5 Ma) is a well-known dinosaur nesting site[26] that has also yielded exceptionally preserved squamate[27] and mammal[16,28] fossils. On the basis of the sedimentology and invertebrate ichnology (Extended Data Figure 3.9.3), we interpret the depositional environment as incipient, well-drained soils formed in semi-arid conditions[29,30] (Supplementary Discussion). The fossils reported herein were recovered as localized, monospecific aggregates from a 56-m^3 volume (7 x 8 x 1 m) at Egg Mountain (Fig. 3.2). They represent a minimum of 22 multituberculate individuals, all of which we refer to *F. primaevus* (Extended Data Figure 3.9.1; Supplementary Discussion). The aggregates are found throughout the quarry, both laterally and vertically (Fig. 3.2; Extended Data Figure 3.9.3).

The sedimentary rock units at Egg Mountain are generally massive and lack clear bedding planes, so the stratigraphic positions of the *F. primaevus* aggregates were recorded on the basis of jackhammer passes (JHP)—stratigraphically parallel cuts that proceeded at ~10 cm-deep intervals through the quarry (Supplementary Methods). The stratigraphically higher aggregates (from JHP 1, 3, 6, and 7) consist of craniodental remains from one or two individuals, except for MOR 11750 from JHP 3, which preserves articulated postcranial remains (Fig. 3.2). In contrast, the four *F. primaevus* aggregates recovered from JHP 8 each comprise two to five individuals, totaling a minimum of 13 individuals represented by articulated postcranial and craniodental elements preserved in close proximity (Fig. 3.2). These JHP 8 aggregates form the basis of the taphonomic description and analysis presented herein (Supplementary Discussion), whereas future preparation and study of the stratigraphically higher aggregates will determine whether those more fragmentary specimens had distinct taphonomic histories.

Two small blocks (MOR 10908) from JHP 8 that were collected less than 40 cm apart from each other preserve five partial skulls and numerous articulated, semi-articulated, and disarticulated (but associated) postcranial remains that together represent at least five individuals of *F. primaevus* (Fig. 3.1; Fig. 3.2c, d; Supplementary Discussion). The morphology of MOR 10908 shows that the aggregate includes individuals of different ontogenetic stages (Extended Data Figure 3.9.4; Supplementary Discussion). MOR10908B and 10908E are classified as subadults by their unfused cranial sutures, unworn cheek teeth, incomplete dental eruption, and unfused femoral epiphyses[31] (Extended Data Figure 3.9.4). In contrast, MOR 10908A, 10908C, and 10908D exhibit traits characteristic of adult individuals: fused cranial sutures, worn cheek teeth, and fused long bone epiphyses[31] (Extended Data Figure 3.9.4). Although the other *F. primaevus* aggregates from JHP 8 have not been fully prepared (Supplementary Table 3.12.1), it is clear that they also constitute a mixture of different ontogenetic stages (Fig. 3.2).

These well-preserved, monospecific aggregates of multiple individuals from multiple ontogenetic stages lead us to hypothesize that the JHP 8 assemblage captures either a single or multiple mortality event(s) of *F. primaevus* that were nesting together in life, likely within burrows. These JHP 8 specimens likely did not accumulate via physical processes[32] (e.g., fluvial transport or attrition), which do not preferentially preserve monospecific assemblages in small, isolated pockets[32]. There is also no sedimentological evidence of aquatic influence, and passive accumulation of vertebrate hardparts would have led to extensive subaerial weathering, which is not supported by the exceptional degree of preservation and articulation of the specimens[32] (Supplementary Discussion).

We propose that these specimens of *F. primaevus* accumulated via biogenic processes[32]. Extrinsic biogenic processes (e.g., predation or scavenging) typically do not produce spatially

restricted and monospecific assemblages[33,34]. The skeletal elements described herein are relatively complete, are often articulated (including teeth in occlusion), and show no signs of bite marks or acid etching from predator ingestion. Although the degree of disarticulation varies among the specimens (Fig. 3.2), the pattern of skeletal element preservation is more consistent with postmortem decay[35,36] and bioturbation[33] than with predatory behaviour[33,34]. Thus, these specimens likely represent a death assemblage (or assemblages) of individuals of *F. primaevus* that aggregated in life[32] (Supplementary Discussion).

The very close proximity of the five individuals in MOR 10908 (< 40 cm^2) is more indicative of gregarious social behaviour[32,38] than of parental care (Supplementary Discussion). The ratio of three adults to two subadults negates the possibility that this was simply a mother-offspring unit[4], even if parental care was protracted across multiple litters (and thus multiple ontogenetic stages)[39]. Further, the permanent cheek teeth that are preserved in the subadult specimens are fully erupted, and MOR 10908B even exhibits minor cheek-tooth wear, indicating nutritional independence from its mother[31]. Nonetheless, because females and their kin form the core of nearly every mammalian social group[1,2], these individuals were probably closely related.

In order to reduce predation pressures, social aggregations of small-bodied mammals such as *F. primaevus* (~27 g[8]) are rarely above ground and usually within a shelter, such as a burrow or a depression[4,6]. After the mortality event (or events), the skeletal remains would have been protected from full disassociation within a burrow[40,41,42] but still would have been subject to some postmortem disarticulation and bioturbation[34,36,42,43]. We have yet to identify a burrow structure at the site in association with specimens of *F. primaevus*, but notably most burrowing mammals do not line their burrows[44], greatly decreasing the preservation potential of these structures[45]. Given the homogenous and bioturbated nature of the Egg Mountain sediments, a

burrow structure would be difficult to identify or even preserve unless it was filled with sediment distinct from that into which the animal dug[42,43] (Supplementary Discussion). Alternatively, the individuals of *F. primaevus* could have nested above ground, perhaps among vegetation or within a small depression. This scenario would require that individuals were buried rapidly, for example, by a massive sediment influx, or else their remains would have been exposed to extensive subaerial weathering. Both the sedimentology and insect trace fossil record at Egg Mountain fail to support this alternative hypothesis[29] and are most consistent with the taphonomic interpretation that the mortality event (or events) occurred within a burrow (Supplementary Discussion).

The functional morphology of *F. primaevus* postcrania also supports the burrowing hypothesis. This animal was capable of powerful shoulder retraction, manual and digital flexion, and elbow extension, as inferred from forelimb features such as (i) a dorsoventrally long, craniocaudally narrow scapula with a prominent acromion process (Fig. 3.3a); (ii) a humerus with well-developed teres and deltopectoral crests and a medially projecting, robust entepicondyle (Fig. 3.3e); and (iii) an ulna with a long and robust olecranon process that has a deep medial fossa, respectively (Fig. 3.3b; Supplementary Discussion)[46,47]. *F. primaevus* was also capable of powerful hip extension and knee flexion, had a habitually flexed knee, and thus was adapted for ambulatory movements on the surface and maneuvering in tight, confined spaces (e.g., burrows) rather than terrestrial running and leaping[12]. The associated features include a (i) long ilium, deep, blade-like, and dorsolaterally flaring ischium (Fig. 3.3g), and large greater trochanter of the femur[48,49] (Fig. 3.3c); and (ii) an anteroposteriorly shallow distal femur with the articular surfaces of the femoral condyles primarily restricted to the posterior portion of the femur[50] (Fig. 3.3c). Moreover, a multivariate analysis[13] of postcranial measurements

demonstrates that *F. primaevus* is morphologically most similar to extant fossorial taxa (Fig. 3.3h; Extended Data Figure 3.9.5), a result that was driven primarily by the robustness of both the humerus and hind limb (Supplementary Discussion). Thus, multiple lines of evidence indicate that *F. primaevus* was a terrestrial, scratch-digging mammal, functionally analogous to the Least Chipmunk, *Neotamias minimus*.

The *F. primaevus* specimens from JHP 8, a monodominant assemblage of 13 individuals from a narrow stratigraphic (~ 9 cm) and geographic (< 32 m^2) interval, likely represent either (1) a single mass mortality event or (2) a series of group mortality events. As of yet, we have not observed marked variation in taphonomic modification within or among the four *F. primaevus* aggregates from JHP 8, suggesting there was little to no time averaging. This lends some support to the single mass mortality hypothesis, but the precise timing and mechanism of mortality is difficult to assess on an ecological time scale. Additional specimen preparation and taphonomic assessment may allow us to distinguish among these two mortality scenarios.

Nevertheless, given that many extant mammalian mass death assemblages accurately reflect the social structure and demographics of the living populations[51], we propose that the multituberculate assemblage from JHP 8 reflects colonial nesting behaviour in *F. primaevus*. Although it is possible that the *F. primaevus* aggregates from JHP 8 reflect ephemeral social groupings where individuals were driven into close proximity via a shared local resource, or were sheltering together for safety from predators or climatic events[1,4,6,52,53], most extant burrowing mammals exhibit protracted, rather than temporary, social behaviours[6]. Colonialism is defined as a prolonged occupation of a restricted geographic area and, among small mammals, is frequently associated with burrowing[1,4,6]. The JHP 8 assemblage preserves 13 individuals of *F. primaevus* in four groups over an area of < 32 m^2; this close proximity, coupled with their likely

preservation within burrows, is reminiscent of extant semi-fossorial mammal colonies (e.g., various rodents and lagomorphs)[1]. Further, if the JHP 8 assemblage, or the Egg Mountain multituberculate assemblage as a whole, reflects a series of group mortality events, that would be evidence of more prolonged occupation of a limited geographic area[32]; such site fidelity would also be consistent with colonial nesting in extant mammals[1,2,4,6].

These exceptionally preserved specimens of *F. primaevus* significantly advance our understanding of early mammalian evolution. Among Mesozoic mammals, they represent the most complete material from North America, the first occurrence of adults and subadults preserved in close association, the oldest-known case of burrowing capabilities in a multituberculate, and the earliest record of social behaviour. Additionally, the rich assemblage and multiple aggregates may represent the earliest evidence of colonial nesting in mammals. Despite accumulating evidence demonstrating that extinct lineages of Mesozoic mammals exploited a diversity of ecological niches approximating the complexity and specialization of extant therian mammals[13,54], sociality has largely been viewed as unique to Placentalia[1,3]. This view is now shifting, with social behaviour being documented in non-mammalian therapsids[55] and stem marsupials[56]. The social behaviour of *F. primaevus* indicates that mammalian sociality extends back to at least the Late Cretaceous, and likely further; the Multituberculata originated by at least the Middle Jurassic[10] and possibly as early as the Late Triassic[7]. Ecology and environment are thought to be central selective drivers of social evolution in placental mammals[5,6], and similar selective drivers likely triggered the evolution of social behaviour in non-therian mammals as well. Sociality appears to be an evolutionarily labile trait that arose independently numerous times throughout the course of mammalian evolution.

3.5 METHODS

All *Filikomys primaevus* specimens described herein were collected during the 2010–2016 field seasons at Egg Mountain (Teton County, Montana, U.S.A.). MOR 10908, 11750, and 11753 were manually prepared by Robert Masek. MOR 10908 was μCT scanned at the University of Washington on a North Star Imaging X5000 CT scanner with a Feinfocus FXE [11164478] Xray source and Perkin Elmer [XRD 1620/1621 AM/AN] detector, 85 kV voltage and 500 μA current. Post-processing and virtual reconstructions of μCT data were performed using Avizo Software (ThermoFisher Scientific, Version 9.2). Measurements were taken on virtually reconstructed elements in Avizo using the 'Measure' tool. Multivariate analyses follow previous methodologies[13]. Phylogenetic parsimony analyses were performed in PAUP* (version 4.0a) based on a previously compiled multituberculate character-taxon matrix[56], and node support was calculated using bootstrapping and Bremer support. For more details about the materials and methods used in this paper see Supplementary Methods.

3.6 ACKNOWLEDGMENTS

We thank the Museum of the Rockies, Beatrice R. Taylor Paleontological Resource Area, and Jack Horner for permission and support to excavate Egg Mountain, and the 2010–2016 Egg Mountain field crews for collecting the specimens described herein; R. Masek for his masterful preparation of the specimens; Misaki Ouchida for preparing the in-situ line drawings, skeletal reconstruction, and artistic reconstruction of the Egg Mountain multituberculates; A.L. Brannick and M. Rivin for μCT scanning specimens; J. Scannella and A. Atwater of the Museum of the Rockies for curatorial assistance; J.R. Moore for his geological insights at Egg Mountain; D.W. Krause for allowing study of the holotype of *Ptilodus kummae*, among other multituberculate

postcranial specimens; C.S. Scott for allowing study of unpublished multituberculate specimens at the Royal Tyrrell Museum; W.A. Clemens and P.A. Holroyd for access to University of California Museum of Paleontology specimens; D.L. Brinkman for facilitating access to the Yale Peabody Museum collections; D.M. Boyer for access to, and advice about, MorphoSource μCT data; D.M. Grossnickle, A.L. Brannick, M.R. Whitney, B.T. Hovatter, J.R. Claytor, P.K. Wilson, and C.A.E. Strömberg for helpful feedback on the manuscript and figures; R.R. Rogers, A.K. Behrensmeyer, and T.M. Bown for helpful discussions about Egg Mountain taphonomy; D.W. Krause, A. Weil, and C.S. Scott for discussions about multituberculates. Financial support was from the National Science Foundation Grants 0847777 (D.J.V.) and 1325674 (D.J.V. and G.P.W.), National Science Foundation Graduate Research Fellowship (L.N.W.), Doris O. and Samuel P. Welles Research Fund (L.N.W.), University of Washington Department of Biology (L.N.W. and G.P.W.), and the Burke Museum (L.N.W. and G.P.W).

3.7 REFERENCES

1. Poole, T. B. *Social Behaviour in Mammals* (Blackie, 1985).
2. Smith, J. E., Lacey E. A. & Hayes, L. D. in *Comparative Social Evolution* Ch. 10 (eds Rubenstein, D. R. & Abbot, P.) 284–319 (Cambridge Univ. Press, 2017).
3. Eisenberg, J. F. *The Mammalian Radiations: An Analysis of Trends in Evolution, Adaptation, and Behaviour* (Univ. Chicago Press, 1981).
4. Crook, J. H., Ellis, J. E. & Goss-Custard, J. D. Mammalian social systems: structure and function. *Anim. Behav*. **24**, 261–274 (1976).
5. Silk, J. B. The adaptive value of sociality in mammalian groups. *Phil. Trans. R. Soc. B* **362**, 539–559 (2007).

6. Ebensperger, L. A. A review of the evolutionary causes of rodent group-living. *Acta Theriol.* **46**, 115–144 (2001).

7. Kielan-Jaworowska, Z., Cifelli, R. L. & Luo, Z.-X. *Mammals from the Age of Dinosaurs: Origins, Evolution, and Structure* (Columbia Univ. Press, 2004).

8. Wilson, G. P. et al. Adaptive radiation of multituberculate mammals before the extinction of dinosaurs. *Nature* **483**, 457–460 (2012).

9. Grossnickle, D. M. & Polly, P. D. Mammal disparity decreases during the Cretaceous angiosperm radiation. *Proc. R. Soc. B* **280**, 20132110 (2013).

10. Luo, Z.-X., Gatesy, S. M., Jenkins, F. A., Jr., Amaral, W. W. & Shubin, N. H. Mandibular and dental characteristics of Late Triassic mammaliaform *Haramiyavia* and their ramifications for basal mammal evolution. *Proc. Natl Acad. Sci. USA* **112**, E7101–E7109 (2015).

11. Yuan, C.-X., Qiang, J., Meng, Q.-J., Tabrum, A. R. & Luo, Z.-X. Earliest evolution of multituberculate mammals revealed by a new Jurassic fossil. *Science* **341**, 779–783 (2013).

12. Kielan-Jaworowska, Z. & Gambaryan, P. P. Postcranial anatomy and habits of Asian multituberculate mammals. *Foss. Strat*. **36**, 1–92 (1994).

13. Chen, M. & Wilson, G. P. A multivariate approach to infer locomotor modes in Mesozoic mammals. *Paleobiology* **41**, 280–312 (2015).

14. Weaver, L. N. & Wilson, G. P. Shape disparity in the blade-like premolars of multituberculate mammals: functional constraints and the evolution of herbivory. *J. Mammal*. (2020).

15. Linnaeus, C. *Systema Naturae per Regna Triae Naturae, Secundum Classes, Ordines, Genera, Species, cum Characteribus, Differentiis, Synonymis Locis; Tomus I. Editio Decima, Reformata* (Laurentii Salvii, Stockholm, 1758).

16. Cope, E. D. The Vertebrata of the Tertiary Formations of the West. Book I. *Report U. S. Geol. Survey Territories, F. V. Hayden in charge* **3**, 1–1009 (1884).

17. McKenna, M. C. in *Phylogeny of the Primates* (eds Luckett, W. P. & Szalay, F. S.) 21–46 (Plenum, New York, 1975).

18. Sloan, R. E. & Van Valen, L. Cretaceous mammals from Montana. *Science* **148**, 220–227 (1965).

19. Lambe, L. M. New genera and species from the Belly River Series (mid-Cretaceous). *Contrib. Canadian Paleont*. **3**, 25–81 (1902).

20. Montellano, M., Weil, A. & Clemens, W. A. An exceptional specimen of *Cimexomys judithae* (Mammalia: Multituberculata) from the Campanian Two Medicine Formation of Montana, and the phylogenetic status of *Cimexomys*. *J. Vertebr. Paleontol*. **20**, 333–340 (2000).

21. Sahni, A. The vertebrate fauna of the Judith River Formation, Montana. *Bull. Am. Mus. Nat. Hist*. **147**, 321–412 (1972).

22. Clemens, W. A. Fossil mammals of the type Lance Formation, Wyoming: part I. introduction and Multituberculata. *Univ. Calif. Publ. Geol. Sci*. **48**, 1–105 (1964).

23. Eaton, J. G. Multituberculate mammals from the Wahweap (Campanian, Aquilan) and Kaiparowits (Campanian, Judithian) formations, within and near Grand Staircase-Escalante National Monument, southern Utah. *Misc. Publ. Utah Geol. Surv*. **02-4**, 1–66 (2002).

24. Wilson, G. P. in *Through the End of the Cretaceous in the Type Locality of the Hell Creek Formation in Montana and Adjacent Areas* (eds Wilson, G. P., Clemens, W. A., Horner, J. R. & Hartman, J. H.) 365–392 (Geol. Soc. Am. Spec. Pap. 503, 2014).

25. Smith, S. M. et al. Early mammalian recovery after the end-Cretaceous mass extinction: a high-resolution view from McGuire Creek area, Montana, USA. *Geol. Soc. Am. Bull*. **130**, 2000–2014 (2018).

26. Horner, J. R. in *Dinosaurs Past and Present, Volume II* (eds Czerkas, S. J. & Olson, E. C.) 50–63 (Natural History Museum of Los Angeles County, 1987).

27. DeMar, D. G., Conrad, J. L., Head, J. J., Varricchio, D. J & Wilson, G. P. A new Late Cretaceous iguanomorph from North America and the origin of New World Pleurodonta (Squamata, Iguania). *Proc. R. Soc. B* **284**, 20161902.

28. Montellano, M. *Alphadon halleyi* (Didelphidae, Marsupialia) from the Two Medicine Formation (Late Cretaceous, Judithian) of Montana. *J. Vertebr. Paleontol.* **8**, 378–382.

29. Freimuth, W. J. & Varricchio, D. J. Insect trace fossils elucidate depositional environments and sedimentation at a dinosaur nesting site from the Cretaceous (Campanian) Two Medicine Formation of Montana. *Palaeogeogr. Palaeoclimatol. Palaeoecol*. **534**, 109262 (2019).

30. Panascí, G. & Varricchio, D. J. A new enigmatic terrestrial trace *Feoichnus martini*, ichnosp. nov., from the Upper Cretaceous Two Medicine Formation (USA). *J. Paleontol*. **94**, 922–930 (2020).

31. Morris, P. A review of mammalian age determination methods. *Mammal Rev*. **2**, 69–104 (1972).

32. Rogers, R. R. & Kidwell, S. M. in *Bonebeds: Genesis, Analysis, and Paleobiological Significance* (eds Rogers, R. R., Eberth, D. A. & Fiorillo, A. R.) 1–64 (Univ. Chicago Press, 2007).

33. Brain, C. K. *The Hunters and the Hunted? An Introduction to African Cave Taphonomy* (Univ. Chicago Press, 1981).

34. Andrews, P. *Owls, Caves and Fossils* (London Nat. Hist. Mus. Publ., 1990).

35. Dodson, P. The significance of small bone in paleoecological interpretations. *Univ. Wyo. Contr. Geol*. **12**, 15–19 (1973).

36. Brand, L. R., Hussey, M. & Taylor, J. Decay and disarticulation of small vertebrates in controlled experiments. *J. Taph*. **1**, 69–95 (2003).

37. Armour-Chelu, M. & Andrews, P. Some effects of bioturbation by earthworms (Oligochaeta) on archaeological sites. *J. Archaeol. Sci*. **21**, 433–443 (1994).

38. Rogers, R. R. Taphonomy of three dinosaur bone beds in the Upper Cretaceous Two Medicine Formation of northwestern Montana: evidence for drought-related mortality. *PALAIOS* **5**, 394–413 (1990).

39. Russell, E. M. Patterns of parental care and parental investment in marsupials. *Biol. Rev*. **57**, 423–486 (1982).

40. Voorhies, M. R. in *The Study of Trace Fossils* (ed Frey, R. W.) 325–350 (Springer, 1975).

41. Behrensmeyer, A. K. & Hook, R. W. in *Terrestrial Ecosystems Through Time* (eds Behrensmeyer, A. K. et al.) 15–136 (Univ. Chicago Press, 1992).

42. Tomassini, R. L. et al. Microvertebrates preserved in mammal burrows from the Holocene of the Argentine Pampas: a taphonomic and paleoecological approach. *Hist. Biol*. **29**, 63–75 (2017).

43. Varricchio, D. J., Martin, A. J. & Katsura, Y. First trace and body fossil evidence of a burrowing, denning dinosaur. *Proc. R. Soc. B* **274**, 1361–1368 (2007).

44. Reichman, O. J. & Smith, S. C. Burrows and burrowing behaviour by mammals. *Curr. Mammal*. **2**, 197–244 (1990).

45. Genise, J. F. & Bown, T. M. New Miocene scarabeid and hymenopterous nests and early Miocene (Santacrucian) paleoenvironments, Patagonian Argentina. *Ichnos* **3**, 107–117 (1994).

46. Stein, B. R. in *Life Underground: The Biology of Subterranean Rodents* (eds Lacey, E. A., Patton, J. L. & Cameron, G. N.) 19–61 (Univ. Chicago Press, 2000).

47. Salton, J. A. & Sargis, E. J. in *Mammalian Evolutionary Morphology: A Tribute to Frederick S. Szalay* (eds Sargis, E. J. & Dagosto, M.) 51–71 (Springer Science, 2008).

48. Argot, C. Functional-adaptive analysis of the hindlimb anatomy of extant marsupials and the paleobiology of the Paleocene marsupials *Mayulestes ferox* and *Pucadelphys andinus*. *J. Morphol*. **253**, 76–108 (2002).

49. Sargis, E. J. Functional morphology of the hindlimb of tupaiids (Mammalia, Scandentia) and its phylogenetic implications. *J. Morphol*. **254**, 149–185 (2002).

50. Krause, D. W. & Jenkins, F. A. The postcranial skeleton of North American multituberculates. *Bull. Mus. Comp. Zool*. **150**, 200–246 (1983).

51. Berger, J. et al. Back-casting sociality in extinct species: new perspectives using mass death assemblages and sex ratios. *Proc. R. Soc. Lond. B* **268**, 131–139 (2001).

52. Schradin, C. et al. Social flexibility and social evolution in mammals: a case study of the African striped mouse (*Rhabdomys pumilio*). *Mol. Ecol*. **21**, 541–553 (2012).

53. Williams, C. T. et al. Communal nesting in an 'asocial' mammal: social thermoregulation among spatially dispersed kin. *Behav. Ecol. Sociobiol*. **67**, 757–763 (2013)

54. Luo, Z.-X. Transformation and diversification in early mammal evolution. *Nature* **450**, 1011–1019 (2007).

55. Jasinoski, S. C. & Abdala, F. Aggregations and parental care in the Early Triassic basal cynodonts *Galesaurus planiceps* and *Thrinaxodon liohinus*. *PeerJ* **5**, e2875 (2017).

56. Ladevéze, S., de Muizon, C., Beck, R. M. D., Germain, D. & Cespedes-Paz, R. Earliest evidence of mammalian social behaviour in the basal Tertiary of Bolivia. *Nature* **474**, 83–86 (2011).

57. Wang, H., Meng, J. & Wang, Y. Cretaceous fossil reveals a new pattern in mammalian middle ear evolution. *Nature* **576**, 102–105 (2019).

3.8 FIGURES

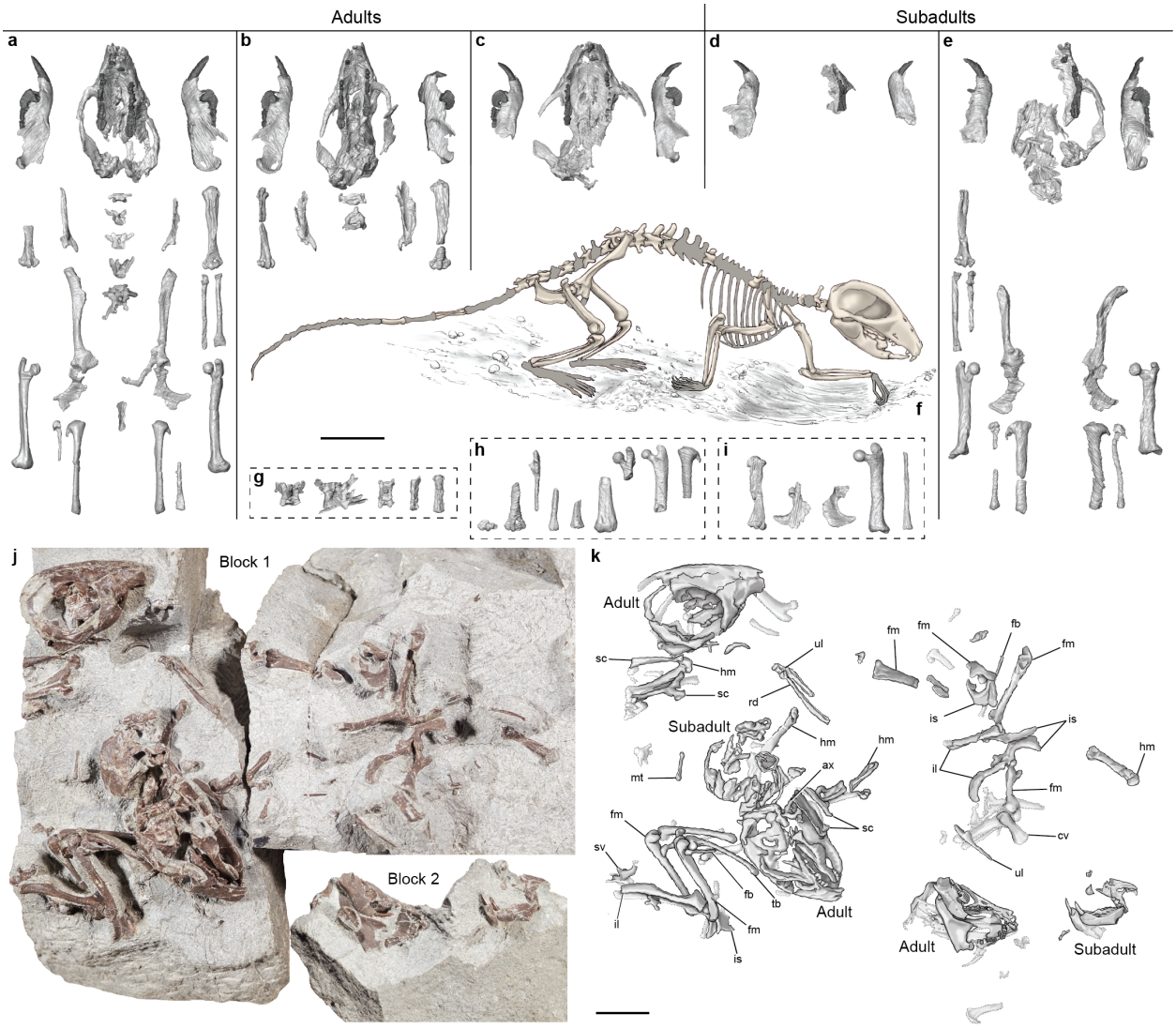

Figure 3.1 | Skeletal elements of the five *Filikomys primaevus* individuals preserved in MOR 10908 at Egg Mountain. **a**–**e**, Craniodental and closely associated postcranial remains of each individual. **a**–**c**, Adult individuals. **d**, **e**, Subadult individuals. **f**, Skeletal reconstruction of *F. primaevus* in a burrowing posture; grey regions represent skeletal elements that are missing (not to scale). **g**–**i**, Postcranial remains that were associated with craniodental remains but were not associated with a particular individual. **g**, Disarticulated vertebrae with unclear associations. **h**, Disarticulated forelimb and hind limb elements of adult individuals. **i**, Disarticulated forelimb,

pelvic, and hind limb elements of subadult individuals. Photographs (**j**) and annotated line drawings (**k**) of MOR 10908. MOR 10908 Block 1 preserves three partial crania and lower jaws, two adults (top and bottom) and one subadult (middle), two articulated pelves and hind limbs, two semi-articulated scapulae and forelimbs, other closely associated limb and girdle elements, articulated to closely associated vertebrae (including an atlas and axis), and a few isolated metapodials and phalanges. MOR 10908 Block 2 preserves two partial skulls and lower jaws, one adult (left) and one subadult (right), and an isolated tibia and distal humerus. These two blocks were found less than 40 cm apart and together represent the remains of five individuals. **Abbreviations**: **ax**, axis; **cv**, caudal vertebra; **fb**, fibula; **fm**, femur; **hm**, humerus; **il**, ilium; **is**, ischium; **mt**, metatarsal; **rd**, radius; **sc**, scapula; **sv**, sacral vertebra; **tb**, tibia; **ul**, ulna. Subadult and Adult labels indicate skulls. Scale bars = 1 cm.

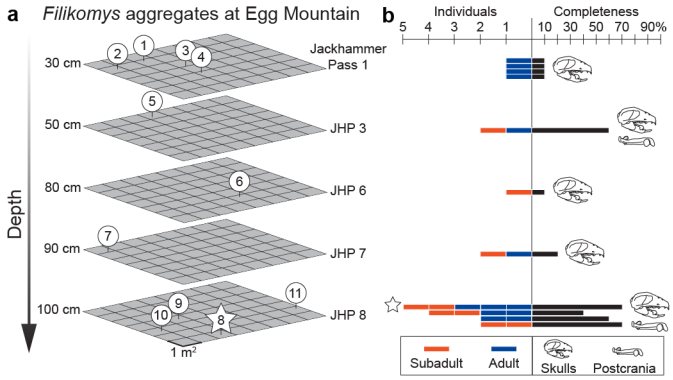

Figure 3.2 | Spatial distribution and composition of the monospecific *Filikomys primaevus* fossil aggregates at Egg Mountain. **a**, Grey boxes are the Egg Mountain quarry map broken into 1 m^2 grids with the numbered pins showing where different aggregates were recovered; these grids are arranged stratigraphically according to the jackhammer pass (JHP, to the right) at which different *F. primaevus* specimens were found (approximate depth in cm to the left). JHPs are stratigraphically parallel cuts that proceeded at ~10 cm-deep intervals through the quarry.

The star indicates MOR 10908, the aggregate highlighted in this paper. **b**, The number of adult and subadult individuals (to the left) and the skeletal completeness and specific elements that are preserved (to the right) are given for each aggregate. Adults are represented by blue bars and subadults are represented by orange bars. Completeness is defined as the percentage of 10 skeletal regions preserved: cranium, dentaries, vertebrae, ribs, pectoral girdle, pelvic girdle, forelimb, hind limb, forefoot, hind foot (e.g., aggregate 9 preserves the cranium, dentaries, forelimb, and hind limb: 40% completeness). Skeletal illustrations indicate whether the aggregate consists of craniodental material, or both craniodental and postcranial material. Note that only MOR 11750, 10908, and 11753 have been manually prepared, so the number of individuals and completeness percentages for the other aggregates are estimates based on those elements exposed on the rock surface. Aggregates: **1**, MOR 11747; **2**, MOR 11755; **3**, MOR 11748; **4**, MOR 11749; **5**, MOR 11750; **6**, MOR 11751; **7**, MOR 11756; **8**, MOR 10908; **9**, MOR 11752; **10**, MOR 11754; **11**, MOR 11753.

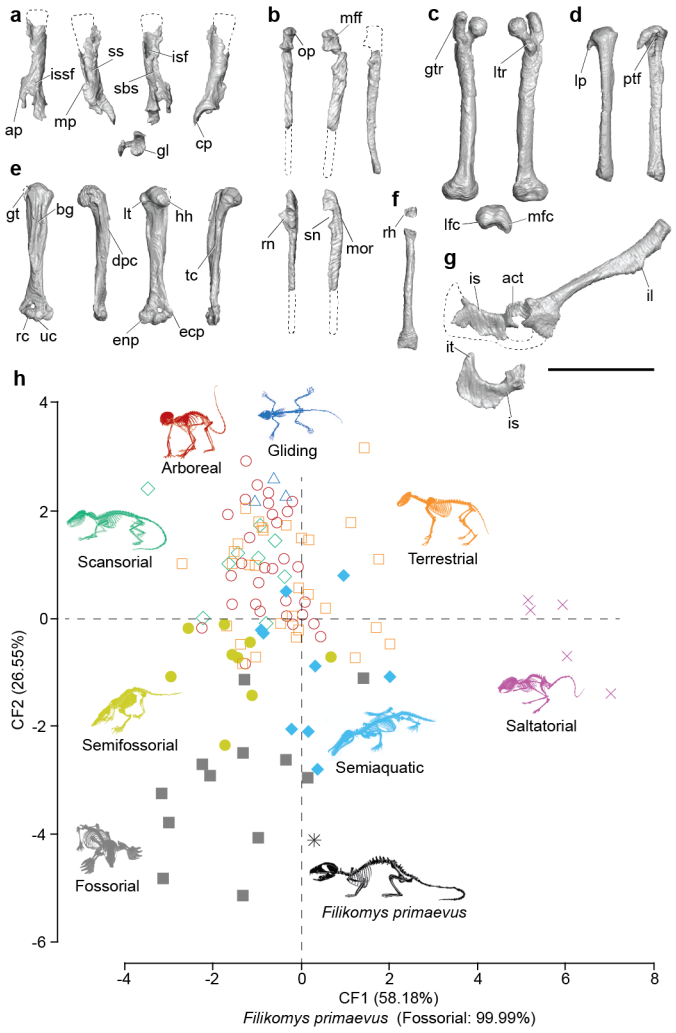

Figure 3.3 | Evidence for burrowing capabilities in *Filikomys primaevus*. **a**–**g**, µCT reconstructions of right limb and girdle elements from MOR 10908; dashed lines indicate damaged portions of the bone. **a**, Scapula in anterior, lateral, posterior, and medial views (left to right), and in ventral view (below). **b**, Ulnae from three individuals (two above, one below) in anterior and medial views (left to right). The top right ulna is reflected. **c**, Femur (reflected) in anterior (left), posterior (right), and distal (below) views. **d**, Tibia (reflected) in anterior and posterior views (left to right). **e**, Humerus (reflected) in ventral, lateral, dorsal, and medial views (left to right). **f**, Radius in anterior (below) and proximal (above) views. **g**, Pelvis in lateral view with complete, disarticulated ischium below. **h**, Results from the canonical variate analysis

(CVA), which plots *F. primaevus* near extant fossorial mammals and classifies *F. primaevus* as fossorial with a 99.99% posterior probability. **Abbreviations**: **act**, acetabulum; **ap**, acromion process; **bg**, bicipital groove; **cp**, coracoid process; **dpc**, deltopectoral crest; **ecp**, ectepicondyle; **enp**, entepicondyle; **gt**, greater tuberosity; **gtr**, greater trochanter; **hh**, humeral head; **il**, ilium; **is**, ischium; **isf**, infraspinous fossa; **issf**, incipient supraspinous fossa; **it**, ischial tuberosity; **lfc**, lateral femoral condyle; **lp**, lateral (hook-like) process; **lt**, lesser tuberosity; **ltr**, lesser trochanter; **mfc**, medial femoral condyle; **mff**, medial flexor fossa; **mor**, medial olecranon ridge; **mp**, metacromion process; **op**, olecranon process; **ptf**, posterior tibial fossa; **rc**, radial condyle; **rh**, radial head; **rn**, radial notch; **sbs**, subscapular spine; **sn**, semilunar notch; **ss**, scapular spine; **tc**, teres crest; **uc**, ulnar condyle. Scale bar = 1 cm.

3.9 EXTENDED DATA FIGURES

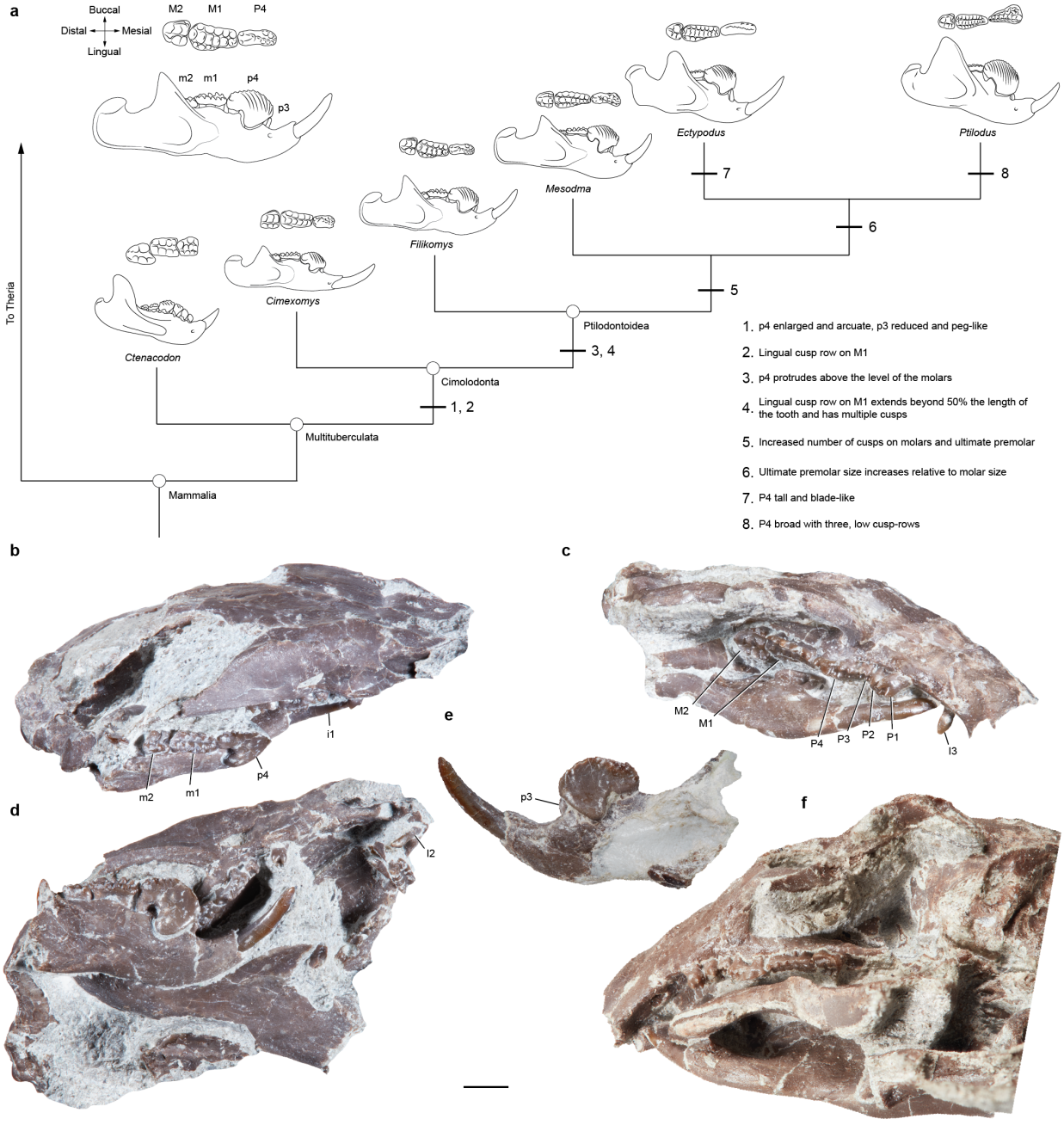

Figure 3.9.1 | Hypothesized phylogenetic relationships and comparative dental morphology of *Filikomys primaevus* and other North American multituberculates. **a**, Simplified cladogram showing changes in cheek tooth morphology among North American cimolodontans. *Filikomys* is morphologically intermediate between basal cimolodontans like *Cimexomys* and

ptilodontoids like *Mesodma*. We place *Filikomys* as a basal ptilodontoid based on a number of shared, derived craniodental character states. See Supplementary Information for further discussion. **b**, MOR 10908D, right lateral view of cranium and occlusal view of right lower dentition. **c**, MOR 10908A, right ventrolateral view of skull and near complete upper dentition (only I2 missing). **d**, MOR 10908D, ventral view of cranium and lateral views of right and left dentaries. **e**, MOR 11750, lateral view of left dentary. **f**, MOR 10908C, left ventrolateral view of skull and complete post-incisor upper dentition. Scale bar = 2 mm.

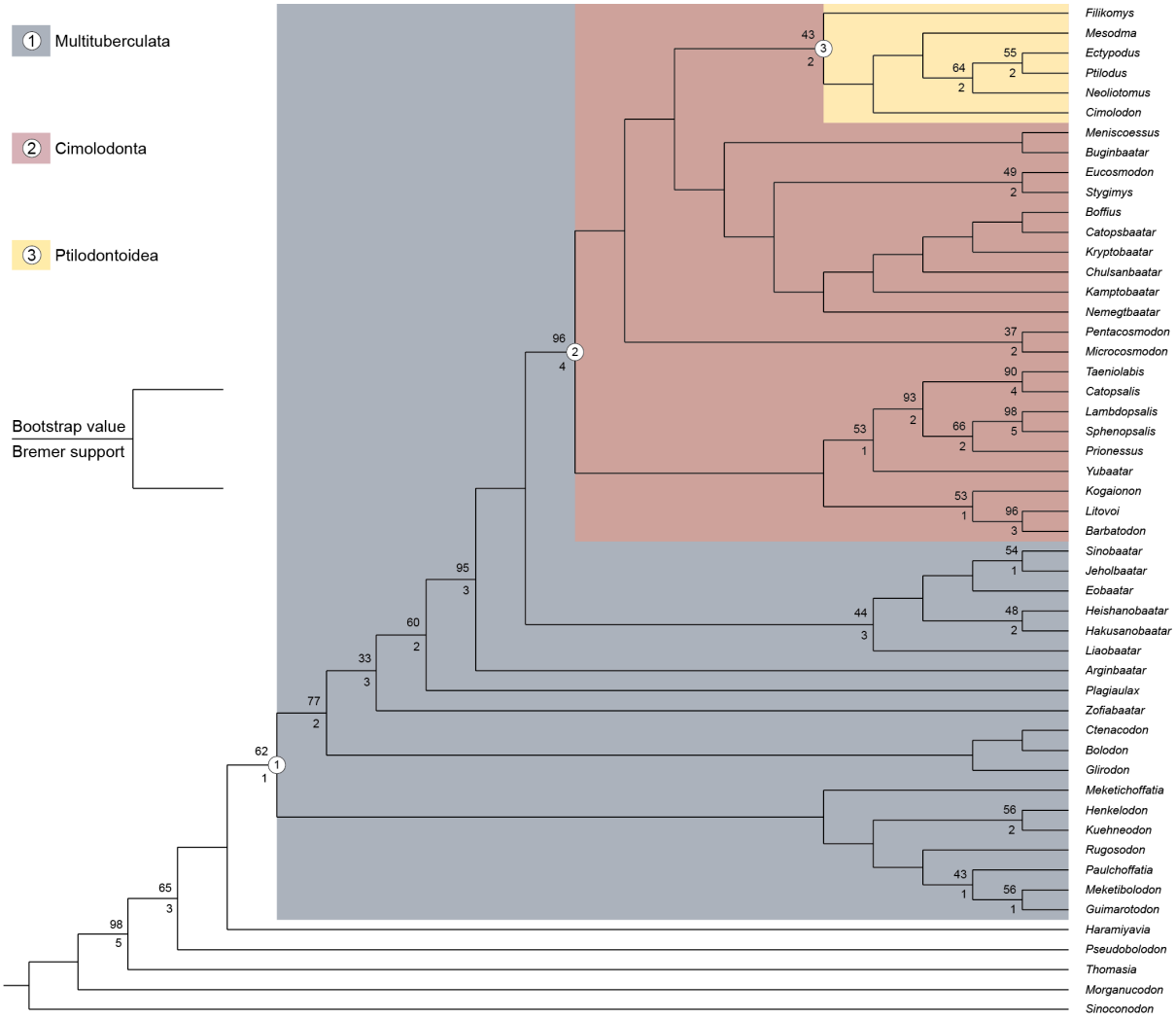

Figure 3.9.2 | Results from phylogenetic parsimony analysis on multituberculate character-taxon matrix containing 51 taxa and 130 characters. Illustrated is the 50% majority-rule consensus tree generated from the 356 shortest trees retained. Tree length = 478; Consistency Index = 0.43; Retention Index = 0.76. The numbers adjacent to certain nodes are bootstrap (above) and Bremer support (below) values; these values were only illustrated for nodes that had a bootstrap value of 40% or more and/or a Bremer support value of 2 or more. Multituberculata (node 1) is highlighted in blue, Cimolodonta (node 2) is highlighted in red, and Ptilodontoidea (node 3) is highlighted in yellow.

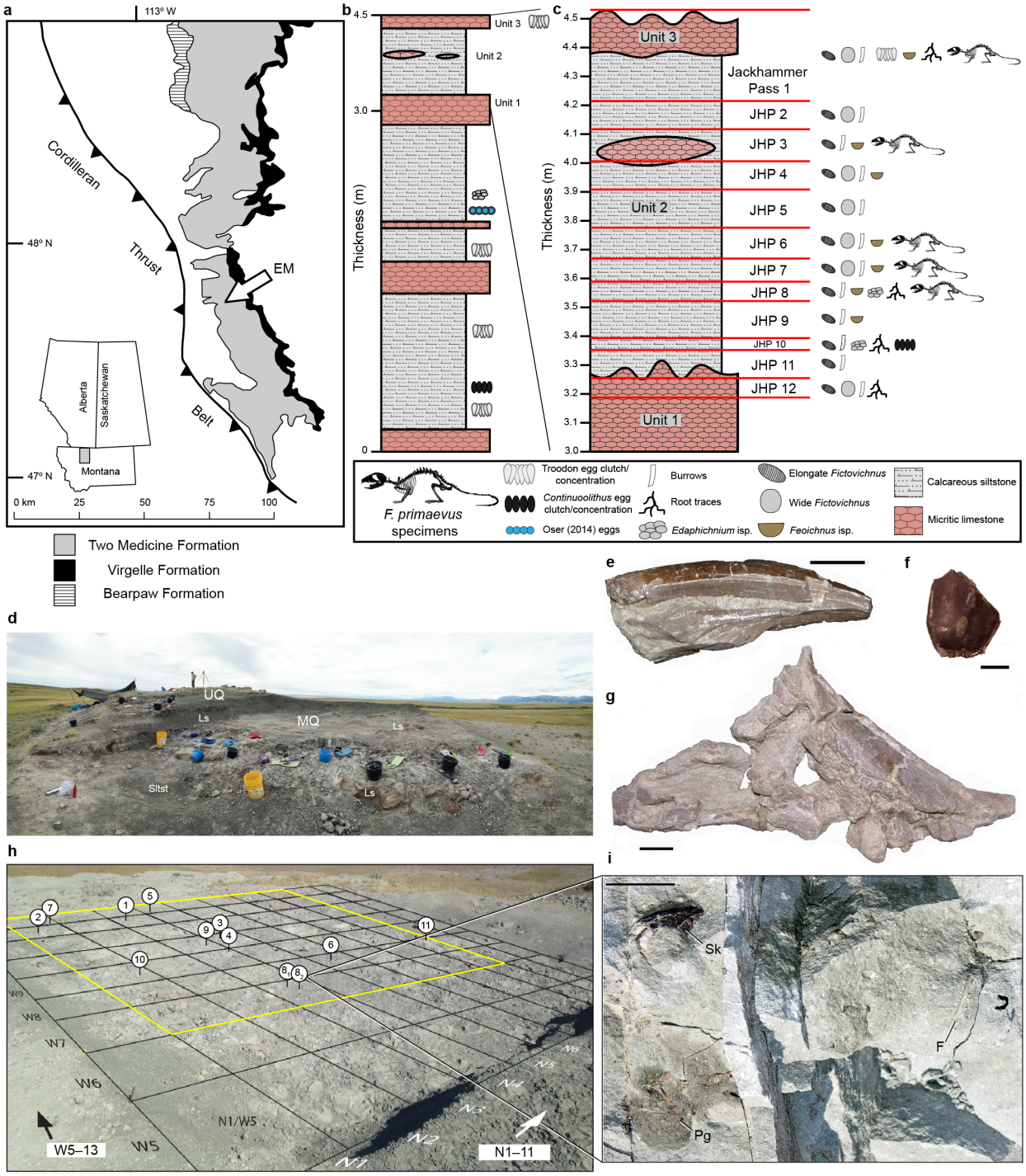

Figure 3.9.3 | The geography, geology, taphonomy, and fossil collecting at the Egg Mountain locality (Museum of the Rockies site TM-006). **a**, Locality map of the field area at the Willow Creek Anticline, Two Medicine Formation near Choteau, Montana, USA. The Egg

Mountain locality (EM) is indicated with an arrow. **b**, Stratigraphic section measured at Egg Mountain. See Supplementary Discussion for detailed discussion of Egg Mountain geology. **c**, Close up of Units 1–3, which were quarried from 2010 to 2016. These sections are subdivided into 12 separate jackhammer passes (JHP). JHPs are stratigraphically parallel cuts that proceeded at ~10 cm-deep intervals through the quarry. The JHPs that produced *F. primaevus* fossils are indicated by the skeleton illustrations. The ichnofauna (see legend below) indicate that Egg Mountain sediments were subaerially exposed. **d**, Photograph of Egg Mountain quarry taken from the north. Note the thick rusty limestones in the foreground, which poke through the siltstone in the main quarry towards the southern quarry wall. A smaller discontinuous limestone lens is visible in the east wall of the main quarry. **e**–**g**, Representative dinosaur specimens from Egg Mountain. **e**, Tyrannosaurid tooth showing the longitudinal fracturing common at the site. **f**, Shed hadrosaur tooth. One of the most common fossils are shed hadrosaur teeth of small dimensions. **g**, Unidentified hadrosaur bone, one of the few large bones recovered from the site. This specimen is from a partial, associated hadrosaur skeleton. In contrast to the bones of small mammals and squamates from the site, these large bones are in poor condition showing surface corrosion and numerous breaks. The close position of the fragments suggests that the breakdown of these bones occurred post depositionally, either subaerially or within the soils. **h**, Grid system of the main quarry (MQ) set up 11 m north by 9 m west (N1–11/W5–13); each quadrant is one square-meter. Yellow square indicates the portion of the quarry where *F. primaevus* fossils were found. Pins labeled 1–11 indicate where specific *F. primaevus* specimens were found (corresponding to Fig. 3.2 in the main text), pins labeled 8_1 and 8_2 represent the location of the two collections that make up MOR 10908. **i**, MOR 10908 as found *in situ* in the field. Skull (MOR 10908A) visible in right lateral view at top left of image with its pelvic girdle visible in

lower left. Portions of its vertebral column were lost in missing block to left. Postcrania of other individuals are partially visible to the right of this specimen, including the impression of a femur. Orientation as in Figure 3.2c in the main text. Parts **a**–**d** and **h** were modified from Freimuth and Varricchio (2019). **Abbreviations: F**, femur; **Ls**, micritic limestone; **MQ**, main quarry; **Pg**, pelvic girdle; **Sk**, skull; **UQ**, upper quarry. Scale bars = 2 cm.

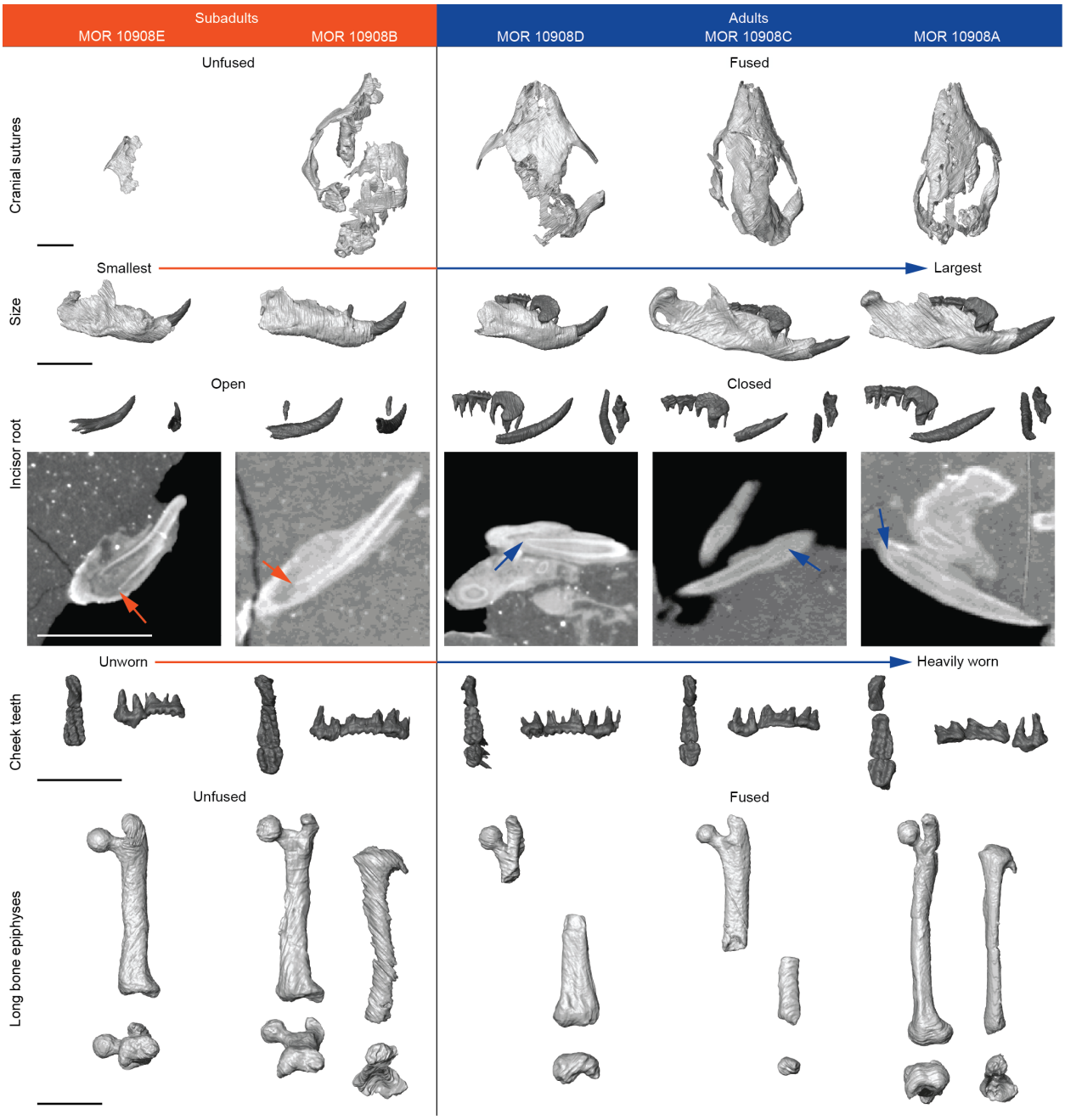

Figure 3.9.4 | Evidence for both subadult and adult individuals of *Filikomys primaevus* at Egg Mountain. MOR 10908E and 10908B exhibit features characteristic of skeletally immature, subadult mammals[25]: (i) unfused cranial sutures, (ii) MOR 10908E is the smallest (based on dentary length) of all the individuals preserved in MOR 10908, (iii) both have open lower incisor roots (orange arrows), indicating that the tooth was still erupting, (iv) MOR 10908E has unworn

cheek teeth and MOR 10908B has only very minor cheek-tooth wear, and (v) the long bones are missing their epiphyses, indicating that they were unfused at the time of death. MOR 10908D, 10908C, and 10908A exhibit features characteristic of skeletally mature, adult mammals[25]: (i) fused cranial sutures, (ii) MOR 10908A is the largest (based on dentary length) of all the individuals preserved in MOR 10908, (iii) all have closed lower incisor roots (blue arrows), indicating that the tooth was fully erupted, (iv) the cheek teeth of MOR 10908C and 10908A are heavily worn, and (v) the long bones have fused epiphyses. See Supplementary Discussion for more information. Scale bars = 5 mm.

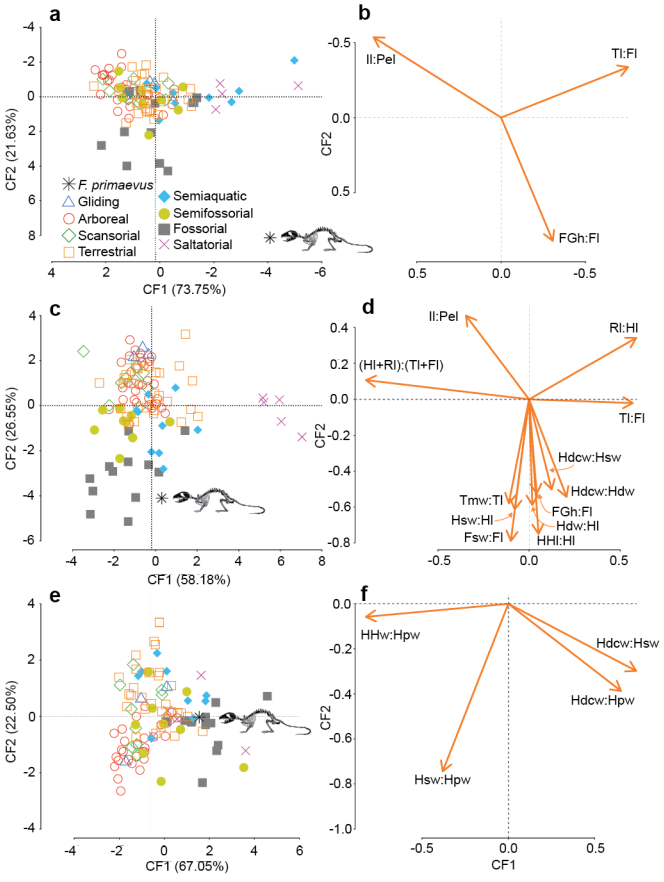

Figure 3.9.5 | Results from canonical variate analyses (CVAs) of linear measurements taken from the postcranial skeleton of *Filikomys primaevus*. **a**, **c**, **e**, Plots of canonical function 1

(CF1) and CF2 from CVA of the right (**a**) and left (**c**) sides of MOR 10908A, and the left side of MOR 10908C (**e**). **b**, **d**, **f**, Plots of structure correlations among the osteological indices and CF1 and CF2 of the right (b) and left (d) sides of MOR 10908A, and the left side of MOR 10908C (**f**). In all three analyses, *F. primaevus* is classified as fossorial. For explanation of osteological index abbreviations see Supplementary Discussion.

3.10 APPENDIX I: SUPPLEMENTARY MATERIALS AND METHODS

Fieldwork. The Egg Mountain multituberculate specimens described here were collected during the 2010–2016 field seasons. The sediments at Egg Mountain are well indurated, so it is nearly impossible to quarry by hand; instead, we made jackhammer passes across the 7 x 11 m quarry to break up the rock, typically to a depth of ~10 cm (Extended Data Figure 3.9.3). The field team then picked through the newly broken-up rock, looked for exposed bone on each piece and on the newly exposed rock face, and broke each loose piece into smaller pieces with a rock hammer and chisel. If bone was found, it was circled, mapped, and the associated blocks were collected, wrapped in foil, and placed into a bag. The *in situ* orientation and association of these blocks was documented through a combination of photographs and detailed field notes. Each collection of bone-bearing blocks found within a small area (~10–30 cm^2) was then given a field number. Given this collecting method, the size, number, and quality of each collection varied greatly; some bone-bearing blocks were very large and associated with multiple pieces, whereas others consisted of only a few small fragments. Each of the Museum of the Rockies specimen numbers referenced herein correspond to a single collection of closely associated to *in situ*, bone-bearing blocks (Supplementary Table 3.12.1), and these specimens have been grouped stratigraphically by the jackhammer pass in which they were discovered (Fig. 3.2; Extended Data Figure 3.9.3).

Specimens. Multituberculate remains were collected from twelve different locations within the Egg Mountain quarry (Supplementary Table 3.12.1), seven of which are composed of multiple individuals (Fig. 3.2). Each collection has been cataloged at the Museum of the Rockies (MOR), and specimens are currently on loan to the University of Washington for ongoing study. See Supplementary Table 3.12.1 for brief descriptions of each collection and their associated MOR numbers. Robert Masek of Chicago, IL mechanically prepared MOR 10908, 11750, and 11753 initially with Paleotools #3 or #4 air scribes until bone was discovered, then a Paleotools #1 air scribe with a very sharp/pointed tip, and finishing with a pin vise.

The multituberculate specimens from Egg Mountain commonly occur as monospecific (*Filikomys primaevus*), spatially restricted aggregates. The multituberculate specimen highlighted in this paper, MOR 10908, consists of two collections that were given different field numbers (7-23-12-26, 'Block 2' in Figure 3.1; 7-23-12-29, 'Block 1' in Figure 3.1) and were discovered adjacent to each other during the same jackhammer pass (JHP 8). Whereas 7-23-12-29 was largely still in place at the time of collection (Extended Data Figure 3.9.3i), 7-23-12-26 was floating loosely in the jumble of rocks surrounding 7-23-12-29. We conservatively estimate the position of 7-23-12-26 in the quarry to be within 40 cm of 7-23-12-29, but it was likely much closer. We count a minimum of five individuals (see Supplementary Table 3.12.7) based on the postcranial remains preserved in 7-23-12-29 and on the total number of skulls preserved in 7-23-12-26 and 7-23-12-29. Although these two collections were not recovered *in situ* next to each other, several lines of evidence support the interpretation that they represent the remains of the same five individuals: (i) the minimum number of individuals represented by postcranial remains in 7-23-12-29 is five, and there are five skulls represented between 7-23-12-26 and 7-23-12-29,

(ii) 7-23-12-26 and 7-23-12-29 both preserve subadult skulls, and there is a minimum of two subadult individuals represented by long bones with unfused epiphyses in 7-23-12-29 (see below), and (iii) differences in size among postcranial elements represented in 7-23-12-29 match the differences in size represented by dentary measurements in both 7-23-12-29 and 7-23-12-26. The five individuals preserved in MOR 10908 are distinguished in the main text, figures, and Supplementary Information by adding a suffix letter (A–E) to the end of the specimen number. MOR 10908A–C refers to the individuals whose three skulls are preserved in the 7-23-12-29 field collection ('Block 1' in Figure 3.1). From top to bottom in Figure 3.1, Block 1, are MOR 10908A, 10908B, and 10908C. MOR 10908D–E refers to the individuals whose two skulls are preserved in the 7-23-12-26 field collection ('Block 2' in Figure 3.1). From left to right in Figure 3.1, Block 2, are MOR 10908D and 10908E.

µCT data. The rock matrix that encases the vertebrate fossils at Egg Mountain is well indurated, so the density contrast between the rock and bone is very slight. As a result, our initial attempts to µCT scan the Egg Mountain specimens were unsuccessful—only the manually prepared elements were distinguishable from the rock. Iterative manipulation of the x-ray tube voltage and current eventually produced images with enough contrast to permit recognition and segmentation of fossil elements that were below the surface of the rock. Nevertheless, the high voltage and low current required to achieve this contrast, coupled with the large size of the fossiliferous blocks, resulted in fairly low-resolution scans (~50 μm^2); thus, fine details preserved on, for example, the teeth were often difficult to recognize. Furthermore, the rock matrix contains many large, dense, rock clasts that have the same greyscale values as the bone; therefore, small, rounded

elements of the skeleton (e.g., tarsal and carpal bones) may have been missed during the segmenting process.

MOR 10908 was μCT scanned at the University of Washington on a North Star Imaging X5000 CT scanner with a Feinfocus FXE [11164478] Xray source and Perkin Elmer [XRD 1620/1621 AM/AN] detector. The specimens were scanned in three batches: (1) the MOR 10908 block containing three skulls, (2) the larger MOR 10908 block containing the second pelvic girdle, and (3) the smallest MOR 10908 block that contains two skulls. All were scanned with 85 kV voltage and 500 μA current.

All post-processing of the μCT scans was done using Avizo Software (ThermoFisher Scientific, Version 9.2). Skeletal elements were segmented individually using the 'Lasso' tool. Given the poor contrast between the rock and the bone, segmenting expedients (e.g., the 'Magic Wand' tool) could not be used; thus, each bone was differentiated from the rock matrix slice-by-slice until the entire bone was segmented and then assigned a unique element in the 'Materials' panel. From the segmented materials label file, 3D renderings of the skeletons were generated using the 'Generate Surface' function in Avizo. All surface renderings were 'compactified' and smoothed. Smoothing was restricted to two iterations of 'unconstrained smoothing' because further smoothing began to obliterate some of the finer morphological details on, for example, the teeth. Each bone was isolated from the rest of the assemblages using the 'Buffer' function in the 'Surface View' properties window and was then oriented in the viewer window and imaged via the 'Snapshot' function.

All μCT tiffstacks are available via MorphoSource:

http://www.morphosource.org/Detail/MediaDetail/Show/media_id/82116.

Measurements. Nearly all of the Egg Mountain multituberculate specimens have been manually prepared in relief and were not prepped out of the rock matrix. Because of this, all measurements were taken from 3D renderings of bones and teeth in Avizo in order to consistently orient and measure each element. All of the μCT data were accurately scaled by entering the voxel size when the .tiff stack was first uploaded into Avizo. 'Landmarks' were placed on the surface of the bones and teeth and the 'Measure' tool was used to take linear measurements between landmarks (e.g., the mesial and distal end of a molar). All measurements were rounded to the nearest 0.01 mm. In many cases these measurements were cross-checked with direct measurements under a microscope, and both measurement techniques are in close agreement (within 0.2 mm). Dentary length was measured from the incisor alveolus to the dentary condyle. Skull length was measured from the anterior-most extent of the nasals to the posterior-most portion of the skull, but this complete measurement was only possible for MOR 10908C; therefore, approximate skull lengths for MOR 10908A and 10908D were taken from the anterior-most to posterior-most portions of the skull that were preserved. The skulls of MOR 10908B and 10908E were too damaged and disarticulated to warrant measuring. Upper-tooth-row length was taken from the mesial-most point on P1 to the distal-most point on M2. Tables listing measurements of the craniodental and postcranial remains of *F. primaevus* can be found in Supplementary Tables 2–6 and 9–10.

Dental terminology. The dental terminology used follows Simpson (1937) and Jepsen (1940). Cusp formulae are presented buccally to lingually (e.g., 5:6:4), except for p4, which is presented as number of serrations, buccal ridges, then lingual ridges. Our p4 measurements and ratios follow Novacek and Clemens (1977) and Hunter et al. (1997), with p4s oriented according to

Novacek and Clemens (1977:fig. 2). Our P4 measurements follow Eaton (2002) and our molar measurements follow Eaton (1995). For premolars and molars (both crown and roots), length refers to the mesiodistal dimension and width refers to the buccolingual dimension. Abbreviations: **L**, length; **W**, width; **H**, height; **L1**, length to the p4 apogee; **H1**, height to the first serration.

Institutional abbreviations. **AMNH FM**, American Museum of Natural History, New York, NY, USA; **MNA**, Museum of Northern Arizona, Flagstaff, AZ, USA; **MOR**, Museum of the Rockies, Bozeman, MT, USA; **NMC**, National Museum of Canada, Ottawa, Canada; **OMNH**, Sam Noble Oklahoma Museum of Natural History, Norman, OK, USA; **UCMP**, University of California Museum of Paleontology, Berkeley, CA, USA; **UW**, University of Wyoming Geological Museum, Laramie, WY, USA.

3.11 APPENDIX II: SUPPLEMENTAL DISCUSSION

3.10.1 ACKNOWLEDGEMENTS

We thank the Museum of the Rockies, Beatrice R. Taylor Paleontological Resource Area, and Jack Horner for permission and support to excavate Egg Mountain, and the 2010–2016 Egg Mountain field crews for collecting of the specimens described herein; R. Masek for his masterful preparation of the specimens; M. Ouchida for preparing the in-situ line drawings, skeletal reconstruction, and artistic reconstruction of the Egg Mountain multituberculates; A.L. Brannick and M. Rivin for μCT scanning specimens; J. Scannella and A. Atwater of the Museum of the Rockies for curatorial assistance; J.R. Moore for his geological insights at Egg Mountain;

D.W. Krause for allowing study of the holotype of *Ptilodus kummae*, among other multituberculate postcranial specimens; C.S. Scott for allowing study of unpublished multituberculate specimens at the Royal Tyrrell Museum; W.A. Clemens and P.A. Holroyd for access to University of California Museum of Paleontology specimens; D.L. Brinkman for facilitating access to the Yale Peabody Museum collections; D.M. Boyer for access to, and advice about, MorphoSource μCT data; D.M. Grossnickle, A.L. Brannick, M.R. Whitney, B.T. Hovatter, J.R. Claytor, P.K. Wilson, and C.A.E. Strömberg for helpful feedback on the manuscript and figures; R.R. Rogers, A.K. Behrensmeyer, and T.M. Bown for helpful discussions about Egg Mountain taphonomy; D.W. Krause, A. Weil, and C.S. Scott for discussions about multituberculates. We also thank A.K. Behrensmeyer and two other anonymous reviewers for comments that improved this manuscript, and L.N. Eoin for handling the manuscript. Financial support was from the National Science Foundation Grants 0847777 (D.J.V.) and 1325674 (D.J.V. and G.P.W.), National Science Foundation Graduate Research Fellowship (L.N.W.), Doris O. and Samuel P. Welles Research Fund (L.N.W.), University of Washington Department of Biology (L.N.W. and G.P.W.), and the Burke Museum (L.N.W. and G.P.W).

3.10.2 GEOLOGIC SETTING

Two Medicine Formation. The Two Medicine Formation is Campanian in age (Upper Cretaceous), with $^{40}Ar/^{39}Ar$ dates near the base and top of the formation, indicating that deposition occurred between 80.044 ± 0.190 and 74.076 ± 0.095 Ma (Rogers et al., 1993) at a paleolatitude of 48º N (Golonka et al., 1994). Sedimentary facies are interpreted as intergrading fluvial and lacustrine systems in a volcanically active area (Lorenz and Gavin, 1984; Rogers et

al., 1993). Abundant caliche nodules (Lorenz and Gavin, 1984) and coprolites from herbivorous dinosaurs (Chin, 2007) suggest that the paleoclimate was seasonal and semi-arid to sub-humid. Taphonomic data (Rogers, 1990) and growth interruptions in conifer fossils (Falcon-Lang, 2003) are also indicative of episodic drought.

Egg Mountain locality. The Egg Mountain locality occurs at the Willow Creek Anticline near Choteau, Montana (Extended Data Figure 3.9.3) and consists of a small hill that rises about 15 m above the surrounding topography. Egg Mountain sits 16.5 m above a bentonite horizon that has produced an $^{40}Ar/^{39}Ar$ date of 75.92 ± 0.32 Ma (Shelton, 2007; Varricchio et al., 2010). Egg Mountain deposition occurred geographically proximal to the emerging Rocky Mountains to the west and distal to the Western Interior Seaway to the east.

Egg Mountain sediments consist of well-indurated micritic limestones and calcareous mudstones and siltstones (Lorenz and Gavin, 1984). Deposits are characterized by a distinct lack of bedding and primary sedimentary structures. Three lithologic units comprise a 1.5-m quarried section through the top of the measured stratigraphic section (Extended Data Figure 3.9.3). The lowermost unit (Unit 1) is a thick (>50 cm) micritic limestone that is roughly laterally continuous throughout the 7 x 11 m quarry and has an irregular upper surface with 10–20 cm of relief. Few medium- to coarse-grained sands and mud rip-up clasts occur. Limestone of Unit 1 is massive and lacks internal structure. The overlying unit (Unit 2) is a ~1-m-thick, grey calcareous siltstone with interfingering micritic limestone lenses, similar in composition to those of Unit 1 but lacking coarse material and rip-up clasts. Unit 3, which overlies Unit 2, is a thin (10–20 cm), irregular, micritic limestone. The upper surface of this unit is variable in topographic relief. Unit

3 preserved a *Troodon* nesting structure and egg clutch (Varricchio et al., 1999). See Extended Data Figure 3.9.3 for more details.

The trace fossil assemblages at Egg Mountain indicate that these sediments were subaerially exposed, and we interpret them as immature paleosols (Bown and Kraus, 1981, 1987). Root traces are found throughout the section (Extended Data Figure 3.9.3), albeit in low abundance. Invertebrate traces—*Fictovichnus* (wasp cocoons; Freimuth and Varricchio, 2019), *Feoichnus* (cicada or other invertebrate feeding chambers; Panascí and Varricchio, 2020), and cf. *Edaphichnium* (invertebrate fecal pellets; Freimuth, 2020)—are indicative of sparsely vegetated, well-drained soils seasonally or perennially above the water table (Genise, 2000; Genise, 2016). Many of these invertebrate traces host root traces on their surface, providing further evidence for both subaerial exposure of Egg Mountain sediments and the emplacement of traces beneath the soil surface (Johnston et al., 1996; Alonso-Zarza et al., 2014). A high concentration of subsurface traces—*Fictovichnus*, *Feoichnus,* cf. *Edaphichnium*, and root traces—are present at jackhammer pass (JHP) 8 (Extended Data Figure 3.9.3), which also produced the largest concentration of articulated, multi-individual multituberculate specimens. The abundance of traces at the JHP 8 interval suggests that there was greater soil development and the substrate was stable for prolonged periods, likely due to a depositional hiatus (*sensu* Bown and Kraus, 1987; Freimuth and Varricchio, 2019). The abundance of cf. *Edaphichnium* in particular (Freimutch, 2020) suggests that this fossiliferous horizon was damp (but not saturated), organic-rich, and situated above the water table at the time of burrowing (Bown and Kraus, 1983; Hembree and Hasiotis, 2007) because deposit-feeding invertebrates are sensitive to soil characteristics such as moisture and organic content (e.g., Lee, 1985; Hopkins and Read, 1992).

The sedimentary succession is largely homogenous in composition, lacking definitive paleosol horizons. Interfingering of detrital siltstones suggests that deposition was frequent enough to interrupt paleosol development (Alonso-Zarza et al., 1998; Kraus, 1999). Nevertheless, the continued and abundant presence of insect trace fossils throughout the Egg Mountain section indicates major depositional events were lacking (Freimuth and Varricchio, 2019). Bioturbation was likely the predominant factor in obliterating bedding planes and other primary sedimentary structures (Lorenz and Gavin, 1984; Freimuth and Varricchio, 2019). The abundant calcium carbonate in the Egg Mountain sediments was likely sourced from Paleozoic marine limestones to the west (Lorenz and Gavin, 1984). Large amounts of calcite are present within the sediments, infilling tectonic fractures, fossil cocoons, and eggshell. Elsewhere in the Two Medicine Formation, calcite is the predominant diagenetic, void-filling mineral in fossil bones (Rogers et al., 2020). Although distinct paleosol horizons are lacking, the trace fossil evidence outlined above suggests that the Egg Mountain limestones are pedogenic in origin (Varricchio et al., 1999; Freimuth and Varricchio, 2019) and are calcretes, formed by the cementation of immature paleosols by infiltrating subsurface waters.

Multituberculate specimens described herein occur in Unit 2, ~30–100 cm below the designated origin point at the top of the section (Extended Data Figure 3.9.3). A grey, well-indurated, calcareous siltstone encases MOR 10908. The sediments are homogenous and lack sedimentary structures. Centimeter-scale lenses of fine-grained, micaceous sandstone immediately underlie the fossil skeletons; these are only visible under 10X magnification on the side of the block containing the skulls of 10908A, 10908B, and 10908C.

3.10.3 SYSTEMATICS AND DESCRIPTION

Systematic Paleontology

Mammalia Linnaeus, 1758

Multituberculata Cope, 1884

Cimolodonta McKenna, 1975

Ptilodontoidea Sloan and Van Valen 1965

Neoplagiaulacidae Ameghino, 1890

Filikomys gen. nov.

Etymology. *Filikós* (Greek), friendly or neighborly, in reference to the inferred social behaviour of this animal; -*mys* (Greek), mouse, a common suffix used for multituberculate genera.

Type species. *Filikomys primaevus* (Lambe, 1902).

Included species. The type species, *F. primaevus* (equal to or including *Mesodma archibaldi* Eaton, 2002 and, in part, *Cimexomys judithae* Sahni, 1972) and, tentatively, *F. minor* (Eaton, 2002).

Distribution. Judithian North American Land Mammal 'age' of the Western Interior of North America, including: Belly River Group of Alberta, Two Medicine and Judith River formations of Montana, 'Mesaverde' Formation of Wyoming, and Kaiparowits Formation of Utah.

Diagnosis. Differing from holotype of *Cimexomys judithae* (p4; AMNH FM 77100) in: (1) the p4 mesiobuccal lobe greatly inflated buccally and expanded mesioventrally, (2) the lingual face flat (whereas the ventral portion of the crown is inflated lingually in AMNH FM 77100), (3) exhibiting nine to 11 serrations and, when only exhibiting nine serrations, the first serration is well developed and contributes to the expanded mesial face of the crown (whereas the first serration is small and projects weakly from the rest of the crown in AMNH FM 77100), (4) ultimate serration with a low ridge on its buccal side that descends ventrally from its apex then curves mesioventrally to form the mesiobuccal cup, (5) either the second and third (for p4s with nine serrations) or third and fourth (for p4s with ten serrations) buccal and lingual ridges converging at an acute angle ventrally (whereas only the first and second buccal and lingual ridges converge in AMNH FM 77100), and (6) lateral profile being more parabolic (rather than roughly triangular) with the apogee occurring at serration four or five, rather than three or four. Differing from all other species of *Cimexomys* in: p4 (1) protruding dorsally over the level of the molars, (2) substantially longer than m1 (average p4:m1 L = 1.58 vs. p4:m1 = 1.08–1.24 among species of *Cimexomys*; Eaton, 2002), (3) having a very large mesiobuccal lobe that projects ventrally, is well separated from the rest of the crown (i.e., pendulous), and is expanded mesioventrally and buccally, (4) serrations more recurved, such that the apices point distodorsally (whereas they are more vertically oriented in *Cimexomys*), (5) ridges are more strongly slanted mesioventrally to distodorsally, such that a horizontal line drawn beneath them forms a more acute angle (whereas that angle is more obtuse in *Cimexomys*), (6) ultimate serration not forming a distinct cusp but rather a cuspule connected to the penultimate serration by a low ridge, and (7) having a weakly developed distobuccal cup that does not project far buccally and never hosts a cuspule (unlike some specimens of *C. minor*, e.g., UCMP 92666);

molar cusps being subcrescentic to crescentic rather than pyramidal; m1 occlusal outline tapering in width near the mesial end of the crown; m2 buccal cusp row being only slightly longer than the lingual cusp row (whereas the lingual cusp row is two-thirds of the length of the buccal cusp row in *Cimexomys*); M1 lingual cusp row (1) extending over 50% of the length of the tooth, (2) not projecting far lingually, (3) not ending abruptly but rather tapering in width mesially, and (4) with up to four distinct cusps.

Resembling members of the Ptilodontoidea in: (1) the lower incisor is slender and completely covered in enamel (the latter characteristic is assumed to be plesiomorphic for Multituberculata), (2) p4 is large, arcuate, and protruding dorsally over the level of the molars, (3) snout is wide and gently incurved medially, anterior to the zygomatic arches, and (4) P4 is mesiodistally long, shaped like an isosceles triangle in lateral view, and protrudes ventrally past the level of the anterior premolars and molars. Resembling members of the Neoplagiaulacidae in: (1) small size (e.g., average m1 L = 2.03 mm) and (2) having a low p4 profile, relative to members of the Cimolodontidae or Ptilodontidae, and (3) a p4:m1 length ratio of 1.43–1.75. Resembling *Mesodma* in: (1) p4 lower crowned than other Paleogene neoplagiaulacids (e.g., *Ectypodus*), (2) nine to 11 p4 serrations (number of serrations ranges from nine to 14 in *Mesodma*; Clemens, 1964; Archibald, 1982; Eaton, 2002), (3) p4 ranging in length from 2.85 to 3.39 mm (*Mesodma* p4 L = 2.7–4.7 mm; Kielan-Jaworowska et al., 2004), (4) P4 medial cusp row maximum height at the distal-most cusp, and (5) P4 medial cusp row climbing ratio lower than in other neoplagiaulacids (e.g., *Ectypodus*).

Differing from *Mesodma* in: p4 profile (1) lower (average H:L = 0.41 vs. 0.47 in *Mesodma*; Weaver and Wilson, 2020), (2) apogee at, or just distal to, the midlength of the crown (average L1:L = 0.53 vs. 0.46 in *Mesodma*; Weaver and Wilson, 2020), (3) a lower mesial face

(average H1:H = 0.59 vs. 0.68 in *Mesodma*; Weaver and Wilson, 2020) that is gently convex (whereas it is often vertical in *Mesodma*), and (4) a shorter first serration relative to the length of the crown (average H1:L = 0.24 vs. 0.32 in *Mesodma*; Weaver and Wilson, 2020); p4 mesiobuccal lobe (1) not extending as far ventrally, (2) prominently inflated buccally (expanding well past the lateral wall of the dentary), and (3) a ventral margin that is mesiodistally broad and gently parabolic (whereas the mesiobuccal lobe tapers more abruptly in mesiodistal width ventrally, forming a blunt triangle in *Mesodma*); p4 ridges are less prominent and do not slant as strongly mesioventrally to distodorsally, such that a horizontal line drawn beneath them forms a slightly more obtuse angle (whereas that angle is slightly more acute in *Mesodma*); P4 medial cusp row lower (H:L = 0.39 vs. 0.4–0.61 in *Mesodma*; Eaton, 2002); m2 ~75% of the length of m1 (m2:m1 = 0.63–0.81 vs. 0.56–0.61 in *Mesodma*; Eaton, 2002); M1 with fewer buccal and medial cusps (M1 cusp formula = 5:6:4 vs. 6–9:8–9:4–7 in *Mesodma*; Eaton, 2002).

Discussion. All of the multituberculate remains that have been recovered from Egg Mountain are very similar morphologically (see 'Description' below), and we argue that they represent a single species. The Egg Mountain multituberculate represents a difficult taxonomic problem because it retains a number of plesiomorphic cimolodontan characters (e.g., lacking prominent ridges on the p4, low number of cusps on the molars and P4, and low number of p4 serrations) that are often associated with the genus *Cimexomys* (Archibald, 1982), but it also exhibits a number of derived characters (e.g., M1 lingual cusp row that extends beyond 50% of the length of the tooth) that are diagnostic of neoplagiaulacids, like *Mesodma* (Archibald, 1982; Montellano et al., 2000; Eaton, 2002). On the basis of the multiple specimens described herein that preserve complete or nearly complete dentitions, we erect a new genus, *Filikomys*, that we distinguish

morphologically from both *Cimexomys* and *Mesodma*. On the basis of extensive morphological comparisons, we also argue that several Judithian species previously assigned to the genus *Mesodma* should be removed from that genus and reassigned to *Filikomys*.

The first multituberculate material described from Egg Mountain was assigned to *Cimexomys judithae* (Montellano, 1992; Montellano et al., 2000). The holotype of *C. judithae* is from the Clambank Hollow local fauna of the Judith River Formation in western Montana (Sahni, 1972). Although Montellano et al. (2000) recognized major morphological differences between the holotype of *C. judithae* (p4; AMNH FM 77100) and the p4 of the Egg Mountain multituberculate specimen (MOR 302), they interpreted them as intraspecific variation (Montellano et al., 2000). In our study, we identify additional morphological differences between the holotype of *C. judithae* and the multituberculate from Egg Mountain, which includes MOR 302 and the new specimens described herein (see 'Diagnosis' above). On the basis of this more extensive catalog of differences, we remove the Egg Mountain multituberculate from the species *C. judithae* as well as the genus *Cimexomys*.

The Egg Mountain multituberculate specimens most closely resemble specimens that were referred to Judithian species of *Mesodma* (*M. primaeva*, *M. archibaldi*, and *M. minor*). Those Judithian species were diagnosed on the basis of isolated teeth and lower jaw fragments. The p4 of the Egg Mountain multituberculate is morphologically identical (or nearly so) to those referred to *Mesodma primaeva* by Lambe (1902:pl. 15, fig. 13, 14; NMC 1890, originally '*Ptilodus primaevus*', but see Clemens, 1964) from the Campanian Oldman Formation, by Sahni (1972:fig. 10, H, I; AMNH FM 77121) from the Campanian Judith River Formation, and by Lillegraven and McKenna (1986:fig. 6, A, B; UW 15539) from the Campanian Mesaverde Formation. The majority of the *M. primaeva* p4 specimens described by those authors fall within

the observed size range of the Egg Mountain sample (p4 L = 2.85–3.58 mm, n = 8), but one specimen (AMNH FM 86305) is larger (p4 L = 3.74 mm; Lillegraven and McKenna, 1986). The p4s of *M. primaeva* also have 11 serrations rather than the nine to 10 serrations observed in our sample. Note that visual inspection of serrations under a microscope was possible for only two p4s; the remainder were inspected via μCT models, which were sometimes of resolution too low to discriminate among individual serrations. Nevertheless, some unpublished p4 specimens from the Belly River Group of Alberta, Canada, which are otherwise identical to the p4s of the Egg Mountain multituberculate, also have 11 serrations. On the basis of these morphological similarities, we consider the Egg Mountain multituberculate to be referable to *M. primaeva*. Nevertheless, the p4s of *M. primaeva* are morphologically distinct from the genus *Mesodma* as it was originally diagnosed (Jepsen, 1940; Clemens, 1964). Furthermore, the original allocation of NMC 1890 to *Mesodma* was 'tentative' and was to be considered 'provisional' (Clemens, 1964:53–54). On the basis of the morphological differences recognized here (see 'Diagnosis' above), we remove *M. primaeva* from the genus *Mesodma* and place it in a new genus, *Filikomys* gen. nov. Because the species epithet '*primaevus*' has priority (Lambe, 1902), we refer the Egg Mountain multituberculate to the species *Filikomys primaevus*, along with all of the p4s previously referred to *M. primaeva* by Clemens (1964), Sahni (1972), and Lillegraven and McKenna (1986).

Other isolated teeth have been assigned to *M. primaeva*, but we do not re-allocate them to *F. primaevus*. The p4 that Montellano (1992) assigned to *M. primaeva* (UCMP 131508) is incomplete and worn, so its morphological similarity to *F. primaevus* is unclear. The m1s, m2s, P2–3, and M2s that were assigned to *M. primaeva* by Sahni (1972) and Montellano (1992) are much larger than those belonging to *F. primaevus*, though they do bear some morphological

resemblance. None of the P4s referred to *M. primaeva* resemble the P4s of *F. primaevus* from Egg Mountain, which are directly associated or in occlusion with the lower dentition. Sahni (1972) tentatively assigned one isolated P4 (AMNH FM 77150) to *M. primaeva*, and since then all other *M. primaeva* P4s have been assigned on the basis of morphological similarity to that specimen (e.g., Lillegraven and McKenna, 1986; Montellano, 1992). These '*M. primaeva*' P4s are much larger than would be expected given the lengths of the p4s assigned to *M. primaeva*, with P4 length either equaling or, more often, exceeding p4 length (Sahni, 1972; Lillegraven and McKenna, 1986; Montellano, 1992). In contrast, the P4s of *F. primaevus* are substantially shorter than the p4s (average P4 L = 1.94 mm vs. average p4 L = 3.15). Thus, the P4s previously assigned to *M. primaeva* belong to a different, larger species of multituberculate.

The M1s of *F. primaevus* are identical in size, shape, and cusp formula to the holotype of *M. archibaldi* (OMNH 24039, an isolated M1) and closely resemble the other M1s referred to that species (Eaton, 2002). No P4s or M2s have been assigned to *M. archibaldi*, but the shape, size, and cusp formulae of m1 and m2 closely match those of *F. primaevus*. Thus, we propose synonymizing *F. primaevus* and *M. archibaldi*. *F. primaevus* has priority (Lambe, 1902), making *M. archibaldi* a junior subjective synonym, and we refer all M1s, m1s, and m2s originally referred to *M. archibaldi* (Eaton, 2002) to *F. primaevus*.

It is unclear whether the p4s referred to *M. archibaldi* closely resemble *F. primaevus*. In one specimen (MNA V7533; Eaton, 2002:fig. 3A), the buccal lobe is cropped away in the figure, and the crown appears lower. In the other specimen (MNA V7531, a partial dentary preserving p4–m2; Eaton, 2002:fig. 4A, B), the p4:m1 length ratio (1.57) and p4 mesiobuccal lobe morphology are similar to *F. primaevus*, but the teeth are significantly damaged, making precise

comparisons impossible. Thus, we tentatively refer these p4 specimens to *Filikomys* sp. cf. *F. primaevus*.

Mesodma minor was differentiated from *M. archibaldi* on the basis of size only (M1s 14% shorter and m1s 16% shorter than those of *M. archibaldi*; Eaton, 2002). Indeed, the isolated teeth referred to *M. minor* closely resemble the morphology of *F. primaevus*. A few of the smaller specimens of *F. primaevus* do overlap in size with larger specimens of *M. minor*; nonetheless, most specimens of *M. minor* are smaller than those of *F. primaevus*. Thus, on the basis of morphological similarity, we remove *M. minor* from the genus *Mesodma* and place it in the genus *Filikomys*. Nevertheless, on the basis of smaller size, we tentatively maintain the species epithet, *Filikomys minor* (Eaton, 2002), for the smallest species of the genus.

Filikomys primaevus (Lambe, 1902)

Holotype. NMC 1890, right dentary fragment with p4 and m1 preserved.

Paratype. MOR 302, transversely crushed fragment of anterior skull and associated dentaries, including fragments of the right dentary with the il-m2, the left dentary with fragments of p3-ml, the right maxilla with P1-M2, the left maxilla with P1-P3, and parts of the premaxillae and nasals.

Referred specimens. MOR 10908, 11747, 11748, 11749, 11750, 11750, 11751, 11752, 11753, 11754, 11755, 11756; all specimens previously assigned to *Cimexomys judithae* by Montellano (1992) and Montellano et al. (2000), except possibly UCMP 131505 (isolated p4); all p4s

previously assigned to '*Mesodma*' *primaeva* by Clemens (1964), Sahni (1972), and Lillegraven and McKenna (1986); all M1s, m1s, and m2s previously assigned to '*M.*' *archibaldi* by Eaton (2002).

Distribution. Same as for genus.

Diagnosis. Same as for genus but differing from *F. minor* in larger size (see Eaton, 2002).

Description. The complete dentition of *F. primaevus* is known from numerous individuals at Egg Mountain. The descriptions of the dentition that are provided here rely primarily on those specimens that have been manually prepared (MOR 10908, MOR 11750). Descriptions of the roots are based on μCT reconstructions. The dental formula of *F. primaevus* is 2:0:4:2/1:0:2:2 and much of the dental morphology has already been described in Montellano et al. (2000), in which they referred the material (MOR 302) to *Cimexomys judithae*. Here, we elaborate upon that earlier description and, given our greater sample size, discuss instances of morphological variation among individuals.

Three I2s are preserved in MOR 10908 and MOR 11750; two are still situated within the premaxilla (one in MOR 10908D, one in MOR 11750), and one is isolated but associated with MOR 10908A. Six I3s are preserved in MOR 10908 and MOR 11750, all of which are situated within the premaxilla (two in MOR 10908A, one in MOR 10908B, 10908C, 10908D, and 11750). I2 is the largest of the two upper incisors, nearly twice the length of I3. I2 is lanceolate, smooth and convex buccally, flattened lingually, and is gently curved distodorsally to mesioventrally. I3 is situated on the palate, approximately 1 mm medial from the lateral edge of

the rostrum, and roughly halfway between I2 and P1. I3 is spade shaped; it is buccolingually wide, mesiodistally short, and tapers in diameter ventrally.

Eight P1s (two in MOR 10908A, 10908C, and 10908D, one in MOR 10908B and 11750), six P2s (two in MOR 10908A and 10908C, one in MOR 10908D and 10908B), and eight P3s (two in MOR 10908A, 10908C, and 10908D, one in MOR 10908B and 10908E) are preserved in MOR 10908 and MOR 11750; all are still situated within the maxilla. These specimens match, in most respects, the description for the anterior upper premolars of MOR 302 in Montellano et al. (2000), but we elaborate on a few characteristics here. All of the anterior upper premolars have two roots, with the mesial and distal roots roughly equal in size, short and wide in cross-sectional dimensions, and tapered in diameter dorsally. Broad interradicular grooves are present along the mesial faces of the distal roots in P1 and P2, and along the distal face of the mesial root in P3. The anterior premolars decrease in size distally, with P1 being the largest and P3 the smallest. In addition to the P2 morphology described by Montellano et al. (2000), in some instances (e.g., MOR 10908D_L) P2 only has three conical cusps that are arranged in a right triangle such that one large mesiobuccal cusp is widely separated from two smaller lingual cusps (one mesial and one distal) that are closer to one another. In other instances, a low, conical cuspule abuts the large mesiobuccal cusp either mesially (as in 10908C_L) or distally (as in 10908A_R). See Supplementary Table 3.12.3 for measurements.

Eight P4s are preserved in MOR 10908 and MOR 11750; seven are still situated within the maxilla (two in MOR 10908A and 10908C, one in MOR 10908B, 10908D, and 10908E), and one is isolated but associated with MOR 11750. These specimens match, in most respects, the description for the P4 of MOR 302 in Montellano et al. (2000), but we elaborate on a few characteristics here. Both roots are short and wide in cross-sectional dimensions, and taper in

diameter dorsally. The mesial root is slightly larger than the distal root and exhibits a broad interradicular groove along its distal face. All P4s, except for MOR 10908E, have only two conical mesiobuccal cusps, with the first cusp slightly smaller and in line buccolingually with the second cusp of the medial cusp row, and the second cusp larger and just distal to the third cusp of the medial cusp row. The P4 preserved in MOR 10908E is identical to the description given in Montellano et al. (2000). See Supplementary Table 3.12.4 for measurements.

Eight M1s are preserved in MOR 10908 and MOR 11750; seven are still situated within the maxilla (two in MOR 10908A and 10908C, one in MOR 10908B, 10908D, and 10908E), and one is isolated but associated with MOR 11750. These specimens match, in most respects, the description for the M1 of MOR 302 in Montellano et al. (2000); however, we elaborate on a few characteristics here. In cross-sectional dimensions, the mesial root is nearly equal in length and width (slightly wider than long) and the distal root is short and wide (~1.5 times the width of the mesial root). Both roots taper in diameter dorsally, and there is a broad interradicular groove present along the distal face of the mesial root. An accessory root is present between the two main roots in some specimens (e.g., MOR 10908C); it is very small and does not project as far dorsally as the mesial and distal roots. In all specimens, the lingual cusp row of M1 extends beyond half the length of the tooth (average lingual-cusp-row:M1 L = 0.62), terminating at a level near the midpoint of the second cusp in the medial cusp row. In most specimens, the cusps on the lingual cusp row have been nearly completely worn away (although a trace of them can be seen in the wear facets); however, in one unworn specimen (MOR 10908E_L), four distinct cusps are present. At the distal end of the crown, the lingual cusp row is expanded buccally, and it then tapers in buccal width mesially. See Supplementary Table 3.12.5 for measurements.

Eight complete M2s are preserved in MOR 10908 and MOR 11750; six are still situated within the maxilla (two in MOR 10908A and 10908C, one in MOR 10908B and 10908D), two are isolated but associated with MOR 10908E and MOR 11750. All specimens are in full agreement with M2 crown descriptions of MOR 302 in Montellano et al. (2000). In cross-sectional dimensions, the mesial root is short and wide, nearly twice the width of the distal root, and the distal root is nearly equal in length and width (slightly wider than long). Both roots taper in diameter dorsally and a narrow and deep interradicular groove is present along the mesial face of the distal root. See Supplementary Table 3.12.5 for measurements.

Eleven complete lower incisors are preserved in MOR 10908 and MOR 11750; all are still situated in the dentary (two in MOR 10908A, 10908B, 10908C, 10908D, and 10908E, one in MOR 11750). All specimens are in full agreement with lower incisor descriptions of MOR 302 in Montellano et al. (2000).

Nine complete p3s are preserved in MOR 10908 and MOR 11750; all are still situated in the dentary (two in MOR 10908A, 10908B, 10908D, and 11750, one in MOR 10908C). The p3 is single rooted, small, and peg-like, situated in a notch beneath the first serration of the p4.

Eight complete p4s are preserved in MOR 10908 and MOR 11750; all are still situated in the dentary (two in MOR 10908A, 10908C, and 10908D, one in MOR 10908B and 11750). These specimens match, in most respects, the description for the p4 of MOR 302 in Montellano et al. (2000), but we elaborate on and modify a few characteristics here. The following description is based primarily on the p4s of MOR 10908D_R and MOR 11750_L, which have been well exposed through manual preparation, although only MOR 11750_L has been prepared to expose both the buccal and lingual sides of the tooth (only the buccal side is exposed in MOR 10908D_R). Description of these new specimens was augmented by our study of casts of MOR

302 (Montellano et al., 2000). Both MOR 10908D_R and MOR 11750_L exhibit minor attritional wear on the apex of the crown. The mesial root is long and narrow in cross-sectional dimensions (over twice the length of the distal root), is slightly concave lingually and greatly expanded and convex buccally, and has a shallow groove descending ventrally along its mesial face. The distal root is short and wide in cross-sectional dimensions, and has a broad interradicular groove that extends ventrally along its mesial face. Both roots taper in diameter ventrally and are slightly curved such that their apices are directed mesially. The p4 crowns have nine to ten serrations, seven to eight buccal ridges, and six to seven lingual ridges. The buccal and lingual ridges are faint and extend from all except the last two serrations on the buccal face and all except the last three serrations on the lingual face. When ten serrations are present (e.g., MOR 10908A and MOR 11750), on both the buccal and lingual sides the first two ridges descend ventrally to meet at an acute angle below the first serration, and the third and fourth ridges descend ventrally to meet at an acute angle below the third serration. When nine serrations are present (e.g., MOR 302; Montellano et al., 2000), on both the buccal and lingual sides the first ridge projects mesioventrally and is well separated from the second ridge, which, in turn, converges with the third ridge at an acute angle ventral to the second serration. All other ridges extend mesioventrally, are mesially convex and widely spaced, and run roughly parallel to one another. The p4 profile is highly arched, protruding dorsally above the level of the molars, and symmetrical (average L1:L = 0.52) with the apogee at the fourth or fifth serration. The mesiobuccal lobe is deep, mesiodistally broad, inflated buccally (overhanging the lateral edge of the dentary when observed in occlusal view), and its mesial face is gently curved to form an obtuse angle with the mesial face of the tooth. There is a shallow concavity on the mesioventral portion of the crown that accommodates a peg-like p3. The height of the first serration is over

halfway between the base and the apex of the crown (average H1:H = 0.58), and in specimens with nine serrations (e.g., MOR 302; Montellano et al., 2000) it forms a prominent cusp at the mesial face of the crown. The first through third serrations are roughly equally spaced, as are the third through eighth (for specimens with nine serrations) or ninth (for specimens with ten serrations); however, the first through third serrations are more widely separated than the third through eighth/ninth. The penultimate serration is conical and is connected to the ultimate serration by a low ridge that descends distoventrally from the distal face of the penultimate serration. The ultimate serration (either the ninth or the tenth) is little more than a cuspule and in MOR 10908A and MOR 11750 it is nearly obliterated by wear. A ridge extends ventrally from the buccal face of the ultimate serration then curves mesioventrally to form a weak distobuccal cup below the penultimate and ultimate serrations. See Supplementary Table 3.12.6 for measurements.

Eight complete m1s are preserved in MOR 10908 and MOR 11750; five are still situated within the dentary (two in MOR 10908A, one in MOR 10908B, 10908C, 10908D), and three are isolated but associated with MOR 10908B, MOR 10908D, and MOR 11750. All specimens are in full agreement with m1 crown descriptions of MOR 302 in Montellano et al. (2000). The mesial and distal roots are roughly equal in size, both are short and wide in cross-sectional dimensions, and they taper in diameter ventrally. A broad interradicular groove is present on the distal face of the mesial root, and both roots occasionally bifurcate ventrally. See Supplementary Table 3.12.5 for measurements.

Six complete m2s are preserved in MOR 10908 and MOR 11750; five are still situated within the dentary (two in MOR 10908A, one in MOR 10908B, 10908C, and 10908D), and one is isolated but associated with MOR 11750. All specimens are in full agreement with m2 crown

descriptions of MOR 302 in Montellano et al. (2000). The mesial and distal roots are roughly equal in size, both are short and wide in cross-sectional dimensions, and they taper in diameter ventrally. A broad interradicular groove is present on the mesial face of the distal root, and both roots occasionally bifurcate ventrally. See Supplementary Table 3.12.5 for measurements.

Filikomys minor (Eaton, 2002)

Holotype. MNA V7525, an isolated right M1.

Referred specimens. See Eaton (2002:6).

Distribution. Kaiparowits Formation of Utah.

Diagnosis. Same as for genus but differing from *F. primaevus* in smaller size.

The Need for a Revised Diagnosis of *Mesodma*

The genus *Mesodma* was first erected on the basis of a dentigerous lower jaw from the Mantua Lentil local fauna (Puercan) from the Polecat Bench Formation of Wyoming (*M. ambigua*; Jepsen, 1940). It was later expanded to include two additional species from the Lance Formation (Lancian) of Wyoming (*M. formosa* and *M. thompsoni*; Clemens, 1964). A third, smaller species of *Mesodma* was later described from the Scollard Formation (Lancian; formerly Edmonton Formation) of Alberta (*M. hensleighi*; Lillegraven, 1969), and the hypodigm includes specimens from multiple Lancian localities, including the Lance and Hell Creek formations. A fourth

species was described from the Tullock Member (Puercan) of the Fort Union Formation of Montana (*M. garfieldensis*; Archibald, 1982) but has since been subsumed within *M. thompsoni* (Smith and Wilson, 2017). The youngest species of *Mesodma* was described from the Gidley Quarry local fauna from the Lebo Member (Torrejonian) of the Fort Union Formation of Montana (*M. pygmaea*; Sloan, 1987). These five species are very difficult to distinguish on the basis of their p4 shape (Novacek and Clemens, 1977; Archibald, 1982; Smith and Wilson, 2017) and are largely distinguished on the basis of size (Lillegraven, 1969; Archibald, 1982; Sloan, 1987; Smith and Wilson, 2017). In addition, several species of *Mesodma* have been described from earlier in the Late Cretaceous (?Cenomanian–Campanian). The genus *Mesodma* has become a 'waste-basket taxon' for any small cimolodontan multituberculate that has a low-crowned p4 with a fairly high serration count (nine and above). As such, an abundance of specimens from the Early–Late Cretaceous boundary (?*Mesodma*; Eaton and Cifelli, 2001), to the late Cenomanian through Santonian (*Mesodma* sp.; Eaton, 2013), to the Aquilan (*M. senecta*; Fox, 1971), and the Judithian (*M. primaeva*, *M. archibaldi*, *M. minor*), have been assigned to *Mesodma*, despite them bearing little resemblance to the Puercan holotype species or the Lancian taxa that were first assigned to the genus. As currently composed, the genus *Mesodma* has a tentative geologic range of nearly 45 million years.

Above we erected a new genus, *Filikomys*, that we morphologically distinguished from *Mesodma*. We also proposed that several Judithian species previously assigned to *Mesodma* should be removed from that genus and reassigned to *Filikomys*. Below, we propose a revision to the contents of the genus *Mesodma* and a corresponding revision to the diagnosis, which more precisely circumscribes the morphological characteristics that distinguish the included species from other small, 'neoplagiaulacid-like' multituberculates. We restrict the genus *Mesodma* to the

holotype species and the other Lancian, Puercan, Torrejonian, and Tiffanian species previously assigned to the genus. Although *Mesodma thompsoni* has been reported from 'Edmontonian' localities (Sloan and Russell, 1974; Diem, 1999), these identifications were based on teeth (P3, M2, and m2) that are difficult to differentiate morphologically from those of other small multituberculates (e.g., *Cimexomys*; Archibald, 1982); thus, the 'Edmontonian' occurrence of *Mesodma* requires further investigation.

Mesodma Jepsen, 1940

Type species. *Mesodma ambigua* (Jepsen, 1940)

Species included. Type species, *M. formosa* (Marsh, 1889; Clemens, 1964), *M. thompsoni* (Clemens, 1964), *M. hensleighi* (Lillegraven, 1969), and *M. pygmaea* (Sloan, 1987).

Species removed. *M. primaeva* (Lambe, 1902; Clemens, 1964), synonymized with *Filikomys primaevus*; *M. senecta* (Fox, 1971), not reassigned to a new genus here; *M. archibaldi* (Eaton, 2002), junior subjective synonym of *F. primaevus*; *M. minor* (Eaton, 2002), tentatively reassigned to *F. minor*.

Revised distribution. Lancian, Puercan, Torrejonian, Tiffanian, and possibly 'Edmontonian' North American Land Mammal 'ages' of the Western Interior of North America.

Revised diagnosis. See Clemens (1964); also, differing from the holotype of '*Mesodma*' *senecta* (p4, UA 5378; Fox, 1971) in: (1) first serration shorter relative to height (average H1:H = 0.68 vs. 0.75 in UA 5378), (2) mesial face close to vertical (whereas it is prominently curved in UA 5378), (3) mesiobuccal lobe projecting much farther ventrally and is well separated from the rest of the crown. Differing from referred specimens of *M. senecta* (P4s, UA 5627–5629, Fox, 1971) in: P4 medial cusp row (1) lower, (2) lower climbing ratio, and (3) lacking complex ornamentation (i.e., vertical ridges). Differing from *Filikomys* in: p4 profile (1) higher (average H:L = 0.47 vs. 0.41 in *Filikomys*; Weaver and Wilson, 2020), (2) reaching its apogee mesial to the midlength of the crown (average L1:L = 0.46 vs. 0.53 in *Filikomys*; Weaver and Wilson, 2020), (3) having a higher mesial face that is often vertical (average H1:H = 0.68 vs. 0.59 in *Filikomys*; Weaver and Wilson, 2020), and (4) having a taller first serration relative to the length of the crown (average H1:L = 0.32 vs. 0.24 in *Filikomys*; Weaver and Wilson, 2020); mesiobuccal lobe (1) descending farther ventrally, (2) not prominently inflated buccally, and (3) having a ventral margin that tapers prominently in mesiodistal width ventrally, forming a blunt triangle; p4 ridges are more prominent and slant more strongly mesioventrally to distodorsally, such that a horizontal line drawn beneath them forms a slightly more acute angle (whereas that angle is slightly more obtuse in *Filikomys*); P4 medial cusp row higher (H:L = 0.4–0.61 vs. 0.39 in *Filikomys*; Eaton, 2002); m2 just over half the length of m1 (m2:m1 = 0.56–0.61 vs. 0.63–0.81 in *Filikomys*; Eaton, 2002); M1 with a greater number of buccal and medial cusps (M1 cusp formula = 6–9:8–9:4–7 vs. 5:6:4 in *Filikomys*; Eaton, 2002).

Discussion. On the basis of this revised diagnosis, we remove *Mesodma primaeva* and *M. minor* from the genus *Mesodma* and reassign them to the genus *Filikomys*. We also propose that *M.*

archibaldi is a junior subjective synonym of *F. primaevus*. We also remove *M. senecta* (Fox, 1971) from the genus *Mesodma* on the basis of this revised diagnosis. '*M.*' *senecta* also does not match the diagnoses for other multituberculate genera (e.g., *Cimolodon*) of equivalent age (Aquilan). The morphological characteristics of the holotype of '*M.*' *senecta* are distinct and likely warrant the erection of a new genus, but that is beyond the scope of this paper.

3.10.4 EVIDENCE FOR DIFFERENT ONTOGENETIC STAGES

There are five lines of evidence demonstrating that both adult and subadult individuals of *F. primaevus* are preserved in our sample from Egg Mountain (Extended Data Figure 3.9.4): (1) state of cranial suture fusion, (2) relative size, (3) incisor eruption stage, (4) magnitude of tooth wear, and (5) state of long bone epiphyseal fusion. Although all of the skulls exhibit some degree of postmortem damage, MOR 10908A, MOR 10908C, and MOR 10908D all exhibit fully fused, yet still detectable, cranial sutures, and breakage occurs independent of suture lines. In contrast, the paired parietals and paired frontals of MOR 10908B are disarticulated, with sediment filling in the gaps between them. Most of the skull is missing in MOR 10908E (only the left maxilla and part of the left frontal are preserved), so its state of cranial fusion is unclear. Nevertheless, the incisor roots are completely open in MOR 10908E (see below), much more so than in MOR 10908B, so it is likely that the cranial sutures were also poorly fused in MOR 10908E. This may have contributed to the loss of these cranial bones postmortem.

There is variation in the size of tooth-bearing elements among the *F. primaevus* individuals preserved in MOR 10908 (but note that tooth size does not differ dramatically). The skulls are too damaged or distorted to get reliable skull lengths, but there are numerous complete dentaries preserved. We observe considerable variation in dentary length across individuals.

MOR 10908A and MOR 10908C are the largest, and they also have the most heavily worn cheek teeth (see below). MOR 10908B is only slightly smaller than MOR 10908A and MOR 10908C, which fits its dental eruption pattern (see below). MOR 10908D is smaller than all three of those individuals and exhibits the least amount of wear among the adult individuals. MOR 10908E, which is the least mature based on incisor eruption stage, is substantially smaller than any of the other individuals. See Table 2 for measurements.

Although there is no evidence of incomplete tooth eruption in any of the cheek teeth in MOR 10908, μCT imaging reveals that the lower incisors are in three separate stages of eruption. In the first stage, which is exhibited by MOR 10908E, the root of i1 is open and the apex is broadly expanded, indicating that the i1 was still in the process of root formation and eruption (Narci, 2008). Additional evidence that the i1s on this specimen were not fully erupted is that they do not entirely fill the i1 alveoli (i.e., there is a large space between the bone wall and the enamel surface). In the second stage, which is exhibited by MOR 10908B, the root of i1 is still open, but the root apex is only slightly expanded, indicating that root formation and eruption were nearly complete (Narci, 2008). In the third stage, which is exhibited by MOR 10908A, MOR 10908C, and MOR 10908D, the incisor root of i1 is closed, with no expansion of the root apex, indicating that root formation had ceased and the tooth was fully erupted (Narci, 2008). The roots of the upper incisors and the cheek teeth are closed in all of the specimens/ontogenetic stages observed. See Extended Data Figure 4 for details.

Tooth wear also varies considerably among the individuals. MOR 10908A and MOR 10908C exhibit heavily worn cheek teeth, such that individual cusps are often difficult to see. In contrast, MOR 10908E exhibits no wear on the cheek teeth. MOR 10908D and MOR 10908B exhibit only moderate wear on the cheek teeth.

One of the most striking differences among the five individuals preserved in MOR 10908 is the variable states of epiphyseal fusion across the individuals. The hind limbs that are associated with MOR 10908B have unfused femoral and tibial epiphyses. On the femora this is true of both the proximal and distal ends, whereas it is only present on the distal tibia. One isolated femur preserved in MOR 10908 also exhibits an unfused distal epiphysis and may be associated with MOR 10908E. That two isolated, but otherwise complete, ischia are found in MOR 10908 provides further evidence for the partial fusion of epiphyses in many of the postcranial skeletal elements. The humerus associated with MOR 10908B appears to be missing its proximal epiphysis, but there are other, non-epiphyseal parts of the proximal end that are damaged so this determination is tentative. Additionally, the condylar process of the right dentary of MOR 10908E is missing its epiphysis. In contrast to these instances, the epiphyses on all of the other long bones preserved in MOR 10908 exhibit fully fused proximal and distal epiphyses, especially those associated with MOR 10908A and MOR 10908C.

3.10.5 TAPHONOMIC ANALYSIS

Methods. We conducted a taphonomic assessment of MOR 10908 by measuring the following standard proxies: 1) representation of skeletal elements; 2) articulation (Behrensmeyer, 1991); 3) breakage (Andrews, 1990); 4) weathering (Behrensmeyer, 1978; Andrews, 1990); 5) abrasion (Shipman, 1981); 6) presence of corrosion by digestion (Andrews, 1990; Fernandez-Jalvo et al., 2016); and 7) presence of tooth or beak marks. A minimum number of individuals (MNI) was determined by tally of the most common single-sided element, and relative abundance was calculated using the following equation (Andrews, 1990):

Relative abundance = N_O / (MNI x N_E)

where N_O is the number of elements observed in the assemblage, and N_E is the number of elements expected per individual.

Results. Element representation of MOR 10908 is summarized in Supplementary Table 3.12.7. Skulls and dentaries are most abundant, yielding an MNI of five. Femora and humeri are the next most abundant elements. Small and light elements—vertebrae, ribs, and distal manual and pedal elements—are comparatively uncommon (but note that many of these may be obscured within the rock matrix). *F. primaevus* specimens MOR 10908 are articulated to disarticulated but associated (Behrensmeyer, 1991) and contained in an area less than 82 cm^2.

Limb elements are largely complete with epiphyses preserved. Those elements that are incomplete display breaks with sharp edges, consistent with category 1 abrasion (Shipman, 1981). The surface bone on limb elements is smooth, regular, and intact across all surfaces, corresponding to category 0 weathering stage (Behrensmeyer, 1978; Andrews, 1990). No marks of predation (tooth or beak marks) or digestion (corrosion of epiphyses or tooth enamel) are present on any *F. primaevus* craniodental or postcranial material. However, detailed investigation of the bone surfaces was only possible for the portions of the skeletons that were manually prepared, so there remains the possibility that some of the skeletal elements embedded within the rock matrix could exhibit these features. Nonetheless, given that marks of predation or digestion are uniformly absent among the numerous skeletal elements that were manually prepared, we consider this possibility to be unlikely.

Taphonomic interpretations. Microvertebrate skeletal assemblages can be concentrated by abiotic (hydraulic, aeolian sorting) and biotic (predators, scavengers, burrowing) processes. These different mechanisms may result in different taphonomic characteristics and different biases inherent to paleoecological and paleoenvironmental interpretation (e.g., Behrensmeyer and Hook, 1992; Lyman, 2004; Rogers and Brady, 2010). Assessing many lines of evidence at different scales offers a holistic interpretation of taphonomic agents of a microvertebrate accumulation.

The following characteristics are observed here in MOR 10908: (1) proportionally high preservation of crania relative to postcrania, with nearly articulated skulls and dentaries present in most individuals; (2) articulated to disarticulated but associated postcrania; (3) apparent scarcity of distal limb bones (but see notes above about difficulties in recognizing these elements in μCT scans); (4) lack of abrasion and weathering; and (5) absence of marks related to predation. These observations are compared to typical characteristics of abiotic (hydraulic processes), extrinsic biotic (predation), and intrinsic biotic (burrowing) factors of skeletal accumulations (Rogers and Kidwell, 2007).

Skulls, dentaries, and femora are the most abundant elements, whereas vertebrae, ribs, and distal limb elements are less common. The elements represented span hydraulic and aeolian sorting categories (*sensu* Voorhies, 1969) for small vertebrates (Dodson, 1973; Korth, 1979; Arriaga et al., 2012), suggesting fluvial or aeolian processes were not the primary agent of accumulation.

Debris flows can also be ruled out as an accumulation mechanism. First, the persistence of insect trace fossils (formed at 5–10 cm depth) throughout the Egg Mountain section indicates that there were no major depositional events (i.e., greater than ~10 cm; Freimuth and Varricchio,

2019). Second, there is no evidence of a turbulent event that would randomly orient (vertically or laterally) the individual skeletons preserved in MOR 10908; all articulated elements are oriented along the same roughly horizontal plane (Fig. 3.1). Third, similar to fluvial processes, a debris flow is unlikely to preserve a multi-individual, monospecific aggregate in such pristine condition (Rogers and Kidwell, 2007).

Although similar patterns of elemental abundance are observed in some owl pellet assemblages (Dodson and Wexlar, 1979; Andrews, 1990), other evidence of predation is lacking. Notably, there is a complete absence of digestive corrosion and predatory markings on *F. primaevus* (but see the note above about our ability to investigate these marks). Some predator assemblages are characterized by prey with no digestive markings and are attributed to "leftover" or discarded prey remains; however, these assemblages are greatly skewed towards cranial elements, with postcrania only sparsely represented (Montalvo and Tallade, 2009; Montalvo et al., 2016). The representation of *F. primaevus* crania compared to postcrania in our sample is even more than observed in discarded prey assemblages. Two individuals (MOR 10908E and MOR 10908B) are interpreted as subadults based partly on unfused long bone epiphyses. Digestive acids preferentially act on epiphyses first (e.g., Fernandez-Jalvo et al., 2016), with higher degrees of modification observed in immature prey items relative to adults (e.g., Lowe, 1980), but subadult *F. primaevus* elements exhibit no modification by digestion. Additionally, skulls and limbs of *F. primaevus* are largely intact and often occur in articulation (with jaws in occlusion). In raptor pellets, prey skulls follow characteristic breakage patterns, characterized by initial loss of basicranial and posterior regions (Andrews, 1990). Postcrania in raptor pellets are also subject to disarticulation and display breakage patterns of proximal and distal ends of long

bones (Andrews, 1990). These patterns are not observed in *F. primaevus* remains here. Hence, the available evidence does not to support accumulation by predators.

The degree of articulated and associated elements and the lack of breakage, weathering, and abrasion suggests rapid burial and/or little to no subaerial exposure (much less than one year; Andrews, 1990; Brand et al., 2003). Conversely, extensive periods of subaerial exposure and infrequent depositional episodes <10 cm in thickness are inferred at the locality (Freimuth and Varricchio, 2019). Thus, it is unlikely that *F. primaevus* remains were preserved and buried at the surface in articulation and without signs of weathering and exposure.

The most parsimonious hypothesis is that *F. primaevus* remains were preserved beneath the surface, prior to any final burial events on the landscape. The eggshell concentrations (n=20) and all the traces (n = 4,794; with potentially the exception of some feeding traces [Freimuth, 2020]) represent buried structures (Supplementary Table 3.12.8). Skeletal remains of large vertebrates display signs of weathering and/or abrasion (e.g., hadrosaur bones and shed dinosaur teeth; Extended Data Figure 3.9.3). We would expect exposed small *F. primaevus* elements to be scavenged, disarticulated, and weathered far more rapidly than elements from Egg Mountain dinosaurs (Behrensmeyer, 1978). A burrow would protect elements from taphonomic modification for 1–10 years (Behrensmeyer and Hook, 1992). Mammal remains that display a similar combination of characteristics described above (i.e., high crania:postcrania, articulated to associated elements, high instances of complete elements, no weathering or abrasion) are associated with burrows from Holocene and modern deposits in Argentina (Montalvo et al., 2017; Tomassini et al., 2017).

Burrow preservation potential at Egg Mountain. In conflict with our hypothesis that MOR 10908 is preserved in a subterranean nest, a definitive burrow structure or chamber for *F. primaevus* has not yet been identified at Egg Mountain. Nevertheless, the taphonomy of the invertebrate ichnofossils at Egg Mountain informs the absence of a burrow for *F. primaevus*. Cocoon and pupation chamber traces of fossorial insects are abundant at Egg Mountain (*Fictovichnus* and *Feoichnus*, n = 4,787; Freimuth and Varricchio, 2019; Panascí and Varricchio, 2020), yet none have been observed in their terminal chamber or associated directly with burrows (whereas cocoons are associated directly with burrows elsewhere in the Two Medicine Formation; Martin and Varricchio, 2011). Further, isolated insect burrow traces are fragmentary and relatively scarce at Egg Mountain (n = 232). This bias towards cocoon and pupation chamber preservation likely reflects the fact that these structures are constructed with discrete walls (made of compacted sediments that enhance density contrast) or linings (typically mucous or fecal pellets) that enhance their preservation potential in paleosols (Genise and Bown, 1994; Genise, 2004; Genise, 2016). In contrast, fossorial insect burrows are typically simple and unlined (i.e., there is no modification of the burrow walls; Evans, 1966; O'Neill, 2001); thus, unless they were backfilled, they are unlikely to be preserved in a paleosol (Genise and Bown, 1994; Genise, 2004; Hembree and Hasiotis, 2006; Freimuth and Varricchio, 2019). If the rate of sedimentation is low, as is commonly the case during paleosol development (Bown and Kraus, 1987), this further limits the preservation potential of unlined burrows (e.g., Berger et al., 1979; Hembree and Hasiotis, 2006). Thus, the inferred low sedimentation rates at Egg Mountain (Freimuth and Varricchio, 2019) may further explain the comparative scarcity of burrow traces relative to cocoons and pupation chambers.

The factors outlined above would also decrease the preservation potential of burrows constructed by mammals because most fossorial mammals construct simple, unlined burrows and terminal chambers (Reichman and Smith, 1990). Further, the abundance of *Fictovichnus* (wasp pupation chambers) at Egg Mountain indicates that these sediments were unconsolidated and well-drained at the time of burrowing, given that those are the soil conditions preferred by modern fossorial wasps (Evans, 1966; O'Neill, 2001) and other insects (Genise, 2000). Unconsolidated and well-drained substrate conditions are also preferred by fossorial mammals (Reichman and Smith, 1990). Unlined mammal burrows within a loose substrate are prone to collapse, leading to a homogenization of the sediment and loss of the original stratigraphy. Such a phenomenon has been documented in modern communal mammal burrow systems (Bocek, 1986; Rafuse et al., 2019). Bioturbation at the surface can also cause burrow collapse (Agha et al., 2015), so the abundant bioturbation apparent at Egg Mountain could have further destabilized the sediment and decreased the burrow preservation potential (e.g., Berger et al., 1979), particularly in unlined burrows. Thus, the absence of associated burrow structures does not falsify the hypothesis that *F. primaevus* individuals were preserved in burrows at Egg Mountain.

The proximity of the five *F. primaevus* individuals that constitute MOR 10908 offers additional support to the hypothesis that they were preserved together in a subterranean nest. White (2005) provided allometric equations that use body mass and ethological category (colonial fossorial, solitary fossorial, and semi-fossorial) to estimate nest chamber volume of a given mammalian taxon. Although the ethological category of *F. primaevus* is unclear, we can use the semi-fossorial and colonial fossorial categories to calculate a minimum value for nest chamber size. Given an estimated body mass of 27 g for *F. primaevus* (formerly referred to *Cimexomys judithae*; Wilson et al., 2012), the expected nest chamber volume is 0.677 L for

colonial fossorial and 0.663 L for semi-fossorial. *F. primaevus* individuals in MOR 10908 are contained in an ellipsoidal area less than 82 cm^2. Assuming a maximum chamber height of 8 cm based on chamber dimensions of the Four-Striped Grass Mouse (*Rhabdomys pumilio*, ~40 g; David and Jarvis, 1985), this yields a nesting chamber of 0.653 L which is near White's (2005) estimates for colonial fossorial and semi-fossorial mammals. This consistency between specimen proximity and nest chamber volume is therefore consistent with the hypothesis that the individuals in MOR 10908 were preserved in a subterranean nest.

Sociality or parental care? The *F. primaevus* assemblage at Egg Mountain is more consistent with gregarious social behaviour (Rogers, 1990; Rogers and Kidwell, 2007) than parental care. The ratio of three adults to two subadults in MOR 10908 largely negates the possibility that this aggregate represents a parent-offspring unit. Nevertheless, there are rare instances among mammals where parental care can be protracted across multiple litters and, therefore, multiple ontogenetic stages (namely, among large-bodied macropodid marsupials; Russell, 1982). In these instances, however, there is significant ontogenetic separation between each litter with the mother caring for an embryo *in utero*, a suckling newborn, and a joey at heel (Russell, 1982). Such a scenario is unlikely in this case given the limited separation between the ontogenetic stages represented in MOR 10908.

No neonatal or juvenile individuals are preserved in MOR 10908, and even the subadult individuals (MOR 10908B, 10908E) appear to have been approaching skeletal maturity at the time of death. The permanent cheek teeth that are preserved in MOR 10908B and 10908E are fully erupted, and MOR 10908B even exhibits minor cheek-tooth wear (Extended Data Figure 4), indicating that this individual was not dependent on its mother for feeding (Morris, 1972).

On the basis of tooth eruption and dental wear, it is possible that there are up to four separate ontogenetic stages of *F. primaevus* in MOR 10908: two subadult stages and two adult stages. MOR 10908B and 10908E differ in their degree of lower incisor eruption; in MOR 10908B the root apices are approaching closure, whereas in MOR 10908E the root apices are fully open (Extended Data Figure 4). This suggests that MOR 10908E was slightly younger than MOR 10908B. Both MOR 10908B and 10908D share similar levels of moderate cheek-tooth wear; therefore, it is possible that MOR 10908D is only slightly older than MOR 10908B. Finally, MOR 10908A and 10908C appear to be the oldest individuals and of roughly equivalent ontogenetic stages, evidenced by their significant cheek-tooth wear (Extended Data Figure 4; Morris, 1972). This close association of relatively skeletally mature subadults and adults is consistent with the demographics of many modern small mammal social groups (Crook et al., 1976; Poole, 1985; Ebensperger, 2001) and is unknown in the parent-offspring units of solitary mammals (Gubernick and Klopfer, 1981). Thus, we reject the parental care hypothesis in favor of the better supported hypothesis that the *F. primaevus* assemblage at Egg Mountain represents multi-generational, group-nesting behaviour.

Taphonomic history of the JHP 8 assemblage relative to other *F. primaevus* aggregates. The *F. primaevus* aggregates from JHP 8 comprise a minimum of 13 individuals preserved in close proximity (Fig. 3.2). As such, these specimens formed the basis of our taphonomic analysis. The stratigraphically higher *F. primaevus* specimens are generally more fragmentary than those from JHP 8, and it is possible that they have distinct taphonomic histories. Manual preparation of the Egg Mountain multituberculate specimens is still underway and the descriptions of the unprepared *F. primaevus* aggregates summarized in Supplementary Table 3.12.1 are based on

those skeletal elements that are exposed on the unprepared rock surfaces. Future preparation and study may reveal that the stratigraphically higher *F. primaevus* specimens are more complete, but as it stands there appears to be a bias towards greater skeletal preservation at JHP 8. Regardless, the abundance of *F. primaevus* specimens at Egg Mountain indicates that these animals were an important and consistent component of the local vertebrate fauna.

3.10.6 FUNCTIONAL MORPHOLOGY OF THE POSTCRANIAL SKELETON

Postcranial features of *Filikomys primaevus* indicate that it was a terrestrial, scratch-digging mammal, functionally analogous to extant chipmunks. The scapula is dorsoventrally long, craniocaudally narrow, and has a prominent, ventrally protruding acromion process (Fig. 3.3a), and the humerus exhibits well-developed teres and deltopectoral crests (Fig. 3.3e). These features suggest that the teres major and deltoid muscles were well developed in *F. primaevus*, and it was, thus, capable of powerful forelimb retraction at the shoulder, a common characteristic of burrowing mammals (Maynard Smith and Savage, 1956; Salton and Sargis, 2008). A deep, trough-like infraspinous fossa makes up the majority of the scapular body, and the supraspinous fossa only occurs as a shallow, triangular depression on the cranial portion of the scapula between the cranial edge of the acromion and the glenoid (i.e., incipient supraspinous fossa, *sensu* Kielan-Jaworowska and Gambaryan, 1994) (Fig. 3.3a). The distal humerus is broad, with a medially projecting and robust entepicondyle (Fig. 3.3e), and the olecranon process of the ulna has a deep fossa on its medial face (termed the medial flexor fossa) that extends distally to form a shallow groove along the proximomedial ulna (Fig. 3.3b). These features indicate that the manual and digital flexors were well developed in *F. primaevus* (Maynard Smith and Savage, 1956; Stein, 2000; Argot, 2001; Sargis, 2002b; Salton and Sargis, 2008). The olecranon process

extends well past the semilunar notch of the ulna and is capped by a mediolaterally broad and rugose protuberance (Fig. 3.3b). This extension of the olecranon process likely functioned in increasing the lever arm and insertion area of triceps brachii, which act to powerfully extend the elbow (Maynard Smith and Savage, 1956; Stein, 2000; Argot, 2001; Salton and Sargis, 2008). Taken together, these features of the shoulder, humerus, and elbow of *F. primaevus* imply that it may have first used its strong manual and digital flexors to gain purchase against a resistant substrate, then initiated forelimb retraction at the shoulder, and finished the digging stroke by powerfully extending the elbow, flushing the loosened sediment backwards (Fig. 3.3f).

The pelvis and hind limb of *F. primaevus* reflect a terrestrial, ambulatory mode of locomotion and the ability to maneuver in tight, uneven spaces. The long ilium (Fig. 3.3g) and large greater trochanter (Fig. 3.3c) imply well-developed gluteal muscles, and the deep, blade-like, and dorsolaterally flaring ischium (Fig. 3.3g) indicates well-developed hamstring muscles. Together, these features indicate that *F. primaevus* was capable of powerful thigh extension and knee flexion (Taylor, 1976; Heinrich and Rose, 1997; Argot, 2002; Sargis, 2002a). Furthermore, the distal femur is mediolaterally broad and anteroposteriorly shallow, with the articular surfaces of the femoral condyles primarily restricted to the posterior portion of the femur (Fig. 3.3c), suggesting that the knee of *F. primaevus* was habitually flexed (Simpson and Elftman, 1928; Krause and Jenkins, 1983). Thus, it is unlikely that *F. primaevus* was a terrestrial runner or leaper (*contra* Kielan-Jaworowska and Gambaryan, 1994) because, although it would have been capable of powerful extension at the hip, it was not powerfully extending its knee, which is typical for terrestrial runners (Sargis, 2002a; Salton and Sargis, 2009) and required for generating long strides (Taylor, 1976; Heinrich and Rose, 1997) or propelling the body upwards from a crouched position (Gebo and Sargis, 1994; Anemone and Covert, 2000). Instead, we

suggest that the hip and knee of *F. primaevus* were adapted for ambulatory movements on the surface and for maneuvering in tight, confined spaces (e.g., burrows, under rocks, between tree roots, etc.). In such spaces, the knee would have had to remain habitually flexed, and propelling the body forward would have required powerful thrust (extension) generated at the hip. The hip joint of *F. primaevus* was also likely mobile and capable of habitual femoral abduction, evidenced by its broad, shallow, and dorsally positioned acetabulum (Fig. 3.3g) and large, spherical femoral head (Fig. 3.3c) (Szalay and Sargis, 2001; Argot, 2002; Sargis, 2002a); however, the range of motion would have been somewhat restricted by the large greater trochanter of the femur (Sargis, 2002a). Rotational movement at the hip joint would facilitate maneuvering in tight spaces because the hind limbs would need to both gain traction in a variety of orientations and brace against the substrate while digging (Salton and Sargis, 2009).

3.10.7 MULTIVARIATE ANALYSIS OF LOCOMOTOR MODE

To infer locomotor mode, we incorporated linear measurements of the appendicular skeleton of *F. primaevus* into a multivariate analysis following Chen and Wilson (2015). Chen and Wilson (2015) successfully predicted locomotor mode among extant small-bodied mammals (< 5 kg) using canonical variate analysis (CVA) of 30 osteological indices of the appendicular skeleton. They used this training set to infer the locomotor mode of extinct species that had only a subset of the osteological indices (Chen and Wilson, 2015; Calede et al., 2019). The dataset of Chen and Wilson (2015) consists of 107 extant, small-bodied mammal species, representing eight locomotor modes, including: gliding, arboreal, scansorial, terrestrial, semiaquatic, semifossorial, fossorial, and saltatorial. For each species, 45 linear measurements were taken and converted to 30 statistically significant and functionally relevant osteological indices. The completeness of the

appendicular skeletons of *F. primaevus* varies in MOR 10908; thus, linear measurements taken on the left and right sides of MOR 10908A and the left side of MOR 10908C (Supplementary Tables 9, 10) were used to calculate osteological indices and run three CVAs (Fig. 3.3h; Extended Data Figure 3.9.5; Supplementary Tables 11–16). Abbreviations for the linear measurements taken are as follows: **Fbdw**, fibula distal width; **Fbl**, fibula length; **Fbmw**, fibula midshaft width; **Fbpw**, fibula proximal width; **Fdw**, femur distal width; **Fgh**, femur greater trochanter height; **Fhd**, femoral head diameter; **Fl**, femur length; **Fsw**, femur midshaft width; **Hdw**, humerus distal width; **Hdcw**, humerus deltopectoral crest width; **Hhl**, humeral head length; **Hhw**, humeral head width; **Hl**, humerus length; **Hpw**, humerus proximal width; **Hsw**, humerus midshaft width; **Il**, ilium length; **Isl**, ischium length; **Pel**, pelvis length; **Rl**, radius length; **Sh**, scapula height; **Sl**, scapula length; **Tdw**, tibia distal width; **Tl**, tibia length; **Tmw**, tibia midshaft width; **Tpw**, tibia proximal width; **Uol**, olecranon process length; **Ul**, ulna length.

In the first CVA, three osteological indices were calculated using measurements from the right side of MOR 10908A, including gluteal index (FGh:Fl), crural index (Tl:Fl), and ilium robustness index (Il:Pel) (Supplementary Table 3.12.11). Our results indicate that CF1 and CF2 account for 73.75% and 21.63% of the variance, respectively, in the dataset (Extended Data Figure 5). In the bivariate plot of CF1 and CF2, fossorial and saltatorial species were relatively well separated from the rest of the locomotor categories (Extended Data Figure 3.9.5a). CF1 is strongly positively correlated with the ilium robustness index but negatively correlated with the gluteal index and the crural index, whereas CF2 is strongly positively correlated with the gluteal index but strongly negatively correlated with both the ilium robustness index and the crural index (Extended Data Figure 3.9.5b; Table 3.12.11). The CVA only correctly classified 33.64 % of 107 extant, small-bodied mammalian species (Supplementary Table 3.12.12). This analysis inferred

F. primaevus as a fossorial species with 99.40% posterior probability (Extended Data Figure 3.9.5a). This result is likely driven by its large greater trochanter and correspondingly high gluteal index given that *F. primaevus* plots far away from the extant species in the bottom right corner of the plot (Extended Data Figure 3.9.5a).

The left side of MOR 10908A includes the best preserved postcranial elements, including both the forelimb and hind limb. Measurements of these postcranial elements were converted to 12 osteological indices, including the humerus robustness index (Hsw:Hl), the humeral head robustness index (HHl:Hl), the deltopectoral crest index (Hdcw:Hsw), deltopectoral crest width to distal humerus width ratio (Hdcw:Hdw), the humeral epicondylar index (Hdw:Hl), the brachial index (Rl:Hl), the intermembral index ((Hl+Rl):(Tl+Fl)), the tibial robustness index (Tmw:Tl), and the fibular robustness index (Fsw:Fl), in addition to the same three indices calculated for the right side of MOR 10908A (Supplementary Table 3.12.13). With more osteological indices, the CVA better segregates extant, small-bodied mammalian species according to locomotor modes, as shown in the bivariate plot of CF1 and CF2, which account for 58.18% and 26.55% variance, respectively, in the dataset. CF1 is strongly positively correlated with the brachial index and the crural index but strongly negatively correlated with the ilium robustness index and the intermembral index (Supplementary Table 3.12.13). The saltatorial species are separated from other species along the CF1 (Extended Data Figure 3.9.5c). CF2 is strongly positively correlated with the brachial index and ilium robustness index but strongly negatively correlated with the humerus robustness index, humeral epicondylar index, humeral head robustness index, deltopectoral crest index, deltopectoral crest width to distal humerus width ratio, gluteal index, femoral robustness index, and tibial robustness index (Supplementary Table 3.12.13). This large set of indices drives the separation of fossorial species in negative

morphospace along CF2 (Extended Data Figure 3.9.5c), driven by their stout postcranial elements (Extended Data Figure 3.9.5d). Nevertheless, the rest of the extant small-bodied mammalian species remain less segregated (Extended Data Figure 3.9.5c). The CVA correctly classified 59.81% of all extant species, particularly with 75.00%, 100%, and 100% for fossorial, gliding, and saltatorial species, respectively (Supplementary Table 3.12.14). *F. primaevus* was unequivocally inferred as a fossorial species with high posterior probability (99.99%). The results from this analysis are also illustrated in Figure 3.3h of the main text.

The left side of MOR 10908C is more poorly preserved and thus only has four forelimb-related osteological indices for the CVA (Extended Data Figure 3.9.5e, f; Supplementary Table 3.12.15, 16). CF1 and CF2 from the CVA of extant, small-bodied species account for 67.05% and 22.50% of the variance, respectively, in the dataset. CF1 is strongly positively correlated with the deltopectoral crest width to proximal humerus width ratio (Hdcw:Hpw) and the deltopectoral crest index (Hdcw:Hsw) but strongly negatively correlated with the humerus midshaft width to proximal humerus width ratio (Hsw:Hpw) and the humeral head width to proximal humerus width ratio (HHw:Hpw). CF2 is strongly negatively correlated with the humerus midshaft width to proximal humerus width ratio (Hsw:Hpw), the deltopectoral crest width to proximal humerus width ratio (Hdcw:Hpw), and the deltopectoral crest index (Hdcw:Hsw). Most osteological indices reflect the robustness of the proximal humerus (Extended Data Figure 3.9.5f). As a result, the CVA did not segregate locomotor modes very well (Extended Data Figure 3.9.5e). The morphometrics model only correctly classified 39.25% of the extant, small-bodied mammalian species (Supplementary Table 3.12.16). Nevertheless, this morphometrics model still indicated that the *F. primaevus* could be a species that is primarily fossorial (45.17% posterior probability). Thus, although the completeness of elements

varied considerably across these three analyses, they all classify *F. primaevus* as a fossorial species.

3.10.8 PHYLOGENETIC ANALYSIS

To assess the phylogenetic relationship of *Filikomys* to other cimolodontan multituberculates, we conducted a cladistic analysis using a modified version of the multituberculate character-taxon matrix recently published by Wang et al. (2019). We removed *Cimexomys* from the matrix because the majority of its character scores were based on MOR 302, a specimen that we have now assigned to *Filikomys primaevus*. All characters were scored for *Filikomys* on the basis of the new craniodental material reported herein. To ensure that our character scorings were not biased by subadult morphology (e.g., poorly-developed muscle scars), only mature, adult specimens (see 'Part E' above) were used for scoring cranial and mandibular characters. Some character scores for other North American cimolodontans were modified to reflect character state polymorphisms that we observed (listed below). Otherwise, the taxa, characters, and scores used in our analysis follow those in Wang et al. (2019).

Our character matrix includes 51 taxa and 130 characters, 19 of which were ordered (see characters listed below). We assembled the matrix in Mesquite (version 3.5) and performed parsimony analyses using PAUP* software (version 4.0a). For the heuristic searches, when a taxon was scored with multiple states for a character that taxon was treated as polymorphic for that character, gaps were treated as missing, starting tree(s) were obtained via stepwise addition, the tree-bisection-reconnection branch-swapping algorithm was used with a reconnection limit of eight, and maximum trees was set at 100,000. Out of 3.6541e+10 rearrangements tried, the score of the most parsimonious tree found was 478, and 356 shortest trees were retained. The

cladogram illustrated in Extended Data Figure 3.9.2 is the 50% majority-rule consensus tree. The consistency index of our most parsimonious tree was 0.4289, homoplasy index was 0.5711, and retention index was 0.7605.

In nearly all of the trees, *Filikomys* was recovered as the basal-most taxon within a clade containing *Mesodma*, *Cimolodon*, *Neoliotomus*, *Ectypodus*, and *Ptilodus*, which we refer to as Ptilodontoidea (Sloan and Van Valen, 1965). To explore the robustness of this topology, bootstrapping analyses were performed and Bremer support values were calculated. Bootstrapping was replicated 100 times with resampling from all 130 characters. Bremer support was calculated by increasing the tree score from the most parsimonious tree by one until all of the nodes collapsed. The bootstrap value for the ptilodontoid node was 43 and Bremer support was 2.

The low bootstrap and Bremer support values indicate that only a few characters support the ptilodontoid node. The character transformations that frequently occur at that node indicate that Ptilodontoidea is largely united by dental characters: gracile lower (Character 15) and upper (C. 19) incisors, p4 that protrudes above the level of the molars (C. 45), M1 lingual cusp row that extends beyond half the length of the tooth (C. 58), molar enamel surface that is often ornamented with pits and ridges (C. 76). All of these synapomorphies have previously been used to diagnose the Ptilodontoidea (e.g., Kielan-Jaworowska and Hurum, 2001), but in almost every case there are other multituberculate groups that exhibit similar characters (although not the same suite of characters). In addition, two cranial characters often unite the ptilodontoid clade: having two nasal vascular foramina (C. 84) and a small and shallow jugular fossa (C. 97).

Taken together, the results of our phylogenetic analysis lend support to the hypothesis that the Ptilodontoidea is monophyletic. Although bootstrap and Bremer support values are low,

this may reflect that few synapomorphies have been recognized among multituberculates (e.g., Simmons, 1993; Kielan-Jaworowska and Hurum, 2001). Indeed, the ptilodontoid clade has higher bootstrap and Bremer support than the majority of clades recovered in our 50% majority-rule consensus tree (Extended Data Figure 3.9.2). Given that cranial character states for *Mesodma*, *Cimolodon*, and *Neoliotomus* are largely unknown, the discovery of more complete specimens of these genera should shed further light on ptilodontoid relationships.

The findings of our phylogenetic analysis are also consistent with the dental observations presented above; in particular, that *Filikomys* shares dental characteristics with neoplagiaulacid ptilodontoids like *Mesodma*. Whether or not *Cimolodon* and *Neoliotomus* belong in the Ptilodontoidea, however, is debatable (e.g., Eaton and Cifelli, 2001; Weil and Krause, 2008). It has been proposed that the character states that support their grouping with more traditionally accepted ptilodontoids (i.e., *Mesodma*, *Ectypodus*, and *Ptilodus*), may be homoplastic (Eaton and Cifelli, 2001; Kielan-Jaworowska and Hurum, 2001). For example, *Cimolodon* retains gigantoprismatic enamel (a presumably plesiomorphic cimolodontan character state), whereas other ptilodontoids have microprismatic enamel (a presumably derived character state; Krause and Carlson, 1987), and *Neoliotomus* has large, rodent-like lower incisors that are more similar to those seen among the Eucosmodontidae and Microcosmodontidae (Weil and Krause, 2008). Teasing apart whether these taxa belong within the Ptilodontoidea will require further study, but our results lend some support to their inclusion in the group. Nevertheless, because of the historical uncertainty of their phylogenetic affinities, *Cimolodon* and *Neoliotomus* were not included in the schematic cladogram illustrated in Extended Data Figure 3.9.1.

Character list used in the phylogenetic analysis and scorings for *Filikomys*

1. Postdentary trough:

(0) Present; (1) Absent.

Filikomys = 1

2. Meckel's sulcus presence:

(0) Present; (1) Vestigial or absent.

Filikomys = 1

3. Anteroventral extension of masseteric fossa to mandibular body below m1:

(0) Absent; (1) Present and extending to below m1; (2) Present and extending more anteriorly than the p4-m1 junction.

Filikomys = 2

4. Coronoid or coronoid scar on mandible:

(0) Present; (1) Absent.

Filikomys = 1

5. Angle of the coronoid anterior margin to the molar alveolar line on the mandibular body:

(0) > 45 degrees; (1) Low < 45 degrees.

Filikomys = 0

6. Coronoid process orientation in parasagittal plane:

(0) Parallel to the rest of the outer wall of the dentary; (1) Flared laterally.

Filikomys = 1

7. Angle between the lower margin of the dentary and alveolar line of the lower p4 and molars:

(0) 11–17 degrees; (1) 18 degrees or above.

Filikomys = 0

8. Gracile and elongate dentary peduncle:

(0) Present; (1) Absent.

Filikomys = 1

9. Mandibular condyle height to the m1-m2 alveolar line:

(0) Opposite or below the level of the molar alveoli; (1) Above the level of the molars.

Filikomys = 1

10. Mandibular angle:

(0) Present; (1) Absent.

Filikomys = 1

11. Number of lower incisors:

(0) Four or more; (1) One.

Filikomys = 1

12. Procumbency and enlargement of the lower anterior-most incisors:

(0) Absent; (1) Present (at least 50% longer than the adjacent incisor).

Filikomys = 1

13. Lower incisor 1 root posterior extension:

(0) Not extending below p3; (1) Extending posteriorly beyond p3-p4 junction.

Filikomys = 1

14. Enlargement diastema in lower incisor-canine region:

(0) Present and behind the canine; (1) Present and behind the posterior incisor.

Filikomys = 1

15. Lower incisor robustness:

(0) Robust; (1) Gracile.

Filikomys = 1

16. Enamel covering of lower incisor:

(0) Of uniform thickness; (1) Thicker on labial surface than on lingual surface; (2) Completely restricted to the labial surface of the tooth.

Filikomys = 0

17. Number of upper incisors (Ordered):

(0) Four or more; (1) Three; (2) Two.

Filikomys = 2

18. Diastema between Upper Incisor 2 and Incisor 3:

(0) No large diastema between the second incisor and third upper incisors; (1) I2-I3 diastema.

Filikomys = 1

19. Upper Incisor 2 (or penultimate incisor) morphology:

(0) Peg-like or single cusp; (1) Two-cusped, or more.

Filikomys = 0

20. Upper Incisor 3 (or ultimate upper incisor) morphology:

(0) Single cusped or peg-like; (1) 2-cusped; (2) 3–4 cusped.

Filikomys = 0

21. Placement of posterior upper incisor (I3):

(0) On the margin of premaxilla; (1) Medial to the margin-crest of the faciopalatal faces of premaxilla; (2) More internal on the palatal part (close to the first premolar).

Filikomys = 1

22. Upper canine — presence vs. absence, and size:

(0) Present and enlarged; (1) Present and small; (2) Absent.

Filikomys = 2

23. Upper canine — number of cusps:

(0) Peg-like with single cusp; (1) Two or more cusps.

Filikomys = ?

24. Lower canine — presence vs. absence:

(0) Present; (1) Absent.

Filikomys = 1

25. Ratio between I3 and first maxillary tooth vs. length of the upper premolars and molars (Ordered):

(0) Below 0.09; (1) Between 0.1–0.19; (2) 0.2 or above.

Filikomys = 2

26. Number of upper premolars (only applicable to taxa with premolar vs. molar differentiation) (Ordered):

(0) Five; (1) Four; (2) Three; (3) Two or one.

Filikomys = 1

27. Root(s) of posterior upper premolar(s):

(0) Double-rooted; (1) Single-rooted; (2) Triple-rooted.

Filikomys = 0

28. Labial cuspules on posterior upper premolars:

(0) Absent; (1) Present.

Filikomys = 0

29. Upper premolars/upper molars length ratio (Ordered):

(0) 1.5 or more; (1) 1.5–0.8; (2) 0.8 or less.

Filikomys = 1

30. Last upper premolar — number and length of cusp rows:

(0) Two main and equal rows of cusps; (1) Two equal rows of cusps and a continuous row of labial cingular cuspules or cingulum; (2) One main row and a shorter buccal row (anterior or posterior); (3) One main row only.

Filikomys = 2

31. P4 (or penultimate upper premolar) — cusp number of the main labial cusp row (excluding the labial cingular cuspules) (Ordered):

(0) 1–4; (1) 5–8; (2) 9–10.

Filikomys = 1

32. Width ratio of the ultimate upper premolar vs. M1 (Ordered):

(0) More than 0.9; (1) 0.9–0.7; (2) 0.69–0.4; (3) 0.39–0.2.

Filikomys = 2

33. Lower p1:

(0) Present; (1) Absent.

Filikomys = 1

34. Lower p2:

(0) Present; (1) Absent.

Filikomys = 1

35. Lower p3 (or penultimate premolar) presence vs. absence:

(0) Present; (1) Absent.

Filikomys = 0

36. p3 (or penultimate lower premolar) laterally compressed to be blade-like:

(0) No (including taxa with a peg-like p3); (1) Yes.

Filikomys = 0

37. Lower p3 (or penultimate premolar) cusp/serration count:

(0) Present, with 3–5 cusps; (1) Present, with 1–2 cusps.

Filikomys = 1

38. Shape of p3:

(0) Single row of cusps; (1) Blade-like rectangular; (2) Blade-like triangular; (3) Peg-like.

Filikomys = 3

39. Labial basal cuspules on p3 (applicable to bladed lower premolars):

(0) Present; (1) Absent.

Filikomys = 1

40. Contact of penultimate and ultimate lower premolars:

(0) Juxtaposition; (1) Staged: p4 overhangs p3.

Filikomys = 1

41. Lower p4 (or ultimate lower premolar) laterally compressed to be blade-like:

(0) No; (1) Yes.

Filikomys = 1

42. Lower p4 (or ultimate premolar) profile in lateral view:

(0) Tricuspate; (1) Rectangular; (2) Arcuate; (3) Triangular.

Filikomys = 1

43. Blade-like p4 serration count (Ordered):

(0) 7 or less; (1) 8–10; (2) More than 10.

Filikomys = 1

44. Lower p4 anterior root — Exoedaenodont at crown-root junction:

(0) Absent; (1) Present.

Filikomys = 1

45. Dorsal margin of p4 to m1:

(0) On the level of molars; (1) Protruding dorsally over molars.

Filikomys = 1

46. p3/p4 maximum length ratio (Ordered):

(0) Above 0.7; (1) 0.7–0.4; (2) 0.39–0.11; (3) 0.10 or less.

Filikomys = 3

47. Buccal basal cuspules on p4 (Ordered):

(0) Absent; (1) Single cusp or simple cingulid; (2) Several—single row; (3) Several—double rows.

Filikomys = 0

48. Ratio of p4:m1 length (Ordered):

(0) Less than 0.99; (1) 1–1.49; (2) 1.5–1.99; (3) 2 or greater.

Filikomys = 2

49. Number of lower molars or molariform postcanines (Ordered):

(0) Three or more; (1) Two.

Filikomys = 1

50. Number of upper molars or molariform postcanines:

(0) Three or more; (1) Two.

Filikomys = 1

51. Total number of upper postcanine loci (Ordered):

(0) More than 8 (including the loci plus the alveoli of shed anterior postcanines); (1) Seven loci;

(2) Six; (3) Five or fewer.

Filikomys = 2

52. Number of lower postcanine loci (Ordered):

(0) Eight or more; (1) Six; (2) Five or less.

Filikomys = 2

53. U-shaped transverse ridge(s) between b1-l1, or b2-l2 cusps in lower molars:

(0) Absent; (1) Present; (2) Sharp crest closes the narrow central valley.

Filikomys = 0

54. Lower molar cusp height:

(0) Uneven; (1) Even.

Filikomys = 1

55. M1 cusp formula:

(0) 2–3:2–4:0; (1) 4–5:4–5:0–1; (2) 5–7:5–8:2–5; (3) 5–11:7–10:6–11.

Filikomys = 2

56. Penultimate upper molar 1 (M1) of multi-rowed upper molar (or postcanines) — cusp height ratio in the lingual row:

(0) Distal cusp or second distal cusp highest, with a gradient of anteriorly decreasing height; (1) Cusps in same row of equal height.

Filikomys = 1

57. M1 posterolingual wing (applicable to molars with multiple rows of multiple cusps):

(0) Absent; (1) Present.

Filikomys = 1

58. M1 posterolingual wing M1 length (applicable to M1 with multiple rows) (Ordered):

(0) Present and below 0.2; (1) Present and between 0.2 and 0.5; (2) Present and more than 0.5.

Filikomys = 2

59. M1 posterolingual wing morphology (applicable only to M1s with posterolingual wing) (Ordered):

(0) Wing smooth; (1) Wing is crested; (2) Wing cuspate with 3–4 cuspules; (3) Wing cuspate with 5 or more cuspules.

Filikomys = 2

60. Off-set alignment of main cusp row(s) of the first and second upper molars:

(0) Absent; (1) Present.

Filikomys = 1

61. Upper M2 (or ultimate upper molar) middle row cusp count (Ordered):

(0) Two cusps; (1) Three cusps; (2) Four cusps or more.

Filikomys = 1

62. Anterior end of middle valley of upper M2 (or ultimate upper molar):

(0) Middle valley absent; (1) Present as a uniform groove along most length but anterior end closed by a crescentic rim; (2) Uniform valley anteriorly open.

Filikomys = 2

63. Middle valley of upper M1 (or penultimate molar):

(0) Middle valley absent; (1) Valley present along the tooth length but its posterior end closed by a rim or rim with tiny cuspules; (2) Valley present along most of the tooth length but posterior end closed by a single enlarged cusp in mid position; (3) Uniform valley posteriorly open; (4) Valley indistinctive owing to inflation of tooth cusps.

Filikomys = 3

64. Curvature of lingual cusp row (applicable to multi-rowed M2):

(0) Straight; (1) Curved posterolabially.

Filikomys = 0

65. M2 middle valley posterior end (applicable to multi-rowed M2):

(0) Valley posteriorly open; (1) Valley closed by a posterior cusp; (2) Valley absent due to inflation of tooth cusps.

Filikomys = 0

66. M2 mesiobuccal ridge:

(0) Absent; (1) Present; (2) Present and expanded to mesial margin labial cusp row.

Filikomys = 1

67. m1 main lingual cusp count:

(0) 4 or fewer; (1) 5; (2) 6 or higher.

Filikomys = 0

68. Lower m1 middle valley:

(0) Middle valley absent; (1) Present and posteriorly open and completely separating distal cusps of lingual vs. labial rows; (2) Middle valley present, but rimmed posteriorly.

Filikomys = 1

69. m2 middle longitudinal valley:

(0) Middle valley absent; (1) Present and completely separating two rows of cusps; (2) Middle valley present and closed distally by a ridge.

Filikomys = 1

70. Coalescence of m2 buccal row cusps (applicable only to teeth with multi-rows of multiple cusps):

(0) Absent; (1) Present.

Filikomys = 0

71. Complete rim of m2 basin (applicable only to teeth with multi-rows of multiple cusps):

(0) Absent; (1) Present.

Filikomys = 0

72. m2 lingual row cusp count (Ordered):

(0) One trenchant anterior cusp; (1) 2–3; (2) 4–5.

Filikomys = 1

73. Ultimate lower molar (or m2) with multi-rows —ratio of row length:

(0) Labial cusp row about equal as lingual cusp row; (1) Labial row is longer (by at least half-cusp length) than lingual row.

Filikomys = 1

74. Cusp shape on lower molars:

(0) Conical; (1) Crescentic; (2) Inflated.

Filikomys = 0

75. Enlarged trenchant second cusp of lingual row enclosed into the basin on lower m1 (applicable only to molars with multi-rows of multiple cusps):

(0) Absent; (1) b2 cusp enlarged; (2) b2 cusp enlarged and encircled into the basin.

Filikomys = 0

76. Molar enamel surface:

(0) Not ornamented; (1) Covered with grooves, pits, and ridges.

Filikomys = 1

77. Enamel microstructure:

(0) Prismless; (1) Gigantoprismatic; (2) Small prismatic.

Filikomys = ?

78. Differentiation of premolars vs. molars:

(0) Absent; (1) Present.

Filikomys = 1

79. Diphyodont dental replacement:

(0) Absent; (1) Present.

Filikomys = 1

80. Infraorbital foramen:

(0) Double; (1) Single.

Filikomys = 1

81. Palatal vacuities:

(0) Absent; (1) Present and single; (2) Present and double.

Filikomys = 1

82. Sharp ridge between the palate and lateral walls of premaxilla:

(0) Absent; (1) Present.

Filikomys = 1

83. Curvature of anterior zygomatic root (best viewed in dorsal view):

(0) Zygomatic root aligned with (or lightly incurved into) facial part of rostrum; (1) Zygomatic root is more transverse and deeply incurved with facial part of rostrum.

Filikomys = 0

84. Number of pairs of vascular foramina on nasal:

(0) Absent; (1) One; (2) Two; (3) Three or more.

Filikomys = 2

85. Posterior-most infraorbital foramen positions (Ordered):

(0) Dorsal to P3 or P4, or more posterior; (1) Dorsal to P2; (2) Dorsal to P1.

Filikomys = 0

86. Base of zygomatic arch as marked by posterior edge:

(0) Dorsal to P4 or more anterior; (1) Dorsal or posterior to P5/M1 or P4/M1 embrasure, or farther posterior.

Filikomys = 0

87. Bony roof over anterior orbital space:

(0) Absent; (1) Present.

Filikomys = 0

88. Postorbital process:

(0) Absent; (1) Present and short; (2) Present and long.

Filikomys = 0

89. Snout length:

(0) < 49 percent of total skull length; (1) > 50 percent of skull length.

Filikomys = 0

90. Frontal/nasal suture pattern:

(0) With subtransverse anterior margins or zigzag line; (1) Pointed anteriorly and not deeply inserted between the nasals; (2) Frontal deeply inserted between the nasals.

Filikomys = 1

91. Frontal-parietal suture:

(0) Roughly V-shaped parietal lappet into frontal; (1) U-shaped.

Filikomys = 0

92. Contacts between nasals and parietals:

(0) Absent; (1) Present.

Filikomys = 0

93. Facial exposure of lacrimal:

(0) Very small and arcuate; (1) Large, roughly rectangular.

Filikomys = 0

94. Thickening in palatal process of premaxilla:

(0) Absent; (1) Present.

Filikomys = 0

95. Incisive foramen positioned:

(0) Within premaxilla; (1) Limited posteriorly by maxilla.

Filikomys = 1

96. Foramen ovale inferium placement:

(0) Medial to foramen masticatorium; (1) Posterior 1254 to foramen masticatorium.

Filikomys = 0

97. Jugular fossa:

(0) Small and shallow; (1) Large and deep.

Filikomys = 0

98. Anterior part of promontorium:

(0) 1.5 or more; (1) Below 1.49.

Filikomys = ?

99. Glenoid fossa length-width ratio (length as measured as maximum dimension from anterolateral to posteromedial end of glenoid for multituberculates):

(0) Oval; (1) Irregular within curvatures on both sides.

Filikomys = 1

100. Post-temporal fossa:

(0) Large (as seen in Ptilodus); (1) Reduced to a small foramen.

Filikomys = 0

101. Width of the snout: skull length ratio:

(0) Above 0.4; (1) Below 0.39.

Filikomys = 1

102. Skull width: length ratio:

(0) 0.79 and below; (1) Above 0.8.

Filikomys = 0

103. Length ratio (R) of ultimate vs. penultimate upper premolar:

(0) subequal (R = 1-1.25); (1) penultimate premolar lengthened, R < 1; (2) penultimate premolar shortened, 3 > R> 1.25; (3) penultimate premolar strongly shortened, R > 3; (4) penultimate premolar lost, only one premolar present.

Filikomys = 3

104. Length ratio (R) of M1 to penultimate premolar (we use the term 'penultimate premolar' topologically, without inferring homology of this tooth position across the sampled taxa):

(0) roughly subequal, 1.5 > R > 1; (1) penultimate premolar elongated, R < 1; (2) penultimate premolar shortened, 3.5 > R > 1.5; (3) penultimate premolar strongly shortened, R > 3.5; (4) penultimate premolar lost, only one premolar present.

Filikomys = 3

105. Length ratio (R) of ultimate upper premolar vs. M1:

(0) premolar and molar subequal, R < 1.5; (1) ultimate premolar shortened, 3 > R > 1.5; (2) ultimate premolar vestigial, R > 3.

Filikomys = 0

106. Ratio (R) of width to length in M1:

(0) M1 wide, R > 0.55; (1) M1 elongated, R ≤0.55.

Filikomys = 1

107. Length ratio (R) of M2 vs. M1:

(0) R > 0.7; (1) M1 elongated, 0.7 > R > 0.5; (2) M1 strongly elongated, R < 0.5.

Filikomys = 1

108. Masseteric ridge:

(0) Weak; (1) Prominent.

Filikomys = 0

109. Masseteric fovea in front of masseteric fossa:

(0) Absent; (1) Present.

Filikomys = 1

110. Coronoid process — form:

(0) Relatively Massive; (1) Low and short; (2) High and short.

Filikomys = 0

111. Dorsal margin of the posterior part of mandible — neck:

(0) Shallow; (1) Deep.

Filikomys = 0

112. Mandibular condyle, size, relative to mandible size:

(0) Large; (1) Small.

Filikomys = 0

113. Mandibular condyle — orientation:

(0) Facing posteriorly; (1) Facing dorsoposteriorly.

Filikomys = 1

114. Lower incisor — tooth crown (rodent-like):

(0) Rounded; (1) Strongly laterally compressed.

Filikomys = 0

115. Two-cusped I2, the posterior cusp: position:

(0) Small cuspule, close to the tip of tooth crown; (1) Small cuspule, more posterodorsal to the tip of tooth crown.

Filikomys = ?

116. Upper incisor 3 — form:

(0) Conical; (1) Triangular or trapezoidal; (2) Transversely wide and anteroposteriorly compressed.

Filikomys = 2

117. Second upper premolar, size, relative to the first upper premolar (for taxa that have four or five upper premolars):

(0) Smaller; (1) Larger.

Filikomys = 0

118. M1/m1 multiple accessory roots:

(0) Absent; (1) Present.

Filikomys = 0

119. Posterobuccal cingulid on m1:

(0) Absent; (1) Present.

Filikomys = 0

120. Post-trigeminal canal (canal for the ramus inferior):

(0) Present; (1) Absent.

Filikomys = 0

121. Stapedial groove:

(0) Absent; (1) Present, running posterolaterally on the promontorium to the oval window; (2) Present, runs wholly posterior to the oval window.

Filikomys = ?

122. Stapes — form:

(0) Columelliform–macroperforate; (1) Columelliform-microperforate (or imperforate); (2) Bicrurate-perforate; (3) Bicrurate-perforate with a large posterior process.

Filikomys = ?

123. The enamel of p4:

(0) Complete; (1) Limited to a part of tooth crown.

Filikomys = 0

124. Tooth crown of the ultimate upper premolar in lateral view, outline:

(0) Relatively flat or conical; (1) Triangular.

Filikomys = 0

125. Penultimate upper premolar, outline:

(0) Triangular or square; (1) Rectangular with length greater than width.

Filikomys = 0

126. Ultimate upper premolar: the length to width ratio:

(0) < 1.4; (1) 1.4–1.7; (2) > 1.7.

Filikomys = 2

127. Ultimate upper premolar: main cusp row count:

(0) 1–4; (1) 5–8; (2) > 8.

Filikomys = 1

128. The reduced upper premolar for taxa that have four upper premolars:

(0) P4; (1) P1; (2) P2.

Filikomys = 0

129. Upper premolar enamel surface:

(0) Not ornamented; (1) Ornamented with ridges.

Filikomys = 0

130. m2, lingual cusp row, facing medially:

(0) Absent; (1) Present.

Filikomys = 0

Character scorings for North American cimolodontans that differ from Wang et al. (2019)

5. Angle of the coronoid anterior margin to the molar alveolar line on the mandibular body:

(0) > 45 degrees; (1) Low < 45 degrees.

Mesodma = 0

19. Upper Incisor 2 (or penultimate incisor) morphology:

(0) Peg-like or single cusp; (1) Two-cusped, or more.

Mesodma = ?

20. Upper Incisor 3 (or ultimate upper incisor) morphology:

(0) Single cusped or peg-like; (1) 2-cusped; (2) 3–4 cusped.

Mesodma = ?

43. Blade-like p4 serration count (Ordered):

(0) 7 or less; (1) 8–10; (2) More than 10.

Mesodma = 1&2

48. Ratio of p4:m1 length (Ordered):

(0) Less than 0.99; (1) 1–1.49; (2) 1.5–1.99; (3) 2 or greater.

Mesodma = 1&2

Cimolodon = 1&2

58. M1 posterolingual wing M1 length (applicable to M1 with multiple rows) (Ordered):

(0) Present and below 0.2; (1) Present and between 0.2 and 0.5; (2) Present and more than 0.5.

Mesodma = 2

59. M1 posterolingual wing morphology (applicable only to M1s with posterolingual wing) (Ordered):

(0) Wing smooth; (1) Wing is crested; (2) Wing cuspate with 3–4 cuspules; (3) Wing cuspate with 5 or more cuspules.

Mesodma = 2&3

67. m1 main lingual cusp count:

(0) 4 or fewer; (1) 5; (2) 6 or higher.

Mesodma = 0&1

Cimolodon = 0&1

72. m2 lingual row cusp count (Ordered):

(0) One trenchant anterior cusp; (1) 2–3; (2) 4–5.

Mesodma = 1&2

109. Masseteric fovea in front of masseteric fossa:

(0) Absent; (1) Present.

Mesodma = 1

113. Mandibular condyle — orientation:

(0) Facing posteriorly; (1) Facing dorsoposteriorly.

Mesodma = ?

Cimolodon = ?

Ptilodus = 1

126. Ultimate upper premolar: the length to width ratio:

(0) < 1.4; (1) 1.4–1.7; (2) > 1.7.

Mesodma = 2

Character scoring for phylogeny

Meniscoessus

1	1	2	1	1	?	0	1	?	1	1	1	1
1	0	0	2	1	1	1	1	2	?	1	2	1
0	0	2	2	0	2	1	1	0	0	1	3	1
1	1	2	1	1	0	3	0	0	1	1	2	2
0	1	2&3	1	1	2	3	1	2	2	3	0	0
1	1	?	1	0	0	2	1	1	0	1	1	1
?	0	2	1	0	?	0	1	?	?	?	?	?
?	?	0	1	?	?	?	?	?	?	?	?	3
1	0	0	?	?	?	?	?	?	0	?	?	?
1	0	?	1	?	0	1	?	1	0	0	0	0

Mesodma

1	1	2	1	0	?	0	1	?	1	1	1	1
1	1	0	2	?	?	?	1	2	?	1	?	1
0	0	?	2	1	1	1	1	0	0	1	3	1
1	1	2	1&2	1	1	3	0	1&2	1	1	2	2
0	1	2	1	1	2	2&3	1	1	2	3	0	0
1	0&1	1	1	0	0	1&2	1	0	0	1	2	1
1	1	?	?	?	?	?	?	?	?	?	?	?
?	?	?	?	?	?	?	?	?	?	?	?	?
0	1	?	0	1	?	0	0	?	0	?	?	?
0	0	0	?	?	0	0	?	2	1	0	0	0

Cimolodon

1	1	2	1	0	?	0	1	?	1	1	1	1
1	?	0	?	?	?	?	?	2	?	1	?	1
0	0	1	2	1	1	1	1	0	0	1	3	1
1	1	2	2	1	1	2	0	1&2	1	1	2	2
0	1	2	1	1	2	2	1	2	2	3	0	0
1	0&1	1	1	0	0	2	1	0	0	1	1	1
1	?	?	?	?	?	?	?	?	?	?	?	?
?	?	?	?	?	?	?	?	?	?	?	2	2
0	1	0	0	?	0	0	0	?	0	?	?	?
0	?	?	?	?	0	0	0	1	1	0	0	0

Ectypodus

1	1	2	1	0	?	0	1	1	1	1	1	1
1	1	0	2	1	0	1	1	2	?	1	0	1
0	0	1	2	2	1	1	1	0	0	1	3	1
1	1	2	2	1	1	3	0	3	1	1	2	2
0	1	2&3	1	1	1	3	1	1	2	3	1	0
1	2	1	1	0	0	2	1	0	0	1	2	1
1	1	1	?	2	?	0	1	0	?	0	?	?
0	?	?	1	1	0	0	1	?	1	0	2	2

0	1	1&2	0	1	0	0	0	0	0	?	?	0
?	0	?	1	?	0	0	0	1	1	0	0	0

Ptilodus

1	1	2	1	0	0	0	1	0	1	1	1	1
1	1	0	2	1	0	0	1	2	?	1	0	1
0	0	0	2	2	1	1	1	0	0	1	3	1
1	1	2	2	1	1	3	0	2	1	1	2	2
0	1	2&3	1	1	1	3	1	1	2	3	1	0
1	2	1	1	0	0	2	1	0	0	1	2	1
1	1	1	1	0	2	0	0	0	?	0	0	0
0	0	0	1	0	0	0	1	0	1	0	2	2
0	1	2	0	0	0	0	0	1	0	?	?	0
0	0	1	1	?	0	0	0	1	1	0	0	0

Neoliotomus

1	1	2	1	1	?	0	1	?	1	1	1	1
1	0	2	?	?	0	?	?	?	?	1	?	1
0	0	1	2	2	1	1	1	0	0	1	3	1
1	1	2	2	1	1	3	0	3	1	1	2	2
0	1	3	1	1	2	3	1	1	2	3	0	0
1	2	1	1	0	0	2	1	1	0	1	2	1
?	?	?	?	?	?	?	?	?	?	?	?	?

? ? ? ? ? ? ? ? ? ? ? 2 2

0 1 2 ? ? ? 0 ? ? ? ? ? ?

? ? ? ? ? 0 0 0 1 1 0 0 0

Pentacosmodon

1 1 2 ? 0 0 1 1 1 1 1 1 1

1 0 1 ? ? ? ? ? ? ? 1 ? ?

? ? ? ? 0 ? 1 1 1 0 ? ? ?

1 1 2 0 1 0 ? 1 0 1 1 ? 2

0 1 ? ? ? 1 ? ? ? ? ? ? ?

? 0 1 1 0 0 1 1 0 0 0 1 1

? ? ? 2 ? ? ? ? ? ? ? ? ?

? ? ? ? ? ? ? ? ? ? ? ? ?

? ? ? 0 0 ? 0 0 0 1 ? ? ?

1 0 ? ? ? 0 ? ? ? ? ? ? 0

Eucosmodon

1 1 2 1 1 ? 1 1 0 1 1 1 1

1 0 2 2 ? 1 1 ? 2 ? 1 ? 2

0 0 ? 2 ? ? 1 1 1 ? ? ? ?

? 1 2 2 1 0 ? 0 1 1 1 2 2

0 1 2 1 1 ? ? 1 ? 2 3 ? ?

1 1 1 1 0 0 2 1 0 0 0 1 1

? 1 ? ? ? ? ? ? ? ? ? ? ?

? ? ? ? ? ? ? ? ? ? ? ? ?

? ? ? 0 0 ? ? ? ? 1 ? ? 0

0 ? ? ? ? 0 0 ? 1 1 ? 0 0

Stygimys

1 1 1 1 1 0 0 1 0 1 1 1 1

1 0 2 2 1 1 1 1 2 ? 1 1 1

0 0 1 2 2 1 1 1 1 ? ? ? ?

? 1 2 2 1 0 ? 1 1 1 1 2 2

0 1 2 1 1 1 2&3 1 1 2 3 0 0

1 2 1 1 0 0 1 1 0 0 0 1 1

? 1 2 1 0 ? 2 0 ? ? ? ? ?

? ? 1 1 ? ? ? ? ? ? ? 2 2

0 1 1 1 1 1 1 0 0 1 0 ? 0

0 0 ? ? ? 0 0 0 1 2 ? 0 0

Microcosmodon

1 1 2 ? 0 ? 0 1 1 1 1 1 1

1 0 1 2 1 1 1 1 2 ? 1 0 1

0 0 1 2 1 2 1 1 0 0 1 2 1

1 1 2 0 1 0 ? 1 2 1 1 2 2

0 1 2 1 1 1 3 1 1 2 3 0 0

1	2	1	1	0	0	1	1	0	0	0	?	1
1	1	0	1	1	?	0	0	0	?	?	?	?
?	?	?	1	?	?	?	1	?	?	?	?	?
0	0	?	?	?	?	?	?	?	1	?	?	?
1	0	?	?	?	0	0	?	2	1	?	0	0

Taeniolabis

1	1	2	1	0	0	0	1	1	1	1	1	1
1	0	2	2	0&1	1	0	0	2	?	1	2	3
1	0	2	2&3	0	3	1	1	1	?	?	?	?
?	0	3	?	0	0	?	1	0	1	1	3	2
0	1	3	1	1	2	3	1	1&2	2	4	0	2
1	2	1	1	0	0	2	0	2	0	0	1	1
1	1	0	1	1	3	0	?	0	?	0	2	0
1	0	0	?	?	?	?	?	1	1	1	4	4
1	1	1	0	1	1	1	1	0	0	?	0	?
0	1	?	?	?	?	0	?	1&2	0	?	0	0

Catopsalis

1	1	2	1	0	0	0	1	0&1	1	1	1	1
1	0	2	2	0&1	1	0	0	2	?	1	2	3
1	0	2	2&3	1	3	1	1	1	?	?	?	?
?	0	3	?	0	0	?	1	0	1	1	3	2

0	1	3	1	1	2	3	1	1	2	4	0	1&2
1	0&1	1	1	0	0	1	0&1	2	0	0	1	1
?	?	?	?	?	?	?	?	?	?	?	?	?
?	?	?	?	?	?	?	?	?	?	?	4	4
1	0	1	0	0	?	?	?	0	0	?	0	?
0	1	?	?	?	0	0	0	1&2	0	?	0	0

Sinoconodon

0	0	0	0	0	0	0	0	0	0	0	0	0
0	0	0	0	0	0	0	0	0	0	0	0	0
0	0	2	?	0	0	0	0	0	0	0	0	?
0	0	0	?	0	0	1	0	0	?	?	0	0
0	0	?	0	?	?	?	0	1	0	0	?	?
0	0	0	0	?	?	?	?	?	?	0	0	0
0	0	0	0	0	1	0	0	0	0	1	0	0
0	0	0	0	?	0	0	0	0	0	0	?	?
?	?	?	0	0	0	0	0	?	?	?	0	1
0	0	?	0	0	0	?	?	?	?	?	?	?

Morganucodon

0	0	0	0	0	0	0	0	0	0	0	0	0
0	0	0	0	0	0	0	0	0	0	0	0	0
0	0	2	?	0	0	0	0	0	0	0	0	?

0 0 0 ? 0 0 1 0 0 0 0 0 0

0 0 ? 0 ? ? ? 0 1 0 0 ? ?

0 0 0 0 ? ? ? ? ? ? 0 0 1

1 0 0 0 0 0 0 0 0 0 1 0 0

0 0 0 0 ? 0 0 0 0 0 0 ? ?

? ? ? 0 0 0 0 0 ? ? ? 0 1

0 0 ? 0 0 0 ? ? ? ? ? ? ?

Thomasia

? ? ? ? ? ? ? ? ? ? 0 1 ?

? 0 0 0 ? 0 0 ? ? ? ? ? 3

0 0 2 0 0 1 ? ? 0 0 0 0 ?

0 0 1 ? 0 0 1 0 0 0 0 ? ?

1 0 ? 0 0 ? ? 0 1 1 3 0 0

0 0 ? 2 0 0 2 0 0 0 0 ? 1

? ? ? ? ? ? ? ? ? ? ? ? ?

? ? ? ? ? ? ? ? ? ? ? ? ?

? 0 0 ? ? ? 0 ? ? ? ? ? ?

? ? ? ? ? 0 ? ? ? ? ? ? ?

Haramiyavia

0 0 0 ? 1 0 0 0 0 0 0 1 0

0 0 0 0 1 0 0 0 1 0 0 ? ?

? ? ? ? ? ? 0 0 0 0 0 0 ?

0 0 0 ? 0 0 ? 0 0 0 0 0 0

1 0 ? 0 0 ? ? 0 1 1 3 0 0

1 0 1 2 0 0 2 0 0 0 0 1 1

? ? ? ? ? ? ? ? 0 ? ? ? ?

? ? ? ? ? ? ? ? ? ? ? ? ?

? 0 0 0 0 0 0 ? ? 0 ? ? ?

0 0 ? ? ? 0 ? ? ? ? ? ? ?

Meketichoffatia

? ? ? ? ? ? ? ? ? ? ? ? ?

? ? ? ? ? ? ? ? 1 1 ? 0 0

0 1 0 0 0 0 ? ? ? ? ? ? ?

? ? ? ? ? ? ? ? ? ? 1 1 ?

? ? 0 0 0 ? ? 1 ? 1 1 ? ?

? ? ? ? ? ? ? ? ? ? 1 ? 1

? 0 0 0 0 ? ? 0 0 ? 0 0 ?

? ? ? 1 1 0 0 0 ? 1 0 0 0

0 0 0 ? ? ? ? ? ? ? ? ? 0

0 ? ? 1 0 ? 0 0 0 0 ? 0 ?

Henkelodon

? ? ? ? ? ? ? ? ? ? ? ? ?

? ? ? 1 0 1 2 0 2 ? ? 0 0

0 1 0 0 0 0 ? ? ? ? ? ? ?

? ? ? ? ? ? ? ? ? ? 1 1 ?

? ? 0 1 0 ? ? 1 ? 1 2 ? ?

? ? ? ? ? ? ? ? ? ? 1 ? 1

1 0 ? ? ? ? ? ? ? ? ? ? ?

? ? ? ? ? ? ? ? ? ? ? 0 0

0 0 ? ? ? ? ? ? ? ? 0 1 0

0 ? ? ? ? ? 0 0 0 0 ? 0 ?

Rugosodon

1 1 1 ? 1 ? 0 1 0 1 1 1 1

1 0 0 1 0 1 1 0 1 1 1 0 0

0 ? 0 0 ? ? 0 0 0 1 ? 1 ?

0 1 1 0 0 1 ? ? 1 1 1 1 1

1 0 0&1 1 0 ? ? 1 0 1 1 1 1

2 0 2 2 1 1 0 0 0 1 1 1 1

1 0 ? ? ? ? 0 ? ? ? 0 ? ?

? 1 1 ? ? ? ? ? ? ? ? 2 0

0 0 0 0 0 0 0 0 0 0 0 1 0

0 0 ? ? ? 0 0 0 0 0 ? 0 0

Paulchoffatia

1 1 1 ? 1 0 0 1 0 1 1 1 0

1 0 0 ? ? ? ? ? ? ? 1 ? ?

? ? ? ? ? ? 0 0 0 1 0 1 0

0 1 1 0 0 1 0 2 1 1 ? ? 1

1 0 0 ? ? ? ? ? ? ? ? ? ?

? 0 2 2 1 1 0 0 0 2 1 1 1

? ? ? ? ? ? ? ? ? ? ? ? ?

? ? ? ? ? ? ? ? ? ? ? ? ?

? ? ? 0 0 0 0 0 0 0 ? ? ?

0 0 ? ? ? 0 ? ? ? ? ? ? 0

Meketibolodon

1 1 1 1 1 0 0 1 0 1 1 1 0

1 0 0 ? ? ? ? ? ? ? 1 ? ?

? ? ? ? ? ? 0 0 0 1 0 1 0

0 1 1 0 0 1 0 3 ? ? ? ? ?

? ? 0 ? ? ? ? ? ? ? ? ? ?

? ? 2 ? ? ? 0 ? ? 2 1 ? 1

? ? ? ? ? ? ? ? ? ? ? ? ?

? ? ? ? ? ? ? ? ? ? ? ? ?

? ? ? 0 0 0 0 0 0 0 ? ? ?

0 0 ? ? ? 0 ? ? ? ? ? ? 0

Guimarotodon

1 1 1 1 1 0 0 1 0 1 1 1 0

1 0 0 ? ? ? ? ? ? ? 1 ? ?

? ? ? ? ? ? 0 0 0 1 0 1 0

0 1 1 0 0 1 0 3 1 1 ? ? 1

1 0 ? ? ? ? ? ? ? ? ? ? ?

? 0 2 2 1 1 0 0 0 2 1 1 1

? ? ? ? ? ? ? ? ? ? ? ? ?

? ? ? ? ? ? ? ? ? ? ? ? ?

? ? ? 0 0 ? 0 0 0 0 ? ? ?

0 0 ? ? ? 0 ? 0 ? ? ? ? 0

Kuehneodon

1 1 1 0 1 0 0 1 0 1 1 1 1

1 0 0 1 0 1 2 0 1 1 1 0 1

0 1 0 0 0 0 0 0 0 1 0 1 0

0 1 1 0 0 1 0 2 1 1 1 2 1

1 0 0 1 0 ? ? 1 0 1 2 1 1

2 0 2 2 1 1 1 0 0 1&2 1 1 1

1 0 ? ? ? ? ? ? 0 ? ? ? ?

? ? ? ? ? ? ? ? ? ? ? 0 0

0 0 0 0 0 0 0 0 0 0 1 ? 0

0 0 ? ? ? 0 0 0 0 0 1 0 0

Pseudobolodon

? ? ? ? ? ? ? ? ? ? ? ? ?

? ? ? 1 0 0 0 ? 0 1 ? ? 0

0 0 ? 1 0 ? ? ? ? ? ? ? ?

? ? ? ? ? ? ? ? ? ? ? ? ?

? ? ? ? ? ? ? ? ? ? ? ? ?

? ? ? ? ? ? ? ? ? ? ? ? ?

? ? ? ? ? ? ? ? ? ? ? ? ?

? ? ? ? ? ? ? ? ? ? ? 0 ?

? ? ? ? ? ? ? ? ? ? ? ? 0

? ? ? 1 2 ? 0 0 0 ? ? 0 ?

Ctenacodon

1 1 1 1 0 ? 1 1 1 1 1 1 1

1 0 0 1 0 1 1 0 1 ? 1 0 0

0 1 0 1 0 0 0 0 0 1 0 1 1

0 1 1 0 0 1 1 2 1 1 1 1 1

0 1 1 1 1 0 0 1 0 2 3 0 0

1 0 1 1 0 0 1 1 0 0 0 0 1

? 0 ? ? 0 ? ? 0 ? ? ? ? ?

? ? ? ? ? ? ? ? ? ? ? 0 0

0 0 0 0 0 0 0 0 0 0 ? ? 0

? 0 ? ? ? 0 1 0 1 0 ? 0 0

Glirodon

1	1	1	1	0	0	1	1	1	1	1	1	1
1	0	1	1	0	1	1	0	1	0	1	0	0
0	1	0	1	0	0	0	0	0	?	0	1	1
0	1	1	0	0	1	1	2	1	1	1	1	1
0	1	0	1	0	?	?	1	0	2	3	0	0
1	0	1	1	0	0	1	1	0	0	0	0	1
?	0	0	1	0	1	1	0	0	?	?	0	?
0	?	?	1	?	?	?	?	?	?	?	0	0
0	0	0	?	?	?	?	?	?	?	?	0	0
0	?	?	?	?	0	0	0	1	0	?	0	0

Bolodon

1	1	1	1	1	?	1	1	?	?	1	1	1
?	0	0	?	?	?	?	?	1	?	1	?	0
0	1	0	1	0	0	0	0	0	1	0	2	1
0	1	1	0	0	1	1	2	?	1	1	1	1
0	1	0	1	1	0	0	1	0	2	3	0	0
1	0	?	1	?	?	1	1	0	0	1	0	1
?	0	0	?	?	?	1	?	?	?	?	?	?
?	?	?	?	?	?	?	?	?	?	?	0	0

0 0 0 0 0 0 0 0 ? 0 ? ? 0

0 0 ? ? ? 0 1 0 1 0 ? 0 ?

Plagiaulax

1 1 1 1 0 0 1 1 1 1 1 1 1

1 0 0 ? ? ? ? ? ? ? 1 ? ?

? ? ? ? ? ? 1 0 0 1 0 2 1

0 1 1 1 0 ? 1 2 ? 1 ? ? 1

0 1 ? ? ? ? ? ? ? ? ? ? ?

1 0 1 1 0 0 1 1 ? 0 0 0 1

? ? ? ? ? ? ? ? ? ? ? ? ?

? ? ? ? ? ? ? ? ? ? ? ? ?

? ? ? 1 0 0 0 0 0 0 ? ? ?

0 0 ? ? ? 0 ? ? ? ? ? ? 0

Zofiabaatar

1 1 1 1 0 0 1 1 1 1 1 1 ?

1 0 ? ? ? ? ? ? ? ? ? ? ?

? ? ? ? ? ? 0 0 0 1 0 1 1

0 1 1 0 0 1 1 2 3 1 ? ? 1

0 1 ? ? ? ? ? ? ? ? ? ? ?

1 0 ? 1 0 0 1 1 0 0 0 0 1

? ? ? ? ? ? ? ? ? ? ? ? ?

? ? ? ? ? ? ? ? ? ? ? ? ?

? ? ? 0 0 0 0 0 0 0 ? ? ?

0 0 ? ? ? ? ? ? ? ? ? ? 0

Sinobaatar

1 1 1 1 0 ? 1 1 0 1 1 1 1

1 0 0 1 1 0 1 ? 2 ? 1 0 0

0 0 0 2 0 1 1 0 0 1 1 2 1

0 1 2 1 1 1 2 1 2 1 1 1 2

0 1 1 1 1 1 0 1 1 2 3 0 0

1 0 1 1 1 0 1 1 0 0 1 0 1

1 1 0 1 ? 1 0 1 0 ? ? ? ?

? 1 ? ? ? ? ? ? ? ? ? 2 0

0 0 0 0 0 0 0 0 0 0 ? 2 0

0 0 ? ? 1 0 1 0 2 0 ? 1 1

Eobaatar

1 1 ? 1 ? ? ? 1 ? 1 1 1 1

1 0 2 ? ? ? ? ? ? ? 1 ? 0

0 0 0 0 0 1 1 0 0 1 0 2 1

0 1 2 1 1 ? 2 1 ? 1 1 1 2

0 1 0 1 1 1 0 1 1 2 3 0 0

1 0 1 1 1 0 1 1 0 0 1 1 1

? ? ? ? ? ? ? ? ? ? ? ? ?

? ? ? ? ? ? ? ? ? ? ? 0 0

0 0 0 ? ? ? ? ? ? 0 ? ? 0

0 0 ? ? ? 0 1 0 2 0 ? 1 1

Jeholbaatar

1 1 1 1 0 0 1 1 0 1 1 1 1

1 0 0 1 1 1 0 0 2 ? 1 0 0

0 0 0 2 0 1 1 0 0 1 1 2 1

0 1 2 1 1 1 2 1 2 1 1 1 2

0 1 1 1 1 1 0 1 1 2 3 0 0

1 0 1 1 1 0 1 1 0 0 1 ? 1

? 1 ? ? 0 ? ? 1 ? 0 ? ? ?

0 ? ? ? ? 1 ? ? 1 ? 0 2 0

0 0 0 0 0 0 0 0 0 0 0 2 0

0 0 ? 2 1 0 1 0 2 0 ? 1 1

Heishanobaatar

1 1 1 1 0 0 1 1 0 1 1 1 1

1 0 0 ? ? ? ? ? ? ? 1 ? ?

? ? ? ? ? ? 1 0 0 1 1 1 1

0 1 2 1 1 1 1 1 2 1 ? ? 2

0 1 ? ? ? ? ? ? ? ? ? ? ?

? 0 1 1 1 0 1 1 0 0 1 ? 1

? ? ? ? ? ? ? ? ? ? ? ? ?

? ? ? ? ? ? ? ? ? ? ? ? ?

? ? ? 0 0 0 0 0 0 0 ? ? ?

0 0 ? ? ? 0 ? ? ? ? ? ? 1

Liaobaatar

1 1 1 1 0 0 1 1 0 1 1 1 1

1 0 0 ? ? ? ? ? ? ? ? ? ?

? ? ? ? ? ? 1 0 0 1 1 2 1

1 1 2 2 1 1 2 1 3 1 ? ? 2

0 1 ? ? ? ? ? ? ? ? ? ? ?

? 0 1 1 1 0 1 1 0 0 1 ? 1

? ? ? ? ? ? ? ? ? ? ? ? ?

? ? ? ? ? ? ? ? ? ? ? ? ?

? ? ? 0 0 0 0 0 0 0 ? ? ?

0 0 ? ? ? 0 ? ? ? ? ? ? 1

Hakusanobaatar

? ? ? ? ? ? ? ? ? ? ? 1 ?

1 0 1 ? ? 1 0 ? 2 ? 1 ? 0

0 0 ? 2 1 1 1 0 0 1 1 1 1

0 1 2 1 1 1 2 1 ? 1 ? ? 2

0 1 1 1 1 1 0 ? ? ? 3 ? ?

? ? ? ? ? ? ? ? 0 0 1 ? 1

? ? ? ? ? ? ? ? ? ? ? ? ?

? ? ? ? ? ? ? ? ? ? ? 0 ?

? ? ? ? 0 ? ? ? ? ? 0 2 0

0 ? ? ? ? 0 0 0 1 1 ? 1 ?

Arginbaatar

? 1 2 1 0 ? ? 1 ? ? 1 1 1

1 0 0 ? ? ? ? ? ? ? 1 ? 0

0 0 0 0 0 1 1 0 0 0 1 2 1

1 1 2 2 1 1 2 0 3 1 1 1 2

0 1 0 1 1 0 0 1 0 2 3 0 0

1 0 1 1 0 0 1 1 0 0 0 1 1

? 0 ? ? ? ? ? ? ? ? ? ? ?

? ? ? ? ? ? ? ? ? ? ? 1 ?

? ? ? 0 0 0 ? ? ? 0 ? ? 0

0 ? ? ? ? 1 0 0 1 0 ? 1 0

Boffius

? ? ? ? ? ? ? ? ? ? ? ? ?

? 0 1 2 ? ? ? ? ? ? ? ? ?

? ? ? ? 1 1 ? ? ? ? ? ? ?

? ? ? ? ? ? ? ? ? 1 ? ? ?

? ? 3 ? 1 2 3 1 ? 2 3 ? ?

1 ? ? ? ? ? ? 1 ? 0 0 1 1

? ? ? ? ? ? ? ? ? ? ? ? ?

? ? ? ? ? ? ? ? ? ? ? 2 2

0 0 ? ? ? ? ? ? ? ? ? ? ?

? ? ? ? ? ? ? 0 ? ? ? ? ?

Buginbaatar

1 1 1 1 1 0 0 1 ? ? 1 1 ?

1 0 0 ? ? ? ? ? ? ? ? ? ?

? 0 ? 2 1 3 1 1 1 ? ? ? ?

? 1 2 0 0 0 ? 0 0 1 1 ? 2

0 1 3 1 1 1 3 1 2 2 3 0 0

1 2 ? 1 0 0 1 1 0 0 0 ? 1

? ? ? ? ? ? ? ? ? ? ? ? ?

? ? ? ? ? ? ? ? ? ? ? ? ?

1 1 1 ? ? ? ? ? ? ? ? ? ?

0 ? ? ? ? 0 ? ? ? ? ? ? ?

Catopsbaatar

1 1 2 1 0 0 1 1 1 1 1 1 1

1 0 2 2 1 0 1 2 2 ? 1 0 2

0	0	2	2	1	2	1	1	0	0	1	3	1
1	1	1	0	0	0	3	0	2	1	1	3	2
0	1	2	1	1	2	3	1	0	2	3	0	0
1	0	1	1	0	0	1	1	0	0	0	1	1
?	1	0	2	2	2	0	1	1	1	1	1	1
0	1	1	0	?	1	1	0	0	0	1	2	2
1	0	1	0	1	2	1	1	1	0	?	0	0
0	0	?	?	?	0	0	0	2	1	2	0	0

Kamptobaatar

1	1	2	1	1	1	0	1	1	1	1	1	1
1	0	1	2	1	0	1	2	2	?	1	0	1
0	0	1	2	1	2	1	1	0	0	1	3	1
1	1	2	1	1	0	3	0	1	1	1	2	2
0	1	1	1	1	0	1	1	1	2	3	0	0
1	0	1	1	0	0	1	1	0	0	0	1	1
?	1	0	2	0	3	2	0	1	0	0	1	1
0	1	1	1	0	1	0	0	0	1	0	3	3
0	0	1	0	1	1	0	1	1	0	?	0	0
0	0	?	1	?	0	0	0	2	1	0	0	0

Chulsanbaatar

1	1	2	1	1	0	1	1	0	1	1	1	1
1	0	2	2	1	0	1	2	2	?	1	0	1
0	0	1	2	1	2	1	1	0	0	1	3	1
1	1	2	1	1	0	3	0	1	1	1	2	2
0	1	1	1	1	0	1	1	1	2	3	0	0
1	0	1	1	0	0	1	1	0	0	0	1	1
1	1	0	2	0	2	2	0	1	0	0	1	1
0	1	1	1	1	1	0	0	0	1	0	2	2
0&1	0&1	2	1	1	1	0	1	0	0	?	0	0
0	0	?	1	1	0	0	0	2	1	0	0	0

Kryptobaatar

1	1	2	1	1	0	0	1	0	1	1	1	1
1	0	2	2	1	0	1	2	2	?	1	0	1
0	0	1	2	1	2	1	1	0	0	1	3	1
1	1	2	1	1	0	3	0	1	1	1	2	2
0	1	1	1	1	0	2	1	2	2	3	0	0
1	0	1	1	0	0	1	1	0	0	0	1	1
1	1	0	2	2	2	1	0	1	1	1	1	1
0	1	1	1	1	1	1	0	0	0	1	2	2
0	0&1	2	0	1	1	0	0	0	0	?	0	0
0	0	0	1	2	0	0	0	2	1	0	0	0

Nemegtbaatar

1	1	2	1	1	0	0	1	0	1	1	1	1
1	0	2	2	1	0	1	2	2	?	1	1	1
0	0	1	2	1	2	1	1	0	0	1	3	1
1	1	2	1	1	0	3	0	1	1	1	2	2
0	1	1&2	1	1	2	2	1	2	2	3	0	0
1	0	1	1	0	0	1	1	0	0	0	1	1
1	1	2	2	0	3	1	0	1	0	0	1	1
0	1	1	1	0	1	0	0	0	1	0	2	3
1	1	2	0	1	1	0	?	1	0	?	0	0
0	0	0	1	?	0	0	0	2	1	0	0	0

Kogaionon

?	?	?	?	?	?	?	?	?	?	?	?	?
?	?	?	2	1	0	1	1	2	?	?	1	1
0	0	0	3	0	1	?	?	?	?	?	?	?
?	?	?	?	?	?	?	?	?	?	1	2	?
?	?	1	1	1	2	2	1	0	2	3	0	0
1	?	?	?	?	?	?	?	?	?	0	?	1
?	1	0	1	1	3	0	0	0	0	0	0	0
0	?	?	1	?	1	?	1	?	1	0	1	1
0	0	0	0	?	?	?	?	?	?	?	0	?
0	?	?	?	?	?	0	1	1	0	?	0	?

Lambdopsalis

1	1	2	1	0	1	1	1	1	1	1	1	1
1	0	2	2	0	0	0	0	2	?	1	2	3
1	0	2	3	0	3	1	1	1	?	?	?	?
?	0	3	?	0	0	?	0	0	1	1	3	2
2	1	3	1	1	2	3	1	0	1	3	0	0
1	0	2	2	0	0	1	1	1	0	0	1	1
1	1	0	1	1	3	0	1	0	1	0	2	0
1	0	0	1	?	1	1	1	1	1	1	4	4
2	1	1	0	1	1	1	1	0	0	?	0	?
0	0	0	2	1	0	0	?	0	0	?	0	0

Sphenopsalis

1	1	?	1	?	?	?	1	?	1	1	1	1
1	0	2	2	0	0	0	0	2	?	1	2	3
1	0	2	3	0	3	1	1	1	?	?	?	?
?	0	3	?	0	0	?	0	0	1	1	3	2
2	1	3	1	1	2	3	1	0	1	3	0	0
1	0	2	2	0	0	1	1	1	0	0	1	1
?	?	0	1	?	?	?	1	?	1	?	2	0
?	?	?	1	?	?	1	?	?	?	?	4	4

2	0&1	0	?	?	?	?	?	?	?	?	?	?
0	0	?	?	?	0	0	?	?	0	?	0	0

Prionessus

1	1	2	1	?	?	?	1	?	1	1	1	1
1	0	2	2	?	?	?	?	2	?	1	?	3
0&1	0	2	3	0	3	1	1	1	?	?	?	?
?	0	3	?	0	0	?	0	0	1	1	3	2
0	1	3	1	1	2	3	1	0	1&2	3	0	0
1	0	1	1	0	0	1	0	0	0	0	1	1
?	?	0	1	?	?	?	1	?	?	?	?	?
?	?	?	?	?	?	?	?	?	?	?	4	4
?	1	1	0	0	?	?	?	?	0	?	?	?
0	0	?	?	?	0	0	?	?	0	?	0	0

Yubaatar

1	1	1	1	0	0	0	1	1	1	1	1	1
1	0	2	?	?	?	?	?	2	?	1	?	1
0	0	1	2&3	0	2&3	1	1	1	?	?	?	?
?	0	2	1	0	0	?	1	0	1	1	2	2
0	1	2	1	1	2	3	1	1	2	3	0	0
1	2	1	1	0	0	2	0	0	0	0	?	1
1	1	1&2	1	1	4	0	1	0	1	?	2	0

0 1 0 ? ? 1 1 1 1 ? ? 0 3

2 1 0 0 0 1 0 0 0 0 ? ? 0

0 0 ? ? ? 0 0 0 2 ? 0 0 0

Litovoi

? ? ? ? ? ? ? ? ? ? 1 1 ?

1 0 1 2 1 1 0 0 2 ? 1 1 1

0 0 3 4 0 1 ? ? ? ? ? ? ?

? ? ? ? ? ? ? ? ? ? 1 2 ?

? ? 4 1 1 2 2 1 0 2 3 0 0

1&2 ? ? ? ? ? ? ? ? ? 0 ? 1

? 1 ? 0 1 ? 0 0 0 0 0 ? 0

0 0 0 1 1 ? 1 1 1 1 0 1 1

0 0 0 ? ? ? ? ? ? ? ? ? 1

0 ? ? ? ? ? 0 1 1 0 0 0 ?

Barbatodon

1 1 2 1 0 1 ? 1 0 1 1 1 ?

1 0 1 2 0 1 0 0 2 ? 1 1 1

0 0 3 4 0 1 1 1 1 ? ? ? ?

? 1 2 1 0 0 ? 1 3 1 1 2 2

0 1 4 1 1 2 2 1 0 2 3 0 0

1 0 1 1 0 0 1 1 0 0 0 ? 1

?	0	?	0	1	3	0	0	0	0	0	?	0
0	0	?	?	?	?	?	?	?	?	?	1	1
0	0	0	0	0	?	1	0	0	0	?	?	1
0	0	0	?	?	0	0	1	1	0	0	0	0

3.10.9 REFERENCES

57. Rogers, R. R., Swisher, C. C., III & Horner, J. R. $^{40}Ar/^{39}Ar$ age and correlation of the nonmarine Two Medicine Formation (Upper Cretaceous), northwestern Montana, U.S.A. *Can. J. Earth Sci.* **30**, 1066–1075 (1993).

58. Golonka, J., Ross, M. I. & Scotese, C. T. in *Pangea: Global Environments and Resources* (eds Embry, A. F., Beauchamp, A. F. & Glass, D. J. B.) 1–48 (Can. Soc. Pet. Geol. Mem. 17, 1994).

59. Lorenz, J. C. & Gavin, W. Geology of the Two Medicine Formation and the sedimentology of a dinosaur nesting ground. *Montana Geol. Soc. Field. Conf., Northwestern Montana*, 175–186 (1984).

60. Chin, K. The paleobiological implications of herbivorous dinosaur coprolites from the Upper Cretaceous Two Medicine Formation of Montana: why eat wood? *Palaios* **22**, 554–566 (2007).

61. Falcon-Lang, H. J. Growth interruptions in silicified conifer woods from the Upper Cretaceous Two Medicine Formation, Montana, USA: implications for palaeoclimate and dinosaur palaeoecology. *Palaeogeogr. Palaeoclimatol. Palaeoecol*. **199**, 299–314 (2003).

62. Shelton, J. A. *Application of sequence stratigraphy to the nonmarine upper Cretaceous Two Medicine Formation, Willow Creek Anticline, northwestern Montana*. MS thesis, Montana State University, Bozeman (Earth Sciences, 2008).

63. Varricchio, D. J. et al. Tracing the Manson impact event across the Western Interior Cretaceous Seaway. *Geol. Soc. Am. Spec. Pap*. **465**, 269–299 (2010).

64. Varricchio, D. J., Jackson, F. & Trueman, C. N. A nesting trace with eggs for the Cretaceous theropod dinosaur *Troodon formosus*. *J. Vertebr. Paleontol*. **19**, 91–100 (1999).

65. Bown, T. M. & Kraus, M. J. Vertebrate fossil-bearing paleosol units (Willwood Formation, Lower Eocene, northwest Wyoming, USA): implications for taphonomy, biostratigraphy, and assemblage analysis. *Palaeogeogr. Palaeoclimatol. Palaeoecol*. **34**, 31–56 (1981).

66. Bown, T. M. & Kraus, M. J. Integration of channel and floodplain suites, I. Developmental sequence and lateral relations of alluvial paleosols. *J. Sediment. Petrol*. **57**, 587–601 (1987).

67. Freimuth, W. J. Paleoecological utility of feeding traces at Egg Mountain, a rich terrestrial vertebrate locality of the Upper Cretaceous Two Medicine Formation, Montana, U.S.A. MS thesis, Montana State University, Bozeman (Earth Sciences, 2020).

68. Genise, J. F. The ichnofamily Celliformidae for *Celliforma* and allied ichnogenera. *Ichnos* **7**, 267–282 (2000).

69. Genise, J. F. *Ichnoentomology: Insect Traces in Soils and Paleosols* (Springer, 2016).

70. Johnston, P. A., Eberth, D. & Anderson, P. K. Alleged vertebrate eggs from Upper Cretaceous redbeds, Gobi Desert, are fossil insect (Coleoptera) pupal chambers: *Fictovichnus* new ichnogenus. *Can. J. Earth Sci.* **33**, 511–525 (1996).

71. Alonso-Zarza, A. M., Genise, J. F. & Verde, M. Paleoenvironments and ichnotaxonomy of insect trace fossils in continental muCFlat deposits of the Miocene Calatayud–Daroca Basin, Zaragoza, Spain. *Palaeogeogr. Palaeoclimatol. Palaeoecol.* **414**, 342–351 (2014).

72. Bown, T. M. & Kraus, M. J. Ichnofossils of the alluvial Willwood Formation (lower Eocene), Bighorn Basin, northwest Wyoming, U.S.A. *Palaeogeogr. Palaeoclimatol. Palaeoecol*. **43**, 95–128 (1983).

73. Hembree, D. I. & Hasiotis, S. T. Paleosols and ichnofossils of the White River Formation of Colorado: insights into soil ecosystems of the North American midcontinent during the Eocene-Oligocene transition. *Palaios* **22**, 123–142 (2007).

74. Lee, K. E. *Earthworms, their ecology and relationships with soils and land use* (Academic Press, 1985).

75. Hopkin, S. P. & Read, H. J. *The biology of millipedes* (Oxford University Press, 1992).

76. Alonso-Zarza, A. M., Silva, P. G., Goy, J. L. & Zazo, C. Fan-surface dynamics and biogenic calcrete development: interactions during ultimate phases of fan evolution in the semiarid SE Spain (Murcia). *Geomorphology* **24**, 147–167 (1998).

77. Kraus, M. J. Paleosols in clastic sedimentary rocks: their geologic applications. *Earth Sci. Rev*. **47**, 41–70 (1999).

78. Rogers, R. R., Regan, A. K., Weaver, L. N., Thole, J. T. & Fricke, H. C. Tracking authigenic mineral cements in fossil bones from the Upper Cretaceous (Campanian) Two Medicine and Judith River formations, Montana. *Palaios* **35**, 1–16 (2020).

79. Simpson, G. G. The Fort Union of the Crazy Mountain Field, Montana, and its mammalian faunas. *U. S. Nat. Mus. Bull*. **169**, 1–287 (1937).

80. Jepsen, G. L. Paleocene faunas of the Polecat Bench Formation, Park County, Wyoming. *Proc. Am. Philos. Soc*. **83**, 217–340 (1940).

81. Novacek, M. & Clemens, W. A. Aspects of intrageneric variation and evolution of Mesodma (Multituberculata, Mammalia). *J. Paleontol*. **51**, 701–717 (1977).

82. Hunter, J. P., Hartman, J. H. & Krause, D. W. Mammals and mollusks across the Cretaceous-Tertiary boundary from Makoshika State Park and vicinity (Williston Basin), Montana. *Univ. Wyo. Contr. Geol*. **83**, 217–340 (1997).

83. Eaton, J. G. Cenomanian and Turonian (early Late Cretaceous) multituberculate mammals from southwestern Utah. *J. Vertebr. Paleontol*. **15**, 761–784 (1995).

84. Ameghino, F. Los plagiaulacideos argentines y sus relaciones zoológicas, geológicas, y geográficas. *Boletín Instituto Geográfico Argentino* **9**, 143–201 (1890).

85. Archibald, J. D. A study of Mammalia and geology across the Cretaceous-Tertiary boundary in Garfield County, Montana. *Univ. Calif. Publ. Geol. Sci*. **122**, 1–286 (1982).

86. Montellano, M. Mammalian fauna of the Judith River Formation (Late Cretaceous, Judithian), northcentral Montana. *Univ. Calif. Publ. Geol. Sci* **136**, 1–115 (1992).

87. Lillegraven, J. A. & McKenna, M. C. Fossil mammals from the “Mesaverde” Formation (Late Cretaceous, Judithian) of the Bighorn and Wind River basins, Wyoming, with definitions of Late Cretaceous North American land-mammal “ages.” *Am. Mus. Novit*. **2840**, 1–68 (1986).

88. Lillegraven, J. A. Latest Cretaceous mammals of the upper part of the Edmonton Formation of Alberta, Canada, and review of marsupial-placental dichotomy in mammalian evolution. *Univ. Kans. Paleontol. Contrib*. **50**, 1–122 (1969).

89. Smith, S. M. & Wilson, G. P. Species discrimination of co-occurring small fossil mammals: a case study of the Cretaceous-Paleogene multituberculate genus *Mesodma*. *J. Mammal. Evol*. **24**, 147–157 (2017).

90. Sloan, R. E. in The Cretaceous-Tertiary Boundary in the San Juan and Raton Basins, New Mexico and Colorado (eds Fassett, J. E. & Rigby, J. K., Jr.) 165–200 (Geol. Soc. Am. Spec. Pap. 209, 1987).

91. Eaton, J. G. & Cifelli, R. L. Multituberculate mammals from near the Early-Late Cretaceous boundary, Cedar Mountain Formation, Utah. *Acta Palaeontol. Pol*. **46**, 453–518 (2001).

92. Eaton, J. G. in At the Top of the Grand Staircase: The Late Cretaceous of Southern Utah (eds Titus, A. L. & Loewen, M. A.) 329–369 (Indiana Univ. Press, 2013).

93. Fox, R. C. Early Campanian multituberculates (Mammalia: Allotheria) from the Upper Milk River Formation, Alberta. *Can. J. Earth Sci*. **8**, 916–938 (1971).

94. Sloan, R. E. & Russell, L. S. Mammals from the St. Mary River Formation (Cretaceous) of southwestern AlbeA. rta. *Life Sci. Contrib. R. Ont. Mus*. **95**, 1–21 (1974).

95. Diem, S. *Vertebrate faunal analysis of the Upper Cretaceous Williams Fork Formation, Rio Blanco County, Colorado* (M.S. thesis, San Diego State University, 1999).

96. Marsh, O. C. Discovery of Cretaceous Mammalia, Part 1. *Am. J. Sci*. **38**, 81–92 (1889).

97. Narci, A. in *Ten Cate's Oral Histology: Development, Structure, and Function, 7th Ed* (ed. Nanci, A.) 79–107 (Mosby, St. Louis, 2008).

98. Behrensmeyer, A. K. in Taphonomy: Releasing the Data locked in the Fossil Record (eds Allison, P. & Briggs, D. E. G.) 291–335 (Plenum, New York, 1991).

99. Behrensmeyer, A. K. Taphonomic and ecological information from bone weathering. *Paleobiology* **4**, 150–162 (1978).

100. Shipman, P. in The Research Potential of Anthropological Museum Collections (eds Cantwell, J. B., Griffin, J. B. & Rothschild, N. A.) 357–385 (NY Acad. Sci., 1981).

101. Fernández-Jalvo, Y. et al. Taphonomy for taxonomists: implications of small mammal studies. *Quat. Sci Rev*. **139**, 138–157 (2016).

102. Lyman, R. L. The concept of equifinality in taphonomy. *J. Taph*. **2**, 15–26 (2004).

103. Rogers, R. R. & Brady, M. E. Origins of microfossil bonebeds: insights from the Upper Cretaceous Judith River Formation of north-central Montana. *Paleobiology* **36**, 80–112 (2010).

104. Voorhies, M. R. Taphonomy and population dynamics of an early Pliocene vertebrate fauna, Knox County, Nebraska. *Univ. Wyo. Contrib. Geol. Spec. Pap*. **1**, 1–69 (1969).

105. Korth, W. A. Taphonomy of microvertebrate fossil assemblages. *Ann. Carnegie Mus*. **48**, 235–285 (1979).

106. Arriaga, L. C., Montalvo, C. I. & Sosa, R. A. Experiments on wind dispersal of modern rodent bones. *Neues Jahrbuch für Geologie und Paläontologie – Abhandlungen* **265**, 185–198 (2012).

107. Dodson, P. & Wexlar, D. Taphonomic investigations of owl pellets. *Paleobiology* **5**, 275–284 (1979).

108. Montalvo, C. & Tallade, P. O. Taphonomy of the accumulations produced by *Caracara plancus* (Falconidae): analysis of prey remains and pellets. *J. Taph*. **7**, 235–248 (2009).

109. Montalvo, C. I., Tomassini, R. L. & Sostillo, R. Leftover prey remains: a new taphonomic mode from the Late Miocene Cerro Azul Formation of Central Argentina. *Lethaia* **49**, 219–230 (2016).

110. Lowe, V. Variation in digestion of prey by the tawny owl (*Strix aluco*). *J. Zool*. **192**, 282–293 (1980).

111. Montalvo, C. I., Fernández, F. J., Bargo, M. S., Tomassini, R. L. & Mehl, A. First record of a Late Holocene fauna associated with an ephemeral fluvial sequence in La Pampa Province, Argentina: taphonomy and paleoenvironment. *J. S. Am. Earth Sci*. **76**, 225–237 (2017).

112. Genise, J. F. Ichnotaxonomy and ichnostratigraphy of chambered trace fossils in palaeosols attributed to coleopterans, ants and termites. *Geol. Soc. Lond. Spec. Publ*. **228**, 419–453 (2004).

113. Berger, W. H., Ekdale, A. A. & Bryant, P. P. Selective preservation of burrows in deep-sea carbonates. *Mar. Geol*. **32**, 205–230 (1979).

114. Evans, H. E. The accessory burrows of digger wasps. *Science* **152**, 465–471 (1966).

115. O'Neill, K. M. *Solitary Wasps: Behavior and Natural History* (Cornell Univ. Press, 2001).

116. Martin, A. J. & Varricchio, D. J. Paleoecological utility of insect trace fossils in dinosaur nesting sites of the Two Medicine Formation (Campanian), Choteau, Montana. *Hist. Biol*. **23**, 15–25 (2011).

117. Deeming, D. C. Ultrastructural and functional morphology of eggshells supports the idea that dinosaur eggs were incubated buried in a substrate. *Palaeontol*. **49**, 171–185 (2006).

118. Agha, M. et al. Nelson's big horn sheep (*Ovis canadensis nelsoni*) trample Agassiz's desert tortoise (*Gopherus agassizii*) burrow at a California wind energy facility. *Bull. S. Calif. Acad. Sci.* **114**, 58–62 (2015).

119. White, C. R. The allometry of burrow geometry. *J. Zool*. **265**, 395–403 (2005).

120. David, J. H. M & Jarvis, J. U. M. Population fluctuations, reproduction and survival in the striped fieldmouse *Rhabdomys pumilio* on the Cape Flats, South Africa. *J. Zool*. **207**, 251–276 (1984).

121. Gubernick, D. J. & Klopfer, P. H. *Parental care in mammals* (Plenum Press, 1981).

122. Maynard Smith, J. & Savage, R. J. G. Some locomotory adaptations in mammals. *J. Linnean Soc. Lond. Zool*. **42**, 603–622 (1956).

123. Argot, C. Functional-adaptive anatomy of the forelimb in the Didelphidae, and the paleobiology of the Paleocene marsupials *Mayulestes ferox* and *Pucadelphys andinus*. *J. Morph*. **247**, 51–79 (2001).

124. Sargis, 2002b. Functional morphology of the forelimb of tupaiids (Mammalia, Scandentia) and its phylogenetic implications. *J. Morph*. **253**, 10–42 (2002b).

125. Taylor, M. E. The functional anatomy of the hindlimb of some African Viverridae (Carnivora*). J. Morph*. **148**, 227–253 (1976).

126. Heinrich, R. E. & Rose, K. D. Postcranial morphology and locomotor behaviour of two early Eocene miacoid carnivorans, *Vulpavus* and *Didymictis*. *Palaeontol*. **40**, 279–305 (1997).

127. Simpson, G. G. & Elftman, H. O. Hind limb musculature and habits of a Paleocene multituberculate. *Am. Mus. Novit*. **333**, 1–19 (1929).

128. Salton, J. A. & Sargis, E. J. Evolutionary morphology of the Tenrecoidea (Mammalia) hindlimb skeleton. *J. Morph*. **270**, 367–387 (2009).

129. Gebo, D. L. & Sargis, E. J. Terrestrial adaptations in the postcranial skeletons of guenons. *Am. J. Phys. Anthropol*. **93**, 341–371 (1994).

130. Anemone, R. L. & Covert, H. H. 2 New skeletal remains of *Omomys* (Primates, Omomyidae): functional morphology of the hindlimb and locomotor behavior of a Middle Eocene primate. *J. Hum. Evol.* **38**, 607–633.

131. Szalay, F. S. & Sargis, E. J. Model-based analysis of postcranial osteology of marsupials from the Palaeocene of Itaboraí (Brazil) and the phylogenetics and biogeography of Metatheria. *Geodiversitas* **23**, 139–302 (2001).

132. Calede, J. J. M., Samuels, J. X. & Chen, M. Locomotory adaptations in entoptychine gophers (Rodentia: Geomyidae) and the mosaic evolution of fossoriality. *J. Morph*. **280**, 879–907 (2019).

133. Kielan-Jaworowska, Z. & Hurum, J. H. Phylogeny and systematics of multituberculate mammals. *Palaeontol*. **44**, 389–429 (2001).

134. Simmons, N. B. in *Mammal Phylogeny: Mesozoic Differentiation, Multituberculates, Montotremes, Early Therians, and Marsupials* (eds Szalay, F. S., Novacek, M. J. & McKenna, M. C.) 146–164 (Springer, 1993).

135. Weil, A. & Krause, D. W. *in Evolution of Tertiary Mammals of North America: Volume 2: Small Mammals, Xenarthrans, and Marine Mammals* (eds Janis, C. M, Gunnell, G. F. & Uhen, M. D.) 19–38 (Cambridge Univ. Press, 2008).

136. Krause, D. W. & Carlson, S. J. Prismatic enamel in multituberculate mammals: tests of homology and polarity. *J. Mammal*. **68**, 755–765.

3.12 APPENDIX III: SUPPLEMENTARY TABLES

Table 3.12.1. Brief summary of *Filikomys primaevus* specimens preserved at Egg Mountain, including where they fall stratigraphically (JHP refers to the jackhammer passes from Extended Data Figure 3.9.3), number of individuals, brief description of the elements preserved, and whether or not the specimen has yet been manually prepared. Note that for the unprepared specimens these descriptions rely on those elements that are exposed on the rock face and there may be more material beneath the surface.

Field No.	MOR No.	JHP	Individuals	Brief Description	Prepared?
7-12-10-08	11747	1	1	Partial maxilla with P2–4 exposed.	No
7-6-14-07	11755	1	1	Fragmentary proximal femora.	No
7-17-10-11	11748	1	1	Palate with P1–4 exposed.	No
7-17-10-16	11749	1	1	Dentary with p4–m1 exposed.	No
7-29-10-35	11750	3	2	Partial skull with maxillae in articulation with lower dentition, at least one dentary from another individual.	Yes

				Forelimb and hind limb in articulation. Numerous vertebrae and ribs, mostly disarticulated.	
7-25-11-24	11751	6	1	Dentary fragment.	No
7-15-14-19	11756	7	2	Three dentaries, edentulous except for incisors. Isolated p4, isolated partial incisor.	No
7-23-12-27	11752	8	4	At least four partial skulls, potentially five. Two in occlusion with maxillae in occlusion with lower dentition. Associated with limb bones obscured by matrix.	No
7-23-12-26	10908	8	2	Two skulls, proximal tibia, distal humerus, bone fragments.	Yes
7-28-12-35	11754	8	2	Two partial skulls. One zygomatic arch exposed, one skull with maxilla in occlusion with lower dentition. Associated with vertebrae and obscured long bones.	No
7-23-12-29	10908	8	5	Three skulls, two articulated pelvic girdles and hind limbs, two partially articulated pectoral girdles and forelimbs, numerous disarticulated limbs and vertebrae.	Yes
7-24-12-32	11753	8	2	Two nearly complete skulls, with maxillae in articulation with lower dentition. Associated with humerus and other limb bones, including a hind limb and foot in articulation.	Ongoing

Table 3.12.2. Length measurements (in mm) of *F. primaevus* skull elements preserved in MOR 10908. Missing measurements (–) indicate that the element was too damaged or incomplete to be

accurately measured. * indicates an element that was distorted, such that the measurement is an estimate.

MOR No.	Dentary	Upper Tooth Row	Skull
10908A	14.98	8.65	21.48*
10908B	14.41	8.11	–
10908C	15.48	7.37	21.17
10908D	13.36	7.72	16.82*
10908E	10.44	–	–

Table 3.12.3. Upper anterior premolar measurements (in mm) and ratios of *F. primaevus* individuals from MOR 10908.

Tooth	MOR No.	L	W	W:L
P1	10908A_R	0.76	0.78	1.03
	10908A_L	0.93	0.79	0.85
	10908B_L	0.81	0.85	1.05
	10908C_R	0.73	0.6	0.82
	10908C_L	0.66	0.69	1.05
	10908D_L	0.64	0.54	0.84
	10908D_R	0.67	0.58	0.87
	Means	0.74	0.69	0.93
P2	10908A_R	0.64	0.83	1.3
	10908A_L	0.73	0.73	1

	10908B_L	0.71	0.9	1.27
	10908C_R	0.55	0.6	1.09
	10908C_L	0.57	0.68	1.19
	10908D_L	0.64	0.57	0.89
	Means	0.64	0.72	1.12
P3	10908A_R	0.54	0.58	1.07
	10908A_L	0.5	0.68	1.36
	10908B_L	0.7	0.67	0.96
	10908C_R	0.32	0.35	1.09
	10908C_L	0.45	0.41	0.91
	10908D_L	0.54	0.54	1
	10908D_R	0.54	0.54	1
	10908E_L	0.55	0.47	0.85
	Means	0.52	0.53	1.03

Table 3.12.4. P4 measurements (in mm), ratios, and cusp formulae of *F. primaevus* individuals from MOR 10908. Because most of the P4s were in approximate occlusion with the lower dentition, measurements of cusp height were only possible for MOR 10908E. Abbreviations: L, length; W, width; H, height; CRL, length of the P4 medial cusp row, from the apex of the mesial-most cusp to the apex of the distal-most cusp; CRH, height of the P4 medial cusp row, from the base of the crown to the apex of the tallest cusp; DL, distal length of P4, measured from the apex of the distal-most cusp to the distal-most portion of the P4 crown.

Specimen	Formula	L	W	H	CRL	CRH	DL	W:L	H:L	DL:L	CRH:CRL

10908A_R	2:5	2.06	0.93	–	–	–	–	0.45	–	–	–
10908A_L	–	2.06	0.77	–	–	–	–	0.37	–	–	–
10908B_L	–	1.92	0.99	–	–	–	–	0.52	–	–	–
10908C_R	–	1.91	0.72	–	–	–	–	0.38	–	–	–
10908C_L	2:5	1.77	0.65	–	–	–	–	0.37	–	–	–
10908D_R	2:5	1.92	0.72	–	–	–	–	0.38	–	–	–
10908E_L	3:5	1.97	0.83	0.76	1.15	0.58	0.71	0.42	0.39	0.36	0.5
Means		1.94	0.8	–	–	–	–	0.41	–	–	–

Table 3.12.5. Molar measurements (in mm), ratios, and cusp formulae of *F. primaevus* individuals from MOR 10908. LCR(M1) refers to the lingual cusp row length of M1. Abbreviations: L, length; W, width. Molar to molar ratios are based on tooth length.

Tooth	Specimen	Formula	L	W	W:L	M1:m1	m2:m1	M2:M1	M2:m2	LCR(M1):M1
m1	10908A_R	6:4	2.09	1.04	0.5	1.27	–	–	–	–
	10908A_L	6:4	2.14	1	0.47	1.18	–	–	–	–
	10908B_R	6:4	2.15	0.86	0.4	–	–	–	–	–
	10908B_L	6:4	2.02	1.04	0.51	1.27	–	–	–	–
	10908C_R	6:4	1.78	0.86	0.48	1.2	–	–	–	–
	10908D_R	6:4	2	0.9	0.45	1.21	–	–	–	–
	10908D_L	6:4	2.04	0.91	0.45	–	–	–	–	–
	Means		2.03	0.94	0.47	1.23	–	–	–	–
m2	10908A_R	3:2	1.54	1.19	0.77	–	0.74	–	–	–
	10908A_L	3:2	1.57	1.19	0.76	–	0.73	–	–	–
	10908B_L	3:2	1.64	1.21	0.74	–	0.81	–	–	–
	10908C_R	3:2	1.33	1	0.75	–	0.75	–	–	–
	10908A_R	3:2	1.25	1.06	0.85	–	0.63	–	–	–
	Means		1.47	1.13	0.77	–	0.73	–	–	–
M1	10908A_R	5:6:2+	2.66	1.36	0.51	–	–	0.64	–	–

	10908A_L	5:6:3+	2.53	1.47	0.58	–	–	0.65	–	–
	10908B_L	5:6:4	2.56	1.43	0.56	–	–	0.61	–	–
	10908C_R	5:6:3+	2.14	1.13	0.53	–	–	0.68	–	–
	10908C_L	5:6:2+	2.26	1.12	0.5	–	–	0.58	–	–
	10908D_R	5:6:4	2.42	1.24	0.51	–	–	0.52	–	–
	10908E_L	5:6:4	2.35	1.3	0.55	–	–	0.64	–	–
	Means		2.42	1.29	0.53	–	–	0.62	–	–
LCR(M										
1)	10908A_R	–	1.64	–	–	–	–	–	–	0.62
	10908A_L	–	1.62	–	–	–	–	–	–	0.64
	10908B_L	–	1.59	–	–	–	–	–	–	0.62
	10908C_R	–	1.3	–	–	–	–	–	–	0.61
	10908C_L	–	1.36	–	–	–	–	–	–	0.6
	10908D_R	–	1.48	–	–	–	–	–	–	0.61
	10908D_L	–	1.46	–	–	–	–	–	–	0.62
	Means		1.49	–	–	–	–	–	–	0.62
M2	10908A_R	1:3:3	1.71	1.68	0.98	–	–	–	1.11	–
	10908A_L	1:3:3	1.64	1.64	1	–	–	–	1.04	–
	10908B_L	1:3:3	1.55	1.53	0.99	–	–	–	0.95	–
	10908C_R	1:3:3	1.45	1.29	0.89	–	–	–	1.09	–
	10908C_L	1:3:3	1.32	1.2	0.91	–	–	–	–	–
	10908D_R	1:3:3	1.25	1.19	0.95	–	–	–	1	–
	10908E_L	1:3:3	1.5	1.46	0.97	–	–	–	–	–
	Means		1.49	1.43	0.96	–	–	–	1.04	–

Table 3.12.6. p4 measurements (in mm) and ratios of *F. primaevus* individuals from MOR 10908 and 11750. Abbreviations: L, length; H, height; L1, length to the p4 apogee; H1, height to the first serration.

Specimen	L	H	L1	H1	H:L	L1:L	H1:H	H1:L	p4:m1	P4:p4
10908A_R	3.34	1.3	1.75	0.76	0.39	0.52	0.58	0.23	1.6	0.62

10908A_L	3.32	1.38	1.85	0.78	0.42	0.56	0.57	0.23	1.55	0.62
10908B_L	3.39	1.42	1.82	0.82	0.42	0.54	0.58	0.24	1.68	0.57
10908C_R	3.11	1.26	1.53	0.79	0.41	0.49	0.63	0.25	1.75	0.61
10908C_L	3.11	1.2	1.69	0.79	0.39	0.54	0.66	0.25	–	0.57
10908D_R	2.85	1.19	1.39	0.63	0.42	0.49	0.53	0.22	1.43	0.67
10908D_L	2.95	1.29	1.58	0.73	0.44	0.54	0.57	0.25	1.45	–
11750_L	3.58	1.48	1.73	0.8	0.41	0.48	0.54	0.22	–	–
Means	3.21	1.32	1.67	0.76	0.41	0.52	0.58	0.24	1.58	0.61

Table 3.12.7. Element representation of *F. primaevus* remains from MOR 10908. Abbreviations: N_O, number of elements; R, right; L, left; MNI, minimum number of individuals; RA (relative abundance) = $N_O/(MNI \times N_E)$, where N_E is number of expected elements in an individual.

Element	N_O	R	L	MNI	RA
Skull	5	n/a	n/a	5	1
Dentary	10	5	5	5	1
Scapula	4	2	2	2	0.4
Humerus	8	4	4	4	0.8
Radius	4	2	2	2	0.4
Ulna	3	2	1	2	0.3
Ischium	6	3	3	3	0.6
Ilium	4	2	2	2	0.4
Femur	8	3	5	5	0.8
Tibia	5	2	3	3	0.5
Fibula	5	2	3	3	0.5

Table 3.12.8. Egg Mountain Fossil Assemblage collected from 2010–2016 in quads N1-N11/W1-W13 (see Extended Data Figure 3.9.3). This is a tentative list based on field identifications and those specimens that have been prepared. Many specimens and fragments remain un-prepared. The assemblage is dominated by terrestrial invertebrates and vertebrates both in trace and body fossils. Aquatic vertebrates are poorly represented at the site comprising only 0.3% of the vertebrate remains and 0.05% of all fossils collected. Note: * total does not include specimens from quads N1-N4 and † total does not include 2016 specimens.

Fossil type	Taxon	No. of Specimens
Traces		
	Fictovichnus sciuttoi (4 morphs) (Freimuth and Varricchio, 2019)	4,692*
	Feoichnus n. sp. (Panascí and Varricchio, 2020)	95
	Coprolites - unidentified droppings and pellet masses	10
	Total	4,797
Eggshell		
	Continuoolithus - 1 whole egg, several partial eggs, and hundreds of frags	1
	Prismatoolithus (*Troodon*)	1
	Unidentified, smooth, thin eggshell	18
	Total	20
Teeth†		
	Unidentified hadrosaur	564

	Theropod (tyrannosaurid, *Troodon*, dromaeosaurid)	95
	Unidentified crocodilian	1
	Total	690
Bone		
	Associated partial hadrosaur, including: caudal vertebrae, chevrons, ribs, pelvic elements. ~40 elements in total	1
	Orodromeus: isolated material	72
	Orodromeus: associated material	3
	All mammals: associated and isolated elements	26
	All squamates: associated and isolated elements	35
	Small unidentified vertebrates	35
	Frog	1
	Turtle	1
	Total	174
Total		5,681

Table 3.12.9. Forelimb measurements (in mm) of *F. primaevus* individuals preserved in MOR 10908. Measurements follow the definitions outlined in Chen and Wilson (2015). Abbreviations: Sl, scapula length; Sh, scapula height; Hl, humerus length; Hsw, humerus midshaft width; Hdw, humerus distal epiphysis width; Hhl, humeral head length; Hpw, humerus proximal epiphysis width; Hhw, humeral head width; Hdcw, deltopectoral crest width; Uol, olecranon process length; Ul, ulna length; Rl, radius length. * indicates that the measured element was damaged.

Specimen	Sl	Sh	Hl	Hsw	Hdw	Hpw	Hhw	Hhl	Hdcw	Uol	Ul	Rl
10908A_R	9.22*	1.1*	–	1.59	3.19	–	–	–	–	–	–	–
10908A_L	7.61*	1.12*	13.3	1.39	3.4	2.68*	1.77*	2.28	0.923	–	11.95*	11.5
10908B_R	–	–	–	1.12	3.14	–	–	–	0.905	1.99*	9.37*	12.57*
10908B_L	–	–	–	–	–	–	–	–	–	–	–	–
10908C_R	8.27*	1.93*	–	1.23	3.37	–	–	–	–	–	–	–
10908C_L	10.03*	2.9*	–	1.25	2.98	2.95	1.76	2.05	1.14	–	–	–

Table 3.12.10. Hind limb measurements (in mm) of *F. primaevus* individuals preserved in MOR 10908. Measurements follow the scheme outlined in Chen and Wilson (2015). Abbreviations: Pel, pelvis length; Il, ilium length; Isl, ischium length; Fl, femur length; Fhd, femoral head diameter; Fgh, greater trochanter height; Fsw, femur midshaft width; Fdw, femur distal epiphysis width; Tpw, tibia proximal epiphysis width; Tl, tibia length; Tmw, tibia midshaft width; Tdw, tibia distal epiphysis width; Fbl, fibula length; Fbmw, fibula midshaft width; Fbpw, fibula proximal epiphysis width; Fbdw, fibula distal epiphysis width. * indicates that the measured element was damaged.

ecimen	Pel	Il	Isl	Fl	Fhd	Fgh	Fsw	Fdw	Tpw	Tl	Tmw	Tdw	Fbl	Fbmw	Fbpw	Fb
08A_R	22.72	16.05	6.81*	16.6	1.99	2.6	1.65*	3.52	3.51	14.88	1.1*	1.61	–	0.49*	1.42	–
08A_L	22.96	15.96	7.42	17.48	2.17	2.38	1.71	3.7	3.31	14.79	1.23	1.81	–	0.702	–	1.3
08B_R	20.03	13	7.08	16.31*	2.06	2.02	1.94	3.33	–	–	–	–	–	–	–	–
08B_L	19.9*	12.71*	6.66	13.99	2.18	1.64	2.03	3.66	4.3	13.64	1.64	1.92	13.06	0.78	1.96	1.4

Table 3.12.11. Structure matrix of canonical variate analysis of the right side of MOR 10908A. See Supplementary Table 3.12.10 for abbreviations.

Osteological index	CF1	CF2	CF3
Ilium robustness index (Il:Pel)	0.755	-0.535	0.665
Gluteal index (FGh:Fl)	-0.306	0.821	0.39
Crural index (Tl:Fl)	-0.752	-0.336	0.411

Table 3.12.12. Classification matrix of the canonical variate analysis of the right side of MOR 10908A.

Locomotor mode	A	F	G	S	Sc	Sq	Sf	T	%
Arboreal (A)	14	2	2	0	6	0	2	4	46.67
Fossorial (F)	0	6	0	0	1	3	1	1	50.00
Gliding (G)	0	0	3	0	0	0	0	0	100.0
Saltatorial (S)	0	0	0	4	0	1	0	0	80.00
Scansorial (Sc)	4	0	0	0	4	0	1	0	44.44

Semiaquatic (Sq)	0	1	1	3	1	3	0	0	33.33
Semifossorial (Sf)	2	1	3	0	1	2	0	0	0.00
Terrestrial (T)	4	5	4	0	9	2	4	2	6.67
Total correct classification									33.64

Table 3.12.13. Structure matrix of morphometric analysis of the left side of specimen MOR 10908A. See Supplementary Tables 9 and 10 for abbreviations.

Osteological index	CF1	CF2	CF3
Humerus robustness index (Hsw:Hl)	-0.079	-0.613	0.127
Humeral epicondylar index (Hdw:Hl)	0.018	-0.588	-0.005
Humeral head robustness index (HHl:Hl)	0.052	-0.749	0.154
Deltopectoral crest index (Hdcw:Hsw)	0.206	-0.543	0.296
Deltopectoral crest width to distal humerus width ratio (Hdcw:Hdw)	0.124	-0.502	0.321
Brachial index (Rl:Hl)	0.588	0.342	0.059
Ilium robustness index (Il:Pel)	-0.346	0.466	0.201
Gluteal index (FGh:Fl)	0.042	-0.525	0.215
Femoral robustness index (Fsw:Fl)	-0.1	-0.788	-0.362
Crural index (Tl:Fl)	0.569	-0.021	-0.513
Intermembral index ((Hl+Rl)/(Tl+Fl))	-0.895	0.107	-0.108
Tibial robustness index (Tmw:Tl)	-0.111	-0.579	-0.031

Table 3.12.14. Classification matrix of the canonical variate analysis of the left side of MOR 10908A.

Locomotor mode	A	F	G	S	Sc	Sq	Sf	T	%
Arboreal (A)	18	0	1	0	2	0	2	7	60.00
Fossorial (F)	0	9	0	0	0	1	2	0	75.00
Gliding (G)	0	0	3	0	0	0	0	0	100.0
Saltatorial (S)	0	0	0	5	0	0	0	0	100.0
Scansorial (Sc)	2	0	1	0	5	0	1	0	55.56
Semiaquatic (Sq)	1	0	0	0	0	5	0	3	55.56
Semifossorial (Sf)	0	1	0	0	1	1	5	1	55.56
Terrestrial (T)	4	0	4	0	3	1	4	14	46.67
Total correct classification									59.81

Table 3.12.15. Structure matrix of canonical variate analysis of the left side of MOR 10908C. See Supplementary Table 3.12.9 for abbreviations.

Osteological index	CF1	CF2	CF3
Humeral midshaft width to proximal humerus width ratio (Hsw:Hpw)	-0.38	-0.744	-0.552

Humeral head width to proximal humerus width ratio (HHw:Hpw)	-0.824	-0.058	0.589
Deltopectoral crest width to proximal humerus width ratio (Hdcw:Hpw)	0.652	-0.387	0.169
Deltopectoral crest index (Hdcw:Hsw)	0.74	-0.298	0.338

Table 3.12.16. Classification matrix of the canonical variate analysis of the left side of MOR 10908C.

Locomotor mode	A	F	G	S	Sc	Sq	Sf	T	%
Arboreal (A)	19	0	1	0	3	0	6	1	63.33
Fossorial (F)	0	6	0	5	0	0	1	0	50.00
Gliding (G)	1	0	0	0	1	1	0	0	0.00
Saltatorial (S)	1	0	0	4	0	0	0	0	80.00
Scansorial (Sc)	3	0	1	0	2	0	0	3	22.22
Semiaquatic (Sq)	1	2	0	2	0	2	0	2	22.22
Semifossorial (Sf)	2	0	1	2	1	1	1	1	11.11
Terrestrial (T)	1	0	1	2	6	5	7	8	26.67
Total correct classification									39.25

CHAPTER 4: MULTITUBERCULATE MAMMALS SHOW EVIDENCE OF A LIFE HISTORY STRATEGY SIMILAR TO THAT OF PLACENTALS, NOT MARSUPIALS

Weaver, LN., Fulghum, HZ., Grossnickle, DM., Brightly, WH., Kulik, ZT., Wilson Mantilla, GP., and Whitney, MR. (In Preparation) Multituberculate mammals show evidence of a life history strategy similar to that of placentals, not marsupials.

4.1 AUTHOR CONTRIBUTIONS

LNW and MRW conceived of the study; LNW and HZF collected the data; LNW, HZF, MRW, and ZTK led histological analyses; DMG and WHB led quantitative analyses; GPWM supervised research activities; LNW wrote the manuscript with substantial input from all coauthors.

4.2 ABSTRACT

The remarkable evolutionary success of placental mammals has been partly attributed to their reproductive strategy of prolonged gestation and birthing of relatively precocial neonates that are weaned quickly. Although this strategy has conventionally been considered derived relative to that of marsupials with short gestation times, highly altricial neonates, and long lactation periods, mounting evidence has challenged this view, suggesting that the placental strategy may be plesiomorphic for therians (metatherian-marsupial and eutherian-placental lineages). Until now, the fossil record has been relatively silent on this debate, but here we establish a framework for studying the life histories of small-bodied fossil mammals. Using a phylogenetically, ecologically, and ontogenetically diverse sample of extant marsupials and placentals, we find that proportions of different bone tissue microstructures in their femoral cortices correlate with

length of lactation period. We then apply this histological correlate of reproductive strategies to Late Cretaceous and Paleocene members of the Multituberculata, an extinct mammalian clade that is phylogenetically stemward of Theria. Multituberculate bone histology closely resembles that of placentals, suggesting that they had similar life history strategies. That a stem-therian clade exhibits evidence of placental-like life histories lends support to the hypothesis that intense maternal-fetal contact characteristic of placentals is ancestral for therians. Alternatively, multituberculates and placentals may have independently evolved prolonged gestation and abbreviated postnatal growth. Our results challenge the hypothesis that the Cenozoic rise of placental mammals was driven by unique life history innovations, and shed new light on the diversification of mammals during the Mesozoic and early Cenozoic.

4.3 INTRODUCTION

Of the myriad biological traits that characterize the three major groups of extant mammals—Monotremata, Marsupialia, Placentalia—disparate life history strategies (here referring to age-specific schedules of birth and development[1]) are the most salient. Monotremes lay eggs (ovipary) that yield extremely altricial hatchlings (undeveloped, completely reliant on mother)[2], whereas both marsupials and placentals give live birth (vivipary). Marsupial young are born extremely altricial and undergo prolonged postnatal development, whereas placental young undergo prolonged prenatal development in the womb and are born comparatively precocial (well-developed, less reliant on mother)[3]. As such, marsupials generally invest more reproductive resources in lactation than gestation to nurture their young, whereas placentals tend to invest more in gestation[4,5]. This divergence in life history strategies between marsupials and placentals has been termed the ‘marsupial-placental dichotomy’[6–8].

Despite extensive research on the reproduction, development, and evolution of marsupials and placentals[9–15], the evolutionary origin of the marsupial-placental dichotomy remains contentious. Some researchers view the life history strategy of marsupials as a constraint on their metabolic, morphological, and behavioral evolution[8,10,16], whereas the placental strategy to invest more heavily in gestation than lactation was a novel evolutionary breakthrough that led to their greater taxonomic and ecological diversity relative to other mammalian lineages (including marsupials)[17]. Thus, the marsupial strategy has been posited to be evolutionarily intermediate to the more plesiomorphic monotreme and more derived placental strategies[6,8,17,18]. Others challenge that interpretation, instead proposing that the marsupial life history strategy is derived and adaptive for greater maternal control over reproductive resources in unpredictable environments[19–21]. Indeed, emerging developmental evidence suggests that the intense maternal-fetal contact characteristic of placental gestation may be plesiomorphic for both marsupials and placentals (i.e., the ancestral condition for Theria)[3,22]. In that scenario, the placental strategy is not unique and may have also been present among extinct stem-therian groups. The debate thus remains unresolved, but understanding the evolutionary history of the marsupial-placental dichotomy is fundamental to understanding mammalian life history evolution.

The study of therian life history strategies has largely focused on extant marsupials and placentals; however, this approach neglects critical data from the fossil record. Metatheria and Eutheria (total-group Marsupialia and total-group Placentalia, respectively) diverged by the Middle to Late Jurassic (> 165 million years ago [Ma])[23], and numerous extinct, non-therian mammalian outgroups proliferated during the Mesozoic and early Cenozoic (ca. 180–60 Ma)[24–26]. The fossil record therefore offers a unique opportunity to investigate the origins and evolution of mammalian reproductive and developmental strategies in deep time. Although the soft tissue

structures relevant to this topic (e.g., the placenta) leave little-to-no trace in the fossil record, bone histology—the study of bone tissue microstructure—can provide insights into the life histories of extinct vertebrates because traits such as growth rate, longevity, and reproductive timing are often reflected in the internal architecture of modern and fossil bones[27–31].

Links between bone histology and life history have been established through decades of comparative and experimental research on extant taxa, wherein researchers observed and measured how developmental variables (e.g., growth rate) influence bone tissue microstructure[31–35]. Although there have been a few broad surveys of mammalian bone histology[36–39], most histological research on extant mammal bones has focused on large-bodied taxa[40,41], individual species[42,43], or has sampled inconsistent skeletal elements that complicate interspecific comparisons[36]. Consequently, systematic studies on how the life histories of extant small-bodied mammals (< 5 kg) are reflected in their bone histology are lacking. Given that most Mesozoic and early Cenozoic mammals were small[44], establishing links between small-mammal life history traits and bone histology is essential for reconstructing the life histories of early mammals.

Multituberculata, an early branching mammalian lineage that spanned the Middle Jurassic through late Eocene (ca. 170–35 Ma), are a therian outgroup that can inform hypotheses about the causes and consequences of the marsupial-placental dichotomy. Multituberculates are phylogenetically intermediate to monotremes and therians[45] (Figure 4.1) and based on pelvic morphology are hypothesized to have been viviparous[46]. Further, long bones suited to histological analyses (e.g., femora) are relatively well represented in the fossil record of multituberculates[47–50] making them an ideal study system for investigating early mammalian life histories. Multituberculates were also among the most numerically abundant and taxonomically

rich groups of Mesozoic and early Cenozoic mammals[44,51], exploited an array of ecological niches[25,50,52], and were one of the only non-therian lineages to diversify after the Cretaceous-Paleogene (K-Pg) mass extinction ca. 66 Ma[25,53]. Nonetheless, multituberculate life histories remain poorly understood, with a histological study on only two Late Cretaceous bones suggesting that they had relatively fast growth rates[37,54]. Thus, reconstructing the life histories of multituberculates has implications for understanding not only the evolution of mammalian life history strategies, but also the diversification and the ecological roles of mammals during the Mesozoic and early Cenozoic.

Here we establish a new framework for inferring the life histories of early mammals. We document the femoral histology of a phylogenetically and ecologically diverse sample of 35 species of extant small-bodied marsupials and placentals, including both adults and subadults (Figure 4.1; Table 4.11.1). We then investigate the correlation between histological metrics (from cortical measurements of different bone tissue types) in this sample and the duration of lactation period of these mammals using analyses performed in a phylogenetic context. We compare the histology of our extant sample to that of 18 multituberculate femora from the latest Cretaceous and earliest Paleocene (ca. 68–65.5 Ma[55,56]) (Figure 4.1; Table 4.11.2) and apply our histological correlates of reproductive strategy to multituberculates to quantitatively estimate their weaning age. Our results provide a new perspective on the marsupial-placental dichotomy and the pattern and timing of mammalian life history evolution.

4.4 RESULTS AND DISCUSSION

Multituberculate Bone Histology Closely Resembles That of Placentals, Not Marsupials. Cross sections from the femoral midshaft of 35 specimens from 35 extant species in our adult

sample and 18 specimens from five multituberculate morphotypes (each likely approximating a genus[49]) consist of an open medullary cavity and a compact cortex composed primarily of lamellar (well-organized) and woven (disorganized) bone (Figure 4.1) (see Supplemental Information and Figure 4.10.1–11 for full descriptions, specimen photographs, and interpretive illustrations). Vascularity is low (< 1% of the total cortical area) for most specimens but increases with body size (Dataset S1 and S2). Primary osteons and simple longitudinal canals constitute most of the vasculature, but radial canals are also present (to varying degrees). Two taxa exhibit secondary osteons (Meerkat, *Suricata suricatta*; Eastern Tree Hyrax, *Dendrohyrax arboreus*). Large nutrient foramina and resorption voids also contribute to the porosity of the cortex in many specimens. Osteocyte lacunae in lamellar bone are generally small, pinched, elongate, sparse, and well organized circumferentially within lamellae, whereas osteocyte lacunae in woven bone are generally large, globular, densely packed, and haphazardly arranged. Lines of arrested growth (LAGs) are present in four taxa (Long-Nosed Bandicoot, *Perameles nasuta*; Senegal Galago, *Galago senegalensis*; American Mink, *Neovison vison*; Eastern Tree Hyrax, *Dendrohyrax arboreus*) but are otherwise absent or obscured due to cortical remodeling.

The cortices in our sample consist of three different bone tissue types: (1) endosteal organized bone (EOB), (2) disorganized bone (DB), and (3) periosteal organized bone (POB) (Figure 4.1). EOB primarily comprises parallel-to-lamellar-fibered bone with little-to-no vascularity and is present in the deep cortex. DB frequently comprises a woven-fibered matrix hosting primary osteons (i.e., fibrolamellar bone); however, it also comprises a mixture of compact fine- and coarse-cancellous bone in many specimens and grades to parallel-fibered bone in a few (Supplemental Information; Figure 4.10.1–11). POB primarily comprises parallel-to-

lamellar-fibered bone with little-to-no vascularity, is present in the superficial cortex, and is often separated from EOB or DB by a sharp 'tide' or 'reversal' line[57] (Figure 4.1).

The most striking aspects of the histological architecture in our sample are the different yet consistent proportions of EOB, DB, and POB in marsupials versus placentals. Adult marsupial cortices are primarily POB and exhibit little-to-no DB (Figure 4.1; Figures S1 and S2). When present, DB is restricted to the deep cortex, never spans more than 50% of the cortical circumference, and forms a gradational contact with POB superficially and a sharp contact with EOB deeply. EOB typically forms a thin rim around the circumference of the medullary cavity and is separated from both POB and DB by a reversal line. In larger-bodied species (e.g., Virginia Opossum, *Didelphis virginiana* [2950 g]; Common Ringtail Possum, *Pseudocheirus peregrinus* [895 g]) most of the cortex exhibits prominent and densely packed radial canals that are distinct from other taxa in our sample, but these canals are hosted within a lamellar bone matrix (Figure 4.1). Although our marsupial sample (n = 7 species) is small relative to placentals (n = 28 species) and multituberculates (n = 18 specimens), these observations are consistent with a previous study on the bone histology of small-bodied marsupials[38].

Adult placental and multituberculate cortices exhibit a consistent histological pattern that is distinct from those of adult marsupials. From the medullary cavity to the periosteal margin of the cortex (left to right in Figure 4.1 panels), EOB grades into DB in the mid-cortex, then a sharp reversal line separates DB from POB in the outermost cortex. The proportions of these three tissues vary among species (Figure 4.1; Figure 4.10.2–11), but in most taxa EOB and DB together make up most of the cortex. Primates (Pygmy Marmoset, *Cebuella pygmaea*; Senegal Galago, *Galago senegalensis*) and chiropterans (bats; California Myotis, *Myotis californicus*; Gray-Headed Flying Fox, *Pteropus poliocephalus*) are the exception to this pattern among the

placentals in our sample. Cortices of the small-bodied primate (*C. pygmaea* [60 g]) and bat (*M. californicus* [4 g]) are primarily POB and they lack DB; as such, their bone histology closely resembles that of small-bodied marsupials (e.g., Elegant Fat-Tailed Mouse Opossum, *Thylamys elegans* [28 g]; Brown Antechinus, *Antechinus stuartii* [26 g]). Cortices of the larger-bodied primate (*G. senegalensis* [108 g]) and bat (*P. poliocephalus* [680 g]) have substantial amounts of DB adjacent to the medullary cavity, but otherwise are primarily POB (Figure 4.1); as such, their bone histology resembles neither that of marsupials nor other placentals in our sample and instead exhibits a pattern 'intermediate' to those two end members. Hereafter, when we refer to the histological pattern of 'placental mammals' we exclude primates and bats unless otherwise stated.

Four of the five femoral morphotypes that make up our multituberculate sample show no striking histological differences (Figure 4.1). The one exception is our single Mu2 specimen (UWBM 106225), the cortex of which is composed almost entirely of EOB and DB (Figure 4.10.9) and therefore closely resembles the histology of subadult placentals represented in our extant sample (which exhibit even greater histological differences from marsupials, see below). Our sample of multituberculate specimens are from just before and after the K-Pg boundary in northeastern Montana, but they exhibit histological patterns that are consistent with those observed in geologically older multituberculate long bones from the Late Cretaceous of Mongolia[37,54]. Thus, the histological patterns observed in our sample and their life history implications (discussed below) may be more broadly applied to multituberculates in general.

The Ontogenetic Origin of Marsupial- and Placental-Like Bone Histology. Our sample includes subadult specimens for 22 of the 35 extant species (Figure 4.1). In comparing the bone

histology of subadults and adults, we find that the patterns of bone growth through ontogeny differ in marsupials and placentals, likely reflecting their distinct life history strategies (Figure 4.2) (see Materials and Methods for details about our classification of subadult and adult specimens). The cortices of subadult marsupials are generally very similar to the adult cortices but have a greater proportion of DB in the deep cortex. In the least skeletally mature specimens of the larger-bodied species (Virginia Opossum, *Didelphis virginiana* [2948 g]; Common Ringtail Possum, *Pseudocheirus peregrinus* [895 g]), DB makes up a substantial portion of the cortex (Figure 4.2); however, in the least skeletally mature specimen of a small-bodied species (Monito Del Monte, *Dromiciops gliroides* [24 g]), DB is still a minor component of the cortex relative to POB (Figures S1 and S2).

Among subadult placentals, the cortices of the least skeletally mature specimens (e.g., Red Tree Vole, *Arborimus longicaudus*; Columbian Ground Squirrel, *Urocitellus columbianus*) are almost entirely composed of fine-to-coarse cancellous bone or well-vascularized woven bone (Figure 4.2). In more skeletally mature specimens, many of those cancellous and vascular voids are filled with circumferential lamellae and there is a greater proportion of EOB (Figure 4.10.2–8). Thus, the cortices of the subadult placentals in our sample are characterized primarily by DB and EOB, and the most substantial difference between placental subadults and adults is that subadults have very little (if any) POB (whereas POB makes up a much greater proportion of the adult cortex).

The greater proportion of DB in the subadult cortices of both marsupials and placentals indicates that in both groups DB forms early in ontogeny relative to organized bone layers (which occur in greater proportions in the adult cortices). This interpretation is consistent with previous research on small-bodied mammals showing that bone formed prenatally and early

postnatally (i.e., perinatally) is composed primarily of porous woven bone that gets compacted later in ontogeny[57–59]. However, the relative scarcity of DB in the cortices of adult marsupials reveals that much of that early DB is resorbed later in ontogeny, whereas a substantial proportion of DB remains in the mid-cortex of adult placentals. In marsupials, this resorption of DB occurs along the endosteal (inside) margin of the cortex, indicated by the sharp reversal line separating the DB layer from the thin EOB layer (Figures 1 and 2), likely driven by the expansion of the medullary cavity[57]. In contrast, bone deposition along the periosteal (outside) margin of the cortex is relatively continuous, indicated by the gradational contact between the DB layer and the thick POB layer (Figures 1 and 2), increasing the diameter of the midshaft throughout femoral growth. Thus, in marsupials, growth of the femoral midshaft is primarily characterized by endosteal resorption and periosteal deposition (with endosteal deposition making up a very minor portion of the adult cortex) (Figure 4.2).

In placentals, growth of the femoral midshaft is more complex and represents a composite of substantial bone deposition at both the endosteal and periosteal margins (Figure 4.2). Most endosteal deposition likely occurs early in ontogeny as the femur lengthens[57], indicated by the gradational contact between DB and EOB layers (Figures 1 and 2) and the greater proportion of EOB to POB in the cortices of our subadult specimens (Figure 4.10.2–8). This period of endosteal deposition is concurrent with or immediately followed by resorption along the periosteal margin, indicated by the sharp reversal line between the DB and POB layers. Most periosteal deposition likely occurs later in ontogeny, indicated by the relative scarcity of POB in the cortices of subadult placentals relative to DB and EOB (Figure 4.2; Figure 4.10.2–8). Periosteal deposition is likely reciprocated by some resorption along the endosteal margin, indicated by the scalloped endosteal margins of many adult placental cortices[57]. This period of

periosteal deposition and endosteal resorption is likely associated with increasing the diameter of the midshaft and the concurrent expansion of the medullary cavity.

We propose a model in which these two divergent modes of bone deposition—the periosteal-dominant bone deposition of small-bodied marsupials and the mixed periosteal and endosteal bone deposition of small-bodied placentals—reflect the marsupial-placental dichotomy (Figures 2 and 3). The femoral cortices of perinatal marsupials and placentals both comprise disorganized and porous bone. However, the midshaft diameter of altricial marsupial perinates is much smaller than that of adults, whereas comparatively precocial placental perinates have midshaft diameters much closer in size to that of placental adults (Figure 4.2). As such, postnatal bone deposition in marsupials is predominantly outward or periosteal, increasing the diameter of the midshaft. This is reflected histologically by a preponderance of POB and an obliteration of most perinatal DB through medullary cavity expansion (Figure 4.2). In contrast, postnatal bone deposition in placentals is first inward or endosteal, reinforcing the perinatal woven-bone scaffolding, then outward as the animal grows to adult size. This is reflected histologically by a greater retention of perinatal DB in the mid-cortex that is sandwiched between layers of endosteal and periosteal bone (Figure 4.2). In sum, marsupial-like histological patterns are characterized by appositional bone growth and likely reflect prolonged postnatal development, whereas placental-like histological patterns are characterized by bone remodeling and likely reflect prolonged prenatal development.

That the life history differences between marsupials and placentals are reflected in their bone histology is also supported by a phylogenetic generalized least squares (PGLS) regression, which reveals a significant positive correlation between the proportion of POB in the femoral midshaft (transformed to isometric log-ratios) and weaning age (log-transformed and size-

corrected) ($p < 0.001$, $r^2 = 0.344$; Figure 4.3*B*; Table 4.1). Notably, the correlation between amount of POB and weaning age is not simply driven by discrete differences between placentals and marsupials but rather falls along a spectrum that is maintained when using a placental-only subsample of our dataset (Table 4.1). In preliminary analyses, we did not find a strong or consistent negative correlation between the amount of POB and gestation length, but the marsupials in our sample have a significantly shorter gestation period ($p < 0.001$; Dataset S4) and less POB ($p < 0.001$; Table 4.11.3) relative to placentals. Thus, whereas most placentals are weaned early, have prolonged gestation, and have a small amount of POB, marsupials are weaned late, have abbreviated gestation, and have a large amount of POB.

The primates and bats are the exceptions to the histological pattern of placentals in our sample. Both groups, like marsupials, have bone histology that is dominated by POB, which is characteristic of prolonged outward growth at the femoral midshaft (Figure 4.1). This fits our conceptual framework for marsupial- versus placental-like histology in that primates and bats have very long and slow postnatal growth compared to all other placentals[60–63], instead resembling marsupials in their pace of postnatal growth. The primates and bats also plot closer to marsupials than other placentals in the regression plot of POB and weaning age (Figure 4.3*B*), which is unsurprising considering their relatively late weaning and high proportion of POB (Datasets S2 and S4). Taken together, our results indicate that the defining features of the marsupial-placental dichotomy—emphasizing offspring nourishment via lactation versus gestation—are reflected in the bone histology of small-bodied marsupials and placentals.

Inferring a Placental-Like Life History Strategy for Multituberculates. The strong similarities of the bone histology of multituberculates and extant placentals in our sample are

borne out quantitatively (Figure 4.3; Datasets S1, S3 and S4; see Materials and Methods for details). POB makes up the highest proportion of marsupial cortices, whereas DB and EOB make up the majority of both placental and multituberculate cortices (Figure 4.3*A*). Analyses of variance (ANOVAs) show that placentals and multituberculates do not have statistically different proportions of POB or DB (transformed to isometric log-ratios) in their cortices, whereas both are significantly different from those of marsupials (Figure 4.3*C*; Table 4.11.3). Further, mixture discriminant analysis (MDA) models trained on our extant dataset consistently classify multituberculates with placentals. These results indicate that the proportions of EOB, DB, and POB robustly distinguish marsupials from placentals but cannot distinguish multituberculates from placentals.

This histological similarity of multituberculates and placentals implies that, like placentals, multituberculates likely exhibited prolonged prenatal growth and abbreviated postnatal growth (Figure 4.2). Using the proportion of POB in the cortex within an ordinary least squares (OLS) regression model, we predict that the weaning age of the multituberculates in our sample was ~30 days (± 10 days) (Figure 4.3*D*), which places them within the range of the smallest-bodied placentals (excluding bats) in our extant sample, such as the rodents (e.g., squirrels and voles) and eulipotyphlans (e.g., shrews) (Dataset S2 and S4). This methodological approach provides an exciting new avenue to quantitatively estimate life history traits in extinct small-bodied mammals. In sum, given the evidence presented here, we infer that the multituberculates in our sample likely had a level of maternal-fetal contact comparable to extant small-bodied placental mammals and that they were weaned relatively rapidly.

Implications for the Marsupial-Placental Dichotomy. The inference that at least some multituberculates had prolonged gestation and abbreviated lactation demonstrates that this life history strategy was not unique to placental mammals (contra[8,17]). It also casts doubt on the hypothesis that the marsupial life history strategy is plesiomorphic for Theria[6,8,18]. That hypothesis is largely based on the extreme altricial state of neonates shared by marsupials and monotremes[6,8]; however, this 'extreme fetalization' may have evolved independently in those two clades[3,22,64,65]. For instance, embryonic development in both the cranium and postcranium of monotremes more closely resembles that of placentals than marsupials[65,66]. The bone histology of monotremes is also distinct from that of both marsupials and placentals[28,36,37,54]. Although there are few comparable histological descriptions of monotremes (e.g., femoral midshaft[37,54]), they show a distinct pattern of alternating 'bands' of highly vascularized woven bone and avascular lamellar bone in the mid-cortex[36,37,54]—no such pattern has been observed among small-bodied marsupials or placentals.

One interpretation of our results is that the inferred similarities in the life histories of multituberculates and placentals evolved in their common ancestor, which is consistent with the hypothesis that the placental strategy is ancestral for therians and perhaps all mammals that give live birth[3,22]. In many ways, the placental strategy to birth relatively precocial young that are less reliant on maternal nourishment is more similar to the presumed ancestral amniote life history strategy[3,67–69]. Indeed, placentals and non-mammalian amniotes share several developmental traits (e.g., advancement of the neural tube, small branchial arches, approximately equal rates of fore- and hind limb development) that are distinct from those of marsupials[65,70]. These lines of evidence suggest that the reproductive and developmental biology of placentals may be conserved relative to that of marsupials. Further, that multituberculates likely had prolonged

gestation and abbreviated postnatal growth is in line with emerging evidence indicating that intense maternal-fetal contact is ancestral for both marsupials and placentals[3,22] and suggests that the roots of this intimate contact between the internally gestating offspring and mother may extend back to at least the Early to Middle Jurassic.

An alternative scenario is that multituberculates convergently evolved a life history strategy similar to that of placentals. Complex morphological structures, such as tribosphenic-like molars[71,72] and tri-ossicular middle ears[73,74], have evolved independently multiple times among mammaliaforms and crown mammals, and we cannot rule out that life history traits, such as prolonged gestation and abbreviated lactation, may have similarly evolved independently in multituberculates and placentals. The multituberculate and placental taxa sampled in our study are all deeply nested within Multituberculata and Eutheria, respectively, and their life history strategies might therefore not be representative of the basal life history strategies of those groups. The multituberculates are members of Cimolodonta, a clade that evolved in the late Early Cretaceous[44], potentially as much as 100 Ma after Multituberculata diverged from other mammals[75]. Similarly, placentals first appear near the K-Pg boundary[76,77], as much as 100 Ma after Eutheria diverged from Metatheria[78]. Although two femoral cortices of stem eutherians from the Late Cretaceous of Mongolia were previously described as primarily consisting of moderately well-organized bone (parallel-fibered)[37,54], similar to descriptions for some small-bodied marsupials[38] (Figure 4.1; Figures S1 and S2), the samples were few and fragmentary, and the published images resemble the cross sections of some eulipotyphlans in our sample (e.g., *Sorex* spp.; Figure 4.10.6). As such, the life history strategies of phylogenetically more basal members of Multituberculata and Eutheria remain unknown. Ultimately, studies on the bone

histology of other early mammals are necessary to test whether the placental-like life histories in multituberculates were inherited from a common ancestor or evolved convergently.

Nevertheless, our results challenge the presumed exceptionalism of placental reproduction and development. One of the hypothesized consequences of the marsupial-placental dichotomy is that placental life history strategies were competitively superior to those of marsupials in the aftermath of the K-Pg mass extinction, facilitating the taxonomic and ecological rise of placentals in the Cenozoic[17]. That interpretation draws primarily from the well-documented North American fossil record of metatherians and eutherians[6,7,17], but neglects the record of contemporaneous multituberculates. In North America, most metatherians went extinct at the K-Pg boundary[55,79,80], and eutherians underwent an adaptive radiation early in the Cenozoic[55,81,82], but multituberculates surpassed both metatherians and eutherians in abundance and diversity in the Late Cretaceous[44,80,83] and exceeded or rivaled eutherians in terms of numerical abundance and taxonomic richness in the early aftermath of the K-Pg mass extinction[80,84].

Thus, if the rise of placental mammals in the Cenozoic was facilitated by the purported ecological, physiological, and behavioral benefits afforded by the combination of mature neonates plus abbreviated lactation (e.g., rapid increases in population size, increased metabolic rates[17]), then the same rationale should apply to multituberculates. Indeed, *Mesodma*, the multituberculate genus likely represented by our Mu1 morphotype, was the most prolific 'bloom taxon' in the immediate aftermath of the K-Pg mass extinction[80,84], and gregarious social behavior, a hypothesized 'secondary evolutionary effect' of placental-like reproduction[17], has now been documented in a Late Cretaceous multituberculate species[50]. However, the fact that eutherians and their placental descendants continued to diversify throughout the Cenozoic,

whereas multituberculate diversity declined precipitously in the late Paleocene (ca. 57 Ma)[53,85] before their eventual extinction in the late Eocene (ca. 35 Ma)[51], calls these mechanisms as the cause for the evolutionary success of placental mammals into question. What drove the decline and extinction of multituberculates remains unresolved, but one hypothesis is that the specialized dentitions of multituberculates constrained their ability to evolve novel dental morphologies[25,53], perhaps leading to their competitive exclusion by placental herbivores[85,86] with more 'evolvable' tribosphenic dentitions[87]. Nonetheless, if sympatric multituberculates and placentals had similar life history strategies then it is unlikely that the Cenozoic ascendency of placentals was driven by their inherent reproductive or developmental 'superiority' to contemporaneous multituberculates (contra[88]) or marsupials (contra[6,8]).

In sum, the evidence presented here that multituberculates had placental-like life history strategies suggests that prolonged gestation and abbreviated lactation either (i) were ancestral for Theria and perhaps viviparous Mammalia more generally[3,22] or (ii) evolved independently in both multituberculates and placentals. In either case, these results challenge the hypothesis that the Cenozoic rise of placental mammals was driven by unique life history innovations[17]. The new comparative approach presented here for inferring life history traits in extinct small-bodied mammals offers an exciting new avenue of research, and future studies on the bone histology of other Mesozoic and early Cenozoic mammals will continue to shed light on the pattern and timing of mammalian life history evolution.

4.5 ACKNOWLEDGMENTS

We thank Jeffrey Bradley and Sharlene Santana (UWBM) for access and permission to histologically sample extant specimens; Christian Sidor, Ronald Eng, Meredith Rivin, and Katherine Anderson (UWBM), David Evans and Kevin Seymour (ROM), David Fox (Bell Museum), and Glenn Stores (CMC) for access and permission to histologically sample fossil specimens; Field crews led by the Wilson Mantilla lab (UWBM), Loris Russell (ROM), and Robert Sloan (Bell Museum) for collecting fossil specimens; Brody Hovatter for μCT scanning; Michael Holland for assistance in casting; Taylor Manske for measuring and sorting fossil specimens; Michaela Leung and Jacqueline Lungmus for help preparing thin sections; John Horner for providing histological photographs of *Ornithorhynchus*; the 2017 ROM Palaeohistology Workshop organizers and attendees for training and discussions; and Kristina Curry Rogers, Russell Main, Michael D'Emic, G. James Kenagy, William Clemens, David Krause, Kathryn Stanchack, Rachel Roston, Lianna Marilao, Savannah Olroyd, Christian Sidor, Caroline Strömberg, Patricia Kramer, Raymond Rogers, Allison Bormet, Alexandria Brannick, Jordan Claytor, Paige Wilson, and Brody Hovatter for thoughtful discussions that improved this manuscript. Funding for LNW was provided by the National Science Foundation Graduate Research Fellowship, Society of Vertebrate Paleontology, Paleontological Society, American Society of Mammalogists, UW Biology, and the Burke Museum. Funding for HZF was provided by the Mary Gates Research Scholarship.

4.6 FIGURES AND TABLES

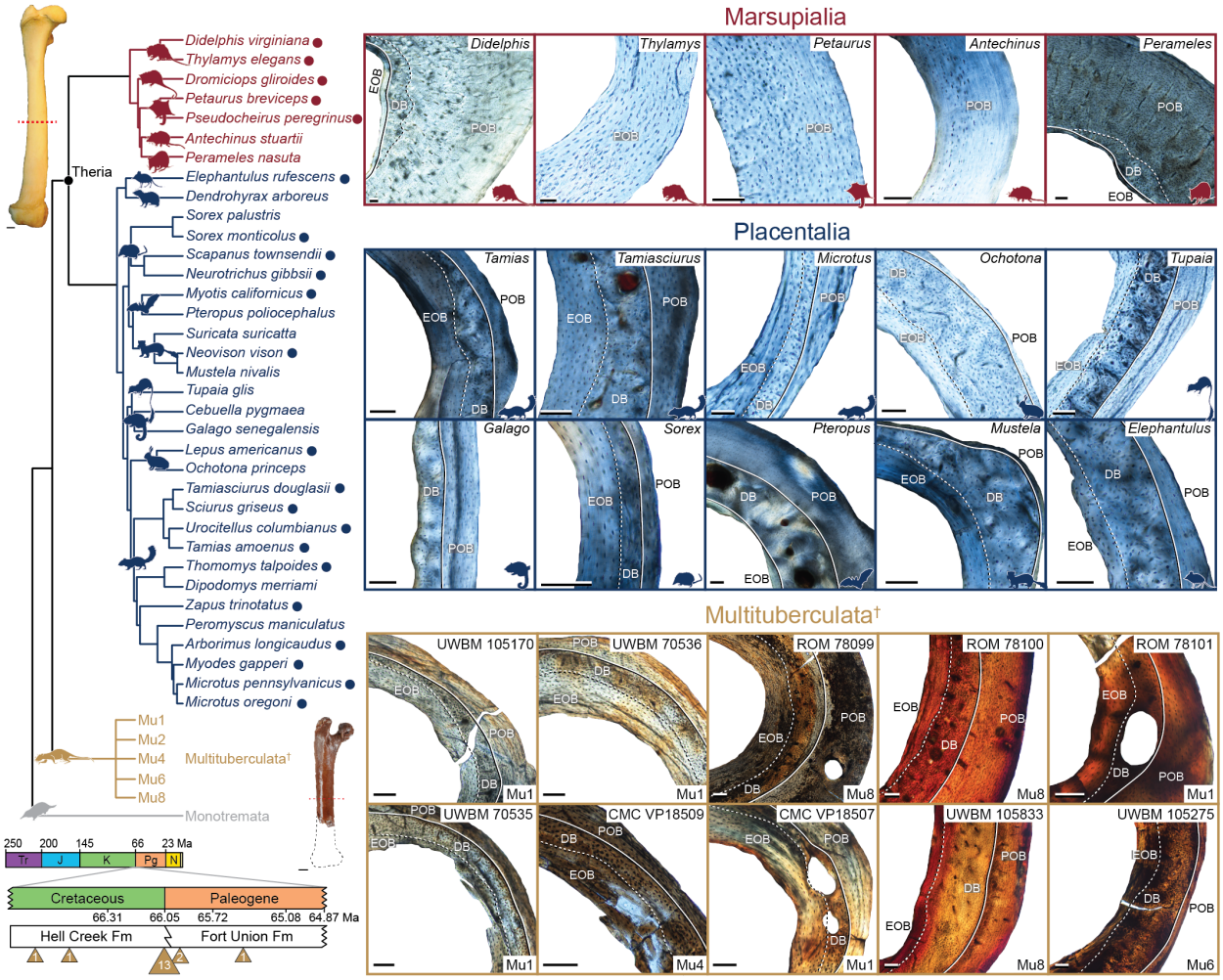

Figure 4.1. Phylogeny, geologic age, and histology of femoral midshaft cross sections from marsupial, placental, and multituberculate mammals. (*Left*) A time-calibrated phylogeny of the marsupials (red), placentals (blue), and multituberculates (gold) included in this study (geologic time scale below). Circles next to the species names indicate that both adult and subadult specimens were included in this study. Silhouettes indicate different Orders (from top to bottom: Didelphimorphia, Microbiotheria, Diprotodontia, Dasyuromorphia, Peramelemorphia, Macroscelidea, Hyracoidea, Eulipotyphla, Chiroptera, Carnivora, Scandentia, Primates,

Lagomorpha, Rodentia, Multituberculata). Most silhouettes are from www.phylopic.org, with credit to Sarah Werning (Microbiotheria, Diprotodontia), Maky (vectorization), Gabriella Skollar (photography), and Rebecca Lewis (editing) (Primates), and Nobu Tamura (vectorized by T. Michael Keesey) (Monotremata) via Creative Common Attribution 3.0 Unported. Didelphimorphia, Rodentia, and Multituberculata silhouettes are by LNW, with the multituberculate based on artwork by Misaki Ouchida. Gold triangles indicate the stratigraphic level of the localities where our multituberculate specimens were collected and the white numbers inside the triangles indicate the number of specimens from that locality (the large triangle indicates the Bug Creek Anthills locality, which hosts a mixed K-Pg fossil assemblage). The extant femur (top) is from the Virginia Opossum (*Didelphis*; scale bar = 2 mm), the multituberculate femur (bottom) is from the Mu1 morphotype (likely *Mesodma*; scale bar = 1 mm). (*Right*) Representative histological samples of marsupials (red, top), placentals (blue, middle), and multituberculates (gold, bottom) in cross-polarized light. Solid lines indicate sharp reversal lines and dashed lines indicate gradational contacts between bone tissue types. Scale bars = 0.1 mm. Abbreviations: EOB = endosteal organized bone, DB = disorganized bone, POB = periosteal organized bone (see main text for details).

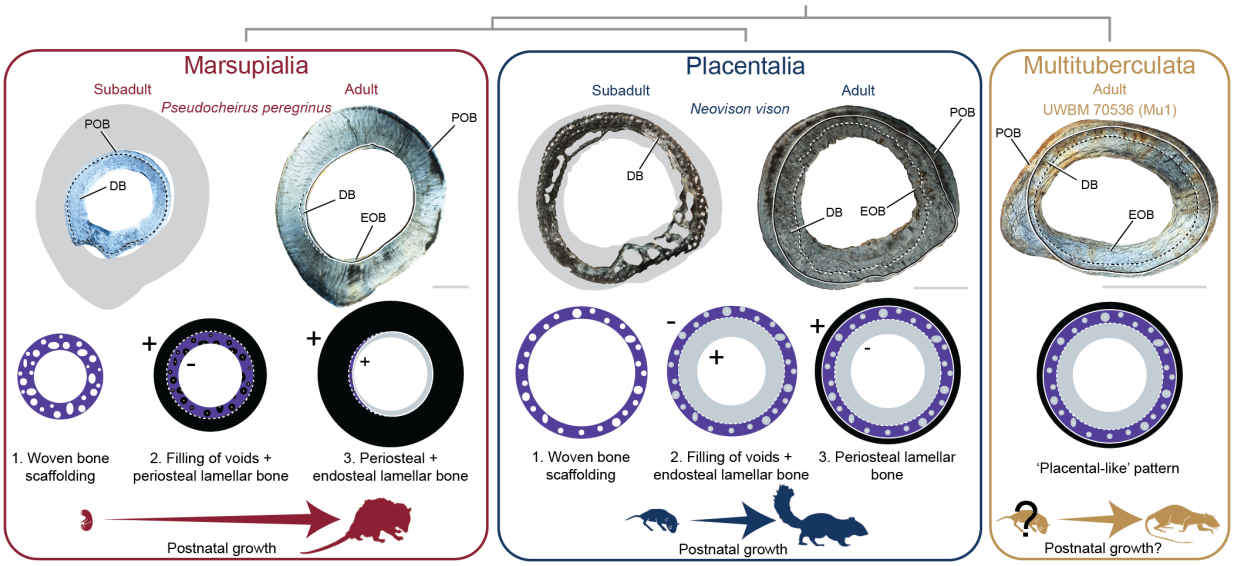

Figure 4.2. Conceptual model for the ontogenetic origins of marsupial- and placental-like histological patterns. (*Top*) Comparisons of subadult versus adult cross sections (scale bar = 1 mm). (*Middle*) Illustrations of our proposed models for bone growth through ontogeny at the femoral midshaft in marsupials versus placentals. Pluses and minuses indicate where bone deposition and resorption, respectively, are likely occurring. (*Bottom*) Illustration of the small perinate size of marsupials versus the relatively large perinate size of placentals. These histological differences likely reflect the prolonged versus abbreviated postnatal growth of marsupials versus placentals, respectively. Multituberculate cross sections of adult specimens exhibit the same histological pattern as placentals, suggesting that they too had abbreviated postnatal growth. See main text for details.

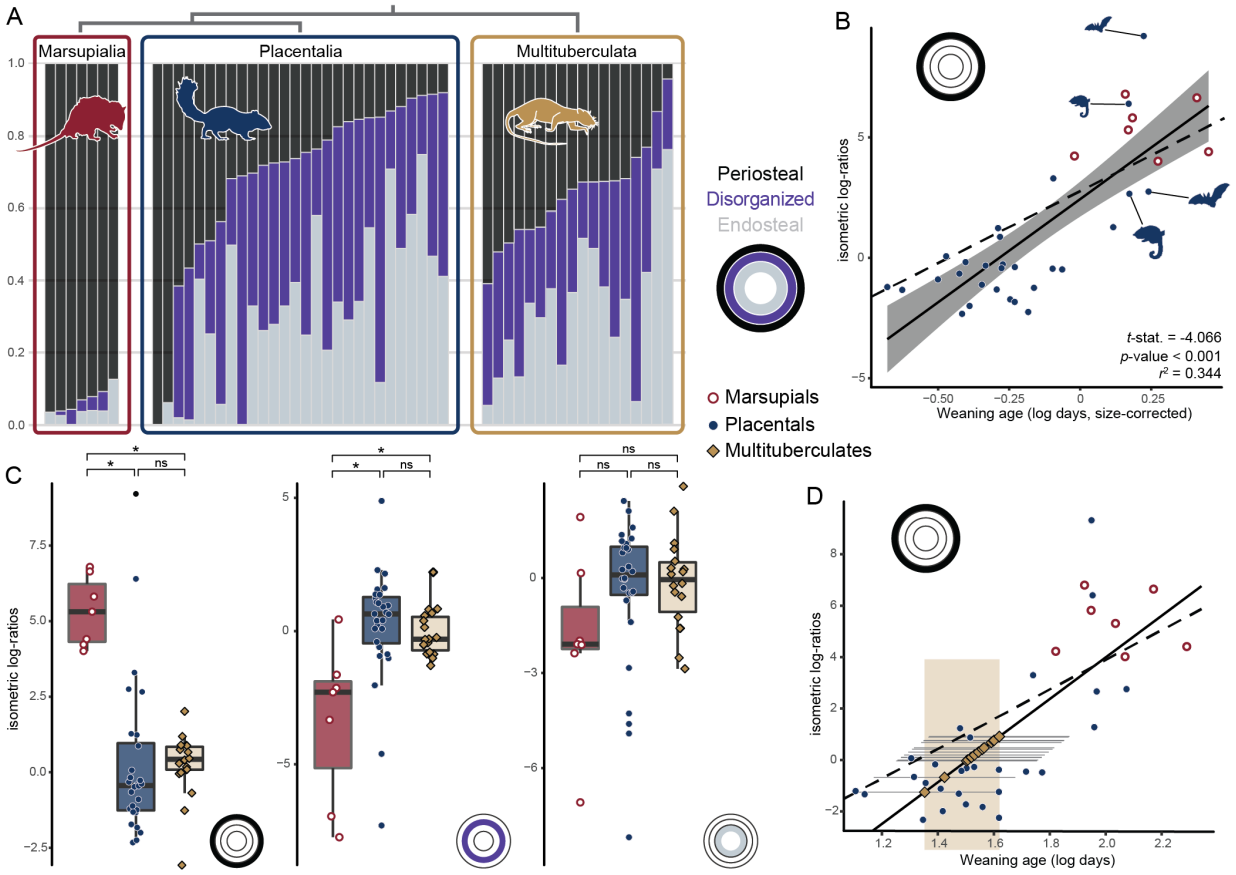

Figure 4.3. Quantitative evidence for histological similarities between multituberculates and placentals, and the relationship between bone tissue microstructure and length of lactation period. (*A*) Stacked bar chart showing the raw proportions of the different tissue types in the cortices of our sample. (*B*) Ordinary least squares (solid line) with 95% confidence intervals and phylogenetic generalized least squares (PGLS; dashed line) regression of the isometric log-ratios (ILR) of periosteal lamellar bone versus weaning age (log days and size corrected via PGLS residuals). (*C*) Box plots of the ILRs of periosteal organized, disorganized, and endosteal organized bone (left to right). Brackets above denote whether the ILRs are significantly different among marsupials, placentals, and multituberculates (via ANOVAs). Significant *p*-values are < 0.001. (*D*) Same plot as (*B*) but regressed against non-size-corrected log weaning age and showing predicted weaning ages (with 95% confidence intervals) for our multituberculate

sample. The gold band highlights the spread of weaning ages predicted by the model, which when converted back to days fall around ~30 days (± 10 days). Note that UWBM 106225 was removed from this predictive regression because it appears to be from a subadult individual, and UWBM 115276 and ROM 78100 were removed because those cross sections were taken from very proximal on the midshaft. See main text for details.

Table 4.1. Summary statistics for phylogenetic generalized least squares (PGLS) regressions of bone cortex tissues against weaning age (measured in days) for our entire therian sample and a placental-only subsample. Prior to analyses, compositional tissue data (percentages of cortex) were transformed into isometric log-ratios, and weaning age was log-transformed and size-corrected (via PGLS regression against adult body mass).

		Cortex tissue	***t*-stat.**	***p*-value**	r^2
Weaning age	Therians	Periosteal	4.066	<0.001	0.344
		Disorganized	-1.575	0.125	0.070
		Endosteal	-1.493	0.145	0.063
	Placentals	Periosteal	3.879	0.001	0.367
		Disorganized	-1.527	0.139	0.082
		Endosteal	-1.419	0.168	0.072

4.7 MATERIALS AND METHODS

Institutional Abbreviations. CMC, Cincinnati Museum Center, Cincinnati, OH; ROM, Royal Ontario Museum, Toronto, ON; UWBM, Burke Museum of Natural History and Culture, Seattle, WA.

Sampling. Our extant sample consists of femora from 35 mammalian species representing nine placental and five marsupial orders and 18 placental and six marsupial families (Figure 4.1; Table 4.11.1). This sample spans a body mass range of 4.25–2,950 g, and the majority of taxa (*n* = 33) weigh < 1 kg (Dataset S2). All extant specimens come from the UWBM Mammalogy collections; most are wild-caught but a small number are zoo specimens (Table 4.11.1). Our sample consists of both skeletally mature and immature specimens; all but one species (*Perameles nasuta*) are represented by a skeletally mature individual (indicated by fused cranial sutures and/or long-bone epiphyses) and 22 species in our sample are represented by both a skeletally mature and immature individual (indicated by incompletely fused or unfused cranial sutures and/or long bone epiphyses). We refer to these skeletally immature individuals as 'subadults,' but the level of skeletal maturity among our subadult sample varies considerably. In one case (*Arborimus longicaudus*) our 'subadult' is a newborn nestling, whereas in most other instances our 'subadult' represents a smaller individual of the species with incompletely fused femoral epiphyses. In Figure 4.2, we highlight a couple of the starkest ontogenetic differences in our sample, but for perspective on the entirety of our subadult and adult sample refer to Figure 4.10.1–8.

Our multituberculates sample (Table 4.11.2) consists of 18 fragmentary, isolated proximal femora from the Hell Creek and Fort Union formations, which span the K-Pg boundary in northeastern Montana[56]. Two of these specimens are from the Hell Creek Formation and are latest Cretaceous in age (ca. 68–67 Ma), four are from the Fort Union Formation and are earliest Paleocene in age (ca. 66–65.5 Ma), and 12 are from the Bug Creek Anthills locality, a fluvial channel deposit in the Hell Creek Formation that hosts a mixed assemblage of latest Cretaceous and earliest Paleocene taxa[89]. All specimens are grouped into femoral morphotypes and tentatively assigned to genera following the work of L. B. DeBey and G. P. Wilson[49] on Hell Creek and Fort Union mammal femora (Table 4.11.2). In total, our sample comprises five morphotypes. Because these specimens are fragmentary, their degree of skeletal maturity cannot be robustly assessed; however, of the specimens that preserve the greater trochanter and femoral head, the epiphyses are entirely fused.

Histological and Life History Data. Prior to embedding, all extant specimens were dehydrated through an alcohol series consisting of two 24-hour baths in 70%, 80%, 95%, and 100% ethanol. Otherwise, thin sections from both extinct and extant specimens were prepared following the procedures outlined by E.-T. Lamm[90]. Histological observations and high-resolution photographs were taken using a Nikon Eclipse LV100POL microscope under plane- and cross-polarized light. Histological measurements were taken from high-resolution photographs using ImageJ[91]. Area measurements of different tissue types and vasculature were taken from the entire cortex. Measurements of osteocyte lacunae were taken from subsets of each tissue type. Only area measurements of different tissue types were taken on our multituberculate sample because these metrics proved most strongly correlated with life history traits in our extant sample (see below).

For a full list of histological measurements see Datasets S1 and S3. Weaning-age and gestation-length data for the species included in our extant sample were compiled from PanTHERIA[92], Ecological Archive[93], Animal Diversity Web[94], or the primary literature (Dataset S2). We focused on these two life history traits because weaning age and gestation length provide measures of post- versus prenatal maternal investment, respectively. Whenever possible we used the body mass recorded for the UWBM specimens from which histological sections were taken.

Comparative Methods. Most analyses were performed in R (v. 4.04[95]). Exploratory analyses on the histological data collected from our extant sample revealed that the proportion of the three primary cortical tissue types (EOB, DB, and POB) were the most informative in differentiating placentals and marsupials (Figure 4.3; Table 4.11.3) and the most strongly correlated with weaning age (Table 4.11.4). Gestation length did not show a strong or consistent linear relationship with any histological traits, but to test whether mean gestation length was significantly different between the marsupials and placentals in our sample we ran a simple *t*-test (assuming unequal variances) in Microsoft Excel. Because our histological data are compositional in nature, we conducted isometric log-ratio (ILR) transformations of the proportions of the three primary cortical tissues, resulting in two transformed variables that were used in subsequent analyses. ILR transformed proportions of each major tissue type (relative to remaining two) were also used for general comparison between the three major taxonomic groups sampled (Figure 4.3*C*; Table 4.1). For further discussion on ILR transformations, our choice to use this transformation method over others (e.g., amalgamated [summed] log-ratio transformations), and sensitivity analyses applying other transformations, see Supplemental Information and Table 4.11.5.

We performed analyses of variance (ANOVAs) with post-hoc tests (Tukey's Honest Significant Difference) on ILR-transformed histological data using three groups: multituberculates, marsupials, and placentals. We were unable to use phylogenetic ANOVAs because the precise phylogenetic relationships of the multituberculate specimens in our sample are unknown (only tentative genus-level identifications). Similarly, we did not size-correct these data before ANOVAs because the adult body masses of the multituberculates are unknown. ILR-transformed histological data were included as predictors in mixture discriminant analysis (MDA[96]) models, with placental or marsupial as the response. MDA is an extension of traditional linear discriminant analysis (LDA), which treats each group of the response as a mix of unobserved subgroups. This approach was taken because it was found to outperform several other methods, including LDA, in this classification problem (Figures S12 and S13). Models were trained using the full extant dataset, with the exception of *Myotis* (small bat) and *Cebuella* (small primate). Additional results including these taxa are presented in the Supplemental Information and Figure 4.10.13. Training of the model included 35 repeats of two-fold cross-validation (Figure 4.10.13*A*). In the MDA model, the placental group was assigned the default three subgroups, whereas marsupials were assigned only one owing to their smaller sample size. Average accuracy during cross-validation was 0.988 (se = 0.004) with an average Kappa of 0.967 (se = 0.011). The no information rate (NIR) of the entire training set was 0.788. No single round of cross-validation returned an accuracy below this level (max = 1.0, min = 0.824). Analysis was completed using the package *caret*[97] as a wrapper for the *mda* package[98]. Weaning age (in days) was log10-transformed, and the influence of body size was accounted for by regressing the weaning age values against adult body mass via phylogenetic generalized least squares (PGLS), with regression residuals used in subsequent regressions. Size correction was

performed because body size is often the most substantial predictor of mammalian life history variation[99] and can therefore obscure other important life history correlates[60,61]. We ran PGLS regressions on the ILR-transformed histological data and transformed life history data. We set Pagel's lambda to one (Brownian Motion) for all PGLS regressions, and these were performed using the *caper* R package[100]. The phylogeny we used for the PGLS regressions is a maximum-clade-credibility (MCC) tree produced from 1,000 randomly chosen phylogenetic trees from the posterior distribution of Upham *et al.*[101] 'completed trees' analysis of mammals. We used *TreeAnnotator*[102] to generate the MCC tree, which was then pruned to the extant species in our sample. To estimate the weaning age of the multituberculates in our sample we used an ordinary least squares (OLS) regression of the ILR-transformed proportion of POB versus log10-transformed weaning age (but non-size-corrected to allow for back-calculation of predicted weaning ages in days). This analysis excluded UWBM 106225 because it is likely a subadult individual (see above; Supplemental Information; Figure 4.10.9) and UWBM 115276 and ROM 78100 because those cross sections were taken from very proximal on the midshaft (Table 4.11.2); none of those specimens were directly comparable to the adult marsupial and placental cross sections from which our predictive regression was derived.

4.8 REFERENCES

1. Boyce, M.S. (1988). Evolution of life histories: theory and patterns from mammals. In Evolution of Life Histories of Mammals: Theory and Pattern, M. S. Boyce, ed. (Yale University Press), pp. 3–30.
2. Griffiths, M. (1978). The Biology of the Monotremes (Academic Press, Inc.).

3. Hayssen, V., Lacy, R.C., and Parker, P.J. (1985). Metatherian reproduction: transitional or transcending? Am. Nat. *126*, 617–632.
4. Renfree, M.B. (1981). Marsupials: alternative mammals. Nature *293*, 100–101.
5. Tyndale-Biscoe, H., and Renfree, M. (1987). Reproductive physiology of marsupials (Cambridge University Press).
6. Lillegraven, J.A. (1969). Latest Cretaceous mammals of upper part of Edmonton Formation of Alberta, Canada, and review of marsupial-placental dichotomy in mammalian evolution. Univ. Kans. Paleontol. Contrib. *50*, 1–122.
7. Lillegraven, J.A. (1974). Biogeographical considerations of the marsupial-placental dichotomy. Annu. Rev. Ecol. Evol. Syst. *5*, 263–283.
8. Lillegraven, J.A. (1975). Biological considerations of the marsupial-placental dichotomy. Evolution *29*, 707–722.
9. Sánchez-Villagra, M.R., and Maier, W. (2003). Ontogenesis of the scapula in marsupial mammals, with special emphasis on perinatal stages of didelphis and remarks on the origin of the therian scapula. J. Morphol. *258*, 115–129.
10. Sears, K.E. (2004). Constraints on the morphological evolution of marsupial shoulder girdles. Evolution *58*, 2353–2370.
11. Smith, K.K. (2006). Craniofacial development in marsupial mammals: developmental origins of evolutionary change. Dev. Dyn. *235*, 1181–1193.
12. Weisbecker, V., Goswami, A., Wroe, S., and Sánchez-Villagra, M.R. (2008). Ossification heterochrony in the therian postcranial skeleton and the marsupial-placental dichotomy. Evolution *62*, 2027–2041.

13. Goswami, A., Weisbecker, V., and Sánchez-Villagra, M.R. (2009). Developmental modularity and the marsupial-placental dichotomy. J. Exp. Zool. B Mol. Dev. Evol. *312B*, 186–195.
14. Weisbecker, V., and Goswami, A. (2010). Brain size, life history, and metabolism at the marsupial/placental dichotomy. Proc. Natl. Acad. Sci. U.S.A. *107*, 16216–16221.
15. Sánchez-Villagra, M.R. (2013). Why are there fewer marsupials than placentals? On the relevance of geography and physiology to evolutionary patterns of mammalian diversity and disparity. J. Mamm. Evol. *20*, 279–290.
16. Fabre, A.-C., Dowling, C., Portela Miguez, R., Fernandez, V., Noirault, E., and Goswami, A. (2021). Functional constraints during development limit jaw shape evolution in marsupials. Proc. R. Soc. B *288*, 20210319.
17. Lillegraven, J.A., Thompson, S.D., McNab, B.K., and Patton, J.L. (1987). The origin of eutherian mammals. Biol. J. Linn. Soc. *32*, 281–336.
18. Russell, E.M. (1982). Patterns of parental care and parental investment in marsupials. Biol. Rev. *57*, 423–485.
19. Kirsch, J.A.W. (1977). Biological aspects of the marsupial-placental dichotomy: a reply to Lillegraven. Evolution *31*, 898–900.
20. Parker, P.J. (1977). An ecological comparison of marsupial and placental patterns of reproduction. In The Biology of Marsupials, B. Stonehouse, E. Gilmour, eds. (University Park Press), pp. 273–286.
21. Low, B.S. (1978). Environmental uncertainty and the parental strategies of marsupials and placentals. Am. Nat. *112*, 197–213.

22. Smith, K.K. (2015). Placental evolution in therian mammals. In Great Transformations in Vertebrate Evolution, K.P. Dial, N. Shubin, E.L. Brainerd, eds. (University of Chicago Press), pp. 205–225.

23. Luo, Z.-X., Yuan, C.-X., Meng, Q.-J., and Ji, Q. (2011). A Jurassic eutherian mammal and divergence of marsupials and placentals. Nature *476*, 442–445.

24. Luo, Z.-X. (2007). Transformation and diversification in early mammal evolution. Nature *450*, 1011–1019.

25. Wilson, G.P., Evans, A.R., Corfe, I.J., Smits, P.D., Fortelius, M., and Jernvall, J. (2012). Adaptive radiation of multituberculate mammals before the extinction of dinosaurs. Nature *483*, 457–460.

26. Grossnickle, D.M., Smith, S.M., Wilson, G.P. (2019). Untangling the multiple ecological radiations of early mammals. Trends Ecol. Evol. *34*, 936–949.

27. Köhler, M., and Moyá-Solá, S. (2009). Physiological and life history strategies of a fossil large mammal in a resource-limited environment. Proc. Natl. Acad. Sci. U.S.A. *106*, 20354–20358.

28. Huttenlocker, A.K., Woodward, H., and Hall, B.K. (2013). The biology of bone. In Bone Histology of Fossil Tetrapods: Advancing Methods, Analysis, and Interpretation, K. Padian, E.-T. Lamm, eds. (University of California Press), pp. 13–34.

29. Amson, E., Kolb, C., Scheyer, T.M., and Sánchez-Villagra, M.R. (2015). Growth and life history of Middle Miocene deer (Mammalia, Cervidae) based on bone histology. C. R. Palevol *14*, 637–645.

30. Kolb, C., Scheyer, T.M., Lister, A.M., Azorit, C., de Vos, J., Schlingemann, M.A.J., Rössner, G.E., Monaghan, N.T., and Sánchez-Villagra, M.R. (2015). Growth in fossil and

extant deer and implications for body size and life history evolution. BMC Evol. Biol. *15*, 1–15.

31. Calderón, T., DeMiguel, D., Arnold, W., Stalder, G., and Köhler, M. (2019). Calibration of life history traits with epiphyseal closure, dental eruption and bone histology in captive and wild red deer. J. Anat. *235*, 205–216.
32. Castanet, J., Curry Rogers, K., Cubo, J., and Boisard, J.-J. (2000). Periosteal bone growth rates in extant ratites (ostriche and emu). Implications for assessing growth in dinosaurs. C. R. Acad. Sci. III *323*, 543–550.
33. de Margerie, E., Robin, J.-P., Verrier, D., Cubo, J., Groscolas, R., and Castanet, J. (2004). Assessing a relationship between bone microstructure and growth rate: A fluorescent labelling study in the king penguin chick (*Aptenodytes patagonicus*). J. Exp. Biol. *207*, 869–879.
34. Cambra-Moo, O., Nacarino-Meneses, C., Díaz-Güemes, I., Enciso, S., García Gil, O., Llorente Rodríguez, L., Rodríguez Barbero, M.A., de Aza, A.H., and González Martín, A. (2015). Multidisciplinary characterization of the long-bone cortex growth patterns through sheep's ontogeny. J. Struct. Biol. *191*, 1–9.
35. Jordana, X., Marín-Moratalla, N., Moncunill-Solé, B., Nacarino-Meneses, C., and Köhler, M. (2016). Ontogenetic changes in the histological features of zonal bone tissues in ruminants: a quantitative approach. C. R. Palevol *15*, 255–266.
36. Enlow, D.H., and Brown, S.O. (1958). A comparative histological study of fossil and recent bone tissues. Part III. Tex. J. Sci. *10*, 187–230.

37. Hurum, J.H., and Chinsamy-Turan, A. (2012). The radiation, bone histology, and biology of early mammals. In Forerunners of Mammals: Radiation, Histology, Biology, A. Chinsamy-Turan, ed. (Indiana University Press), pp. 249–270.

38. Werning, S.A. (2013). Evolution of bone histological characters in amniotes, and the implications for the evolution of growth and metabolism. University of California, Berkeley, CA.

39. Kolb, C., Scheyer, T.M., Veitschegger, K., Forasiepi, A.M., Amson, E., Van der Greer, A.A.E., Van den Hoek Ostende, L.W., Hayashi, S., and Sánchez-Villagra, M.R. (2015). Mammalian bone palaeohistology: a survey and new data with emphasis on island forms. PeerJ *3*, e1358.

40. Köhler, M., Marín-Moratalla, N., Jordana, X., and Aanes, R. (2012). Seasonal bone growth and physiology in endotherms shed light on dinosaur physiology. Nature *487*, 358–361.

41. Nacarino-Meneses, C., and Köhler, M. (2018). Limb bone histology records birth in mammals. PLoS One *13*, e0198511.

42. Chinsamy, A., and Warburton, N.M. (2021). Ontogenetic growth and the development of a unique fibrocartilage entheses in *Macropus fuliginosus*. Zoology *144*, 125860.

43. Montoya-Sanhueza, G., Bennett, N.C., Oosthuizen, M.K., Dengler-Crish, C.M., and Chinsamy, A. (2021). Bone remodeling in the longest living rodent, the naked mole rat: interelement variation and the effects of reproduction. J. Anat., 10.1111/joa.13404.

44. Kielan-Jaworowska, Z., Cifelli, R. L., and Luo, Z.-X. (2004). Mammals from the Age of Dinosaurs: Origins, Evolution, and Structure (Columbia University Press).

45. Luo, Z.-X., Kielan-Jaworowska, Z., and Cifelli, R. L. (2002). In quest for a phylogeny of Mesozoic mammals. Acta Palaeontol. Pol. *47*, 1–78.

46. Kielan-Jaworowska, Z. (1979). Pelvic structure and nature of reproduction in Multituberculata. Nature *277*, 402–403.

47. Krause, D.W., and Jenkins, F.A., Jr. (1983). The postcranial skeleton of North American multituberculates. Bull. Mus. Comp. Zool. *150*, 199–246.

48. Kielan-Jaworowska, Z., and Gambaryan, P.P. (1994). Postcranial anatomy and habits of Asian multituberculate mammals. Foss. Strat. *36*, 1–92.

49. DeBey, L.B., and Wilson, G.P. (2014). Mammalian femora across the Cretaceous–Paleogene boundary in eastern Montana. Cretac. Res. *51*, 361–385.

50. Weaver, L.N., Varricchio, D.J., Sargis, E.J., Chen, M., Freimuth, W.J., and Wilson Mantilla, G.P. (2021). Early mammalian social behaviour revealed by multituberculates from a dinosaur nesting site. Nat. Ecol. Evol. *5*, 32–37.

51. Weil, A., and Krause, D.W. (2008). Multituberculata. In Evolution of Tertiary Mammals of North America. Vol. 2, C.M. Janis, G.F. Gunnell, M.D. Uhen, eds. (Cambridge University Press), pp. 19–38.

52. Chen, M., and Wilson, G.P. (2015). A multivariate approach to infer locomotor modes in Mesozoic mammals. Paleobiology *41*, 280–312.

53. Weaver, L.N., and Wilson, G.P. (2020). Shape disparity in the blade-like premolars of multituberculate mammals: functional constraints and the evolution of herbivory. J. Mammal., 10.1093/jmammal/gyaa029.

54. Chinsamy, A., and Hurum, J.H. (2006). Bone microstructure and growth patterns of early mammals. Acta Palaeontol. Pol. *51*, 325–338.

55. Clemens, W.A. (2002). Evolution of the mammalian fauna across the Cretaceous-Tertiary boundary in northeastern Montana and other areas of the Western Interior. In The Hell Creek Formation and the Cretaceous-Tertiary Boundary in the Northern Great Plains: An Integrated Continental Record of the End Cretaceous, J.H. Hartman, K.R. Johnson, D.J. Nichols, eds. (Geological Society of America, Special Paper 361), pp. 217–245.
56. Sprain, C.J., Renne, P.R., Wilson, G.P., Clemens, W.A. (2015). High-resolution chronostratigraphy of the terrestrial Cretaceous-Paleogene transition and recovery interval in the Hell Creek region, Montana. Geol. Soc. Am. Bull. *127*, 393–409.
57. Enlow, D.H. (1963). Principles of Bone Remodeling: An Account of Post-Natal Growth and Remodeling Processes in Long Bones and the Mandible (Charles C. Thomas, Publisher).
58. Bach-Gansmo, F.L., Weaver, J.C., Hartmann Jensen, M., Leemreize, H., Mader, K.S., Stampanoni, M., Brüel, A., Thomsen, J.S., and Birkedal, H. (2015). Osteocyte lacunar properties in rat cortical bone: differences between lamellar and central bone. J. Struct. Biol. *191*, 59–67.
59. Bortel, E.L., Duda, G.N., Mundlos, S., Willie, B.M., Fratzl, P., and Zaslansky, P. (2015). Long bone maturation is driven by pore closing: a quantitative tomography investigation of structural formation in young C57BL/6 mice. Acta Biomater. *22*, 92–102.
60. Read, A.F., and Harvey, P.H. (1989). Life history differences among the eutherian radiations. J. Zool., Lond. *219*, 329–353.
61. Promislow, D.E.L., and Harvey, P. H. (1990). Living fast and dying young: a comparative analysis of life-history variation among mammals. J. Zool., Lond. *220*, 417–437.

62. Barclay, R.M.R., and Harder, L.M. (2003). Life history of bats: life in the slow lane. In Bat Ecology, T.H. Kunz, M.B. Fenton, eds. (University of Chicago Press).

63. Jones, J.H. (2011). Primates and the evolution of long, slow life histories. Curr. Biol. *21*, R708–R717.

64. Hopson, J.A. (1973). Endothermy, small size, and the origin of mammalian reproduction. Am. Nat. *107*, 446–452.

65. Smith, K.K. (2001). The evolution of mammalian development. Bull. Mus. Comp. Zool. *156*, 119–135.

66. Weisbecker, V. (2011). Monotreme ossification sequences and the riddle of mammalian skeletal development. Evolution *65*, 1323–1335.

67. Case, T. J. (1978). Endothermy and parental care in the terrestrial vertebrates. Am. Nat. *112*, 861–874.

68. Farmer, C.G. Parental care, destabilizing selection, and the evolution of tetrapod endothermy. Physiology *35*, 160–176.

69. Hoffman, E.A., and Rowe, T.B. (2018). Jurassic stem-mammal perinates and the origin of mammalian reproduction and growth. Nature *561*, 104–108.

70. Sears, K.E. (2009). Differences in the timing of prechondrogenic limb development in mammals: The marsupial-placental dichotomy resolved. Evolution *63*, 2193–2200.

71. Luo, Z.-X., Cifelli, R.L., and Kielan-Jaworowska, Z. (2001). Dual origin of tribosphenic mammals. Nature *409*, 53–57.

72. Davis, B.M. (2011). Evolution of the tribosphenic molar pattern in early mammals, with comments on the “dual-origin” hypothesis. J. Mammal. Evol. *18*, 227–244.

73. Meng, J., Bi, S., Zheng, X., and Wang, X. (2018). Ear ossicles morphology of the Jurassic euharamiyidan *Arboroharamiya* and the evolution of mammalian middle ear. J. Morphol. *279*, 441–457.

74. Luo, Z.-X., and Manley, G.A. (2020). Origins and early evolution of mammalian ears and hearing function. In The Sense: A Comprehensive Reference, Vol. 2, B. Fritzsch, B. Grothe, eds. (Elsevier Academic Press), pp. 207–252.

75. Zheng, X., Bi, S., Wang, X., and Meng, J. (2013). A new arboreal haramiyid shows the diversity of crown mammals in the Jurassic period. Nature *500*, 199–202.

76. Wible, J.R., Rougier, G.W., Novacek, M.J., Asher, R.J. (2007). Cretaceous eutherians and Laurasian origin for placental mammals near the K/T boundary. Nature *447*, 1003–1006.

77. Wilson Mantilla, G.P., et al. (2021). Earliest Palaeocene purgatoriids and the initial radiation of stem primates. R. Soc. Open Sci. *8*, 210050.

78. King, B., and Beck, R.M.D. (2020). Tip dating supports novel resolutions of controversial relationships among early mammals. Proc. R. Soc. B *287*, 20200943.

79. Wilson, G.P. (2005). Mammalian faunal dynamics during the last 1.8 million years of the Cretaceous in Garfield County, Montana. J. Mammal. Evol. *12*, 53–76.

80. Wilson, G.P. (2014). Mammalian extinction, survival, and recovery dynamics across the Cretaceous-Paleogene boundary in northeastern Montana, USA. In Through the End of the Cretaceous in the Type Locality of the Hell Creek Formation in Montana and Adjacent Areas, G.P. Wilson, W.A. Clemens, J.R. Horner, J.H. Hartman, eds. (Geological Society of America, Special Paper 503), pp. 365–392.

81. Alroy, J. (1999). The fossil record of North American mammals: evidence for a Paleocene evolutionary radiation. Syst. Biol. *48*, 107–118.

82. Wilson, G.P. (2013). Mammals across the K/Pg boundary in northeastern Montana, U.S.A.: dental morphology and body-size patterns reveal extinction selectivity and immigrant-fueled ecospace filling. Paleobiology *39*, 429–469.

83. Clemens, W.A. (1964). Fossil mammals of the type Lance Formation, Wyoming, Part I. Introduction and Multituberculata. Univ. Calif. Publ. Geol. Sci. *48*, 1–105.

84. Smith, S.M., Sprain, C.J., Clemens, W.A., Lofgren, D.L., Renne, P.R., and Wilson, G.P. (2018). Early mammalian recovery after the end-Cretaceous mass extinction: a high-resolution view from McGuire Creek area, Montana, USA. Geol. Soc. Am. Bull. *130*, 2000–2014.

85. Krause, D.W. (1986). Competitive exclusion and taxonomic displacement in the fossil record: the case of rodents and multituberculates in North America. In Vertebrates, Phylogeny, and Philosophy, K.M. Flanagan, J.A. Lillegraven, eds. (Contributions to Geology, University of Wyoming, Special Paper 3), pp. 95–117.

86. Van Valen, L., and Sloan, R.E. (1966). The extinction of the multituberculates. Syst. Zool. *15*, 261–278.

87. Chen, M., Strömberg, C.A.E., Wilson, G.P. (2019). Assembly of modern mammal community structure driven by Late Cretaceous dental evolution, rise of flowering plants, and dinosaur demise. Proc. Natl. Acad. Sci. U.S.A. *116*, 9931–9940.

88. Hopson, J.A. (1967). Comments on the competitive inferiority of the multituberculates. Syst. Zool. *16*, 352–355.

89. Lofgren, D.L. (1995). The Bug Creek problem and the Cretaceous-Tertiary transition at McGuire Creek, Montana. Univ. Calif. Publ. Geol. Sci. *140*, 1–185.

90. Lamm, E.-T. (2013). Preparation and sectioning of specimens. In Bone Histology of Fossil Tetrapods: Advancing Methods, Analysis, and Interpretation, K. Padian, E.-T. Lamm, eds. (University of California Press), pp. 55–160.

91. Rueden, C.T., Schindelin, J., Hiner, M.C., DeZonia, B.E., Walter, A.E., Arena, E.T., and Eliceiri, K.W. (2017). ImageJ2: ImageJ for the next generation of scientific image data. BMC Bioinformatics *18*, 1–26.

92. Jones, K.E., et al. (2009). PanTHERIA: A species-level database of life history, ecology, and geography of extant and recently extinct mammals. Ecology *90*, 2648–2648.

93. Myhrvold, N.P., Baldridge, E., Chan, B., Sivam, D., Freeman, D.L., and Ernest, S.M. (2015). An amniote life history database to perform comparative analyses with birds, mammals, and reptile: Ecological Archives E096–269. Ecology *96*, 3109–3109.

94. Myers, P., Jones, T., Espinosa, R., Dewey, T., Hammond, G. (2020). The Animal Diversity Web. Accessed June 15.

95. R Core Team. (2021) R: A language and environment for statistical computing. *R Foundation for Statistical Computing*.

96. Hastie, T., and Tibshirani, R. (1996). Discriminant analysis by Gaussian mixtures. J. R. Stat. Soc. *58*, 155–176.

97. Kuhn, M. (2020). Caret: Classification and regression training. <https://cran.r-project.org/web/packages/caret/index.html>

98. Leisch, K., Hornik, K., Ripley, B.D., and Narasimhan, B. (2020). MDA: Mixture and flexible discriminant analysis. <https://cran.r-project.org/web/packages/caret/index.html>

99. Perrin, M.R. (1989). Alternative life-history styles of small mammals. In Alternative Life History Styles of Animals, M.N. Brunton, ed. (Kluwer Academic Publishers), pp. 209–242.
100. Orne, D. (2018). The caper package: comparative analysis of phylogenetics and evolution in R. R package version 1.0.1 *5*, 1–36.
101. Upham, N., Esselstyn, J.A., and Jetz, W. (2019). Inferring the mammal tree: species-level sets of phylogenies for questions in ecology, evolution, and conservation. PLoS Biol. *17*, e3000494.
102. Drummond, A.J., Suchard, M.A., Xie, D., Rambaut, A. (2012). Bayesian phylogenetics with BEAUti and the BEAST 1.7, Mol. Biol. Evol. *29*, 1969–1973.

4.9 APPENDIX I: SUPPLEMENTARY INFORMATION TEXT

Institutional Abbreviations

CMC, Cincinnati Museum Center, Cincinnati, OH; ROM, Royal Ontario Museum, Toronto, ON; UCMP, University of California Museum of Paleontology, Berkeley, CA; UWBM, Burke Museum of Natural History and Culture, Seattle, WA.

Histological Descriptions

The following are descriptions of cross sections from the femoral midshaft. Our extant sample included both adults and subadults and, where applicable, we describe both sections for each species in the same paragraph. The extant adult cortices lack trabeculae and consist of a compact cortex and open medullary cavity. The same is true for the majority of the subadult specimens

unless otherwise stated. Osteocyte lacunae in organized tissues (most frequently lamellar, but sometimes grading into parallel-fibered bone) are pinched, elongate, sparse, and well-organized along circumferential lamellae, whereas osteocyte lacunae in disorganized tissues (most frequently woven, but sometimes grading into parallel-fibered bone) are large, globular, and haphazardly arranged. Below, we describe all of the extant thin sections included in this study. For high-resolution images and our interpretive annotations of these thin sections see Figure 4.10.1–8.

Extant Marsupials. *Antechinus stuartii* (Adult, UWBM 68914). In cross section, there is a lack of trabeculae and dense cortical bone with a few radiating vascular canals opening to the endosteal surface. Endosteal deposition and cortical drift is evident on the lateral side, opposite to the medial side that contains abundant Sharpey's fibers. The endosteal lamellar bone layer is separated from the rest of the cortex by a sharp reversal line. Moving periosteally, a band of varying thickness contains plump and large osteocyte lacunae in parallel-to-lamellar-fibered bone. However, the majority of the cortex, including the endosteal band, can be characterized by flattened and organized osteocyte lacunae that form circumferential layers. The bone matrix is parallel-to-lamellar fibered and an external fundamental system (EFS) is visible at the periosteal surface. See Figure 4.10.1.

Didelphis virginiana (Adult, UWBM 35526; Subadult UWBM 34284). Both the subadult and adult exhibit a thick cortex of primarily parallel-to-lamellar-fibered tissue and a narrow medullary cavity. The cortex is densely vascularized with longitudinally-oriented canals towards the endosteal and periosteal surfaces in the subadult and largely radially oriented in the adult. Secondary remodeling and resorption cavities are evident on the medial side of the subadult. In

the subadult, there is a thin layer of endosteal lamellar bone anteromedially, separated from a relatively thick and irregular layer of woven bone superficially by a sharp reversal line. The woven bone layer is thickest medially and posteriorly and contains densely packed primary osteons. In the adult, the woven bone layer is much thinner and primary located just superficial to a thin endosteal lamellar bone layer at the anterior and lateral portions of the cortex. Also in the adult, presumably subsequent periosteal deposition is less vascularized and has radial osteons. The bone matrix is parallel-to-lamellar fibered and the osteocyte lacunae are well-organized and lenticular. See Figure 4.10.1.

Dromiciops gliroides (Adult, UWBM 78641; Subadult, UWBM 78631). The subadult cortex is thin, largely avascular, primarily made up of parallel-to-lamellar-fibered bone matrix; however, there is a thin strut of woven bone that extends from the lateral portion of the endosteal margin into the mid-cortex posteriorly. Two large resorption voids are present in this woven layer. The adult cross-section has a larger diameter and relatively narrow cortex compared to the medullary cavity. Osteocyte lacunae are much more circumferentially flattened and become sparse in the periosteal lamellar tissue. An EFS is present in the adult. See Figure 4.10.1.

Perameles nasuta (Subadult, UWBM 68919). The cortex is generally composed of vascularized tissue with a variety of orientations found in a range of matrix organizations. At the posterolateral portion of the cortex, a thin layer of woven tissue is present adjacent to the medullary cavity. The mid-cortex is composed of simple, radially oriented canals in parallel-to-lamellar-fibered bone. The remainder of the outer cortex is composed of lamellar tissue that steadily decreases in vascularity although some radially oriented canals occupy that portion of the cortex. The endosteal woven layer found at the posterolateral side pinches out towards the lateral and medial sides. Throughout the cortex, the periosteal-most tissue is separated by a line

of arrested growth (LAG) and is generally avascular. Additional LAGs are apparent, especially towards the posterolateral side and are reminiscent of an EFS. See Figure 4.10.1.

Petaurus breviceps (Adult, UWBM 68906; Subadult, UWBM 68904). The subadult cortex is thin and generally composed of vascular parallel-to-lamellar-fibered bone, save for the endosteal surface on the posterior and medial side that contains only a few radially oriented canals in woven matrix. Here, the endosteal tissue has a scalloped surface that is nearly continuous along the open medullary cavity, except for the posteromedial side where there is thin layer of endosteal lamellar tissue. The periosteal-most surface is composed of a very narrow band of lamellar tissue. The adult cortex is much more robust and generally homogenous although there are slight differences in the endosteal and periosteal portions of the cortex. More endosteally-positioned tissue is composed of parallel-to-lamellar-fibered bone with plump osteocyte lacunae. Some radial canals are present on the posterolateral surface in woven matrix. Here, the endosteal edge has been eroded by a large resorption cavity that is partially lined by lamellar tissue. The more peripheral tissue in the cortex is composed of lamellar bone with abundant, well-organized osteocyte lacunae. See Figure 4.10.1.

Pseudocheirus peregrinus (Adult, UWBM VP 120076; Subadult, UWBM 68925). The subadult cortex is robust and primarily composed of well-vascularized fibrolamellar tissue. Longitudinally-oriented canals with some osteonal deposition are organized in layers within a woven matrix. A single secondary osteon is present on the posterior portion of the cortex as well as Sharpey's fibers indicative of a site of muscle attachment. Here, the endosteal cortex is lined with a region of lamellar tissue that is thicker than the remainder of the endosteal surface which is narrowly lined with endosteally-deposited lamellar tissue. The periosteal surface also deviates from the primary fibrolamellar organization with more radially-oriented canals that are open to

the periosteal surface, creating a scalloped edge in and parallel-to-lamellar-fibered tissue with scarce osteocyte lacunae. Radially oriented simple canals in parallel-to-lamellar-fibered bone constitute the majority of the adult cortex although some woven tissue is apparent on the lateral and posterior sides of the adult cortex. The periosteal surface of the adult specimen contains an EFS. See Figure 4.10.2.

Thylamys elegans (Adult, UWBM 49000; Subadult, UWBM 49026). The subadult cortex is primarily composed of avascular lamellar-to-parallel-fibered bone that generally contains plump and organized osteocyte lacunae. More of the posteromedial side of the outer cortex is made up of lamellar bone whereas the anterior side is predominantly composed of parallel-fibered tissue. Posteromedially there is a thin band of endosteal lamellar bone that is separated from a layer of woven bone superficially by a sharp reversal line. The adult cortex is slightly more robust especially towards the anteromedial side where the matrix is primarily organized in parallel fibers rather than the lamellar organization of the rest of the cortex. No EFS is present in the adult specimen, although the generally composition of the cortex is lamellar avascular tissue. See Figure 4.10.2.

Extant Placentals. *Arborimus longicaudus* (Adult, UWBM 34486; Newborn, UWBM 78043). A poorly ossified newborn section contains loosely organized trabeculae and calcified cartilage. A very thin cortex consists of disorganized and haphazardly arranged osteocyte lacunae. In the adult section, the cortex is composed of dense, low vascularized cortical bone with no trabeculae evident in the medullary cavity. Generally, the cortex is composed of flattened, well-organized osteocytes in lamellar bone matrix, particularly on the lateral side. However, a band of fibrolamellar, vascularized tissue is evident in the adult section in the anteromedial and

posterolateral regions. This band runs asymmetrically and incompletely around both cross-sections and is reduced to small wedges of vascularized bone in the adult, sandwiched between endosteal and periosteal avascular bone. In the adult, there are multiple, smaller LAGs stacked at the periosteum, akin to an EFS. See Figure 4.10.2.

Cebuella pygmaea (Adult, UWBM 39005). The cortex is relatively narrow with an open medullary cavity. The cortex is comprised of parallel-to-lamellar-fibered bone tissue and contains many severely flattened osteocyte lacunae. A thin margin of lamellar bone lines the medial surface of the medullary cavity. The cortex and avascular and no definitive EFS is apparent. See Figure 4.10.2.

Dendrohyrax arboreus (Adult, UWBM 39083). The endosteal surface is lined with a thin margin of lamellar tissue and occasional radial vascular canals that extend towards fibrolamellar tissue that makes up the deep cortex. Some secondary remodeling is evident on the medial side of this tissue layer that is largely composed of longitudinally oriented vascular canals. This fibrolamellar layer is bordered by a sharp reversal line superficially that separates it from parallel-to-lamellar-fibered tissue with occasional simple, longitudinally-oriented canals. This layer also contains organized and flatted osteocyte lacunae. Finally, two LAGs are evident on the lateral and medial periosteal surfaces. See Figure 4.10.2.

Dipodomys merriami (Adult, UWBM 12576). A thick, avascular cortex is made of primarily parallel-to-lamellar-fibered bone with flattened osteocyte lacunae organized circumferentially. The cortex thickens laterally where remnants of disorganized compact coarse cancellous bone (CCCB) remain sandwiched between endosteal and periosteal layers of bone matrix. More peripherally, a narrow band of disorganized woven bone can be found on the anteromedial side of the thin section. The osteocyte lacunae in this band are occasionally

plumper than those found in the rest of the cortex, however, for the most part, they are similarly sized. This thin-section lacks an EFS or mid-cortical LAGs. See Figure 4.10.3.

Elephantulus rufescens (Adult, UWBM 35466; Subadult, UWBM 34170). The subadult cortex largely consists of well-vascularized, disorganized, fibrolamellar bone sandwiched between thin layers of endosteal and periosteal parallel-fibered to lamellar tissue. Osteocyte lacunae are plump and disorganized in the vascularized regions and well-organized and flattened in avascular regions. In the adult, a band of disorganized vascularized tissue is present along the anterolateral and anteromedial sides and is similarly sandwiched between avascular parallel-to-lamellar-fibered tissue endosteally and periosteally. Along the posterior side of the cross-section, avascular lamellar bone makes up the entire cortex and pinches out on the medial and lateral sides, making the lamellar tissue discontinuous around the cross section. Simple radial canals are present in this section of otherwise avascular tissue. No EFS is present. See Figure 4.10.3.

Galago senegalensis (Adult, UWBM 35394). The cortex is composed of thin cortical walls of variable thickness and tissue types. A layer of disorganized, vascular tissue is continuous around the medullary cavity and is separated by a sharp reversal line from periosteal tissue that varies in thickness. In the anterior and posterior regions, more of the cortex is made up of periosteal parallel-to-lamellar-fibered tissue, whereas the medial region is largely composed of disorganized tissue with a thin layer of periosteal lamellar tissue. Along the endosteal margin, there is evidence of scalloping of the disorganized layer suggesting active resorption. Interestingly, there are distinctions between the posterior and anterior sides of the periosteal tissue. The posterior region contains occasional longitudinally-oriented canals in a parallel-fibered matrix. By contrast, the anterior region is composed of avascular parallel-to-lamellar-fibered matrix with at least one distinct LAG. See Figure 4.10.3.

Lepus americanus (Adult, UWBM 33264; Subadult, UWBM 16859). The cortex is thicker in the subadult than in the adult. Both cortices are composed primarily of plexiform primary bone tissue in woven-to-parallel-fibered matrix. In the adult, a thin margin of endosteal and periosteal, largely avascular, lamellar bone is present along the open medullary cavity and superficial-most cortex, respectively. Scarce radial canals extend from the open medullary cavity to the primary plexiform tissue. See Figure 4.10.3.

Microtus oregoni (Adult, UWBM VP 120069; Subadult, UWBM 69372). The cortex of the subadult is composed of two major bands of tissue, a thick endosteal region of avascular lamellar tissue, and a thin band of woven bone with very scarce primary osteons. The endosteal lamellar bone has organized and lenticular osteocyte lacunae. More peripherally, the woven bone has surprisingly organized osteocyte lacunae. Along the posterolateral region, a very thin band of lamellar bone lines the sub-periosteal surface. In the adult, the cortex has varying bands of tissues that have been reworked such that they do not form a complete circle around the entire cortex. These layers are largely composed of lamellar, avascular bone with organized and flatted osteocyte lacunae. The lateral to posterior portion of the section, however, has a narrow band consisting of disorganized woven bone with no vasculature. See Figure 4.10.3.

Microtus pennsylvanicus (Adult, UWBM 73937; Subadult UWBM 78145). In the subadult, the cortex consists of two tissue types, a band of disorganized vascular tissue that spans the majority of the mid-to outer cortex, a relatively thin band of endosteal, avascular lamellar tissue. There is also a thin band of periosteal lamellar tissue at the anteromedial portion of the cortex. In the adult, the disorganized band borders the medullary cavity laterally and forms the mid-cortex medially. Deep to this disorganized band is a thin layer of endosteal lamellar bone anteromedially to posteromedially. The remainder of the cortex is composed of periosteal

lamellar bone. Scarce, simple radial vascular canals extend from the open medullary cavity into the deeper cortex. The outer cortex is completely avascular. See Figure 4.10.4.

Mustela nivalis (Adult, UWBM 83059). The thick cortex is endosteally lined with multiple layers of lamellar avascular tissue with organized and flattened osteocyte lacunae. Towards the periosteal surface on the posterolateral side, the tissue grades from lamellar to the fibrolamellar complex with longitudinally-oriented canals and plump, disorganized osteocyte lacunae. No EFS is present at the periosteal surface of the adult. See Figure 4.10.4.

Myodes gapperi (Adult, UWBM VP 120070; Subadult, UWBM 55755). Thin cortical walls are composed of a chimera of tissue bands that do not run continuously around the cortex. At the anteromedial portion of the cortex, bone tissue is arranged in a parallel-fibered matrix with abundant radially-oriented vasculature. Layers of lamellar tissue line the anterolateral and posteromedial portions of this vascularized tissue. Remnants of woven bone is evident in both a narrow band on the posterior portion of the cortex with plump, disorganized osteocyte lacunae, and in a fibrolamellar complex with a single row of longitudinally oriented canals on the lateral portion of the cortex. See Figure 4.10.4.

Myotis californicus (Adult, UWBM 67064; Subadult, UWBM 82534). The subadult and adult cortex are remarkably uniform and avascular. The bone matrix is lamellar endosteally, and transitions to parallel-to-lamellar-fibered bone more peripherally. Osteocyte lacunae are sparse within the cortex and are flattened and well organized. There is no evidence of an EFS. See Figure 4.10.4.

Neovison vison (Adult, UWBM 82362-4; Subadult, UWBM 79566). The subadult has a thin cortex composed of disorganized tissue that is highly vascularized. In the deep cortex, large trabecular spaces grade into reticular vascular canals that are open to the periosteal edge

posterolaterally. Large vascular canals sit in a woven matrix that is densely packed with plump osteocyte lacunae. In the adult, a similar degree of disorganized tissue persists as a band in the middle cortex, sandwiched between two regions of organized bone endosteally and periosteally. Interestingly, the disorganized tissue extends to the periphery on the posteromedial side of the cross-section. The endosteal organized tissue is less organized than the periosteal tissue. It is a myriad of tissue types ranging from a thin band of lamellar tissue that lines the medullary cavity, to a convoluted mix of parallel-fibered bone with radial canals that occasionally merge with a band of longitudinal canals in woven bone matrix along the posterior side. This mixture of tissue grades into the disorganized tissue mentioned above, and is not separated by a reversal line. However, periosteally deposited tissue is separated from the disorganized vascular tissue by a sharp reversal line. On the medial side, tissue shifts from fibrolamellar tissue with small longitudinal canals to avascular lamellar tissue, following the reversal line. In other regions of the cortex, the periosteal tissue is completely avascular and made up of lamellar bone matrix, similar to an EFS. See Figure 4.10.5.

Neurotrichus gibbsii (Adult, UWBM 67585; Subadult, UWBM 64764). The subadult cortex is composed of a narrow band of avascular tissue. The endosteal half of the cortex is composed of organized lamellar tissue with flattened osteocyte lacunae. The more periosteally dominated tissue is composed of more disorganized tissue with plumper osteocyte lacunae. In the adult, a narrow cortex is composed of a small portion of endosteally deposited lamellar tissue that contain flattened and organized osteocyte lacunae. This endosteal tissue is distinct from a layer of more periosteally positioned disorganized bone in woven to parallel-fibered matrix. Within this tissue layer, rare but large longitudinally oriented osteons are present. There is a very

thin margin of lamellar tissue along the anterior and lateral sides of the outermost periosteal surface. See Figure 4.10.5.

Ochotona princeps (Adult, UWBM 60067). The cortex is robust and consists of two tissue layers that compose the anterior and posterior portions of the cortex. Although the endosteal surface of the posterior portion of the cortex is lined with lamellar tissue, the posterior tissue layer mostly consists of woven matrix with longitudinally orient canals that frequently anastomose. Towards the posteromedial and posterolateral portions of the cortex, this layer pinches out and the cortex becomes largely composed of parallel-to-lamellar-fibered bone with radially oriented vascular canals. See Figure 4.10.5.

Peromyscus maniculatus (Adult, UWBM 30367). The adult cortex is largely made up of disorganized vascularized tissue in a woven matrix. Lamellar tissue that is largely acellular, makes up the endosteal and periosteal margins, sandwiching the disorganized vascular tissue. See Figure 4.10.5.

Pteropus poliocephalus (Adult, UWBM 35471). The cortex is robust and composed of multiple tissue types that form nearly continuous bands of either vascularized or avascular tissue. The endosteally positioned tissue is composed of disorganized tissue with large irregularly shaped vascular canals in woven bone matrix on the anterolateral side, whereas the posteromedial side is composed of parallel-to-lamellar-fibered tissue with small, longitudinal canals. A reversal line separates this vascularized tissue from more peripheral, avascular tissue composed of parallel-fibered tissue that grades into lamellar tissue most peripherally. Osteocytes are small and organized circumferentially in this organized tissue. No EFS is present. See Figure 4.10.5.

Scapanus townsendii (Adult, UWBM VP 120075; Subadult, UWBM 33304). The inner cortex of the subadult cortex consists of loose trabecular bone. This tissue quickly grades into regions of woven, disorganized matrix surrounding large, longitudinal vascular canals along the posterior and medial margins, or lamellar tissue along the lateral margin, and later grades to disorganized bone tissue more peripherally. The majority of the tissue architecture looks like unfilled cancellous bone. In the adult, vascular canals are surrounded by disorganized matrix around the periphery of the cross section, indicative of fine- to coarse-cancellous bone. This tissue type isn't continuous around the cross section and appears the most patchily on the posterior side. The remainder of the cortex is composed of lamellar tissue with well-organized osteocyte lacunae. See Figure 4.10.6.

Sciurus griseus (Adult, UWBM 83018; Subadult, UWBM 76268). Both the subadult and adult cortices are composed of a region of disorganized vascularized bone and organized tissue that sits periosteally and endosteally to it. The subadult endosteal tissue is lamellar and completely surrounds the open medullary cavity, becoming exceedingly thin along the anteromedial side. The middle cortex is made up of disorganized woven bone with primary osteons. This woven tissue is thickest along the medial region and thinnest along the lateral region, where it narrowly sits along the outermost periosteal edge. A thin band of periosteal lamellar tissue surrounds the entire bone circumference except in the lateral region where woven, disorganized tissue persists. In the adult, the woven, disorganized, vascularized tissue sits in the deep-middle cortex, whereas the outer cortex is composed of avascular, organized tissue in parallel-to-lamellar-fibered matrix. See Figure 4.10.6.

Sorex monticolus (Adult, UWBM VP 120074; Subadult, UWBM 58432). Both the subadult and adult have extremely thin cortices that are completely avascular and include woven,

parallel-fibered, and lamellar bone matrix. In the subadult, the endosteal region is composed of lamellar matrix with concentrically organized osteocyte lacunae. Peripherally, lamellar bone grades into a composite of woven-to-parallel-fibered bone. In the adult, more of the cortex is composed of lamellar matrix with flattened, circumferentially organized osteocyte lacunae, but in the mid cortex there is a layer of parallel-fibered bone that grades to woven bone medially. The superficial-most cortex is composed of avascular lamellar bone. See Figure 4.10.6.

Sorex palustris (Adult, UWBM 80433). The adult cortex is robust and consists of a thick margin of endosteal lamellar tissue that makes up at least half of the cortical thickness. More periosteally, parallel-fibered bone makes up the cortex, except on the posterior side where plump and disorganized osteocytes lacunae sit in woven bone matrix. Posterolaterally, the superficial-most portion of the cortex is composed of avascular lamellar bone. See Figure 4.10.6.

Suricata suricatta (Adult, UWBM 35469). An uneven yet thick cortex consists of a myriad of tissue types that largely grade from endosteal lamellar trabeculae along the lateral margin of the medullary cavity, to a thick region of disorganized, vascular tissue with abundant primary osteons laterally and posteromedially. Peripherally, this disorganized layer is separated by a sharp reversal line and followed by lamellar matrix with lower vascularity consisting of simple canals and scarce primary osteons. An EFS can be traced along the outermost circumference of the cortex in all but the posterior region where a rugose muscle scar is present. See Figure 4.10.7.

Tamias amoenus (Adult, UWBM VP 120071; Subadult, UWBM 74048). The inner cortex the subadult cross-section consists of a thick and continuous band of lamellar tissue with small, well-organized osteocyte lacunae. The middle cortex has remnant islands of compact coarse cancellous bone (CCCB) along the posterolateral and anteromedial regions, in an

otherwise woven-to-parallel-fibered cortex. Within the CCCB, there are simple longitudinal canals and primary osteons. Osteocyte density is fairly high. In the adult, avascular lamellar tissue makes up the majority of the cortex, particularly in the endosteal region. A thin and discontinuous band of woven, vascularized tissue is present along the anteromedial, anterior, lateral, and posterolateral margins. Most peripherally, there is a very thin layer of lamellar periosteal tissue. See Figure 4.10.7.

Tamiasciurus douglasii (Adult, UWBM 83017; Subadult, UWBM 81943). The inner cortex of the subadult consists of lamellar tissue that surrounds an empty medullary cavity. Large primary osteons sit within a woven matrix in all but the posterior region of the middle cortex. Vascular canals are surrounded by dense osteocyte lacunae in a convoluted, whorling, woven matrix. Cortical drift interrupts this disorganized tissue along the anterior region, leaving two islands of disorganized tissue sandwiched between endosteal and periosteal lamellar tissue. The rest of the outer cortex is made up of lamellar tissue with distinctively lower lacunar density than in the woven bone of the middle cortex. In the adult, more of the cortex is made up of periosteal lamellar tissue, however, regions of vascularized, woven tissue are present in the deep-middle cortex, particularly on the lateral and medial sides. The remainder of the cortex is avascular lamellar tissue with organized osteocyte lacunae in circumferential layers. See Figure 4.10.7.

Thomomys talpoides (Adult, UWBM VP 120072; Subadult, UWBM 34613). The subadult has a thin cortex largely consisting of woven bone with disorganized longitudinal canals. From endosteal to periosteal margins, the cortical tissue grades from a thin, continuous band of avascular, lamellar tissue surrounding the medullary cavity, to vascularized disorganized tissue, to a somewhat continuous band of avascular lamellar tissue. The periosteal lamellar tissue is thickest in the anteromedial and posterolateral regions of the cortex, making up the entirety of

the posterior portion, and is absent on the anterolateral and posteromedial sides of the cortex. The variable thickness of both the disorganized vascular tissue and organized periosteal bone tissue indicate cortical remodeling in this subadult individual. In the adult, the cortex is nearly entirely avascular. Small, simple vascular canals sit region of woven bone that varies in thickness in the middle cortex. This woven tissue is sandwiched between a thick region of endosteal, lamellar tissue. More peripherally, parallel-fibered to lamellar tissue composes the outer cortex. See Figure 4.10.8.

Tupaia glis (Adult, UWBM 34266). The cortex is relatively thick and the medullary cavity is open. Endosteal lamellar bone lines the entirety of the medullary cavity, and grades superficially into a band of woven bone packed with primary osteons that spans the circumference of the mid-cortex. This woven layer is separated superficially from a layer of periosteal lamellar bone by a sharp reversal line. The periosteal lamellar bone forms the superficial-most portions of the cortex. See Figure 4.10.8.

Urocitellus columbianus (Adult, UWBM 80405; Subadult, UWBM 39193). The subadult cortex has extremely different tissues on the anterior and posterior sides. The anterior side is thin, compact and made up of a margin of lamellar tissue, followed by a reversal line that separates disorganized vascular tissue more peripherally. On the posterior side, the cortex only consists of a woven bone scaffold that is extremely scalloped on both the endosteal and periosteal surface. Trabecular building is also present on the endosteal surface. This woven, disorganized vascular tissue continues along the medial and lateral sides of the cross-section and becomes more compact and buttressed by woven matrix. The adult cortex is thick and composed of alternating layers of organized avascular and disorganized vascular tissue. Endosteally, the cortex has simple radial canals in a parallel-to-lamellar-fibered matrix. The middle cortex is

made up of disorganized vascular canals in woven matrix. This disorganized tissue continues to the periosteal edge on the anterolateral side. In all other areas of the cortex, a reversal line separates avascular lamellar tissue more peripherally. On the lateral side, another layer of vascularized tissue is present more peripheral to the reversal/lamellar tissue. Finally, the outermost cortex is composed of lamellar tissue that occasionally grades into parallel-fibered bone with simple vascular canals, particularly on the anterior side. See Figure 4.10.7.

Zapus trinotatus (Adult, UWBM VP 120073; Subadult, UWBM 80587). The subadult has a thin cortex with a thin region of simple longitudinal vascular canals sandwiched between endosteal and periosteal organized bone tissue. The endosteal region consists of parallel-fibered to lamellar tissue that is avascular. The vascularized middle cortex is composed of fine-to-coarse compact cancellous bone that is present in all but the anterolateral region. The sub-periosteal surface is made up of lamellar tissue that has well-organized, lenticular osteocyte lacunae. The adult has a similarly thin cortex but more of it is made up of endosteal lamellar bone. Small islands of vascular tissue persist in the middle cortex in areas of woven bone along the anterolateral, anterior, and medial sides. Similar to the subadult specimen, the outermost cortex is made up of lamellar tissue that varies slightly in thickness. An EFS is not present. See Figure 4.10.8.

Multituberculates. The majority of the femoral cross sections from our multituberculate sample were taken near the midshaft (n = 9) or just proximal to the midshaft (n = 7), but two were taken from the proximal femur (a few millimeters distal to the lesser trochanter). For a complete list of where the different thin sections were taken please refer to Table 4.11.2. All of the multituberculate cross sections are mediolaterally broad and anteroposteriorly narrow, exhibit a

thick compact cortex, and lack trabeculae. The osteocyte lacunae in organized tissues (most frequently lamellar, but sometimes grading into parallel-fibered bone) are pinched, elongate, sparse, and well-organized along circumferential lamellae, whereas osteocyte lacunae in disorganized tissues (most frequently woven, but sometimes grading into parallel-fibered bone) are large, globular, and haphazardly arranged. Below, we describe the histology of each femoral cross section individually, and the full sections and our interpretive annotations can be found in Figure 4.10.9–11.

UWBM 105170 (Mu1). This thin section is nearly complete, with only two minor fractures extending through the cortex in the anterolateral and anteromedial regions. There is slight scalloping along the endosteal margin. The deep cortex is composed of avascular lamellar bone that is thickest anteromedially and thinnest anterolaterally. This endosteal lamellar bone layer grades superficially into a band of woven bone, except at the posteromedial portion of the cortex where these endosteal lamellar and woven bone layers are separated by a sharp reversal line. The band of woven bone spans the circumference of the mid-cortex and hosts sparse primary osteons and one large longitudinal vascular canal at the lateral portion of the cortex. The superficial cortex is composed of lamellar bone and is separated from the woven layer by a sharp reversal line deeply. This periosteal lamellar layer hosts one simple longitudinal vascular canal laterally and one large vascular canal (likely the nutrient foramen) posteromedially. See Figure 4.10.9.

UWBM 106225 (Mu2). This thin section is substantially damaged; only the anterior and medial portions of the cortex are preserved. The majority of the cortex is composed of lamellar bone that borders the medullary cavity, but it grades to parallel-fibered bone in some portions of the anterior cortex. This endosteal lamellar bone hosts a few small, simple longitudinal vascular canals at the posterior portion of the cortex and grades into woven bone posteromedially to

anteromedially. The woven bone layer hosts sparse primary osteons and forms the entirety of the superficial cortex medially and posteromedially. A thin layer of periosteal lamellar bone is preserved at the anterior end of the cortex and is separated deeply from both the endosteal lamellar and woven bone layers by a sharp reversal line. The preponderance of woven bone at the periosteal edge of the cortex coupled with the relatively minor amount of periosteal lamellar bone bears some resemblance to the bone histology of some subadult placentals in our extant sample. It is possible that this individual was not fully skeletally mature at the time of death, but the proximal end of the femur was damaged, such that the degree of epiphyseal fusion could not be evaluated. See Figure 4.10.9.

UWBM 105833 (Mu8). This thin section is damaged, missing portions of the outer cortex anteriorly, medially, and laterally; nonetheless, enough of the cortex is preserved to interpolate between these missing sections. A layer of endosteal lamellar bone borders the medullary cavity and is crosscut by a few narrow radial canals that open into the medullary cavity. This endosteal lamellar bone layer grades superficially into a complex amalgamation of both parallel-fibered and woven bone. This parallel-fibered and woven-bone complex makes up the majority of the mid-cortex and is densely packed with primary osteons. Large resorption voids are present laterally and medially and are partially filled with circumferential lamellae. A few radial canals are also present medially. This parallel-fibered and woven-bone complex is separated superficially from a relatively thick layer of periosteal lamellar bone by a sharp reversal line. The periosteal lamellar bone layer hosts sparse, simple longitudinal vascular canals. See Figure 4.10.9.

UWBM 106224 (Mu1). This thin section contains a lot of opaque mineral inclusions, making it quite dark even though it is ground very thin. Further, the specimen is damaged, such

that portions of the posterior and anterior cortex are missing. Nonetheless, the major tissue types that make up the cortex are still discernable. The lateral portion of the endosteal surface is scalloped, suggesting it was in the process of being resorbed, but otherwise the endosteal margin is smooth and regular. The medullary cavity is bordered by a layer of endosteal lamellar bone that is evenly distributed around the deep cortex until pinching out posterolaterally. This endosteal lamellar layer grades superficially into a layer of woven bone that hosts sparse primary osteons. The woven bone layer spans the circumference of the cortex and is primarily located in the mid-cortex, except posterolaterally where it abuts the medullary cavity. This woven bone layer is separated from a relatively thick layer of periosteal lamellar bone superficially by a sharp reversal line. This periosteal lamellar layer hosts a few, small, simple longitudinal vascular canals. See Figure 4.10.9.

UWBM 115275 (Mu6). This thin section is largely undamaged, except for minor cracks medially and laterally; however, opaque mineral inclusions obscure some portions of the cortex. In cross section, this specimen is the most circular of those represented in our multituberculate sample, and is only slightly mediolaterally broad and anteroposteriorly narrow. Endosteal lamellar bone borders the entirety of the medullary cavity and is slightly thicker medially than laterally. This endosteal lamellar layer is crosscut by narrow radial canals anteriorly and posteriorly that open into the medullary cavity. Endosteal lamellar bone grades superficially into a relatively thick layer of woven one that is packed with primary osteons and spans the circumference of the mid-cortex. This woven bone layer is separated from a layer of periosteal lamellar bone superficially by a sharp reversal line. This periosteal lamellar bone layer is very thick laterally but thins considerably medially, and it is largely avascular except for one large longitudinal vascular canal in the posterolateral portion of the cortex. See Figure 4.10.9.

UWBM 115276 (Mu8). This thin section exhibits considerable diagenetic alteration, presumably due to microbial or fungal activity. Nonetheless, nearly the entire cortex is preserved (with a few cracks anteriorly and posteriorly) and the diagenetic alterations only obscure splotches of the cortex; as such, the general tissue types can still be observed with confidence. Endosteal lamellar bone is relatively evenly distributed around the circumference of the medullary cavity and is crosscut by fairly broad radial canals that open into the medullary cavity. This endosteal lamellar bone layer grades superficially into a layer of woven bone that spans the circumference of the mid-cortex and hosts densely packed primary osteons. This woven bone layer is separated from a layer of thick periosteal lamellar bone superficially by a sharp reversal line. This periosteal lamellar bone layer hosts a few sparse, small, simple longitudinal canals and one large void (potentially a nutrient foramen) located at the anteromedial portion of the cortex. See Figure 4.10.9.

UWBM 70535 (Mu1). This thin section is missing the anteromedial portion of the cortex and exhibits some minor damage to the anterior portion of the endosteal margin that occurred during grinding. A relatively thick layer of endosteal lamellar bone borders the medullary cavity and hosts a few small, simple longitudinal vascular canals as well as two fairly large longitudinal canals at the lateral portion of the cortex. This endosteal lamellar layer grades superficially into a fairly thin layer of woven bone that hosts densely packed primary osteons and is located in the mid-cortex. This layer of woven bone is separated from a layer of periosteal lamellar bone superficially by a sharp reversal line. This periosteal lamellar layer hosts a few, small, simple longitudinal vascular canals concentrated at the posterolateral extension of the cortex. The posterolateral protuberance of the cortex also exhibits muscle scarring. See Figure 4.10.10.

UWBM 70536 (Mu1). This thin section is complete and undamaged. The medullary cavity is bordered by a thick layer of endosteal lamellar bone that thins slightly laterally. This endosteal lamellar layer hosts a few, sparse, simple longitudinal canals and grades superficially into a layer of woven bone that spans the circumference of the mid-cortex. This woven bone layer hosts densely packed primary osteons and also gives rise to a few radial canals (concentrated medially and anteromedially) that extend deeply into the endosteal lamellar layer. This woven layer is separated from a layer of periosteal lamellar bone superficially by a sharp reversal line. This periosteal lamellar bone is avascular and is relatively uniform in thickness until expanding at the lateral protuberance of the cortex. See Figure 4.10.10.

UWBM 70974 (Mu1). This thin section is heavily brecciated, is missing the anteromedial portion of the cortex, and exhibits considerable amount of opaque mineral inclusions obscuring portions of the cortex. Nonetheless, the major tissue types that make up the cortex can still be identified. The endosteal margin is relatively smooth and regular except laterally where a large resorption void extends into the cortex. The medullary cavity is bordered by a layer of avascular endosteal lamellar bone that grades superficially into a layer of woven bone in the mid-cortex. This woven bone layer hosts primary osteons, which are sparse through the majority of the layer but more densely packed laterally. The woven layer is separated from a layer of avascular periosteal lamellar bone superficially by a sharp reversal line. This layer of periosteal lamellar bone is relatively uniform in thickness around the circumference of the superficial cortex. See Figure 4.10.10.

CMC VP18507 (Mu1). This thin section is relatively complete except for a small portion of the anterior cortex. Small cracks are present throughout the cortex. The endosteal margin is relatively smooth and regular except at the anterior end where large resorption voids extend into

the cortex. A thick layer of endosteal lamellar bone borders the entirety of the medullary cavity, is thickest posteromedially, and thinnest anterolaterally. This endosteal lamellar layer is avascular but exhibits two large resorption voids anteriorly. Posterolaterally to anteromedially the endosteal lamellar layer grades superficially to a woven bone layer located in the mid-cortex, but posteromedially the endosteal lamellar layer is separated from a layer of periosteal lamellar bone by a sharp reversal line. The woven bone layer hosts a few sparse primary osteons in the lateral portion of the cortex, along with two large resorption voids. The woven bone layer pinches out posteriorly and anteromedially and is separated from the periosteal lamellar layer by a sharp reversal line along the posterolateral to anteromedial portions of the cortex. The periosteal lamellar layer exhibits a few small, simple longitudinal vascular canals, is very thin posteriorly and medially, and is thick anteriorly and laterally. See Figure 4.10.10.

CMC VP18508 (Mu1). This thin section is complete but is substantially diagenetically altered, likely due to microbial or fungal activity. Although the microbial damage obscures most of the osteocyte lacunae and vasculature, the primary tissue types that make up the cortex can still be observed. Endosteal lamellar bone bordered the entirety of the medullary cavity and is relatively uniform in thickness. This endosteal lamellar bone layer grades superficially into a layer of woven bone that spans the entirety of the mid-cortex. Primary osteons can be observed in this woven bone layer medially and laterally. The woven layer is separated from a layer of periosteal lamellar bone superficially by a sharp reversal line. The periosteal lamellar bone is relatively uniform in thickness and spans the entirety of the circumference of the superficial cortex. See Figure 4.10.10.

CMC VP18509 (Mu4). This thin section is missing the anterolateral cortex and portions of the lateral cortex, and also exhibits some damage to the endosteal margin. Despite this

damage, the endosteal margin appears to be smooth and regular anteriorly and medially, but is highly irregular posteriorly and laterally, exhibiting large resorption voids that extend into the cortex. Endosteal lamellar bone borders the majority of the medullary cavity, and it is relatively thick anteriorly to posteriorly but pinches out laterally. This endosteal lamellar layer grades superficially into a layer of woven bone that hosts sparse primary osteons. This woven layer borders the medullary cavity laterally, forms the outermost margin of the cortex anteromedially, but pinches out anterolaterally. The woven bone layer is separated from a layer of periosteal lamellar bone by a sharp reversal line laterally, posteriorly, and medially. This periosteal lamellar layer hosts a few sparse, simple longitudinal vascular canals, pinches out anteromedially, but its anterolateral extent is obscured due to damage. See Figure 4.10.10.

CMC VP18510 (Mu8). This thin section is missing small portions of the posterolateral and medial cortex and portions of the endosteal margin, and it exhibits substantial taphonomic alteration with opaque mineral inclusions and microbial or fungal damage. Nonetheless, the major tissues constituencies of the cortex can still be observed. The endosteal margin, where preserved, is smooth and regular. Avascular, endosteal lamellar bone borders the entirety of the medullary cavity and is thickest posteromedially and thinnest anterolaterally. This endosteal lamellar layer grades superficially into a layer of woven bone that spans the entirety of the mid-cortex. This woven layer is packed with primary osteons and is thickest posteromedially and thinnest anterolaterally. The woven layer is separated from a layer of periosteal lamellar bone superficially by a sharp reversal line. The periosteal lamellar layer is avascular, fairly thick laterally to anteriorly, and thin posteromedially. See Figure 4.10.11.

ROM 78099 (Mu8). This thin section is complete and only exhibits a few minor cracks posteriorly, anteriorly, and medially. There is a moderate amount of taphonomic alteration with

opaque mineral inclusions and some microbial or fungal damage, but not enough to obscure the majority of the histological features. The endosteal margin is smooth and regular. Avascular endosteal lamellar bone borders the entirety of the medullary cavity, is relatively uniform in thickness, and grades superficially into a layer of woven bone that spans the circumference of the mid-cortex. The woven layer is relatively thick, hosts densely packed primary osteons, and extends into the lateral protuberance of the cortex laterally. The woven layer is separated from a layer of periosteal lamellar bone superficially by a sharp reversal line. The periosteal lamellar layer is relatively uniform in thickness, spans the entirety of the superficial cortex, hosts sparse and small simple longitudinal vascular canals and one large circular void (possibly a nutrient foramen) at the anteromedial portion of the cortex. See Figure 4.10.11.

ROM 78100 (Mu8). This thin section is complete with only minor cracks anteriorly and posteriorly. The endosteal margin is smooth and regular. There is a thin rim of avascular endosteal lamellar bone bordering the medullary cavity. This endosteal lamellar layer grades superficially into a layer of mixed woven and parallel-fibered bone. This woven and parallel-fibered bone complex hosts densely packed primary osteons, one large resorption void laterally, and spans the circumference of the mid-cortex. Woven bone is primarily concentrated at the lateral, posterolateral, and medial portions of the cortex, but grades to parallel-fibered bone anteriorly and posteriorly. The mixed woven/parallel-fibered layer is separated from a thick layer of periosteal lamellar bone superficially by a sharp reversal line. The periosteal lamellar layer hosts numerous simple longitudinal canals and one large circular void (possibly a nutrient foramen). See Figure 4.10.11.

ROM 78101 (Mu1). This thin section is missing the anteromedial portion of the cortex and exhibits cracks laterally and posteriorly. The endosteal margin is smooth and regular. A thick

layer of endosteal lamellar bone borders the entirety of the medullary cavity, is thickest posteriorly and medially, and is thinnest laterally. The endosteal lamellar layer hosts a few small simple longitudinal vascular canals and is crosscut by a couple radial canals that open to the medullary cavity laterally. The endosteal lamellar layer grades superficially into a layer of woven bone that spans the circumference of the mid-cortex. This woven layer is very thin anteriorly, posteriorly, and medially, but expands laterally where it hosts a few primary osteons and one large resorption void. The woven layer is separated from a layer of periosteal lamellar bone superficially by a sharp reversal line. The periosteal lamellar layer is relatively thin, avascular, and is thickest at the lateral portion of the cortex. See Figure 4.10.11.

ROM 78102 (Mu1). This thin section exhibits substantial brecciation and dislocation of portions of the cortex laterally. There is also moderate taphonomic alteration, with opaque mineral inclusions and some microbial or fungal damage, but not enough to obscure any of the primary histological features. The endosteal margin is relative smooth and regular but there is some slight scalloping anteriorly and laterally. Avascular endosteal lamellar bone makes up the majority of the cortex and borders the entirety of the medullary cavity. The endosteal lamellar layer grades superficially into a layer of woven bone that hosts densely packed primary osteons. This woven layer is fairly thick anteriorly and anterolaterally where it forms the outermost portion of the cortex, but it thins posteriorly and eventually pinches out. Except where it forms the outermost cortex, this woven layer is separated from a layer of periosteal lamellar bone superficially by a sharp reversal line. The periosteal lamellar layer spans most of the superficial circumference of the cortex but pinches out anterolaterally. See Figure 4.10.11.

ROM 78106 (Mu1). This thin section is complete and undamaged. The endosteal margin is relatively smooth and regular, though there is moderate scalloping anteriorly and posteriorly.

A thick layer of endosteal lamellar bone borders the entirety of the medullary cavity and hosts a few sparse radial canals that open to the medullary cavity. This endosteal lamellar layer grades superficially into a layer of primarily woven bone that spans the circumference of the mid-cortex. Anteriorly and posterolaterally this woven layer hosts a few sparse primary osteons, and it grades into parallel-fibered bone laterally and posteromedially. This woven layer is separated from a layer of periosteal lamellar bone superficially by a sharp reversal line. The periosteal lamellar layer is thin medially but thickens laterally where it hosts a few sparse simple longitudinal canals. See Figure 4.10.11.

Comparative and Discriminant Analyses

The quantitative data collected for these analyses reflect the relative proportions of different histological tissues, with change in one necessarily influencing one or more of the others. They are therefore compositional in nature, which necessitated additional treatment before standard statistical techniques could be applied (1). We conducted isometric log-ratio (ILR) transformation on the three primary cortical tissues, resulting in two new "coordinates" that were used in subsequent analyses. The balance tree for this transformation was {periosteal, {disorganized, endosteal}}, and the new "coordinates" thus correspond approximately to the proportion of cortex which is periosteal deposition, and the proportion of non-periosteal cortical deposition which is endosteal (2, 3). This particular confirmation was judged to be the most biologically meaningful of the (three) potential options. Prior to transformations, values of zero were replaced with small non-zero values (0.001). Transformations were performed in the R statistical environment (v. 4.0.4; ref. 4) using the *compositions* package (5). We also ILR transformed the relative cortical and medullary proportions of each section (resulting in one

transformed variable) prior to incorporating those data into discriminant analyses. In addition to the mixture discriminant analysis (MDA) results discussed in the main text we compared two other methods, linear discriminant analysis (LDA), and random forest (RF), both of which were found to perform marginally worse than MDA (Figure 4.10.12). Average accuracy during cross validation was slightly higher in MDA (MDA = 0.99, LDA = 0.97, RF = 0.96), with more substantial differences observed in average kappa values (MDA = 0.97, LDA = 0.93, RF = 0.91). The latter is consistent with MDA's tendency to perform well at discriminating minority groups when there are significant sample size differences (6), as was the case with our sample. MDA results were also more consistent between cross validation iterations, than either LDA or RF (Figure 4.10.12). Overall, although all three models performed well, MDA performed marginally better in all metrics, for this particular problem.

Two genera of placental mammals (*Myotis* and *Cebuella*) were excluded from our final discriminant analyses (see discussion in main text). We also ran these analyses including these two taxa in the placental class to see how sensitive our results were to their exclusion. Predictably, model performance was worse when including these taxa (Figure 4.10.13). In MDA models, average accuracy dropped from 0.99 (se < 0.01) to 0.88 (se = 0.01) and average kappa values from 0.97 (se = 0.01) to 0.65 (se = 0.03). Performance was worse on average for the marsupial group, likely as a result of models favoring the majority group where there was overlap in morphological space (i.e., as a result of the inclusion of these two genera). Differences between methods, discussed above, persisted with average accuracy and kappa values lower for both LDA (acc = 0.87, K = 0.64) and RF (acc = 0.87, K = 0.6). Although model performance was negatively impacted, group predictions for multituberculates were unchanged, with each strongly supported as belonging to the placental group.

There is debate about what type of transformations are most appropriate when working with compositional data. ILR transformation, although possessing desirable mathematic properties often leads to difficulty in interpreting transformed data in context of the original biological question. This has prompted some authors to advocate alternatives (e.g., ref. 7). The relatively small number of components included here alleviates some of these issues, however we ran our phylogenetic comparative analyses using amalgamated (summed) log-ratios (7), and found that our biological interpretations were unchanged, with the strongest relationship being recovered between the proportion of periosteal deposition and weaning age, and other results near-significant or non-significant (Table 4.11.5).

4.10 APPENDIX II: SUPPLEMENTAL INFORMATION FIGURES

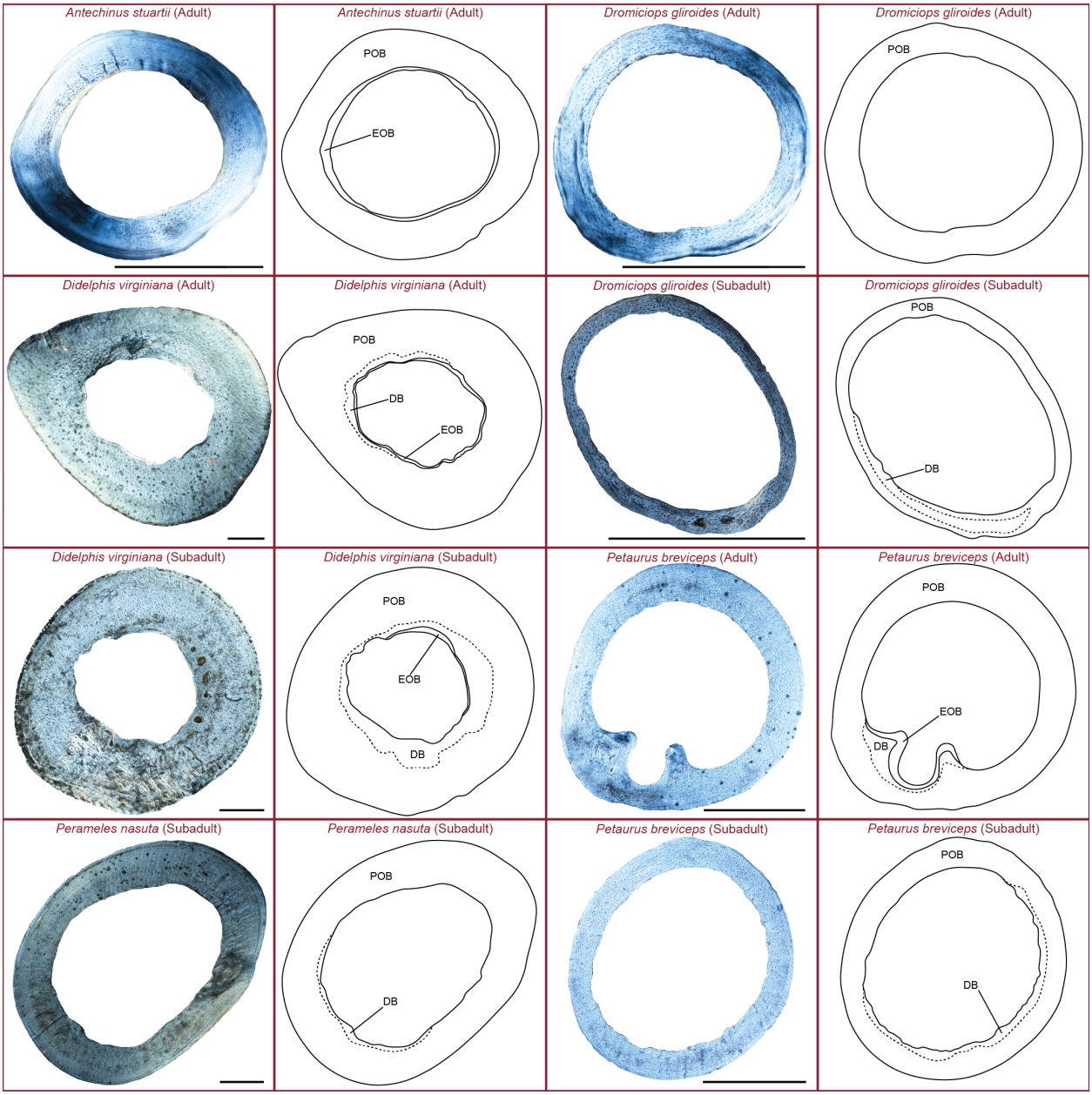

Figure 4.10.1. Full histological cross sections in cross-polarized light and line drawings showing where we classified tissues as endosteal organized bone (EOB), disorganized bone (DB), and periosteal organized bone (POB) for *Antechinus stuartii* (Adult, UWBM 68914), *Didelphis virginiana* (Adult, UWBM 35526 [reflected]; Subadult UWBM 34284), *Dromiciops gliroides* (Adult, UWBM 78641; Subadult, UWBM 78631), *Perameles nasuta* (Subadult, UWBM 68919),

and *Petaurus breviceps* (Adult, UWBM 68906; Subadult, UWBM 68904). Red boxes/text = marsupials, Blue boxes/text = placentals, Gold boxes/text = multituberculates. Anterior = top, lateral = left. Scale bars = 1 mm (unless otherwise stated).

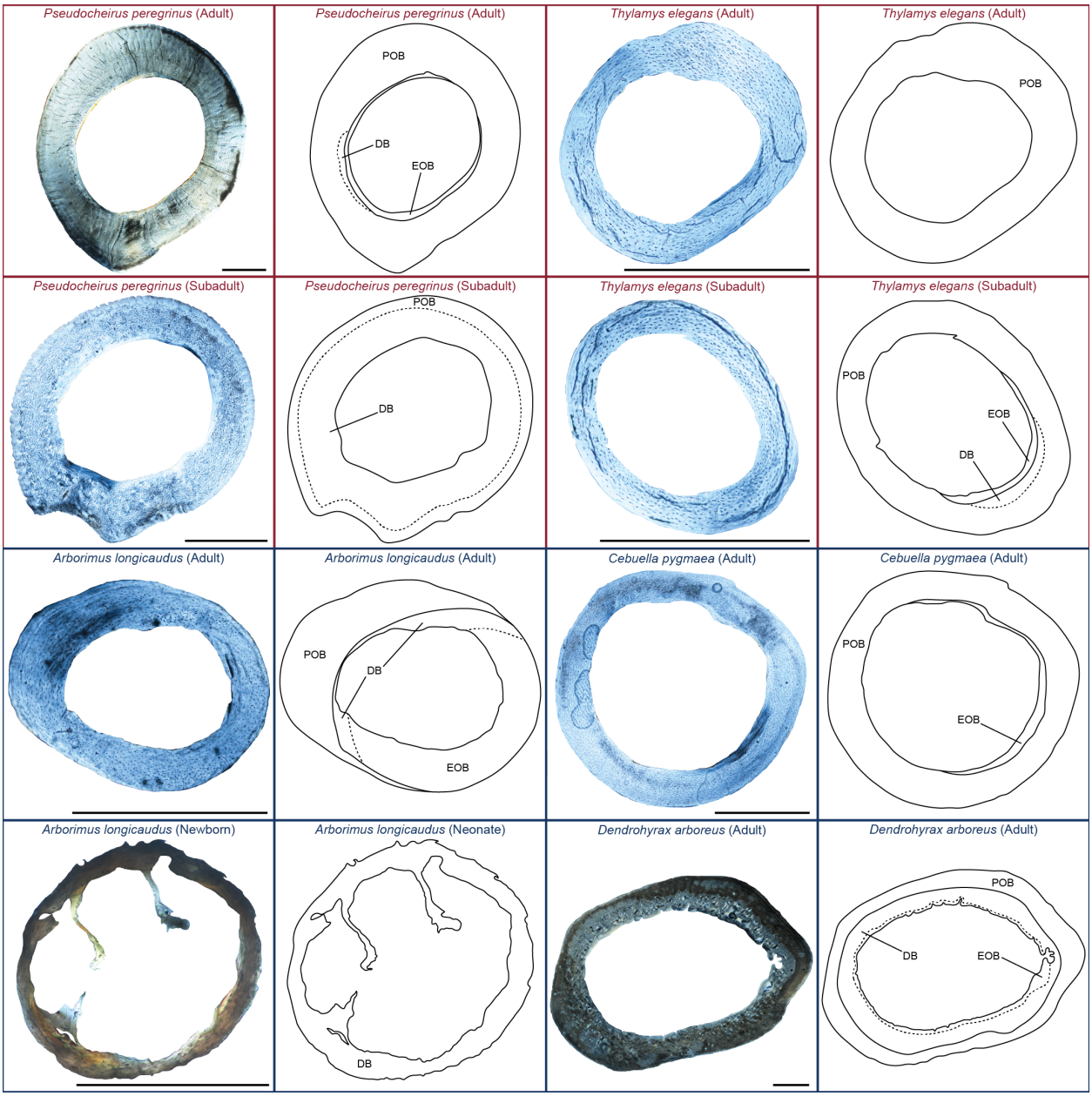

Figure 4.10.2. Same as Figure S1, but for *Pseudocheirus peregrinus* (Adult, UWBM VP 120076; Subadult, UWBM 68925), *Thylamys elegans* (Adult, UWBM 49000 [reflected]; Subadult, UWBM 49026 [reflected]), *Arborimus longicaudus* (Adult, UWBM 34486 [reflected]; Newborn, UWBM 78043 [scale bar = 0.5 mm]), *Cebuella pygmaea* (Adult, UWBM 39005; [reflected]), and *Dendrohyrax arboreus* (Adult, UWBM 39083).

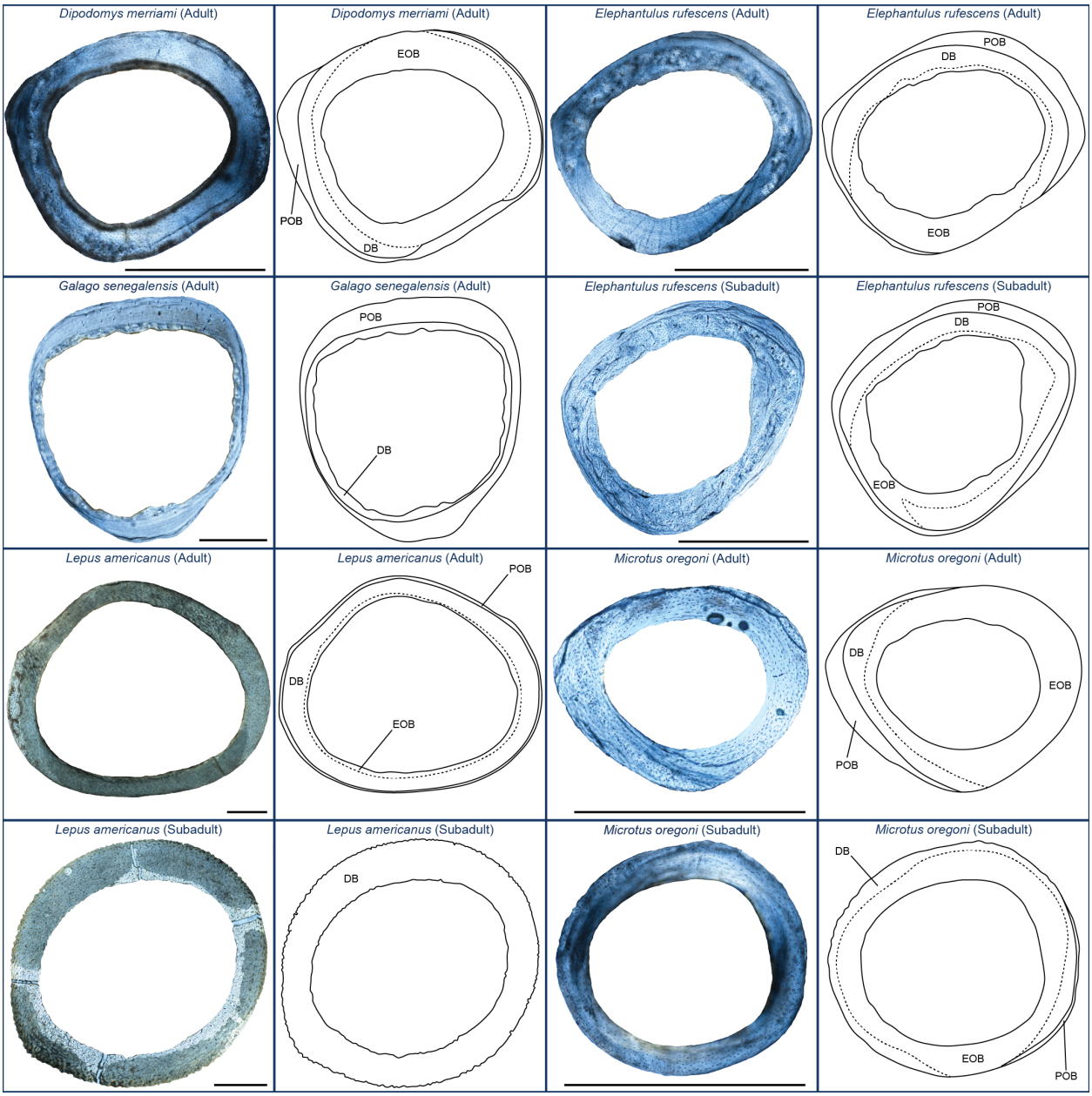

Figure 4.10.3. Same as Figure S1, but for *Dipodomys merriami* (Adult, UWBM 12576), *Elephantulus rufescens* (Adult, UWBM 35466; Subadult, UWBM 34170), *Galago senegalensis* (Adult, UWBM 35394), *Lepus americanus* (Adult, UWBM 33264; Subadult, UWBM 16859), and *Microtus oregoni* (Adult, UWBM VP 120069; Subadult, UWBM 69372).

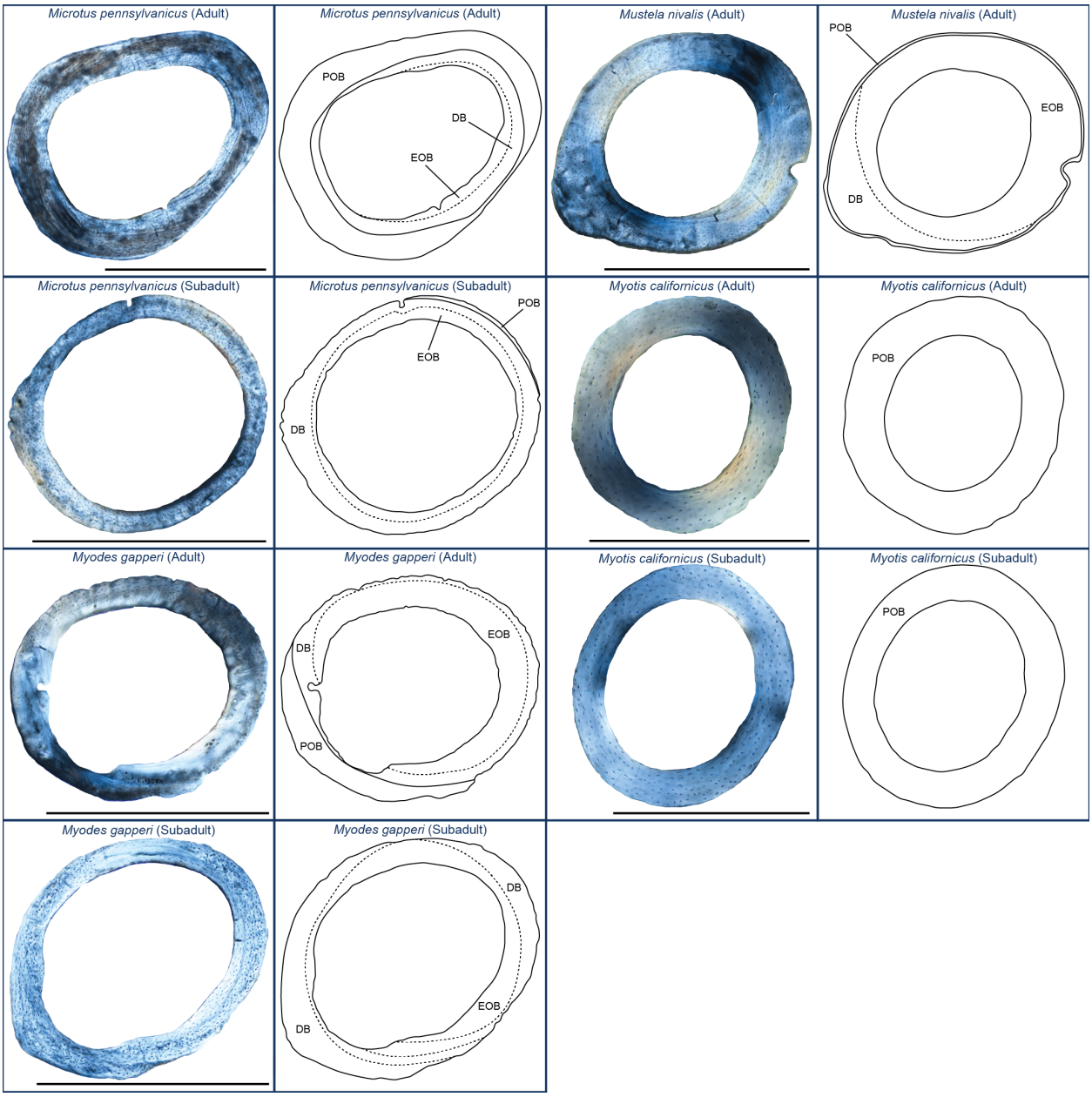

Figure 4.10.4. Same as Figure S1, but for *Microtus pennsylvanicus* (Adult, UWBM 73937; Subadult UWBM 78145), *Mustela nivalis* (Adult, UWBM 83059), *Myodes gapperi* (Adult, UWBM VP 120070; Subadult, UWBM 55755), and *Myotis californicus* (Adult, UWBM 67064 [scale bar = 0.5 mm]; Subadult, UWBM 82534 [scale bar = 0.5 mm]).

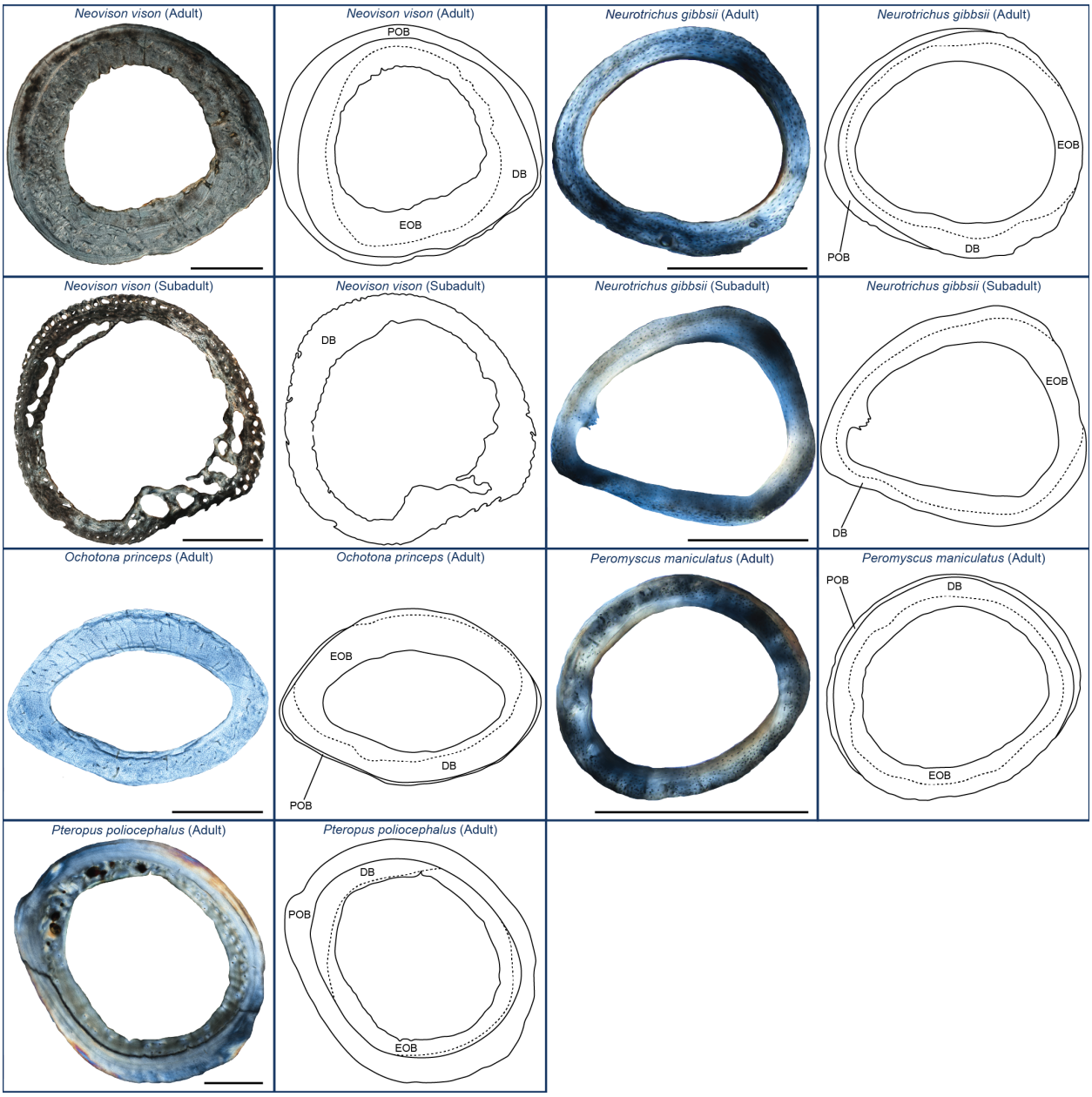

Figure 4.10.5. Same as Figure S1, but for *Neovison vison* (Adult, UWBM 82362-4; Subadult, UWBM 79566), *Neurotrichus gibbsii* (Adult, UWBM 67585 [scale bar = 0.5 mm]; Subadult, UWBM 64764 [scale bar = 0.5 mm]), *Ochotona princeps* (Adult, UWBM 60067), *Peromyscus maniculatus* (Adult, UWBM 30367), and *Pteropus poliocephalus* (Adult, UWBM 35471 [reflected]).

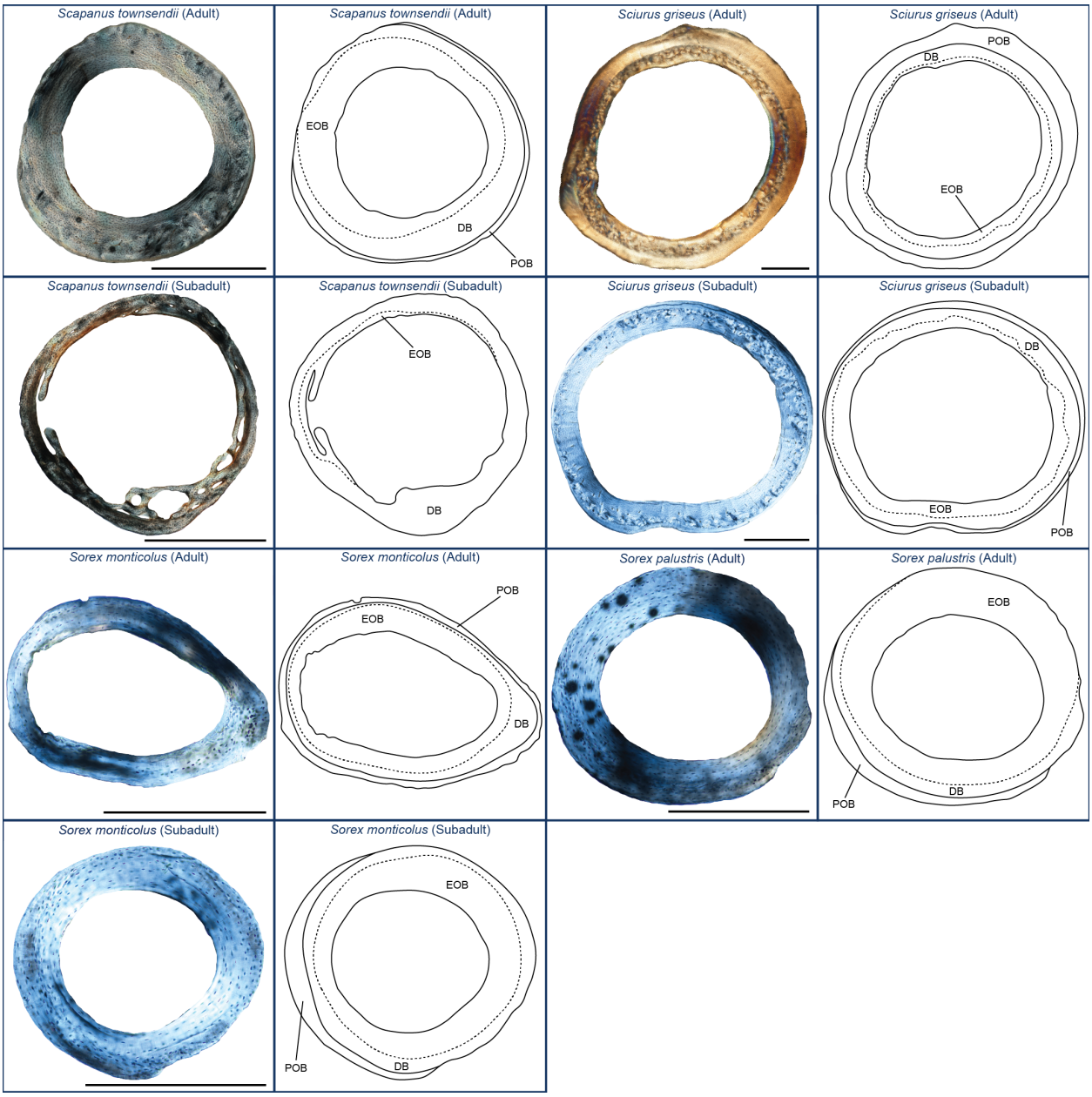

Figure 4.10.6. Same as Figure S1, but for *Scapanus townsendii* (Adult, UWBM VP 120075; Subadult, UWBM 33304), *Sciurus griseus* (Adult, UWBM 83018; Subadult, UWBM 76268), *Sorex monticolus* (Adult, UWBM VP 120074 [scale bar = 0.5 mm]; Subadult, UWBM 58432 [scale bar = 0.5 mm]), and *Sorex palustris* (Adult, UWBM 80433 [scale bar = 0.5 mm]).

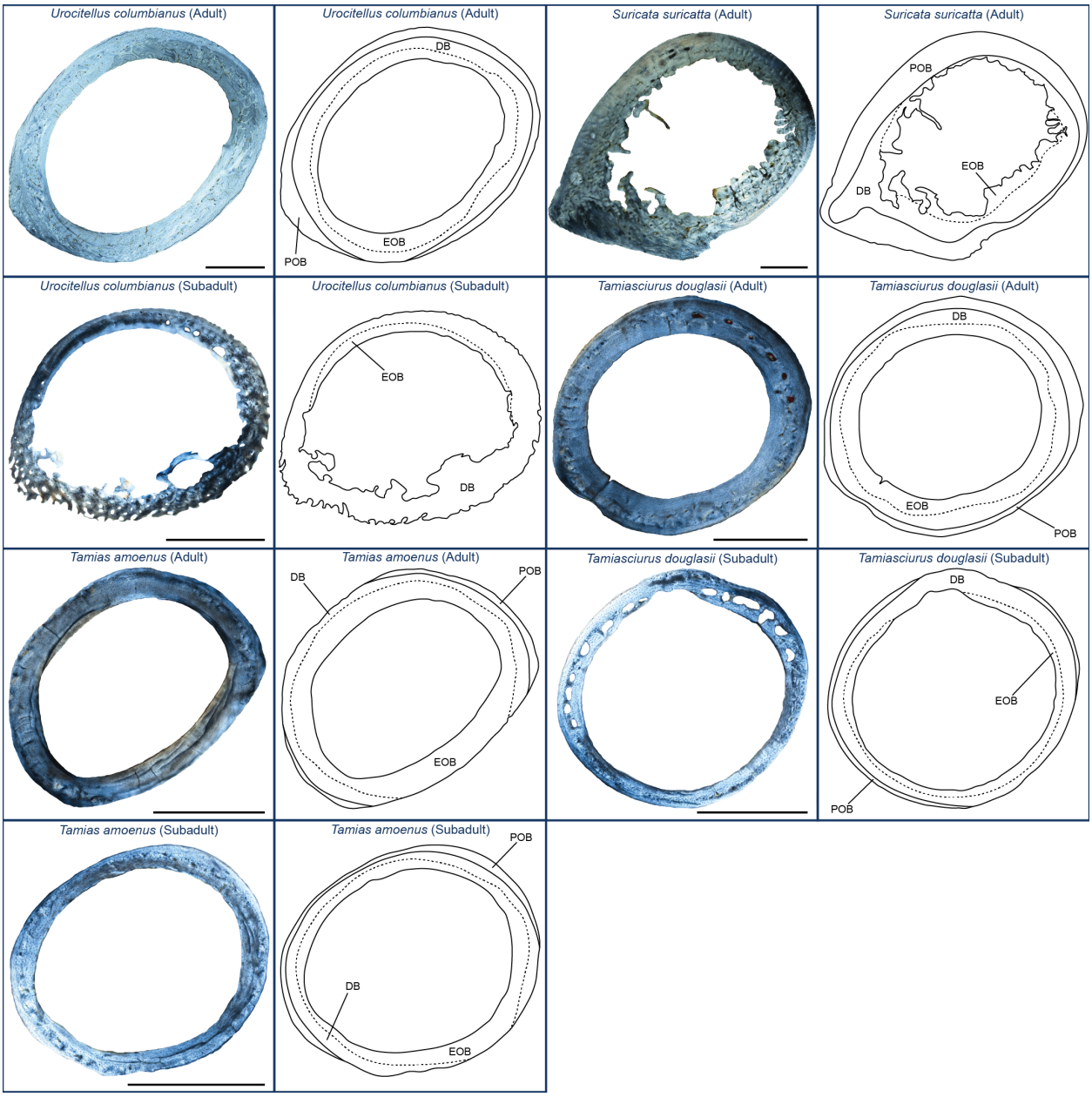

Figure 4.10.7. Same as Figure S1, but for *Urocitellus columbianus* (Adult, UWBM 80405; Subadult, UWBM 39193 [reflected]), *Suricata suricatta* (Adult, UWBM 35469), *Tamias amoenus* (Adult, UWBM VP 120071; Subadult, UWBM 74048 [reflected]), and *Tamiasciurus douglasii* (Adult, UWBM 83017; Subadult, UWBM 81943).

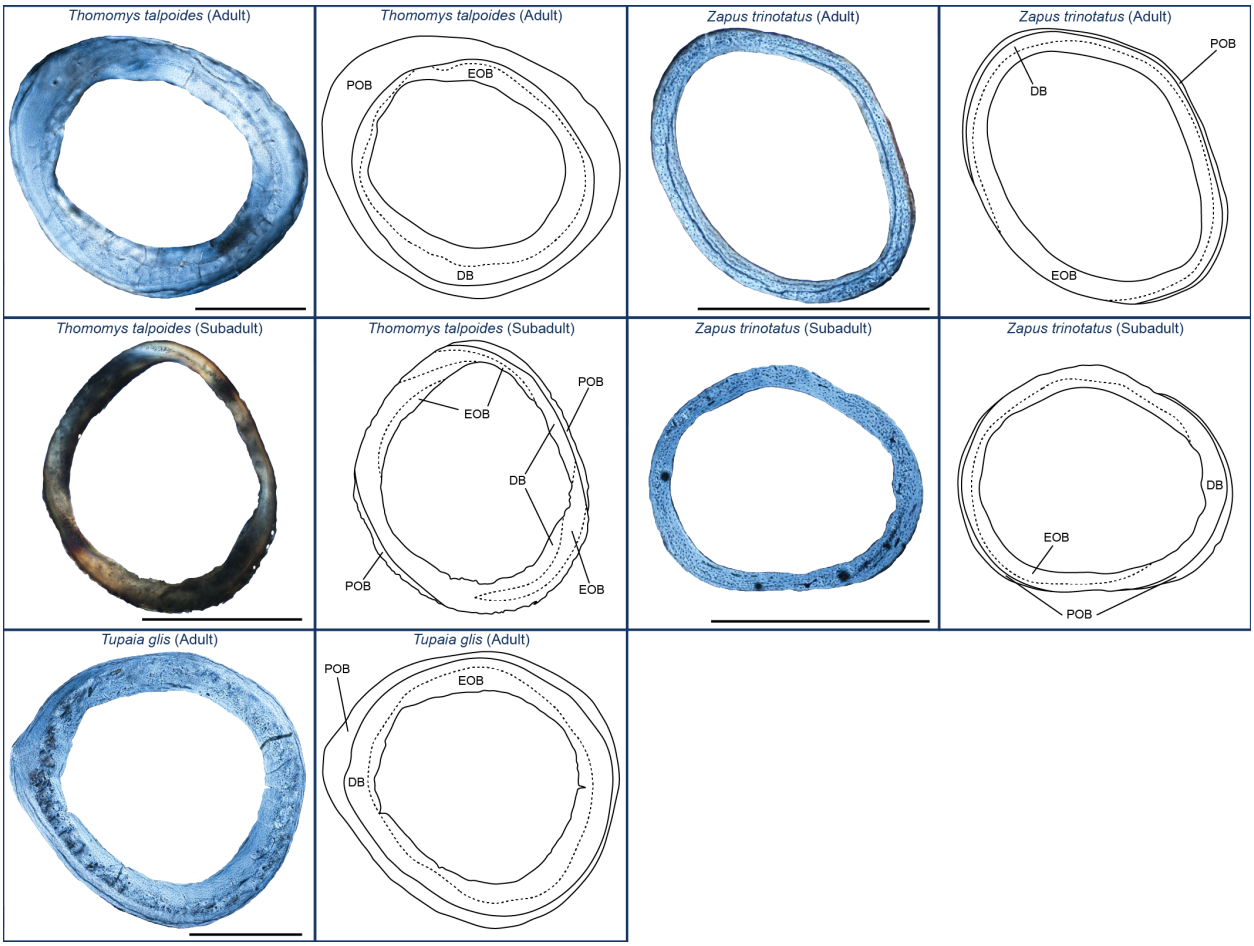

Figure 4.10.8. Same as Figure S1, but for *Thomomys talpoides* (Adult, UWBM VP 120072 [reflected]; Subadult, UWBM 34613 [reflected]), *Tupaia glis* (Adult, UWBM 34266 [reflected]), and *Zapus trinotatus* (Adult, UWBM VP 120073 [reflected]; Subadult, UWBM 80587).

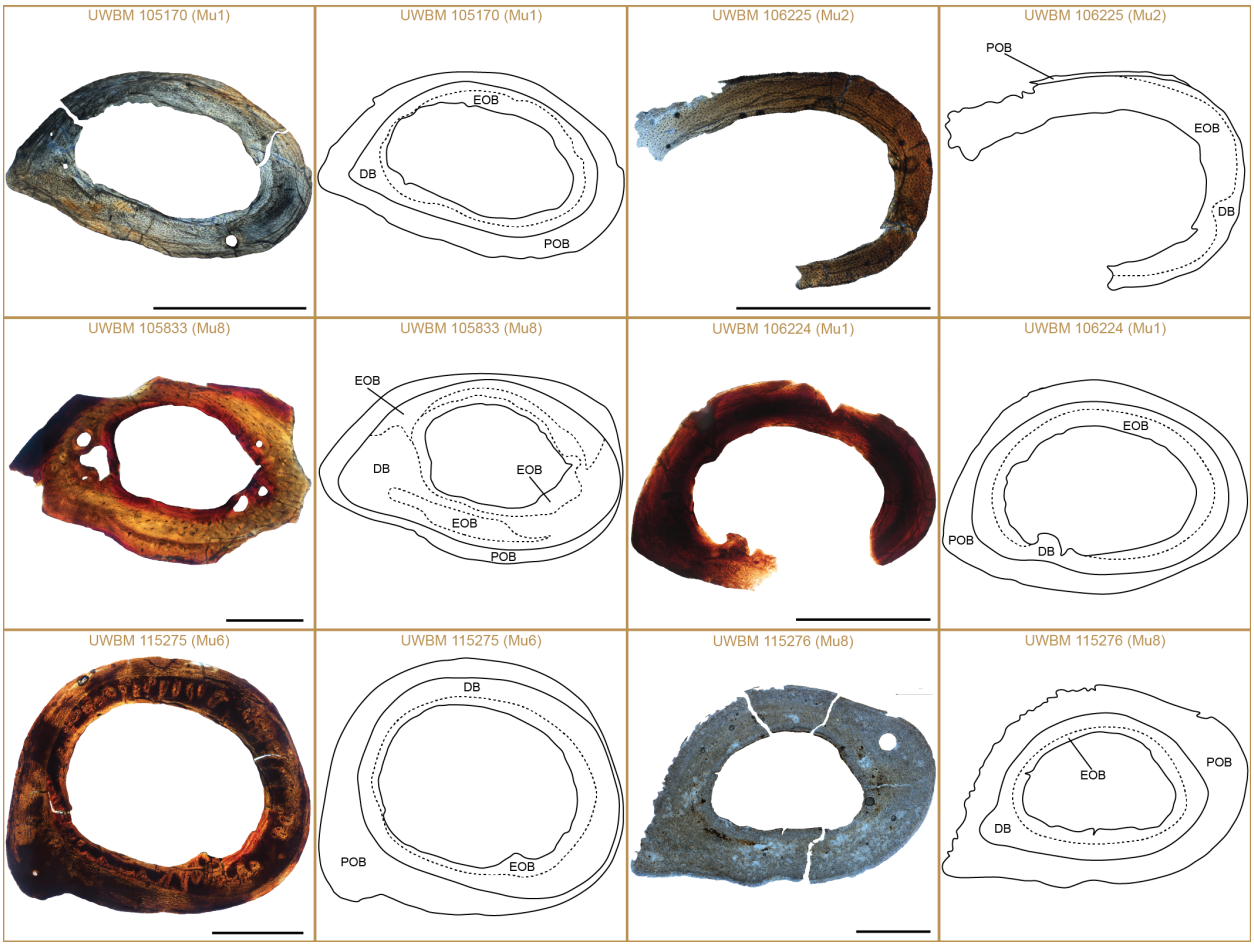

Figure 4.10.9. Same as Figure S1, but for UWBM 105170 (Mu1), UWBM 106225 (Mu2; reflected), UWBM 105833 (Mu8), UWBM 106224 (Mu1), UWBM 115275 (Mu6; reflected), and UWBM 115276 (Mu8; reflected).

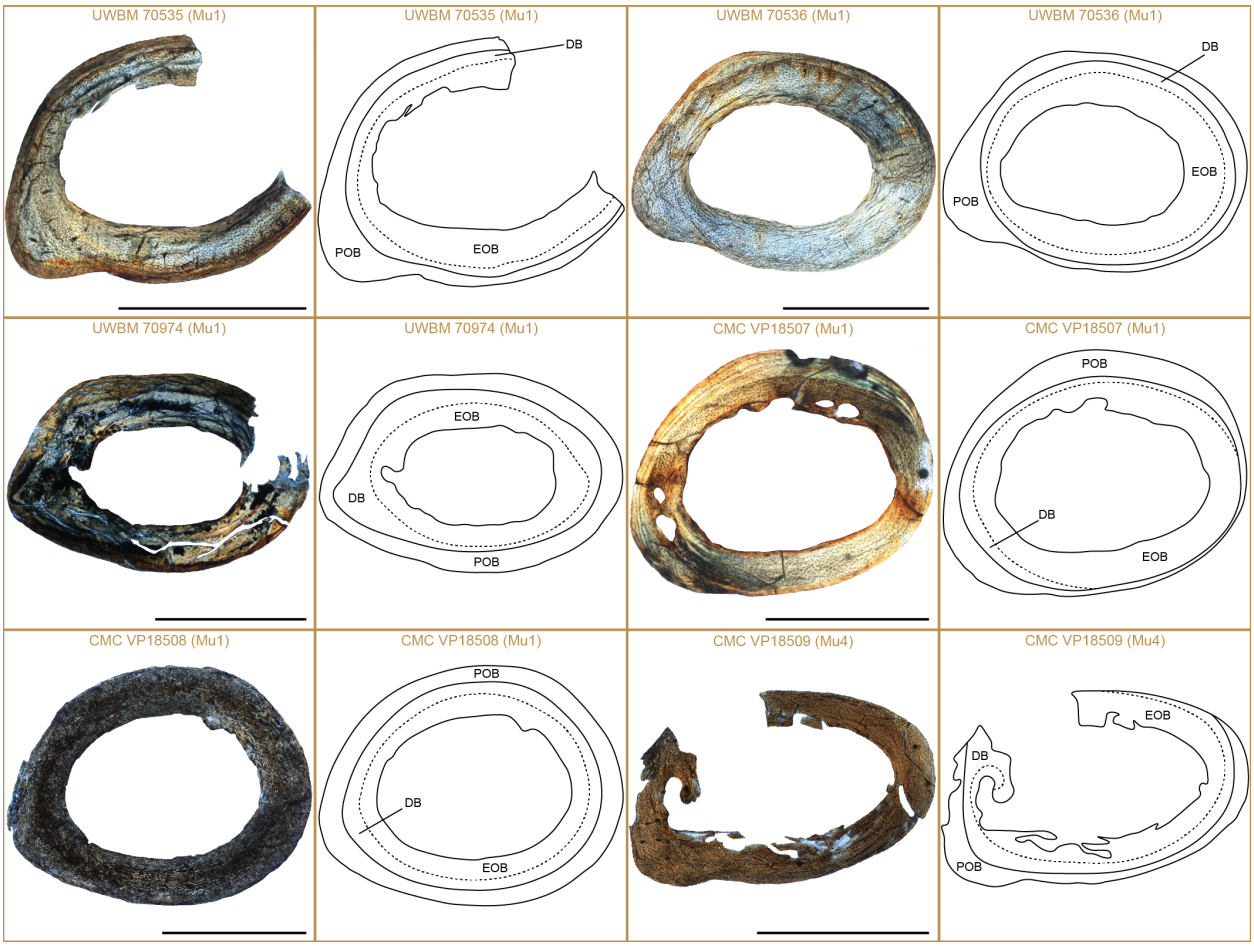

Figure 4.10.10. Same as Figure S1, but for UWBM 70535 (Mu1), UWBM 70536 (Mu1; reflected), UWBM 70974 (Mu1; reflected), CMC VP18507 (Mu1), CMC VP18508 (Mu1; reflected), and CMC VP18509 (Mu4).

Figure 4.10.11. Same as Figure S1, but for CMC VP18510 (Mu8), ROM 78099 (Mu8; reflected), ROM 78100 (Mu8; reflected), ROM 78101 (Mu1; reflected), ROM 78102 (Mu1), and ROM 78106 (Mu1).

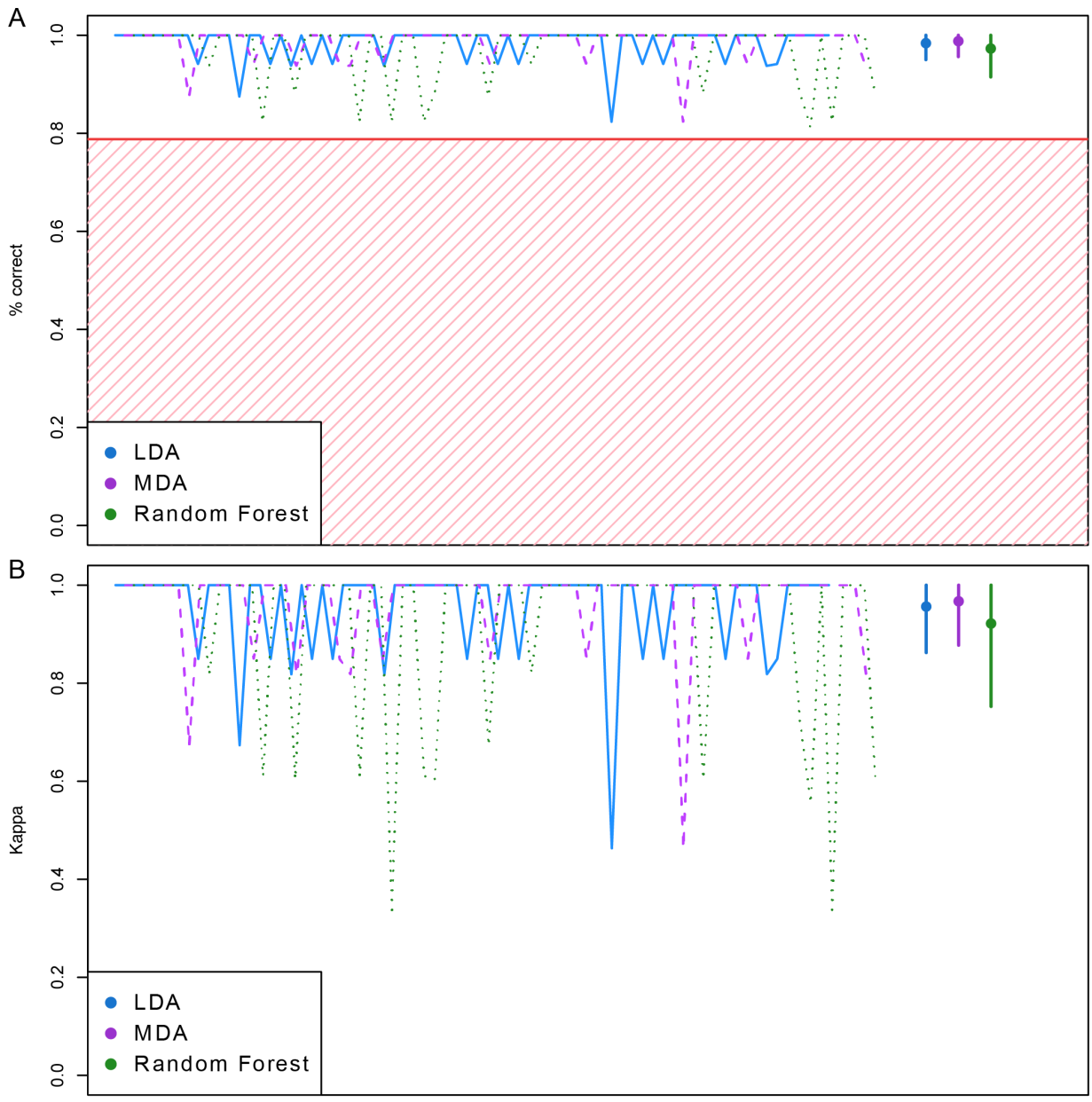

Figure 4.10.12. Model performance during cross-validation for linear discriminant analysis (LDA), random forest (RF), and mixture discriminant analysis (MDA). Lines show each round of cross validation and points show final averages, error bars represent standard error. (*A*) Model accuracy, with the area below the no information rate (0.788) shaded in red. (*B*) Model kappa values. In both metrics, MDA performs slightly better than the other two methods.

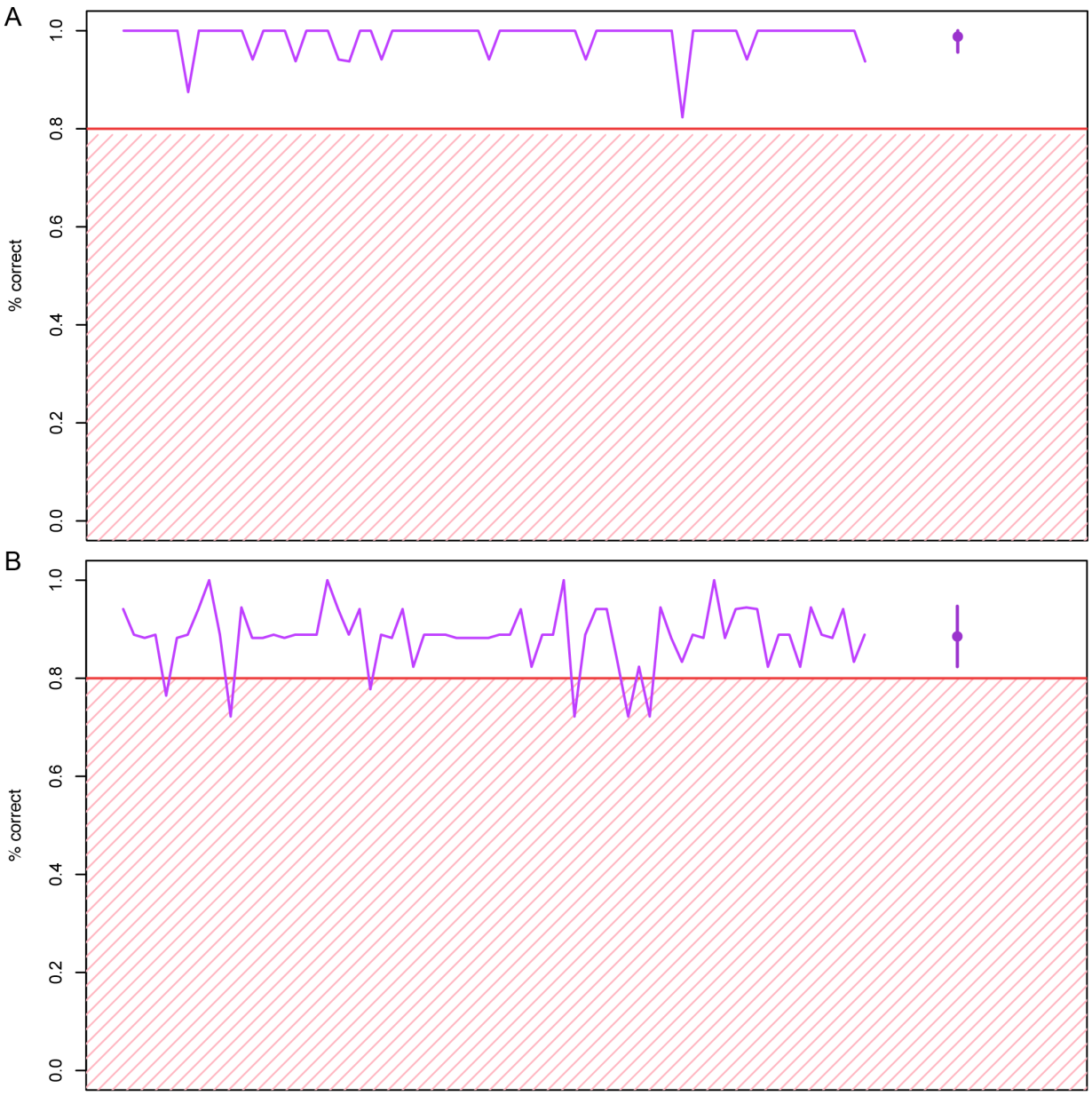

Figure 4.10.13. Impact on mixture discriminant analysis (MDA) model performance when *Myotis* and *Cebuella* are included in the placental class during model fitting. Lines show model accuracy during each round of cross validation, and points show final averages, error bars represent standard error. The area below the no information rate (NIR) is shaded in red. (*A*) MDA model accuracy when *Myotis* and *Cebuella* are excluded. NIR = 0.788. (*B*) MDA model accuracy when *Myotis* and *Cebuella* are included. NIR = 0.8.

4.11 APPENDIX III: SUPPLEMENTAL INFORMATION TABLES

Table 4.11.1. Extant marsupial and placental specimens used in this study. * = Woodland Park Zoo specimens (Seattle, WA).

Infraclass	Order	*Genus*	*Species*	Common Name	UWBM	Ontogenetic Stage
Marsupialia	Didelphimorphia	*Didelphis*	*virginiana*	Virginia Opossum	35526	Adult
Marsupialia	Didelphimorphia	*Didelphis*	*virginiana*	Virginia Opossum	34284	Subadult
Marsupialia	Didelphimorphia	*Thylamys*	*elegans*	Elegant Fat-Tailed Mouse Opossum	49000	Adult
Marsupialia	Didelphimorphia	*Thylamys*	*elegans*	Elegant Fat-Tailed Mouse Opossum	49026	Subadult
Marsupialia	Microbiotheria	*Dromiciops*	*gliroides*	Monito Del Monte	78641	Adult
Marsupialia	Microbiotheria	*Dromiciops*	*gliroides*	Monito Del Monte	78631	Subadult
Marsupialia	Diprotodontia	*Petaurus*	*breviceps*	Sugar Glider	68906	Adult
Marsupialia	Diprotodontia	*Petaurus*	*breviceps*	Sugar Glider	68904	Subadult
Marsupialia	Diprotodontia	*Pseudocheirus*	*peregrinus*	Common Ringtail Possum	VP 120076	Adult
Marsupialia	Diprotodontia	*Pseudocheirus*	*peregrinus*	Common Ringtail Possum	68925	Subadult
Marsupialia	Dasyuromorphia	*Antechinus*	*stuartii*	Brown Antechinus	68914	Adult
Marsupialia	Peramelemorphia	*Perameles*	*nasuta*	Long-Nosed Bandicoot	68919	Adult
Placentalia	Macroscelidea	*Elephantulus*	*rufescens*	E. African Long-Eared Elephant Shrew	35466*	Adult
Placentalia	Macroscelidea	*Elephantulus*	*rufescens*	E. African Long-Eared Elephant Shrew	34170*	Subadult
Placentalia	Hyracoidea	*Dendrohyrax*	*arboreus*	Eastern Tree Hyrax	39083*	Adult
Placentalia	Eulipotyphla	*Sorex*	*palustris*	Water Shrew	80433	Adult
Placentalia	Eulipotyphla	*Sorex*	*monticolus*	Montane Shrew	VP 120074	Adult
Placentalia	Eulipotyphla	*Sorex*	*monticolus*	Montane Shrew	58432	Subadult

Placentalia	Eulipotyphla	*Scapanus*	*townsendii*	Townsend's Mole	VP 120075	Adult
Placentalia	Eulipotyphla	*Scapanus*	*townsendii*	Townsend's Mole	33304	Subadult
Placentalia	Eulipotyphla	*Neurotrichus*	*gibbsii*	American Shrew Mole	67585	Adult
Placentalia	Eulipotyphla	*Neurotrichus*	*gibbsii*	American Shrew Mole	64764	Subadult
Placentalia	Chiroptera	*Myotis*	*californicus*	California Myotis	67064	Adult
Placentalia	Chiroptera	*Myotis*	*californicus*	California Myotis	82534	Subadult
Placentalia	Chiroptera	*Pteropus*	*poliocephalis*	Gray-Headed Flying Fox	35471*	Adult
Placentalia	Carnivora	*Suricata*	*suricatta*	Meerkat	35469	Adult
Placentalia	Carnivora	*Neovison*	*vison*	American Mink	82362-4	Adult
Placentalia	Carnivora	*Neovison*	*vison*	American Mink	79566	Subadult
Placentalia	Carnivora	*Mustela*	*nivalis*	Least Weasel	83059	Adult
Placentalia	Scandentia	*Tupaia*	*glis*	Common Tree Shrew	34266	Adult
Placentalia	Primates	*Cebuella*	*pygmaea*	Pygmy Marmoset	39005*	Adult
Placentalia	Primates	*Galago*	*senegalensis*	Senegal Galago	35394*	Adult
Placentalia	Lagomorpha	*Lepus*	*americanus*	Snowshoe Hare	33264	Adult
Placentalia	Lagomorpha	*Lepus*	*americanus*	Snowshoe Hare	16859	Subadult
Placentalia	Lagomorpha	*Ochotona*	*princeps*	American Pika	60067	Adult
Placentalia	Rodentia	*Tamiasciurus*	*douglasii*	Douglas's Squirrel	83017	Adult
Placentalia	Rodentia	*Tamiasciurus*	*douglasii*	Douglas's Squirrel	81943	Subadult
Placentalia	Rodentia	*Sciurus*	*griseus*	Western Gray Squirrel	83018	Adult
Placentalia	Rodentia	*Sciurus*	*griseus*	Western Gray Squirrel	76268	Subadult
Placentalia	Rodentia	*Urocitellus*	*columbianus*	Columbian Ground Squirrel	80405	Adult
Placentalia	Rodentia	*Urocitellus*	*columbianus*	Columbian Ground Squirrel	39193	Subadult
Placentalia	Rodentia	*Tamias*	*amoenus*	Yellow-Pine Chipmunk	VP 120071	Adult
Placentalia	Rodentia	*Tamias*	*amoenus*	Yellow-Pine Chipmunk	74048	Subadult
Placentalia	Rodentia	*Thomomys*	*talpoides*	Northern Pocket Gopher	VP 120072	Adult
Placentalia	Rodentia	*Thomomys*	*talpoides*	Northern Pocket Gopher	34613	Subadult
Placentalia	Rodentia	*Dipodomys*	*merriami*	Merriam's Kangaroo Rat	12576	Adult
Placentalia	Rodentia	*Zapus*	*trinotatus*	Pacific Jumping Mouse	VP 120073	Adult

Placentalia	Rodentia	*Zapus*	*trinotatus*	Pacific Jumping Mouse	80587	Subadult
Placentalia	Rodentia	*Peromyscus*	*maniculatus*	Deer Mouse	30367	Adult
Placentalia	Rodentia	*Arborimus*	*longicaudus*	Red Tree Vole	34486	Adult
Placentalia	Rodentia	*Arborimus*	*longicaudus*	Red Tree Vole	78043	Subadult
Placentalia	Rodentia	*Myodes*	*gapperi*	Southern Red-Backed Vole	VP 120070	Adult
Placentalia	Rodentia	*Myodes*	*gapperi*	Southern Red-Backed Vole	55755	Subadult
Placentalia	Rodentia	*Microtus*	*pennsylvanicus*	Meadow Vole	73937	Adult
Placentalia	Rodentia	*Microtus*	*pennsylvanicus*	Meadow Vole	78145	Subadult
Placentalia	Rodentia	*Microtus*	*oregoni*	Creeping Vole	VP 120069	Adult
Placentalia	Rodentia	*Microtus*	*oregoni*	Creeping Vole	69372	Subadult

Table 4.11.2. Multituberculate specimens used in this study. All are isolated, fragmentary proximal femora from the Hell Creek and Fort Union formations of northeastern Montana. Tentative identification of genus based on ref. 8. Abbreviation: K/Pg, Cretaceous/Paleogene.

Tentative Genus	Morphotype	Specimen no.	Location of femoral cross section	Locality no.	Formation	Geologic age
Mesodma	Mu1	UWBM 105170	Midshaft	UWBM C1103	Hell Creek	latest Cretaceous
Mesodma	Mu2	UWBM 106225	Midshaft	UWBM C1113	Hell Creek	latest Cretaceous
Stygimys	Mu8	UWBM 105833	Proximal midshaft	UWBM C1665	Fort Union	earliest Paleocene
Mesodma	Mu1	UWBM 106224	Midshaft	UCMP V84193	Fort Union	earliest Paleocene
Cimexomys	Mu6	UWBM 115275	Midshaft	UWBM C1678	Fort Union	earliest Paleocene

Stygimys	Mu8	UWBM 115276	Proximal	UWBM C1665	Fort Union	earliest Paleocene
Mesodma	Mu1	UWBM 70535	Proximal midshaft	UCMP V65127	Hell Creek	mixed K/Pg
Mesodma	Mu1	UWBM 70536	Midshaft	UCMP V65128	Hell Creek	mixed K/Pg
Mesodma	Mu1	UWBM 70974	Midshaft	UCMP V65129	Hell Creek	mixed K/Pg
Mesodma	Mu1	CMC VP18507	Midshaft	UCMP V65130	Hell Creek	mixed K/Pg
Mesodma	Mu1	CMC VP18508	Midshaft	UCMP V65131	Hell Creek	mixed K/Pg
Cimexomys	Mu4	CMC VP18509	Proximal midshaft	UCMP V65132	Hell Creek	mixed K/Pg
Stygimys	Mu8	CMC VP18510	Proximal midshaft	UCMP V65133	Hell Creek	mixed K/Pg
Stygimys	Mu8	ROM 78099	Proximal midshaft	UCMP V65134	Hell Creek	mixed K/Pg
Stygimys	Mu8	ROM 78100	Proximal	UCMP V65135	Hell Creek	mixed K/Pg
Mesodma	Mu1	ROM 78101	Proximal midshaft	UCMP V65136	Hell Creek	mixed K/Pg
Mesodma	Mu1	ROM 78102	Midshaft	UCMP V65137	Hell Creek	mixed K/Pg
Mesodma	Mu1	ROM 78106	Proximal midshaft	UCMP V65138	Hell Creek	mixed K/Pg

Table 4.11.3. Summary statistics for analyses of variances (ANOVAs) and pairwise post-hoc tests (Tukey's Honest Significant Difference) that compare cortex tissues of three clades: marsupials (Mar), placentals (Pla), and multituberculates (Mul). Prior to analyses, compositional tissue data (percentages of cortex) were transformed into isometric log-ratios. Reported values for post-hoc tests are *p*-values.

	***F*-stat.**	***p*-value**	**Mar-Pla**	**Mar-Mul**	**Pla-Mul**
Periosteal	18.46	<0.001	<0.001	<0.001	0.996
Disorganized	9.56	<0.001	<0.001	0.001	0.901
Endosteal	1.70	0.227	0.264	0.175	0.886

Table 4.11.4. Summary statistics for phylogenetic generalized least squares (PGLS) regressions of all histological measurements collected from our extant sample against weaning age (in days). Prior to analyses, compositional data were transformed into isometric log-ratios, and weaning age was log-transformed and size-corrected (via PGLS regression against adult body mass).

Life history trait	**Histology trait**	***t*-stat.**	***p*-value**
Weaning age (days)	Cortex % (ILR)	0.454	0.653
(size-corrected)	**Periosteal % (ILR)**	**4.065**	**<0.001**
	Disorganized % (ILR)	-1.575	0.125
	Endosteal % (ILR)	-1.493	0.145
	Vascular area %	0.654	0.517
	Ave osteocyte density (#/mm^2)	-1.634	0.112
	Ave osteocyte size (mm^2)	0.507	0.616

Table 4.11.5. Summary statistics for PGLS regressions on weaning age but using a summed log-ratio (SLR) transformation instead of IRL.

Life history trait	Histology trait	*t*-stat	*p*-value
Weaning age (days)	Periosteal % (SLR)	3.481	0.001
(size corrected)	Endosteal/Disorganized (SLR)	0.013	0.990

4.11.1 SUPPLEMENTARY INFORMATION REFERENCES

1. Aitchinson, J. (1982). The statistical analysis of compositional data. R. Stat. Soc. *44*, 139–177.
2. Egozcue, J.J., Pawlowsky-Glahn, V., Mateu-Figueras, G., and Barceló-Vidal, C. (2003). Isometric logratio transformations for compositional data analysis. Math. Geol. *35*, 279–300.
3. Morton, J.T., et al. (2017). Balance trees reveal microbial niche differentiation. mSystems *2*, e00162–16.
4. R Core Team. (2021). R: A language and environment for statistical computing. R Foundation for Statistical Computing.
5. van den Boogaart, K.G., Tolosana-Delgado, R., and Bren, M. (2021). compositions: compositional data analysis. R package version *2.0-1*. <https://CRAN.R-project.org/package=compositions>.

6. Holden, J.E., Finch, W.H., Kelley, K. (2011). A comparison of two-group classification methods. Educ. Psychol. Meas. *71*, 870–901.
7. Greenacre, M. (2020). Amalgamations are valid in compositional data analysis, can be used in agglomerative clustering, and their logratios have an inverse transformation. Appl. Comput. Geosci., 10.1016/j.acags.2019.100017.
8. DeBey, L.B., and Wilson, G.P. (2014). Mammalian femora across the Cretaceous–Paleogene boundary in eastern Montana. Cretac. Res. *51*, 361–385.
9. Jones, K.E., et al. (2009). PanTHERIA: a species-level database of life history, ecology, and geography of extant and recently extinct mammals. Ecology *90*, 2648–2648.
10. Myers, P., Jones, T., Espinosa, R., Dewey, T., Hammond, G. (2020). The Animal Diversity Web. Accessed June 15.
11. Myhrvold, N.P., Baldridge, E., Chan, B., Sivam, D., Freeman, D.L., and Ernest, S.M. (2015). An amniote life history database to perform comparative analyses with birds, mammals, and reptile: Ecological Archives E096–269. Ecology *96*, 3109–3109.
12. Gusztak, R.W., and Campbell, K. L. (2004). Growth, development and maintenance of American water shrews (*Sorex palustris*) in captivity. Mammal Study *29*, 65–72.
13. Pedersen, R.J. (1963). The life history and ecology of Townsend's mole *Scapanus townsendii* (Bachman) in Tillamook County Oregon. Oregon State University, Corvallis, OR.

CHAPTER 5: CONCLUSION

The rise and fall of multituberculate mammals represents one of the most compelling stories in mammalian evolution, and in no other place in the world is this story as well-documented as in the Western Interior of North America. Though now extinct, multituberculates remain the longest-lived mammalian group, and they exceeded all other mammals in terms of numerical abundance and taxonomic diversity for much of that interval. In this dissertation, I made an attempt to better understand this iconic lineage by focusing on perhaps the most successful multituberculate group of them all, the Cimolodonta.

In Chapter 2, my co-author and I suggest that Cimolodonta either evolved early in the Early Cretaceous, or they diversified rapidly near the Early-Late Cretaceous boundary. The specialized slicing-then-grinding chewing cycle of cimolodontans likely acted as a functional constraint of their p4 morphology, and perhaps their dentition more broadly. The cimolodontan groups that escaped this constraint were among the most herbivorous taxa, and they did so by shifting the slicing/cutting burden of the p4 to their gliriform incisors, and reducing the size of p4 relative to the molars. That this was the solution, rather than modifying the p4 to a broader and multi-cusped tooth, suggests that the derived, blade-like dentitions of cimolodontans may have constrained their ability to exploit folivorous niches, perhaps putting them at a competitive disadvantage relative to tribosphenic eutherians in the late Paleocene and Eocene.

In Chapter 3, my co-authors and I erect a new multituberculate genus, *Filikomys*, that is likely phylogenetically intermediate between more basal cimolodontans (e.g., *Cimexomys*) and more deeply nested neoplagiaulacids (e.g., *Mesodma*), and I revise the diagnosis for *Mesodma*. Skeletons of *Filikomys primaevus* from Egg Mountain exhibit postcranial adaptations for digging, and on the basis of the sedimentology and ichnology of the site and the preservation of

the fossils, it is likely that they were preserved in burrows (the traces of which were likely obliterated through subsequent bioturbation). That we find numerous individuals packed together, constituting a mixture of subadults and adults, indicates that these individuals of *F. primaevus* represent a gregarious social group. This represents the earliest evidence of mammalian social behavior, predating that in any therian mammals.

In Chapter 4, my co-authors and I find that modern placentals and marsupials have distinct bone tissue microstructures, and that these differences are driven by their divergent life history strategies; in particular, reflecting the abbreviated gestation and prolonged lactation periods of marsupials versus the prolonged gestation and abbreviated lactation periods of placentals. Multituberculate bone histology is nearly identical to that of placentals, implying that they had similar life history strategies, and those multituberculates represented in our sample likely were weaned around 30 days. That multituberculates likely had placental-like life histories lends support to the hypothesis that the intense maternal-fetal contact characteristic of placental reproduction is in fact ancestral for viviparous mammals; but, it is also possible multituberculates and placentals independently evolved similar strategies. Nonetheless, this finding challenges the hypothesis that the rise of placentals was driven by their unique life history strategy.

In sum, these results imply that, in many ways, multituberculates approached the level of biological complexity of small-bodied placental mammals. Yet, despite their long reign, the highly specialized and adaptive multituberculates eventually succumbed to the changing climate and newly radiating placental herbivores. It does not seem likely, however, that they declined on the basis of some inferiority of behavioral complexity or reproduction. Instead, it may have been the highly-specialized dentitions of multituberculates, which facilitated their dominance for tens of millions of years, that ultimately led to their demise.

The Mesozoic mammals constituted a little world of their own. In their society were all the fundamental adaptive types of a recent mammalian fauna. Some were chiefly insectivorous, others predaceous, while still others were herbivorous. It is the latter, the Multituberculata, which we have studied. They were the most successful of Mesozoic mammals, for, appearing as early as the very first, they occur at every mammal-bearing horizon in the Mesozoic and even linger into the beginning of the age of mammalian dominance without any remarkable change. They undoubtedly owed this longevity to their complete and successful adaptation, and also to the fact that they alone among Mesozoic mammals did not have to face heavy reptilian competition for food, as did the small insectivores and carnivores. When the more progressive plant-eating mammals of the Paleocene appeared, the days of the multituberculates were numbered. Yet, so perfect was their adaptation, even then they lingered on until the very moment when the Paleocene herbivores were themselves doomed by the invasion of the modernized mammals, beginning in the earliest true Eocene.

—George Gaylord Simpson, “The Multituberculates as Living Animals,” 1926